

Ex libris
UNIVERSITATIS
ALBERTAE NSIS





Digitized by the Internet Archive
in 2019 with funding from
University of Alberta Libraries

<https://archive.org/details/Johnston1993>

UNIVERSITY OF ALBERTA
RELEASE FORM

NAME OF AUTHOR: STEPHEN T. JOHNSTON

TITLE OF THESIS: THE GEOLOGIC EVOLUTION OF NISLING
ASSEMBLAGE AND STIKINE TERRANE IN THE
AISHIHIK LAKE AREA, SOUTHWEST YUKON

DEGREE: DOCTOR OF PHILOSOPHY

YEAR THIS
DEGREE GRANTED: 1993

PERMISSION IS HEREBY GRANTED TO THE UNIVERSITY OF ALBERTA
LIBRARY TO REPRODUCE SINGLE COPIES OF THIS THESIS AND TO LEND OR
SELL SUCH COPIES FOR PRIVATE, SCHOLARLY OR SCIENTIFIC RESEARCH
PURPOSES ONLY.

THE AUTHOR RESERVES OTHER PUBLICATION RIGHTS, AND
NEITHER THE THESIS NOR EXTENSIVE EXTRACTS FROM IT MAY BE
PRINTED OR OTHERWISE REPRODUCED WITHOUT THE AUTHOR'S WRITTEN
PERMISSION.

UNIVERSITY OF ALBERTA

**THE GEOLOGIC EVOLUTION OF NISLING ASSEMBLAGE AND STIKINE
TERRANE IN THE AISHIHIK LAKE AREA, SOUTHWEST YUKON**

BY

STEPHEN T. JOHNSTON



A THESIS

SUBMITTED TO THE FACULTY OF GRADUATE STUDIES AND RESEARCH
IN PARTIAL FULFILMENT OF THE REQUIREMENTS FOR THE DEGREE OF
DOCTOR OF PHILOSOPHY

IN
GEOLOGY

DEPARTMENT OF GEOLOGY

EDMONTON, ALBERTA
(FALL) (1993)

UNIVERSITY OF ALBERTA

FACULTY OF GRADUATE STUDIES AND RESEARCH

The undersigned certify that they have read, and recommend to the Faculty of Graduate Studies and Research for acceptance a thesis entitled **Geologic evolution of Nisling Assemblage and Stikine terrane in the Aishihik Lake area, southwest Yukon**, submitted by Stephen T. Johnston in partial fulfilment of the requirements for the degree of Doctor of Philosophy in Geology.

ABSTRACT

The Nisling Assemblage in the Aishihik Lake region in southwest Yukon is more than 10 km thick and consists of quartzite, a 4 km thick amphibolite - marble sequence, and Early Mississippian orthogneiss. Late Triassic-Early Jurassic deformation and tectonic burial of Nisling Assemblage to deep crustal levels occurred during subduction beneath the Cache Creek Terrane and resulted in the cessation of arc volcanism on the Cache Creek Terrane and in the deposition of molasse, including the Laberge Group and the Inklin Formation.

The Aishihik Batholith ($187.0 \pm 9.7/-0.9$) intruded deeply buried strata of Nisling Assemblage. The batholith is characterized by a magmatic foliation and by a solid-state fabric that is thought to reflect magmatic ballooning. Intrusion metamorphosed the Nisling Assemblage; isograds parallel the contact, form a hot-side-up metamorphic aureole, and define an increase in grade towards the batholith. Geothermometry data are consistent with this interpretation. Metamorphic minerals, including kyanite which developed at the expense of staurolite, and geobarometry data are indicative of pressures of 8 kbar to 10 kbar. The batholith is characterized by magmatic epidote indicative of emplacement at pressures of 8 kbar.

The Aishihik Batholith is part of the Klotassin Plutonic Suite and developed during subduction, probably of the Windy-McKinley Terrane, beneath the Nisling Assemblage. A change in the the Aishihik-Klotassin arc occurred in the latest Early Jurassic; the batholith and the Nisling Assemblage were intruded by leucocratic pink quartz monzonite of the Long Lake Suite within 10 Ma of emplacement of the Aishihik Batholith, and the arc was rapidly uplifted (between 0.075 and 0.35 cm/year). Uplift and the change in the magmatic character of the arc resulted from the entry of buoyant crust, possibly of Insular Superterrane, into the subduction zone beneath Nisling Assemblage.

The Ruby Range Batholith is a composite plutonic body that intrudes the Nisling Assemblage. The margins of the batholith were emplaced between 68 and 90 Ma; the core of the batholith may be as young as 58 Ma. The youngest parts of the batholith may correlate with widespread Eocene sillimanite-grade metamorphism in southwest Yukon.

ACKNOWLEDGEMENTS

Financial support for this thesis was provided by Dr. Philippe Erdmer, and the Boreal Institute of the University of Alberta. The Whitehorse Geology office of the Department of Indian and Northern Affairs provided helicopter and logistical support. Northern Affairs also sponsored my attendance at the 1987 Yukon Geoscience Forum. The Department of Geology at the University of Alberta provided me with teaching and research assistantships throughout my tenure as a graduate student; the Geological Survey of Canada provided field equipment; and Shell Canada provided logistical support in the preparation of the thesis. Access to the microprobe at the University of Calgary was provided by Dr. Ed Ghent; Dr. Henry Charlesworth made available the TRIPOD program; and Dr. Bud Baadsgaard welcomed me into his geochronology lab at the University of Alberta. U-Pb zircon and sphene separates were analyzed at the GSC geochronology lab by Dr. Jim Mortensen. Neutron activation analyses were performed by John Duke at the Slow Poke reactor at the University of Alberta.

Able field assistance was provided by Paul Baxter and Siegfried Joiner. John Mahatchek provided expert assistance in operating the microprobe at the University of Calgary. Assistance with microprobe studies was also provided by Dr. Mike McDonut and Dr. James Sevigny. Geothermobarometry results were tabulated by Dr. Tim Grover. Assistance in using TRIPOD was provided Dr. Charlesworth, Bruce Wrightson, and J Guidos. Bruce Wrightson assisted in formatting and plotting out structural data. Dr. Bud Baadsgaard is thanked for teaching me the druidic rituals involved in U - Pb isotopic studies. Geochronological studies conducted at the University of Alberta were assisted by Dr. Pat Cavell, John (that is the worst possible thing you could have done) Duke, Steve Prevec, Alex Stelmach, and Wayne. John Duke, Steve Prevec and Alex Stelmach assisted with additional geochemical studies. Brian Turner provided advice and assistance with photographs and brewery tours. Expert drafting assistance was provided by Eva Necas.

The idea for this thesis arose out of discussions with Dr. Philippe Erdmer, who first introduced me to exciting world of Yukon geology. Dr. Dirk Tempelman-Kluit also helped to define the thesis.

This thesis benefited from critical readings by Dr. Philippe Erdmer and Dr. Don Murphy. Parts of the thesis were critically reviewed by John Duke, Dr. Jim Mortensen, Dr. Derek Thorkelson, and Craig Hart (who turned very red and blotchy after reading an

early version of the concluding chapter). Additional helpful review were provided by Dr. Bud Baadsgaard, Dr. Tom Chacko, Dr. Rob Creaser, Dr. F.W. Jones, and Dr. George Gehrels.

Discussions with colleagues at conferences, at the University of Alberta, at Shell Canada, and at the Canada-Yukon Geoscience office were instrumental in shaping my political leanings and my interpretations. In particular I would like to thank Dante Canil, John Duke, Jennifer Smith, Steve Prevec, Kevin Ansdell, Bill Styan, Clay Oberg, Don Murphy, Derek Thorkelson, Craig Hart, Mitch Mihalynuk, Mike McDonough, Grant Abbott, Philippe Erdmer, Jim Mortensen, Dirk Tempelman-Kluit and Donald Hyndman.

The following people are thanked for providing leadership and encouragement during my prolonged passage through the halls of McGill University and the University of Alberta: Dr. Andrew Hynes and Dr. Eric Mountjoy at McGill instilled in me a love for geology and a desire to carry on my studies at the graduate level; Dr. Henry Charlesworth, who suffered through my M.Sc., dispensed fatherly advice at timely intervals, and taught me the importance of rigorous, quantitative analysis; Dr. Chris Scarfe and Dr. R. St. J. Lambert, both deceased, were important influences - Chris for his compelling enthusiasm for geology, and Dr. Lambert for the twinkle (was that a wink?) in his eye and for his incomparable breadth of knowledge. Both are sorely missed.

The support of my family has been (almost) unwavering. To my parents, who show up at geological conferences, clap the loudest after my talks and heckle those who criticize my work, my sincerest thanks and appreciation. My wife, Sheila-Dale, was vigilant in reminding me that I had a thesis to complete. My daughter, Callie Helen, assisted with keeping me up at night.

TABLE OF CONTENTS

CHAPTER	page
I. INTRODUCTION	1
1.1 Statement of the problem	1
1.2 Previous work	6
II. ROCK TYPES AND STRATIGRAPHIC CORRELATIONS	7
2.1 Introduction	7
2.2 The Nisling Assemblage	7
2.3 The Aishihik Batholith	25
2.4 Long Lake Suite pink quartz monzonite	30
2.5 The Ruby Range Batholith	32
2.6 Age, stratigraphic and terrane relations	32
III. U-PB GEOCHRONOLOGY	37
3.1 Introduction	37
3.2 Analytical results	37
3.3 Discussion and Conclusions	49
IV. STRUCTURAL GEOLOGY	52
4.1 Introduction	52
4.2 Structure of the Aishihik Batholith	54
4.2.1 Mesoscopic structures	54
4.2.2 Microscopic structures	78
4.2.3 The nature of S_m and S_t	83
4.3 Structure of the Nisling Assemblage	83
4.3.1 Mesoscopic structures	83
4.3.2 Microscopic structures	97
4.3.3 The nature of the planar fabrics	106
4.4 The shape of the Aishihik Batholith and the nature of the west margin of the batholith	110
4.5 Steep faults	115
4.6 Discussion	116
4.7 Conclusions	121

V. METAMORPHIC PETROLOGY	123
5.1 Introduction	123
5.2 The distribution and morphology of metamorphic minerals and migmatite in pelitic rocks	124
5.3 Mineral isograds	153
5.4 Estimate of metamorphic conditions	158
5.4.1 Petrogenetic relations	158
5.4.2 Geothermometry and geobarometry	162
5.5 The nature of the metamorphic events	167
5.6 Pressure - temperature - time displacement	171
5.7 Discussion	174
5.8 Conclusions	176
VI. DISCUSSION	178
6.1 Towards a tectonic model	178
6.2 Conclusions	185
VII. REFERENCES	187
APPENDICES	
2.1 Sample locations	196
2.2 Sample descriptions	204
3.1 Geochronological methods	235
3.2 Sample locations	237
3.3 Sample descriptions	238
4.1 Structural methods - TRIPOD	240
5.1 Sample locations	241
5.2 Sample descriptions	246
5.3 Geothermobarometry data	263
ENCLOSURES	
2.1 1:50 000 scale sample location maps	
4.1 TRIPOD structural data (3.5 inch computer disk)	

LIST OF TABLES

TABLE		page
3.1	U-Pb analytical data	39
5.1	Characteristic mineral assemblages for M ₂ mineral zones	159
5.2	Geothermobarometric sample mineral assemblages	163
5.3	Geothermobarometric data	164
5.4	Geothermobarometric temperature and pressure estimates	166

LIST OF FIGURES

Figure 1.1	Major tectonostratigraphic terranes of the Northern Cordillera. The Aishihik Lake map-area is indicated.	2
Figure 1.2	General geology of part of the Aishihik Lake map area. The boxes indicate study areas referred to in the text.	5
Figure 2.1	Detailed maps showing the distribution of map units.	8
Figure 2.2	Cross-sections, the locations of which are indicated on the maps in Figure 2.1.	13
Figure 3.1	A map of the bedrock geology in the vicinity of Aishihik Lake with U-Pb geochronology sample locations indicated.	38
Figure 3.2	U - Pb concordia plot for zircon from two mica orthogneiss of the Nisling Assemblage.	41
Figure 3.3	U - Pb concordia plot for zircon and titanite fractions from the Aishihik Batholith.	42
Figure 3.4	U - Pb Concordia plots for zircon from the Long Lake Suite.	43
Figure 3.5	U - Pb Concordia plot for zircon from the Ruby Range Batholith.	44
Figure 4.1	General geology of part of the Aishihik Lake map-area.	53
Figure 4.2	Detailed maps showing orientation data.	55
Figure 4.3	Cross-sections, the locations of which are indicated on the maps in Figure 4.2.	60
Figure 4.4	Equal area plots for planar and linear orientation data.	65

Figure 4.5	A line drawing made from a thin section.	98
Figure 4.6	A regional cross-section, the location of which is indicated in Figure 4.1.	111
Figure 5.1	Detailed maps showing metamorphic mineral paragenesis and mineral isograds.	125
Figure 5.2	Cross-sections, the locations of which are indicated on the maps in Figure 5.1.	130
Figure 5.3	The relative timing of metamorphic mineral nucleation and growth.	154
Figure 5.4	A map showing the distribution of isograd bound metamorphic mineral zones.	156
Figure 5.5	A calibrated petrogenetic Pressure - Temperature grid.	161
Figure 5.6	Geothermometry results.	168
Figure 5.7	Pressure - temperature - time displacement diagrams.	172
Figure 6.1	Tectonic model for the early- to middle-Mesozoic of the northern Cordillera.	182

LIST OF PLATES

Plate 2.1	Micaschist of the Nisling Assemblage.	16
Plate 2.2	Grey quartz gneiss from the South Aishihik Lake area.	17
Plate 2.3	Brown quartzite from the South Aishihik Lake area.	18
Plate 2.4	Hornblende amphibolite from the North Aishihik Lake area.	21
Plate 2.5	Marble from the South Aishihik Lake area.	23
Plate 2.6	Banded graphitic quartzite from the Upper Nisling River area.	24
Plate 2.7	Foliated hornblende granodiorite of Aishihik Batholith.	27
Plate 2.8	A photomicrograph of biotite hornblende granodiorite of Aishihik Batholith.	28
Plate 2.9	A photomicrograph of biotite hornblende granodiorite of Aishihik Batholith.	29
Plate 2.10	A photomicrograph of quartz monzonite of the Long Lake Suite.	31
Plate 2.11	A photomicrograph of biotite granite of Ruby Range Batholith.	33
Plate 2.12	Granodiorite of Aishihik Batholith overlying schist of Nisling	

Assemblage.	35
Plate 4.1 A mafic enclave in Aishihik Batholith.	63
Plate 4.2 A quartzite inclusion in Aishihik Batholith.	64
Plate 4.3 A band of annealed mylonite in Aishihik Batholith.	68
Plate 4.4 Gneissic banding in Aishihik Batholith.	69
Plate 4.5 Granodiorite orthogneiss of Aishihik Batholith.	70
Plate 4.6 Migmatite in Aishihik Batholith.	71
Plate 4.7 Sheared granodiorite of Aishihik Batholith.	73
Plate 4.8 Folded aplite vein in Aishihik Batholith.	74
Plate 4.9 Ptygmatic folds of aplite in Aishihik Batholith.	75
Plate 4.10 Kink folding of quartz diorite of Aishihik Batholith.	76
Plate 4.11 A photomicrograph of hornblende granodiorite of Aishihik Batholith.	79
Plate 4.12 A photomicrograph of annealed mylonite from Aishihik Batholith.	80
Plate 4.13 A photomicrograph of sheared quartz diorite of Aishihik Batholith.	81
Plate 4.14 A photomicrograph of annealed mylonite from Aishihik Batholith.	82
Plate 4.15 Deformed quartzite of Nisling Assemblage.	85
Plate 4.16 Sheared rocks of Nisling Assemblage.	86
Plate 4.17 Gneissic banding in Nisling Assemblage.	89
Plate 4.18 Sheared rocks of Nisling Assemblage.	90
Plate 4.19 Deformed quartzite of Nisling Assemblage.	93
Plate 4.20 An F_3 antiform affecting quartzite and marble of Nisling Assemblage.	94
Plate 4.21 Grey quartz gneiss of Nisling Assemblage.	96
Plate 4.22 A photomicrograph of sillimanite schist of Nisling Assemblage.	99
Plate 4.23 A photomicrograph of micaschist of Nisling Assemblage.	101
Plate 4.24 A photomicrograph of garnet micaschist of Nisling Assemblage.	102
Plate 4.25 A photomicrograph of staurolite micaschist of Nisling Assemblage.	103
Plate 4.26 A photomicrograph of sillimanite micaschist of Nisling Assemblage.	104
Plate 4.27 A photomicrograph of micaschist of Nisling Assemblage.	105
Plate 4.28 A photomicrograph of crenulated micaschist of Nisling Assemblage.	107
Plate 4.29 A photomicrograph of annealed mylonitic quartzite of Nisling	

Assemblage.	108
Plate 4.30 Quartzite next to a steep brittle fault.	117
Plate 4.31 A photomicrograph of mylonitized marble.	118
Plate 4.32 A steep fault that offsets the Aishihik Batholith-Nisling Assemblage contact.	119
Plate 5.1 A photomicrograph of a garnet porphyroblast.	132
Plate 5.2 A migmatite lense in Nisling Assemblage.	134
Plate 5.3 A photomicrograph of a spongy garnet.	136
Plate 5.4 A photomicrograph of a garnet porphyroblast.	137
Plate 5.5 A photomicrograph of sillimanite staurolite kyanite schist of Nisling Assemblage.	139
Plate 5.6 A photomicrograph of micaceous orthogneiss of Nisling Assemblage.	140
Plate 5.7 A photomicrograph of garnet kyanite micaschist of Nisling Assemblage.	141
Plate 5.8 A photomicrograph of andalusite schist of Nisling Assemblage.	144
Plate 5.9 A photomicrograph of andalusite staurolite schist of Nisling Assemblage	145
Plate 5.10 A photomicrograph of andalusite micaschist of Nisling Assemblage	147
Plate 5.11 A photomicrograph of cordierite micaschist of Nisling Assemblage.	148
Plate 5.12 A photomicrograph of cordierite micaschist of Nisling Assemblage.	150
Plate 5.13 A photomicrograph of micaschist of Nisling Assemblage.	151
Plate 5.20 A photomicrograph of sericitized andalusite staurolite micaschist of Nisling Assemblage.	152

LIST OF ABBREVIATIONS

(used in appendices)

Minerals

chl	- chlorite	di	- diopside
bi ₍₂₎	- biotite - phlogopite, Metamorphic Event Indicated (MEI)	ep	- epidote
mu ₍₂₎	- muscovite, MEI	al	- allanite
gt	- garnet	tr	- tremolite - actinolite
pyp	- pyrope garnet	ta	- talc
alm	- almandine garnet	sc	- sericite - pyrophyllite
sps	- spessartine garnet	id	- idocrase
gro	- grossular garnet	rt	- rutile
si ₍₂₎	- sillimanite, MEI	op	- unidentified opaque minerals
ad ₍₂₎	- andalusite, MEI	mt	- magnetite
ky	- kyanite		
st	- staurolite		
cd ₍₂₎	- cordierite, MEI		
hbl	- hornblende		
ag	- augite		
pyx	- pyroxene		
ol	- olivine		
qt	- quartz		
fs	- feldspar		
pl ₍₃₀₎	- plagioclase anorthite content indicated		
ks	- potassium feldspar		
ab	- albite		
an	- anorthite		
or	- orthoclase		
zr	- zircon		
ap	- apatite		
tt	- titanite		
to	- tourmaline		
cc	- calcite		

I. INTRODUCTION

1.1 Statement of the problem

The Mesozoic tectonic evolution of the Northern Cordillera (Figure 1.1) is dominated by the development of the Lewes River arc, a part of the Stikine terrane, and its interaction with neighbouring terranes, including North America (Tempelman-Kluit, 1979). Tempelman-Kluit (1979) defined the arc as consisting of Late Triassic andesitic volcanic and sedimentary rocks of the Lewes River Group; and foliated hornblende granodiorite of the Klotassin Suite, interpreted as the plutonic root of the volcanic arc.

The Lewes River arc was thought to have developed on a continental fragment, represented by metamorphosed continental clastic and carbonate rocks with minor amphibolite of the Nisling Assemblage (Figure 1.1). The basis for this idea is the interpretation that, within the Aishihik Lake map-area in southwest Yukon, rocks of the Nisling Assemblage are in intrusive contact to the east with foliated hornblende granodiorite of the Aishihik Batholith, inferred to be part of the Klotassin Suite (Tempelman-Kluit, 1974).

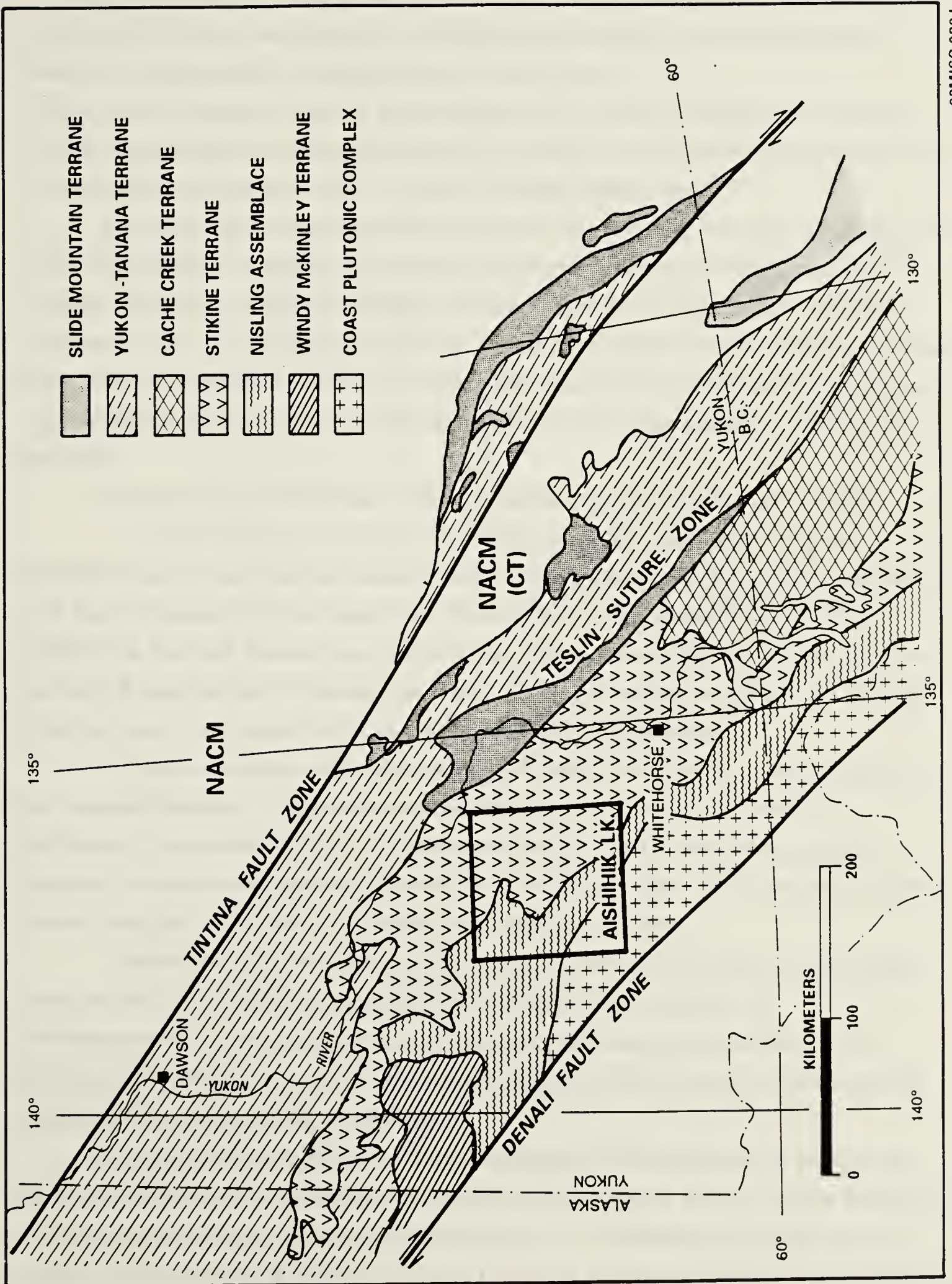
More recent studies have shown that the definition of the arc is problematic. U - Pb zircon geochronological studies of Klotassin Suite intrusions indicate that the intrusions range in age from 209 Ma to 185 Ma (Woodsworth *et al.*, 1991; Tempelman-Kluit, 1974; Tempelman-Kluit and Wanless, 1980; Mortensen and Jilson, 1985; Gabrielse and Reesor, 1974; Mortensen, 1992; Currie, 1991). The Early Jurassic Klotassin Suite is, therefore, too young to represent the plutonic root of the Late Triassic Lewes River volcanic arc.

The interpretation that the Aishihik Batholith intrudes the Nisling Assemblage is also suspect. The contact between the Aishihik Batholith and rocks of the Nisling Assemblage is concordant and sheared. No satellite intrusions, dykes, or sills, related to the batholith have been observed intruding rocks of the Nisling Assemblage. Early metamorphism of rocks of the Nisling Assemblage is thought to be Paleozoic in age (Tempelman-Kluit, 1974). In northern British Columbia foliated hornblende granodiorite of the Hale Mountain plutonic suite, thought to be correlative with the Aishihik Batholith, is faulted against rocks of the Nisling Assemblage (Currie, 1992; 1991). These observations suggest that the contact between the Aishihik Batholith and the Nisling Assemblage may be faulted rather than intrusive.

The goals of this thesis are to determine:

- Is the Aishihik Batholith part of the Early Jurassic Klotassin Plutonic Suite?
- Alternatively, the batholith may be Early Triassic and represent part of the plutonic root of

Figure 1.1 Major tectonostratigraphic terranes of the Northern Cordillera, modified after Wheeler and McFeely (1991). NACM - North American continental margin, includes CT - Cassier terrane, a portion of the continental margin which has been transported at least 450 km to the north along the Tintina strike-slip fault. Suspect terranes are stippled. Rocks of the Stikine terrane underlie and define the Whitehorse Trough. The Aishihik Lake map-area is indicated.



the Lewes River volcanic arc;

- Does the Aishihik Batholith intrude rocks of the Nisling Assemblage? The contact between the Nisling Assemblage and Klotassin Suite intrusions may be faulted, and therefore be a potentially important terrane boundary; and
- What is the timing and nature of metamorphism of the Nisling Assemblage? Was the Nisling Assemblage metamorphosed during the intrusion of the Aishihik Batholith, or was it metamorphosed and deformed as a result of terrane interactions?

To answer these questions a two-part study was initiated. Part one involved 1:50 000 - scale geologic mapping and sample collection in three areas which straddle the Aishihik Batholith - Nisling Assemblage contact. These are: 1) the Southern Aishihik Lake area; 2) the North Aishihik Lake area; and 3) the Upper Nisling River area. All three study areas are contained within the Aishihik Lake map area in southwest Yukon (Figure 1.2). Mapping and sample collection was completed during the summers of 1985, 1986 and 1987.

The second part of the study involved laboratory-based studies and included:

- U - Pb zircon and titanite geochronology of plutonic rocks that crop out within the study area, including foliated hornblende granodiorite of the Aishihik Batholith; pink quartz monzonite of the Long Lake Plutonic Suite (Woodsworth *et al.*, 1991) intrudes the Aishihik Batholith and rocks of the Nisling Assemblage; diorite to granite of the Ruby Range Batholith (Tempelman-Kluit, 1974), part of the northern Coast Plutonic Complex; and orthogneiss that forms part of the Nisling Assemblage.

- Macro- and micro-structural analysis of rocks of the Nisling Assemblage and of the Aishihik Batholith. Quantitative assessment of macrostructural elements was facilitated by the use of TRIPOD (Charlesworth *et al.*, 1989), a computer program designed to assist in the processing of structural orientation data. Thin-sections cut from oriented samples were used to document microstructural fabrics.

- Determination of the metamorphic history of rocks of the Nisling Assemblage, based on the study of hand-samples and thin-sections. Documentation of the metamorphic mineral paragenesis, and microprobe-based geothermometric and geobarometric studies, are used to constrain the pressure and temperature conditions of metamorphism of the Nisling Assemblage.

These studies show that: a) Nisling Assemblage is characterized by orthogneiss, the precursor of which was emplaced in the Early Mississippian; b) the Aishihik Batholith is correlative with other Klotassin Suite intrusions; c) a component of inherited zircon present in both Aishihik Batholith and Long Lake pink quartz monzonite suggests that the crust in the source area is characterized by an Early Proterozoic average age; d) Aishihik

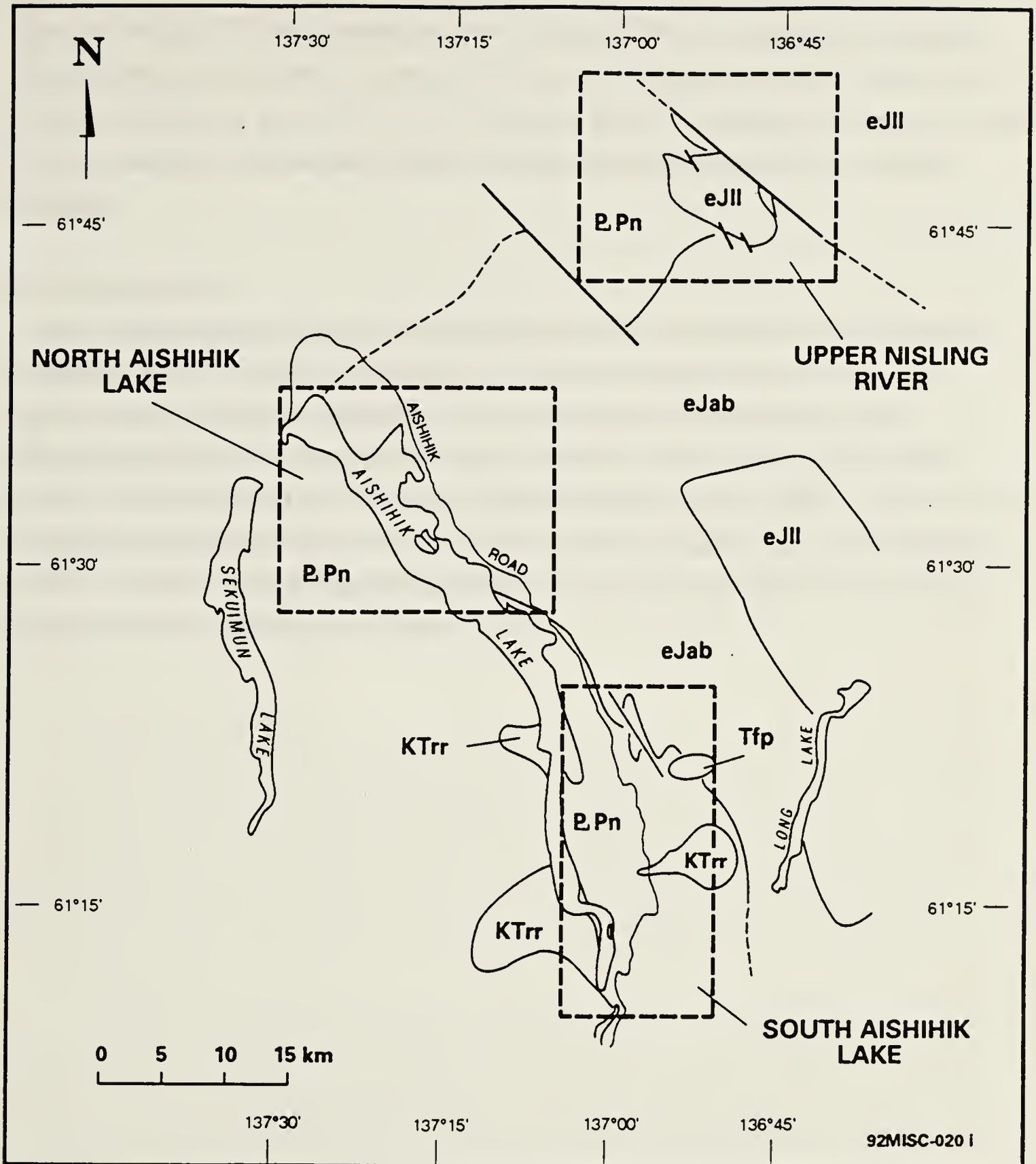


Figure 1.2 General geology of part of the Aishihik Lake map-area in southwest Yukon, modified after Tempelman-Kluit (1974). PPn - the Nisling Assemblage; eJab - the Aishihik Batholith; eJll - Long Lake Suite intrusions; KTrr - the Ruby Range Batholith and satellite intrusions; Tfp - Tertiary feldspar porphyry. The boxes indicate study areas referred to in the text.

Batholith intruded Nisling Assemblage; and e) that the Nisling Assemblage was rapidly uplifted from crustal depths in excess of 25 km to the near surface after the intrusion of Aishihik Batholith at about $187.0 \pm 9.7/-0.9$ Ma but before the intrusion of Long Lake pink quartz monzonite, which intruded within 10 Ma of the emplacement of the Aishihik Batholith.

1.2 Previous work

The Aishihik Lake map area is located between the latitudes of 61° and 62° N and longitudes of 136° and 138° W (Figure 1.2). Previous work in the area includes a reconnaissance report by Cockfield (1927) on the southern part of the map area. Tempelman-Kluit (1974) mapped the area at 1:250 000 - scale, and reported on the geology of the Aishihik Lake, Snag Lake and Stewart map sheets. A B.Sc. thesis on rocks cropping out along part of the west side of the lake was completed at that time (Gordey, 1973). 1:50 000 - scale geological mapping to document copper skarns in the vicinity of Hopkins Lake was conducted by Morin (1981).

II. ROCK TYPES AND STRATIGRAPHIC CORRELATIONS

2.1 Introduction

In the Aishihik Lake map-area of southwest Yukon (Figure 1.1), the Nisling Assemblage (Wheeler and McFeely, 1991), a suite of metamorphosed clastic, carbonate, volcanic, and plutonic rocks, is in contact to the east with foliated granodiorite of the Aishihik Batholith (Tempelman-Kluit, 1974). Plutons of pink quartz monzonite of the Long Lake Suite (Woodsworth *et al.*, 1991) intrude both the Nisling Assemblage and the Aishihik Batholith. In the southwest part of the Aishihik Lake map-area, the Nisling Assemblage is intruded by hornblende quartz diorite to biotite granite of the Ruby Range Batholith (Tempelman-Kluit, 1974). These relationships are shown in 3 maps of the study area (Figure 2.1; a, b, and c), the locations of which are indicated in Figure 1.2, and a series of cross-sections (Figure 2.2). Sample locations are indicated on maps contained in Enclosure 2.1. Sample location coordinates and sample descriptions are given in Appendices 2.1 and 2.2, respectively.

2.2 The Nisling Assemblage

Rocks of the Nisling assemblage underlie the area west and north of the Aishihik Batholith and northeast of the Ruby Range Batholith (Figures 2.1 a, b, and c). The terrain is typically recessive. Rocks crop out along ridge tops and adjacent to north-trending, feldspar-porphyry dykes. Good exposures are present adjacent to the Ruby Range Batholith; along the east shore of Aishihik Lake; and along ridge crests in the Upper Nisling River area.

Rocks of the Nisling Assemblage dip homoclinally to the east throughout both the South and North Aishihik Lake areas and to the north in the Upper Nisling River area (Figure 2.1 a, b, and c) and plunge gently to the north throughout the study area. The result is that the deepest structural levels of the Nisling Assemblage crop out in the southwest part of the South Aishihik Lake Area (Figure 2.1 a) with progressively shallower structural levels exposed towards the north. Regional amphibolite facies metamorphism is suggested by the presence of staurolite, kyanite, and sillimanite and by the widespread development of migmatite. Deformation and metamorphism has obliterated all primary stratigraphic relationships.

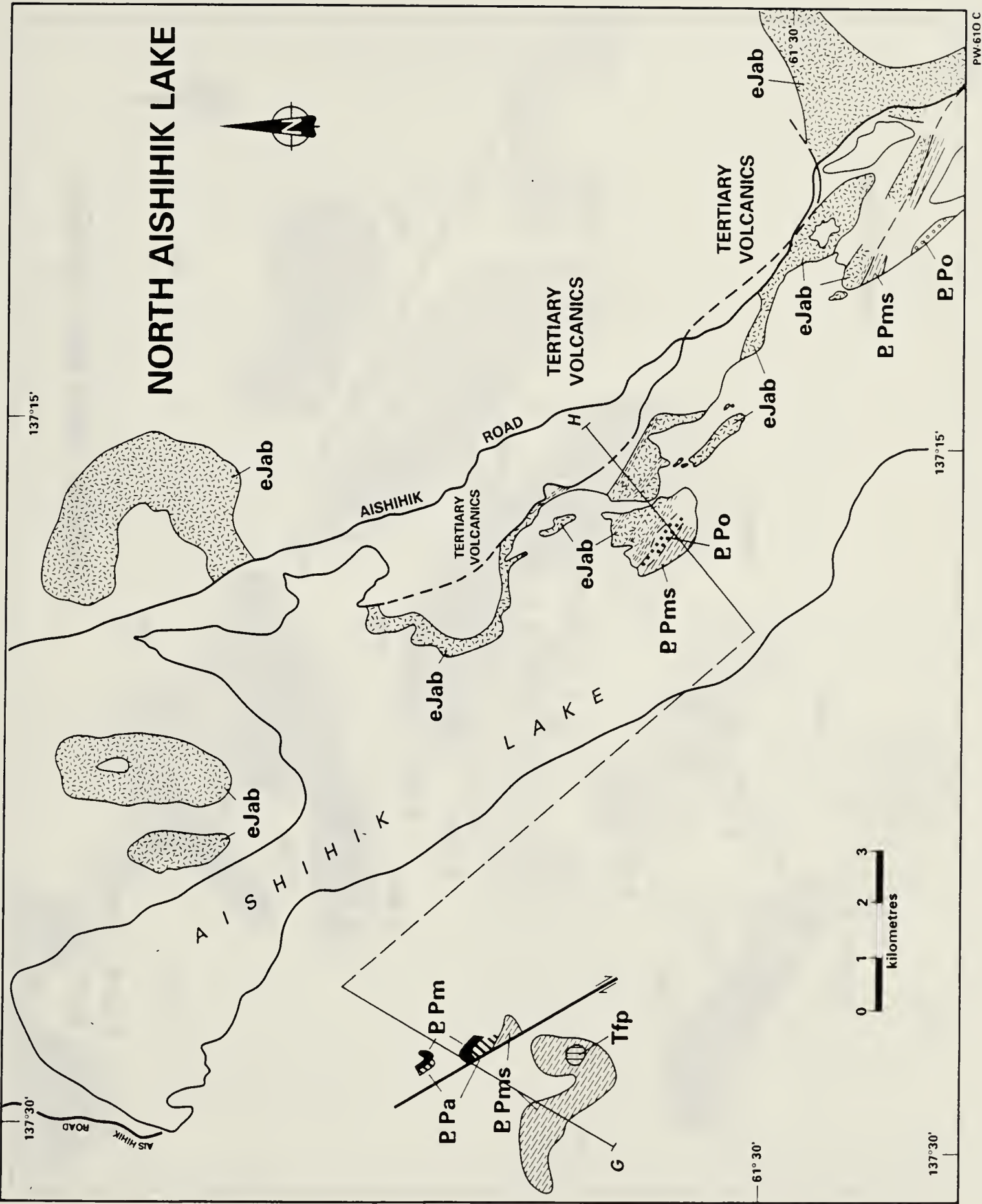
Five units were mapped, including: 1) a heterogeneous micaschist unit (PPms); 2) an amphibolite unit (PPa); a marble unit (PPm); and a brown quartzite unit (PPbq). The distribution of these units is shown in Figures 2.1 and 2.2.

Mica-schist (PPms): The mica-schist unit is a thick and heterogeneous package

Figure 2.1 Detailed maps showing the distribution of map units for each of: a) the South Aishihik Lake area; b) the North Aishihik Lake area; and c) the Upper Nisling River area. The location of these maps is shown in Figure 1.2.

The map displays the following geological units and features:

- Geological Units:**
 - EPms:** Early Proterozoic metasediments, shown with a stippled pattern.
 - EPa:** Early Proterozoic amphibolites, shown with a horizontal line pattern.
 - EPo:** Early Proterozoic orthogneiss, shown with a vertical line pattern.
 - EPm:** Early Proterozoic mafic rocks, shown with a cross-hatch pattern.
 - KTrr:** Keweenaw Terrane, shown with a pattern of small circles.
 - Tfp:** Tertiary foliated gneiss, shown with a diagonal line pattern.
 - eJab:** Early Jurassic andesite basalt, shown with a dotted pattern.
 - F:** Fault zones, indicated by dashed lines.
- Geographical Features:**
 - Aishihik Road:** A dashed line running through the center of the map.
 - Hopkins Lake:** A large lake in the central-eastern part of the map.
 - Giltana Lake:** A smaller lake in the southern part of the map.
 - Aishihik Lake:** The main body of water in the southern part of the map.
- Structural Features:**
 - Faults:** Indicated by dashed lines labeled F, D, and E.
 - Geological Boundaries:** Indicated by solid lines separating different geological units.
- Map Elements:**
 - North Arrow:** Located in the top left corner.
 - Scale Bar:** Located in the bottom right corner, showing distances in kilometers (0, 1, 2, 3).
 - Coordinates:** The map is bounded by 137°00' and 61°15' on the left and right sides, and 61°15' and 137°00' on the top and bottom sides.



UPPER NISLING RIVER



136°45'

137°00'



136°45'

137°00'

TERTIARY
VOLCANICS

61°45'

PW-610 B

LEGEND

PLUTONIC ROCKS

METAMORPHIC ROCKS

TERTIARY



FELDSPAR PORPHYRY

heterogeneous igneous suite which includes plugs and small plutons (open symbols) of orange and pink weathering, flesh colored, miarolitic, massive, felspar and quartz - feldspar porphyry; and dykes (lined pattern which reflects the trend of the dykes) of brown and dark green weathering, green to buff colored, feldspar and hornblende feldspar porphyry.

CRETACEOUS & TERTIARY



RUBY RANGE BATHOLITH

grey to tan weathering, grey to dark grey, medium to coarsely crystalline, massive to mildly foliated, hornblende and biotite hornblende diorite and granodiorite to nebulitic hornblende biotite granite.

EARLY JURASSIC



LONG LAKE PLUTONIC SUITE

orange weathering, orange and pink colored, coarsely crystalline to porphyritic, massive, miarolitic, quartz and biotite quartz monzonite.

STIKINE TERRANE



AISHIHIK BATHOLITH

grey to light grey weathering, grey to dark grey colored, coarsely crystalline, equigranular to K-feldspar megacrystic, hornblende and biotite hornblende granodiorite to quartz diorite. A foliation, defined by the alignment of mineral grains, is commonly developed (random stipple). A second foliation, defined by protomylonitic, and gneissic banding, is locally developed and overprints the mineral foliation (aligned stipple).

NISLING ASSEMBLAGE

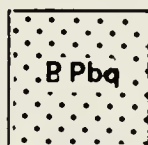
DEVONO-MISSISSIPPIAN



ORTHO GNEISS

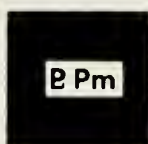
tan weathering, light grey colored, medium to coarsely crystalline, feldspar augan, muscovite and biotite muscovite orthogneiss (open squares); and dark grey weathering, dark grey colored, medium grained, hornblende and biotite hornblende diorite and quartz diorite orthogneiss (filled squares).

PALEOZOIC & OLDER



BROWN QTZITE

dark to light brown weathering, brown to buff colored, medium to fine grained, locally graphitic, micaceous and feldspathic quartzite. Includes thin and discontinuous marble, amphibolite and micaschist lenses.



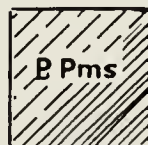
MARBLE

light grey to light brown weathering, white to grey colored, fetid, coarsely crystalline, laminated calcite marble. Includes minor skarn, amphibolite, and calc-silicate



AMPHIBOLITE

dark green to black weathering, green colored, fine to coarsely crystalline, gneissic to well foliated, hornblende and biotite hornblende quartzite, micaschist and marble, and significant amounts of pistachio green, epidote hornblende diopside calc-silicate



MICASCHIST

Brown weathering, dark to light grey colored, medium to coarsely crystalline, well foliated to gneissic, migmatitic, muscovite biotite schist with minor grey quartz gneiss (continuous stipple) and brown weathering, tan colored, medium grained, foliated, micaceous & feldspathic quartzite (discontinuous stipple). Includes minor amphibolite and marble.

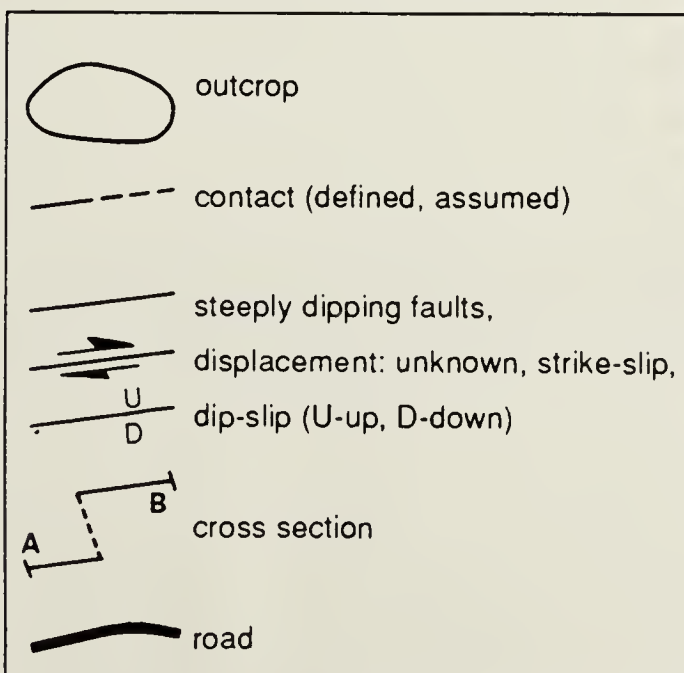
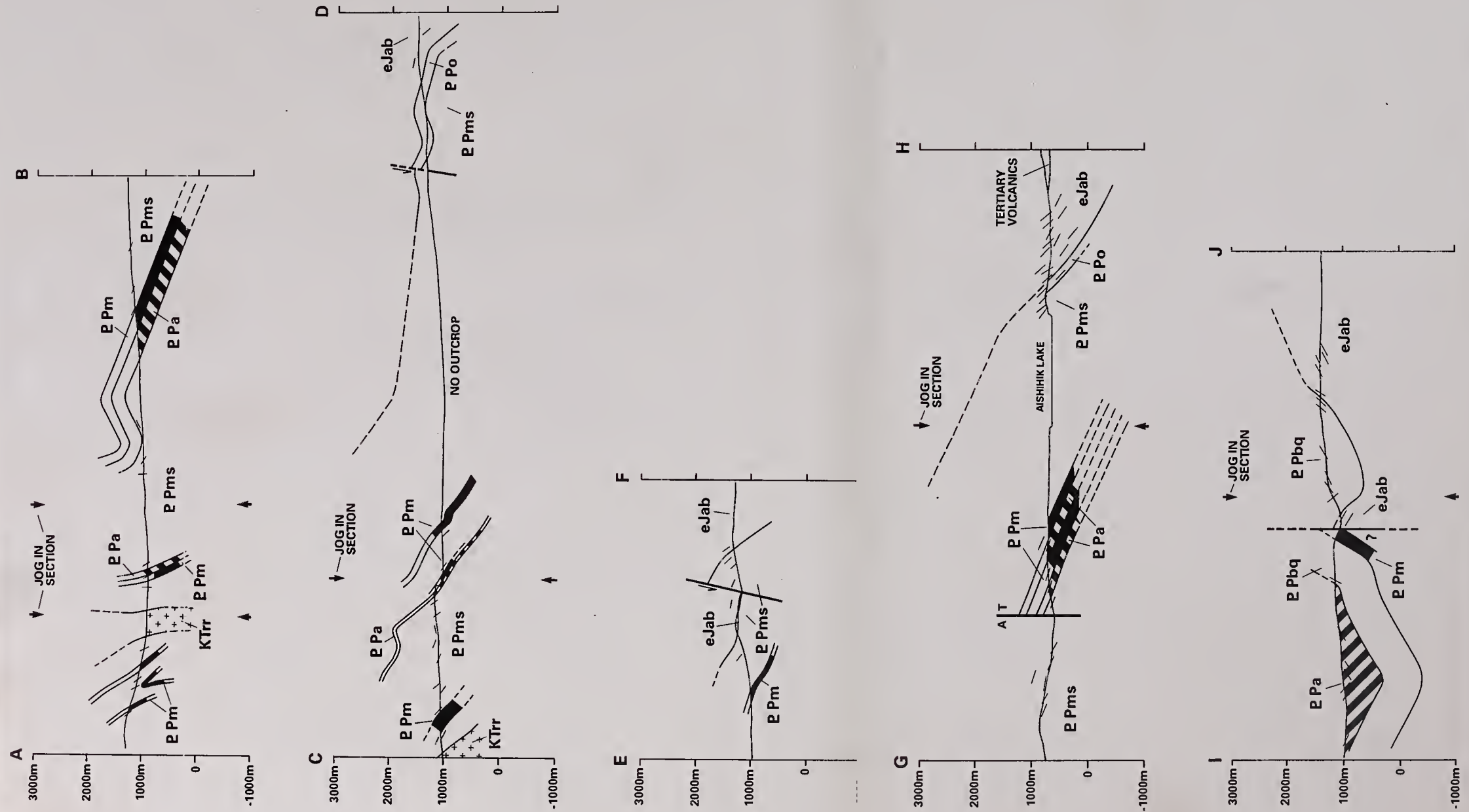


Figure 2.2 Cross-sections, the locations of which are indicated on the maps in Figure 2.1. Symbols are defined in the legend to Figure 2.1. Marble is colored black; amphibolite is indicated by a striped pattern. The apparent dip of foliation is indicated.



that consists largely of quartzofeldspathic mica-schist, but also includes brown quartzite and minor amounts of grey quartz paragneiss, marble, calc-silicate rock, and amphibolite. The unit occupies the lowest structural levels of the Nisling Assemblage and crops out west of the Aishihik Batholith in both the South and North Aishihik Lake areas (Figures 2.1 a and b; and 2.2).

Quartzofeldspathic mica-schist weathers a pink-purple to dark grey colour. Fresh surfaces are usually characterized by a dark grey to medium grey-brown colour. Mica-schist occurs as continuous horizons tens of meters thick or as thin and discontinuous lenses several cm long surrounded by quartzite. Major mineral constituents includes biotite, muscovite, quartz, andesine plagioclase, and potassium feldspar. Metamorphic porphyroblasts include garnet, andalusite, cordierite, staurolite, kyanite, and sillimanite (fibrolite). Accessory minerals include apatite, tourmaline, rutile, sphene, zircon, pyrite, magnetite, graphite, and ilmenite. Migmatite is common, and is characterized by the development of lenses quartz - feldspar leucosome 2 to 100 cm long. Common alteration products include chlorite, sericite, and cryptocrystalline talc (?). The parallel alignment of coarsely crystalline biotite and muscovite define a wavy and irregular schistosity (Plate 2.1).

Continuous horizons of grey quartzofeldspathic gneiss that weathers light to dark grey are intimately interfoliated with mica-schist (Plate 2.2). Fresh surfaces vary in colour from light to medium grey. Gneissic bands, defined by colour and compositional, and grain size variations, vary from 2 to 5 cm in width. Grain-size varies from medium to coarsely crystalline. Gneiss consists of 80% to 100% quartz with lesser amounts of plagioclase, potassium feldspar, mica, and garnet. Accessory minerals include apatite, zircon, rutile, pyrite, ilmenite and graphite.

The mica-schist unit also includes poorly exposed brown quartzite. In the South Aishihik Lake area (Figure 2.1 a), the brown quartzite overlies and is separated from underlying feldspathic mica-schist by about 500 m of amphibolite and marble.

Quartzite typically weathers a tan brown colour and is characterized by colour banding defined by colour variations. Fresh surfaces are flesh coloured (Plate 2.3). Grain-size varies from finely crystalline in clean quartzite, to coarsely crystalline in dirtier, more feldspathic and micaceous quartzite. Quartz is the major mineral constituent, with minor to trace amounts of feldspar, mica, garnet, kyanite, sillimanite, and staurolite.

Brown quartzite included in the mica-schist unit is similar to and may be at least in part equivalent to the brown quartzite unit described below (PPbq). However, more detailed mapping is required to determine if brown quartzite included in the mica-schist unit can be broken out as a separate unit and is correlative with the PPbq brown quartzite

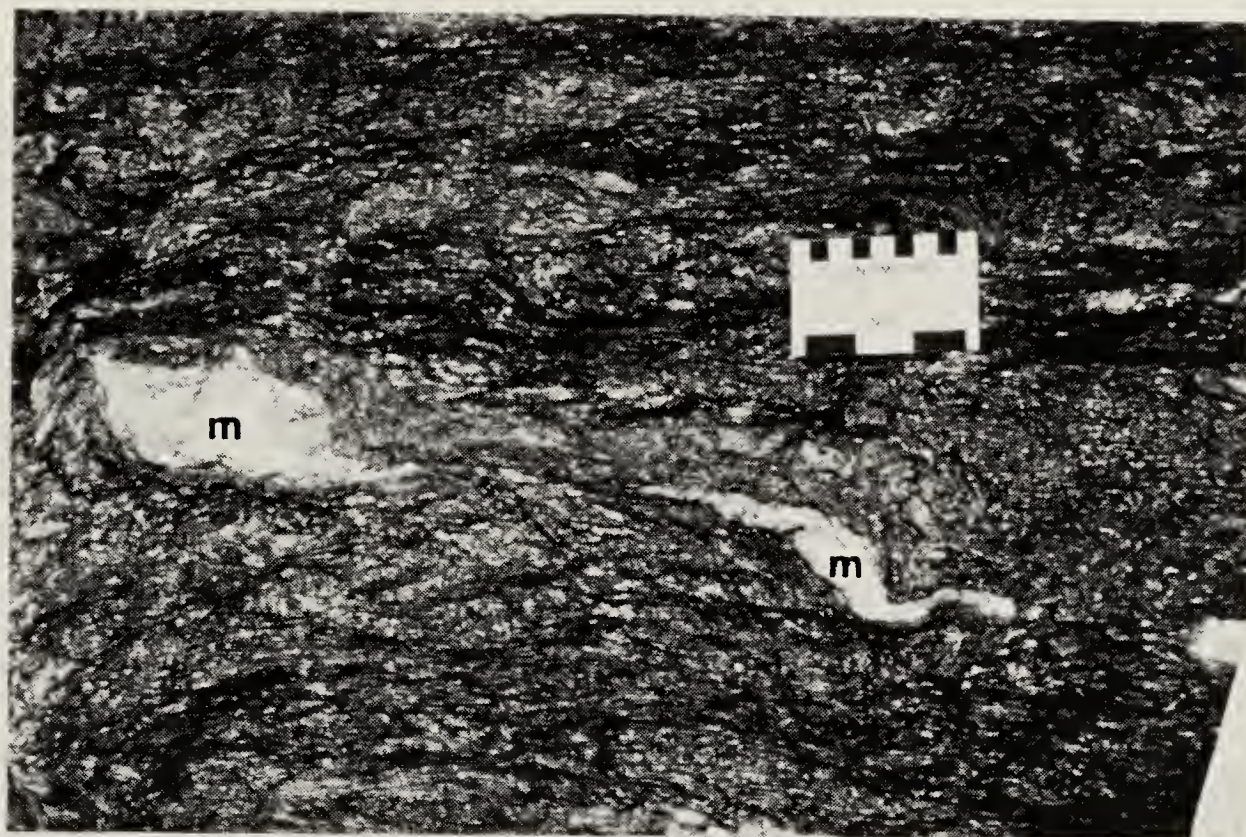


Plate 2.1 Typical, crenulated, migmatitic micaschist of the Nisling Assemblage, observed in the South Aishihik Lake area. Irregular migmatite pods (m) pinch and swell and extend along the plane of schistosity.



Plate 2.2 Folded grey quartz gneiss from the South Aishihik Lake area. Thin recessive bands are more micaceous than the adjacent, more resistant, quartzose bands. The knife is 4 cm long.



Plate 2.3 Brown quartzite from the South Aishihik Lake area. The arrows indicate the axial surface trace of a fold affecting bands defined by variations in color. The lense cap is 6.5 cm wide.

unit.

Discontinuous lenses, 2 cm to 50 cm in width and up to several meters in length, of marble, amphibolite, and calc-silicate rock are present throughout the mica-schist unit. Amphibolite and calc-silicate rock are similar in every way to the amphibolite described below for the amphibolite unit (PPa). Similarly, marble is identical to that described below for the marble unit (PPm).

The mica-schist unit occupies the lowest structural position in the Nisling Assemblage. Metamorphism and deformation have, however, resulted in the obliteration of primary stratigraphic relationships. The current complicated layering is the result of tectonism and its relationship to the original stratigraphic succession remains unknown. The unit is in contact with hornblende granodiorite of the overlying Aishihik Batholith. The base of the Nisling Assemblage was not observed. The mica-schist unit is at least 5 km thick measured perpendicular to foliation (Figure 2.2).

Amphibolite (PPa): The amphibolite unit includes a broad range of hornblende rich rocks including hornblende-amphibolite, quartz hornblende schist, and calc-silicate gneiss. Amphibolite is recessive and is characteristically fractured and jointed. Outcrops commonly consist of blocks of amphibolite debris. Amphibolite was observed in all three map areas, although it is most extensively developed in the Upper Nisling River area (Figure 2.1 c).

Amphibolite exhibits a wide range of colour, but typically weathers black to dark green and appears dark green on freshly exposed surfaces. Micaceous horizons impart a brown green coloration. Deformation and recrystallization produced a schistose to gneissic foliation (Plate 2.4). Hornblende amphibolite consists of 50% to 100% hornblende, 0% to 35% labradorite plagioclase, and minor amounts (less than 10%) of tremolite, quartz, K-feldspar, biotite, garnet, and epidote. Biotite amphibolite schist, with 10 to 25% biotite, is locally interfoliated with hornblende amphibolite and varies from discontinuous lenses several cm wide to continuous horizons several metres thick. Along the contacts between amphibolite and mica-schist and/or quartzite amphibolite is commonly more quartz rich. Accessory minerals include sphene, zircon, apatite and allanite. Alteration products include chlorite, biotite, epidote, calcite, sericite and pyrophyllite. Chloritization of hornblende is common, as is sericitization of feldspar.

Pistachio green, fine to coarsely crystalline, calc-silicate gneiss is commonly found transitional between hornblende amphibolite and marble. Calc-silicate gneiss consists of variable amounts of hornblende, diopside, calcite, epidote, and quartz. Tremolite is common and replaces diopside. Accessory minerals include sphene, magnetite, garnet and mica.



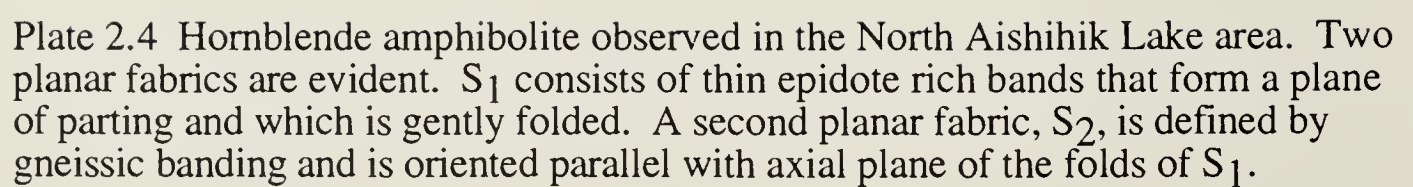


Plate 2.4 Hornblende amphibolite observed in the North Aishihik Lake area. Two planar fabrics are evident. S_1 consists of thin epidote rich bands that form a plane of parting and which is gently folded. A second planar fabric, S_2 , is defined by gneissic banding and is oriented parallel with axial plane of the folds of S_1 .



Amphibolite occurs as thin (< 50 m thick) and discontinuous horizons in mica-schist and as thicker (200 m thick) more continuous horizons associated with marble units. In the Upper Nisling River area a sequence of amphibolite over 750 m thick overlies the brown quartzite unit (PPbq) and occupies the highest structural levels exposed in the study area (Figures 2.1 c and 2.2).

Marble (PPm): Marble occurs as discontinuous lenses or continuous horizons throughout all three map-areas (Figure 2.1). Weathered surfaces are characterized by a bleached white colour. Fresh surfaces are white to grey coloured and emit a strong fetid odour. Well developed flow banding, defined by graphitic horizons, thin continuous chert bands, and by horizons of tremolite rosettes, is typically present (Plate 2.5).

Marble is coarsely crystalline and consists of 80% to 100% calcite, with minor amounts of quartz, diopside, garnet, epidote, and phlogopite. Fine graphite-rich horizons are common. Tremolite is common and occurs along cross-cutting veins and as rosettes that overgrow and replace diopside. Thin and discontinuous, finely crystalline chert laminae are common. Chert laminations weather to a brown colour and are dark grey to black on fresh surfaces.

Marble is commonly brecciated and converted to skarn where intruded by quartz feldspar porphyry dykes. Skarn consists of diopside, garnet, epidote, calcite and magnetite. Copper mineralization is common and consists of disseminated, fine grained pyrite and chalcopyrite. Azurite and malachite characterize the weathered surfaces of skarns.

Individual marble horizons in mica-schist and quartzite are typically 30 to 50 m thick and are continuous for hundreds of meters. Marble also occurs as discontinuous pods in the hinge zones of macroscopic folds. The pods can be 10 to 50 m thick and up to 100 m long. Thicker (> 200 m thick) and more continuous marble is closely associated with thick (> 300 m) sections of amphibolite and appears to define a boundary between underlying feldspathic mica-schist and overlying brown quartzite of the mica-schist unit (Figures 2.1 a, and 2.2).

Brown quartzite (PPbq): Homogenous brown quartzite underlies much of the Upper Nisling River area (Figure 2.1 c). The quartzite weathers a tan brown to dark grey colour. Fresh surfaces are flesh coloured. The quartzite is characteristically tightly folded, and exhibits well developed banding defined by colour variations and by dark grey, graphitic laminations (Plate 2.6). Grain size varies from finely crystalline in clean quartzite, to coarsely crystalline in dirtier, more feldspathic and micaceous quartzite.

Quartz is the major mineral constituent, with minor to trace amounts of feldspar and mica. Accessory minerals include garnet, sillimanite, apatite, zircon, rutile, pyrite, and



Plate 2.5 Laminated calcite marble observed in the southern part of the South Aishihik Lake area. Discontinuous dark laminations consist of brown weathering chert that separate light grey, coarsely crystalline calcite marble. The hinge of a fold affecting compositional banding is indicated by the arrow. A hammer, located just to the right of the arrow, is shown for scale.

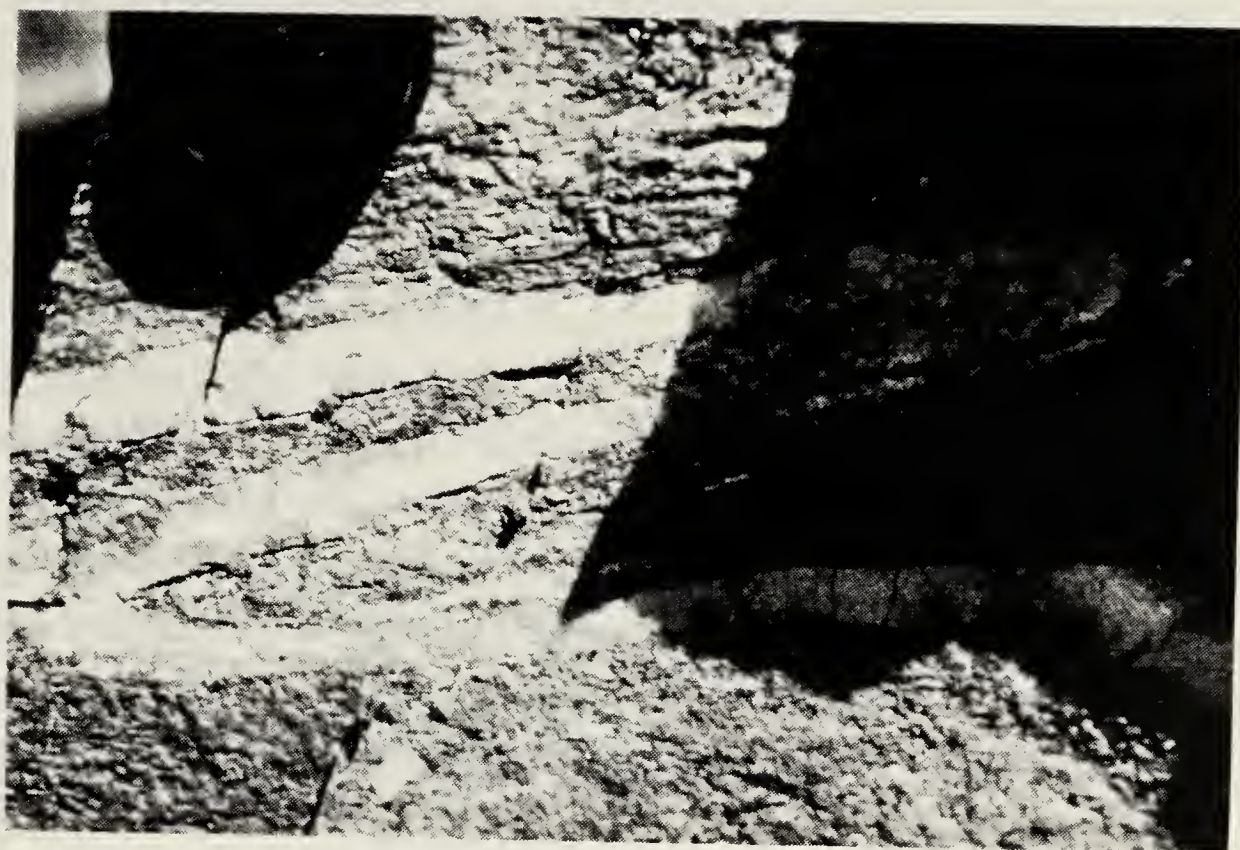


Plate 2.6 Banded graphitic quartzite from the Upper Nisling River area. A thin, light colored non-graphitic, band of clean quartzite is apparent and defines a tight, asymmetric fold. The lense cap at upper left is 6.5 cm wide.

graphite. Discontinuous lenses of marble, calc-silicate, and amphibolite are present.

The brown quartzite unit occurs at shallow structural levels in the Nisling Assemblage, overlies hornblende granodiorite of the Aishihik Batholith, and is in turn overlain to the north by a thick section of amphibolite. Over 1 km of quartzite is present (Figure 2.2). The unit is similar to and may be, at least in part, equivalent to brown quartzite which crops out west of and dips east beneath the batholith and which is included in the mica-schist unit (PPms).

Orthogneiss (PPO): Orthogneiss is interfoliated with brown quartzite of the mica-schist unit (PPms) in both the South and North Aishihik Lake areas (Figure 2.1 a and b). Two distinct types of orthogneiss, including biotite - muscovite (two mica) granitic orthogneiss and hornblende to hornblende quartz diorite orthogneiss are recognized.

Two mica granitic orthogneiss weathers light brown to brown grey. Fresh surfaces are white to light grey. Orthogneiss is characteristically coarsely crystalline and ranges in composition from granite to quartz-monzonite. Major mineral constituents include quartz, potassium feldspar, and albitic plagioclase. Significant amounts of muscovite are commonly present, and minor to trace amounts of biotite. Accessory minerals include zircon, apatite, tourmaline, and pyrite.

Gneissic banding is commonly well developed and pink potassium feldspar augen occur locally. A foliation, usually defined by weakly developed gneissic banding and by the parallel alignment of plagioclase and hornblende laths, is commonly developed. Muscovite locally occurs as large continuous sheets that parallel the gneissic banding and which define a schistosity.

Hornblende quartz diorite weathers light grey. Fresh surfaces are dark grey. Orthogneiss is fine- to medium-grained and ranges in composition from mafic hornblende diorite to hornblende - biotite granodiorite. Major mineral constituents are hornblende, andesine plagioclase, and quartz. Minor amounts of biotite and potassium feldspar are common. Accessory minerals include zircon, apatite, sphene, and magnetite.

2.3 Aishihik Batholith (eJab)

The Aishihik Batholith crops out east of the Nisling Assemblage and underlies the topographically subdued plateau east of the Aishihik Lake (Figures 1.2 and 2.1). Good outcrops are present along the margins of the batholith. In the unglaciated central-eastern parts of the Aishihik Lake map-area (Tempelman-Kluit, 1974) exposure is poor and is limited to isolated outcrops of highly weathered rock.

Granodiorite of the batholith weathers light grey. Locally, weathering has resulted in the development of pink and pistachio green colours. Fresh granodiorite is

characterized by an overall dark grey to grey colour. Little variation in grain size was observed; granodiorite is typically coarsely crystalline and equigranular. Locally a coarsely crystalline porphyritic texture, the result of the presence of potassium feldspar megacrysts, is apparent (Plate 2.7).

Little variation in the composition of the batholith is evident. Granodiorite and quartz-monzodiorite are the most common rock types; quartz-diorite and quartz-monzonite occur less commonly (Tempelman-Kluit, 1974). Major mineral phases include andesine plagioclase, potassium feldspar, and hornblende. Minor amounts of quartz and minor to trace amounts of biotite are characteristically present. Accessory minerals include apatite, sphene, zircon, epidote, allanite, and magnetite. Alteration products include sericite, pyrophyllite, epidote, hematite, and chlorite.

Andesine plagioclase occurs as mildly zoned, euhedral laths, and appears chalky white in hand specimen. Potassium feldspar occurs both as anhedral grains interstitial to plagioclase and locally as large poikilitic megacrysts containing hornblende grains. Feldspar megacrysts are commonly associated with the presence of microveins that consist of potassium feldspar, indicating a late, possibly post-magmatic origin. Myrmekitic intergrowths of feldspar and quartz frequently mantle the megacrysts. Potassium feldspar usually appears grey in hand specimen but weathers to a light pink. Sericitization of feldspar grains is common throughout the batholith and imparts a chalky white to slightly pink colour on the rock. Quartz occurs interstitially to other grains. Mafic minerals commonly account for less than 15% of the rock. Hornblende is the dominant mafic mineral and occurs as euhedral black to dark green prisms. Significant quantities of biotite are only locally present. Epidote grains are typically cored by allanite; are intimately intergrown with biotite; appear to have grown at the expense of hornblende and plagioclase; and are interpreted as being primary magmatic grains (Plates 2.8 and 2.9). The Aishihik Batholith is characteristically foliated. The nature, distribution and significance of foliation is discussed in Chapter IV.

Migmatite complexes, consisting of networks of aplite veins and discontinuous pods of leucosome mantled by thin mafic selvages, occur along the western margin of the batholith. Aplite veins also occur in non-migmatitic parts of the batholith, but are rare.

Microdiorite and microgranitoid enclaves are common. Microdiorite enclaves are up to a meter long and consist largely of well foliated fine-grained hornblende and locally of hornblende, biotite and plagioclase. They occur both as foliaform lenses that extend parallel with foliation in the enclosing granodiorite, and as discordant globules. Microgranitoid lenses are smaller, rarely exceeding 50 cm in length, and are distinguished from the host granodiorite only on the basis of grain size; the enclaves are fine-grained.



Plate 2.7 Foliated, potassium feldspar megacrystic, hornblende granodiorite. The field of view is 5 cm in width. Foliation parallels the top and bottom margins of the plate. Hornblende grains are black, plagioclase grains are white, and small grey grains interstitial to plagioclase and hornblende are quartz. The large grey poikilitic megacryst at center consists of potassium feldspar. The arrow points to a hornblende inclusion within the feldspar grain.

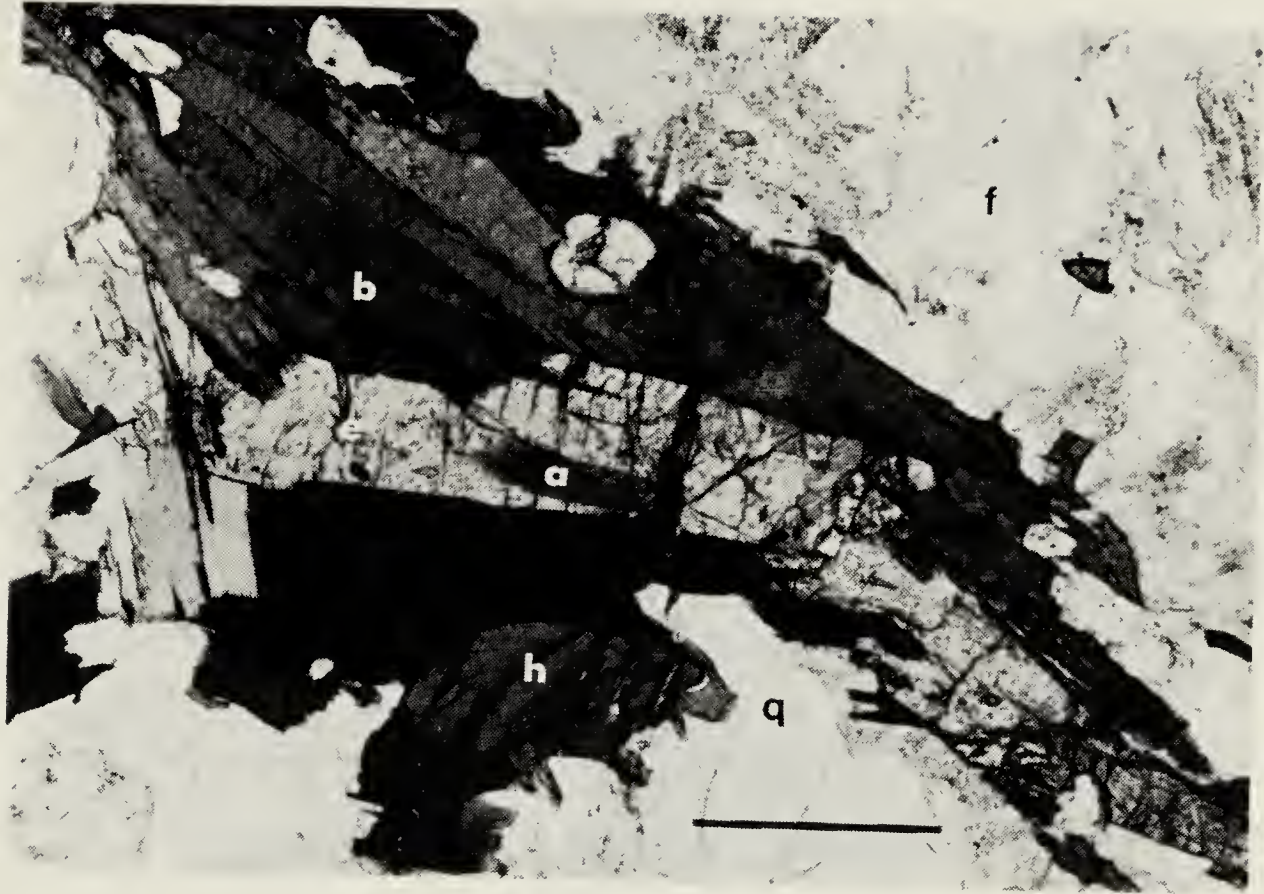


Plate 2.8 A photomicrograph, taken with plane polarized light of biotite hornblende granodiorite of the Aishihik Batholith (sample no. 141). An epidote grain (e), cored by allanite (a) at center is intergrown with biotite (b). Epidote - biotite grain boundaries are euhedral to subhedral. An anhedral hornblende grain (h) is mantled by biotite at lower center; q - quartz; f - feldspar. These textural relationships suggest the coprecipitation of biotite and epidote at the expense of hornblende. The scale bar represents 250 μm .



Plate 2.9 A photomicrograph, taken with plane polarized light of biotite hornblende granodiorite of the Aishihik Batholith (sample no. 141). An epidote grain (e), cored by allanite (a), and a biotite grain (b), surround and appear to have grown at the expense of an anhedral hornblende grain (h). The contact between the epidote grain and a large plagioclase feldspar grain (f) is wormy and is characterized by fine, dark biotite grains; q - quartz. These textures are interpreted to indicate the nucleation and growth of biotite and epidote at the expense of hornblende and plagioclase feldspar. The scale bar represents 250 μm .

Tabular inclusions are rare but are commonly up to several metres in length. Inclusions consist of garnetiferous muscovite - biotite schist and micaceous quartzite are similar to mica-schist of the adjacent Nisling terrane.

Cross-cutting pegmatite veins, including thin grey potassium feldspar veins 1 to 3 mm thick, and coarsely crystalline, pink and white pegmatite veins up to 1 m wide. The larger pegmatite veins consist of graphic intergrowths potassium feldspar and quartz, oligoclase plagioclase, individual grains of both potassium feldspar and quartz, and traces of chloritized mica. Pegmatite veins commonly intersect foliation at a high angle and locally include clasts of foliated granodiorite. Along the west margin of the batholith pegmatite veins are locally deformed. This is further discussed in Chapter IV.

Highly altered granodiorite is commonly present adjacent to surface exposures of younger feldspar porphyry dykes. The altered granodiorite is commonly characterized by quartz and quartz - calcite veins and by trace amounts of disseminated chalcopyrite.

2.4 Long Lake Suite pink quartz monzonite

Plutons of the Long Lake plutonic suite underlie much of the central, unglaciated part of the Aishihik Lake map-area (Fig. 1.2). Good, in-situ exposures are rare; exposures typically consist of weathered, frost heaved blocks.

Weathered surfaces are bright orange. Fresh surfaces are grey to pink. Little compositional variation was observed. The plutons consist of largely leucocratic, biotite and biotite - hornblende pink quartz monzonite (Plate 2.10). The major mineral phases which constitute the quartz monzonite intrusions include albitic plagioclase, quartz, and potassium feldspar. Mafic minerals include biotite, and less commonly, hornblende. Accessory minerals include zircon, apatite, and pyrite. Alteration products include sericite, calcite, epidote, and hematite.

Albitic plagioclase occurs as coarsely crystalline laths and as fine grained, acicular crystals. Plagioclase grains are commonly characterized by normal zonation with slightly more calcic cores. Phenocrysts are often altered entirely to clay. Potassium feldspar occurs as subhedral, poikilitic phenocrysts which include plagioclase and biotite. It also commonly mantles plagioclase phenocrysts and displays antiperthitic exsolution lamellae and cross-hatch twinning. Quartz occurs as fine to coarse grained, anhedral eyes. Mafic minerals, where present, never constitute more than 3% or 4% of the rock. Biotite is the most common mafic mineral and occurs as medium-grained euhedral booklets. Locally both biotite and fine-grained hornblende are present.

The quartz monzonite plutons are pervasively fractured. The fractures are characterized by calcite, epidote, quartz, and hematite mineralization and are associated



Plate 2.10 A photomicrograph, taken with crossed nicols, of typical, massive, coarsely crystalline quartz monzonite of the Long Lake Suite (sample no. 67); k - potassium feldspar; p - plagioclase; q - quartz. The scale bar represents 1 mm.

with sericitization of the feldspars. The fractures and the related disseminated hematite appear to be responsible for the fissile nature and bright orange colour of the weathered monzonite.

2.5 Ruby Range Batholith

The Ruby Range Batholith forms the west margin of the Nisling terrane in the study area (Figures 1.2). The more resistant batholith underlies the glaciated highlands south of the Aishihik Lake and stands in high relief relative to the adjacent schists of the Nisling terrane.

The batholith is composed of a heterogeneous suite of intrusions. Weathered surfaces range in colour from grey to light brown. Fresh surfaces range in colour from dark grey to light grey. Quartz diorite and granodiorite are the most common phases; diorite and nebulitic granite are less common (Plate 2.11). Major mineral phases includes albitic to labradoritic plagioclase, potassium feldspar, quartz, and hornblende. Biotite is a common but minor mineral phase. Accessory minerals include spene, apatite, zircon, and magnetite. Chlorite, sericite, pyrophyllite, calcite, and epidote alteration is present.

Plagioclase is albitic to labradoritic, euhedral, exhibits normal and reverse compositional zoning, and both Carlsbad and albite twinning. Potassium feldspar locally exhibits cross-hatch twinning and occurs as anhedral grains which mantle and are interstitial to other grains and as subhedral phenocrysts. Hornblende and, to a lesser extent, biotite together constitute up to 30% of the rock and usually occur as coarse-grained glomeroporphyritic clots. Mafic enclaves, usually consisting of hornblendite, are common. Plagioclase is mildly sericitized. Biotite is slightly to totally replaced by chlorite and pyrophyllite. Calcite and epidote veins are locally present.

A mild foliation is commonly present and varies from a subtle, nebulitic banding, which appears to highlight relict migmatitic textures, to a weak alignment of hornblende and plagioclase laths.

2.6 Age, stratigraphic and terrane relations

Nisling Assemblage - No fossils, and therefore no direct evidence of the age of the Nisling Assemblage was observed. An Early Mississippian U - Pb zircon age for orthogneiss (PPo) (Chapter III) indicates that the host PPms unit is pre-Mississippian. The rocks are assumed to be Proterozoic to Cambrian in age based on their similarity to Proterozoic to Cambrian rocks of the North American continental margin (Wheeler and McFeely, 1991).

For a complete review of the evolution of current and historical nomenclature regarding the Nisling Assemblage see Mortensen (1992). The Nisling Assemblage,

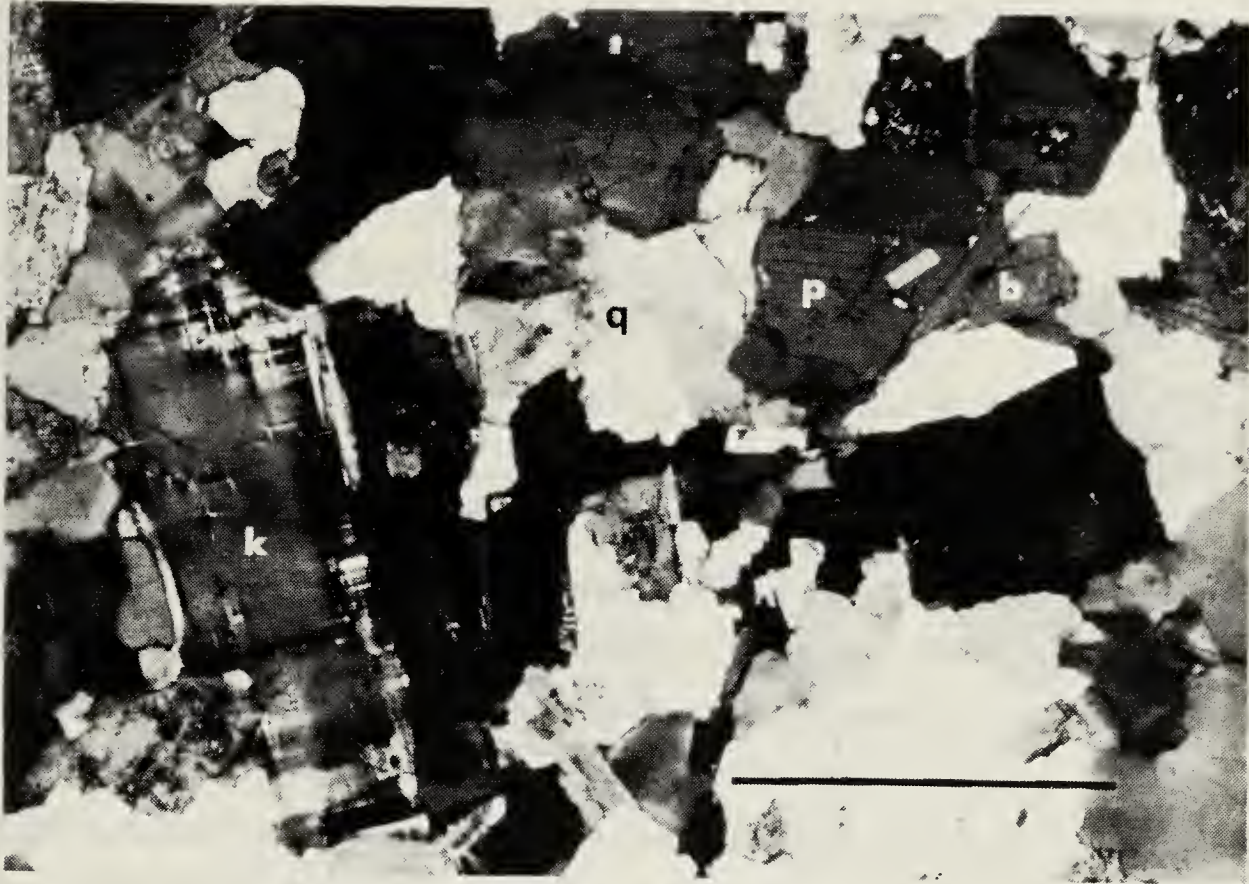


Plate 2.11 A photomicrograph of typical, medium-grained, massive biotite granite of the central part of the Ruby Range batholith (sample no. 135); k - potassium feldspar (characterized by cross-hatch twinning); p - plagioclase; q - quartz; b - biotite. The scale bar represents 250 μm .

together with brown and black quartzite of the Nasina Assemblage (not present in the study area), define the Nisling Terrane (Wheeler and McFeely, 1991). The Nisling Terrane has been interpreted as: 1) a continental fragment which forms the basement of the Stikine terrane (Tempelman-Kluit, 1979); 2) the metamorphosed and deformed equivalent of strata that are part of and continuous with the North American continental margin (Hansen, 1990); and 3) equivalent to and correlative with the Yukon - Tanana terrane (Mortensen, in press).

Aishihik Batholith - U - Pb zircon geochronology indicates that the batholith crystallized at $187.0 \pm 9.7/-0.9$ Ma (Chapter III).

At the west margin of the batholith, hornblende granodiorite overlies mica-schist of the Nisling Assemblage. The contact is concordant with foliation in the overlying granodiorite and with schistosity in the underlying mica-schist, and dips homoclinally to the east, beneath the batholith. The contact is commonly characterized by a discrete plane (Plate 2.12). Locally granodiorite grades into feldspathic schist over a 1 m wide interval and no distinct contact can be discerned. No discordant dykes or sills of granodiorite that intrude mica-schist of the Nisling Assemblage were observed. Mylonitization of both granodiorite above the contact and schist beneath the contact is common (Chapter IV).

Along the north margin of the batholith the contact is less well defined and is poorly exposed. Micaceous quartzite of the Nisling Assemblage overlies granodiorite of the batholith. The contact is concordant with foliation in the underlying granodiorite and with schistosity in the overlying mica-schist, and dips to the north, away from the batholith. Granodiorite appears to grade into micaceous quartzite over an interval of tens of meters. No sharp, discrete contact was observed. No dykes or sills of granodiorite that intrude the Nisling Assemblage were observed.

The nature of the batholith's contact with the Nisling Assemblage is a matter of conjecture. The sharp discrete nature of the contact, and its association with shearing and mylonitization has led to speculation that the west margin of the batholith represents a major shear zone (Wheeler and McFeely, 1991). D. Tempelman-Kluit (pers. comm., 1992) has suggested that the contact represents the northward continuation of the Tally Ho shear zone, a Late Triassic - Early Jurassic shear zone which bounds the east margin of the Nisling Assemblage near the Yukon - British Columbia border (Hart and Radloff, 1990; Hansen *et al.*, 1989). Alternatively, the contact may represent a moderate to deep crustal intrusive contact. Intrusions emplaced at moderate to deep crustal levels are commonly characterized by concordant contacts and lack associated dyke swarms. This interpretation is consistent with the coarsely crystalline, equigranular nature of the granodiorite, and with the crystallization of magmatic biotite and epidote at the expense of

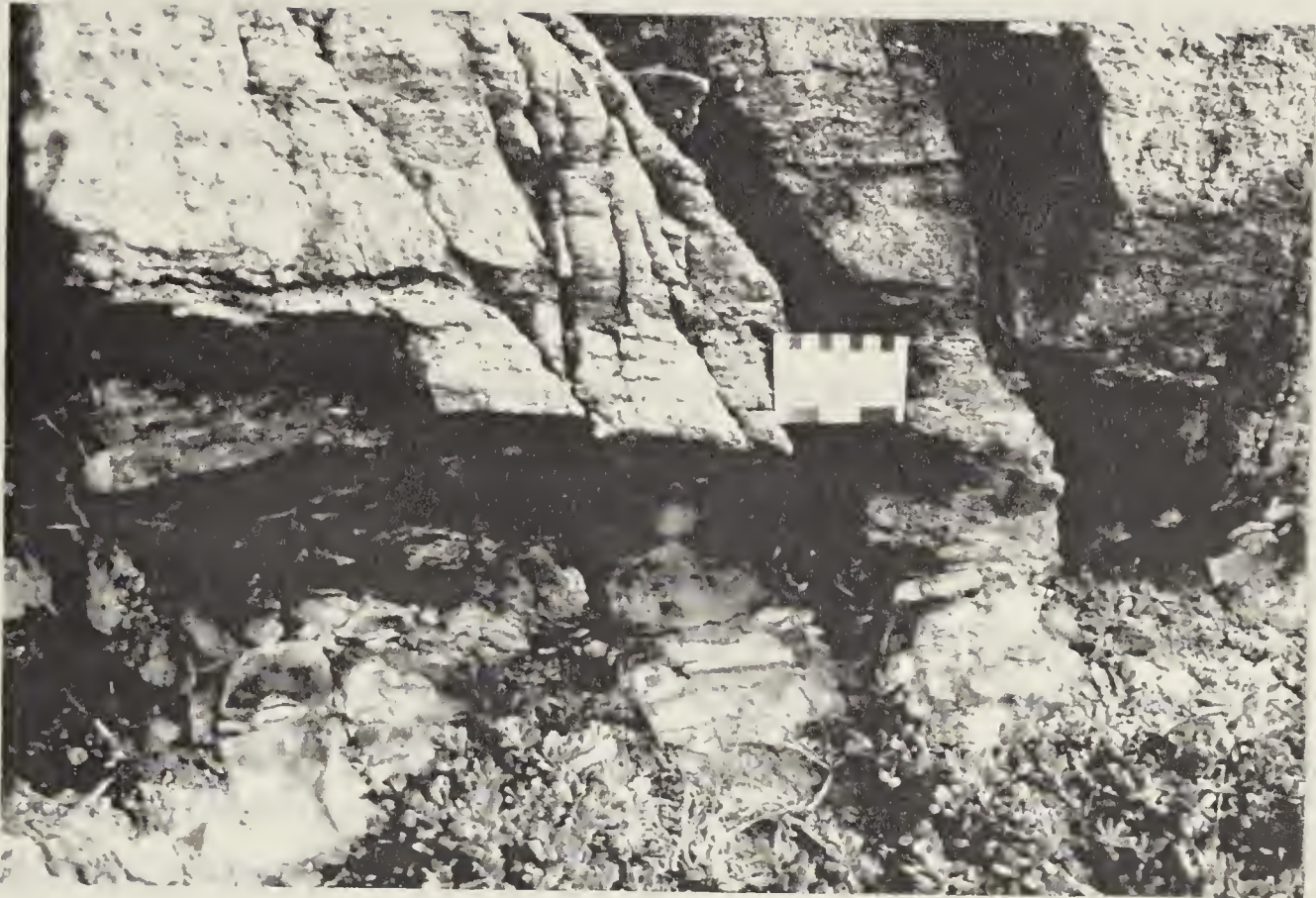


Plate 2.12 This photograph, taken looking to the northeast, shows resistant foliated hornblende granodiorite of the Aishihik Batholith overlying more recessive schist and marble of the Nisling Assemblage. The contact parallels foliation in both the overlying granodiorite and in the underlying schist, dips to the northeast (into the photo), and consists of a sharp plane evident just below and to the left of the scale card (cm at top and inches at bottom).

melt, hornblende and plagioclase (Plates 2.8 and 2.9) (Zen, 1989; Zen and Hammarstrom, 1984). Mica-schist inclusions, though rare, are similar to schist of the Nisling Assemblage.

The batholith is thought to represent part of the Klotassin Suite of intrusions. This correlation is based on common mineralogy and geologic setting (Tempelman-Kluit, 1979).

Long Lake Suite - Field relations and U - Pb zircon and titanite geochronology indicates that the plutons of pink quartz monzonite post-date and crystallized within 10 Ma of the of the Aishihik Batholith (Chapter III). Massive, unfoliated plutons of the Long Lake Suite intrude and truncate foliated rocks of the Aishihik Batholith and plug the Aishihik Batholith - Nisling Assemblage contact. Dyke swarms extend out from pink quartz monzonite plutons and intrude both Aishihik Batholith and Nisling Assemblage.

Pink quartz monzonite is spatially associated with hornblende granodiorite of the Aishihik Batholith. It underlies much of the central part of the Aishihik Batholith but is rare outside of the batholith. This relationships suggests a genetic link between the Long Lake Suite and the older hornblende granodiorite.

Ruby Range Batholith - U - Pb zircon geochronology indicates that the Ruby Range Batholith is a composite plutonic body. The margins of the batholith were emplaced between 68 and 90 Ma; the core of the batholith may be as young as 58 Ma (Chapter III).

The Ruby Range Batholith and related plutons intrude the Nisling Assemblage. Pluton margins are commonly concordant with schistosity in the Nisling Assemblage but are locally discordant and cross-cutting (Figure 2.1 c). Numerous discordant mafic dykes and plugs intrude the Nisling Assemblage in the vicinity of the batholith.

The batholith is on strike with the Coast Plutonic Complex (Roddick and Hutchison, 1970; Brew and Morrell, 1983; Woodsworth *et al.*, 1989), and is thought to represent its most northerly element.

III. U-Pb GEOCHRONOLOGY

3.1 Introduction

In the Aishihik Lake area metamorphosed continental clastic, carbonate and amphibolitic rocks of Nisling Assemblage are in contact with the Stikine terrane (Figure 1.1). The four suites of plutonic rocks recognized within the study area (Figure 3.1) include: 1) orthogneiss within the Nisling Assemblage; 2) the Aishihik Batholith, included in Stikinia; 3) Long Lake Suite pink quartz monzonite; and 4) the Ruby Range Batholith.

This chapter, based on the results of U - Pb analyses of zircon separates, reports on the crystallization ages of each of these four plutonic suites. U - Pb analyses of titanite from samples of the Aishihik Batholith and the Long Lake Suite, are also reported.

3.2 Analytical results

Analytical data and calculated ages of zircon fractions determined in this study are presented in Table 3.1 and are shown on conventional U - Pb concordia plots in Figures 3.2 to 3.5. Errors in age estimates are quoted at the 2 sigma level. Methods of U and Pb extraction and analysis for zircon and titanite are presented in Appendix 3.1. Sample location coordinates and petrographic descriptions are given in Appendices 3.2 and 3.3, respectively.

Nisling Assemblage Orthogneiss (PPO):

Six fractions of abraded zircons from Nisling two-mica orthogneiss (sample 1; Figure 3.1) were analyzed (Table 3.1). The zircon grains are typically stubby, euhedral, pale to medium pink crystals with aspect ratios of 1 to 2. No xenocrystic cores were observed, and grains are generally clear with rose coloured bubbles and rod-shaped inclusions.

The data points lie beneath the concordia curve between 315 Ma and 365 Ma and do not form a linear array (Figure 3.2). The scatter is interpreted to result from inheritance of an older zircon component, compounded by post-crystallization Pb loss. The combination of Pb loss and inheritance of a component of older zircon, together with the lack of concordant data points prevents the assignment of an unequivocal emplacement age for the protolith of the orthogneiss. The most concordant analysis was obtained from fraction A and yields a $^{207}\text{Pb}/^{206}\text{Pb}$ age of 351.5 ± 2.0 Ma. A two point regression line through this analysis and that of fraction E yields lower and upper intercepts of 343.8 ± 0.8 Ma and 2.01 ± 0.14 Ga, respectively. The $^{207}\text{Pb}/^{206}\text{Pb}$ age of

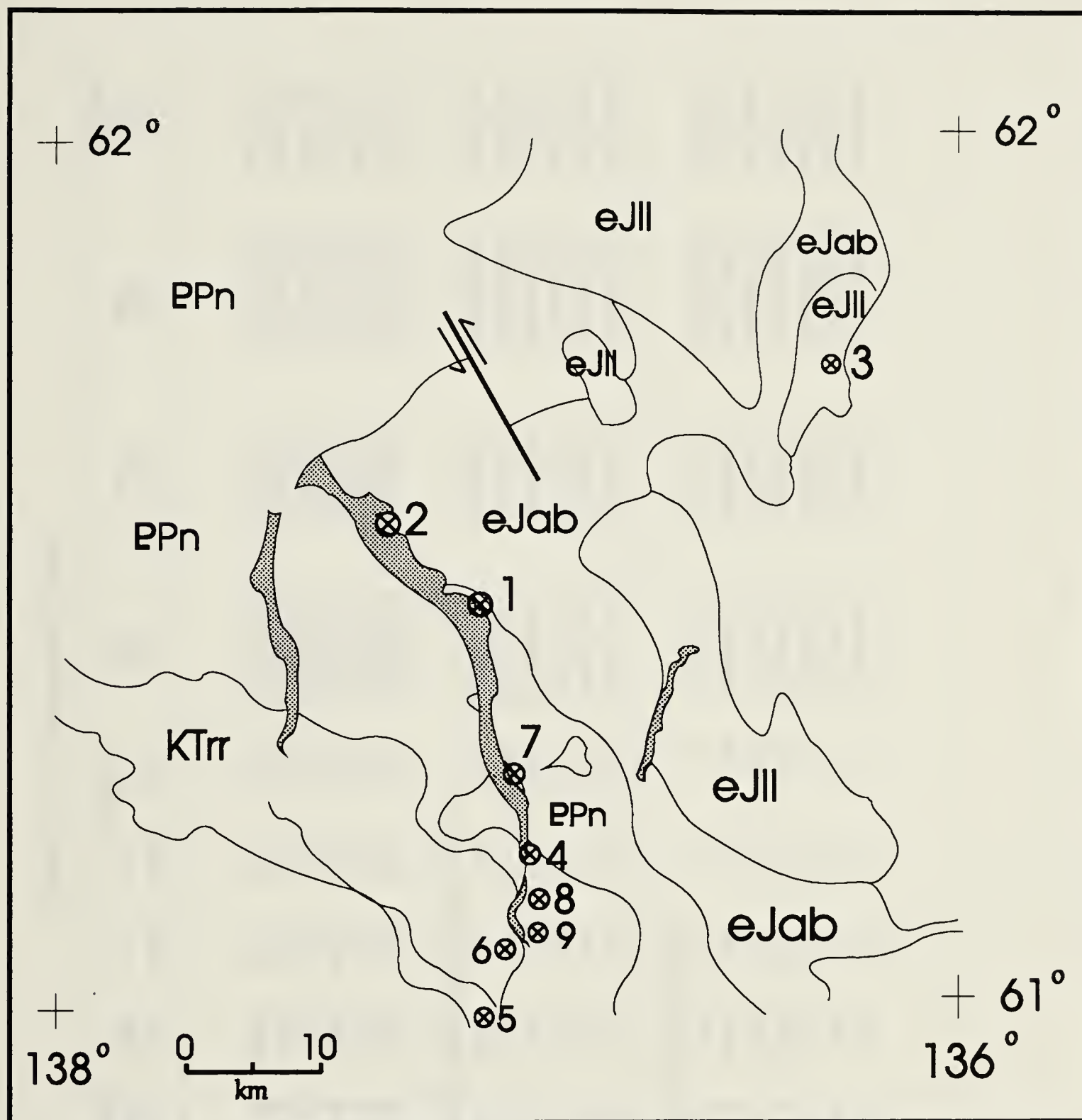


Figure 3.1 A map of the bedrock geology in the vicinity of Aishihik Lake. The location of samples collected for U - Pb geochronometry studies is indicated. PPn - Nisling Assemblage, including orthogneiss (PPo); eJab - Aishihik Batholith; eJll - Long Lake Suite; KTrr - Ruby Range Batholith.

Table 3.1. U - Pb analytical data

Sample	Fraction ^a	Sample weight (mg)	$\frac{^{206}\text{Pb}}{^{204}\text{Pb}}$	U (ppm)	Pb (ppm)	Common Pb (%)	$\frac{^{206}\text{Pb}}{^{238}\text{U}}$	$\frac{^{207}\text{Pb}}{^{235}\text{U}}$	$\frac{^{207}\text{Pb}}{^{206}\text{Pb}}$	Age ^d (Ma)
Two Mica Orthogneiss										
1)	A(*,A,N1)	0.10	7904	470	26.0	0.77	0.05490(0.1)	0.4052(0.1)	0.05353(0.04)	351.5(2.0)
1)	B(*,A,N1)	0.10	8126	701	34.2	0.76	0.04878(0.1)	0.3729(0.1)	0.05544(0.04)	429.8(1.7)
1)	C(*,A,N1)	0.06	1873	394	22.0	3.21	0.05562(0.1)	0.4421(0.2)	0.05765(0.10)	516.4(4.6)
1)	D(*,A,N1)	0.09	7079	448	24.3	0.87	0.05437(0.1)	0.4067(0.1)	0.05427(0.05)	382.1(2.1)
1)	E(*,A,N1)	0.12	6459	459	25.9	0.94	0.05601(0.1)	0.4260(0.1)	0.05516(0.05)	418.8(2.2)
1)	F(*,A,N1)	0.06	2807	537	26.8	2.17	0.04998(0.1)	0.3708(0.1)	0.05380(0.09)	362.7(4.1)
Aishihik Batholith - foliated hornblende granodiorite										
2)	A(*,A,N1)	0.05	1693	323	9.7	3.51	0.02936(0.1)	0.2022(0.2)	0.04996(0.12)	193.2(5.7)
2)	B(*,A,N1)	0.15	4397	321	10.1	1.38	0.03095(0.1)	0.2150(0.1)	0.05038(0.05)	212.6(2.4)
2)	C(*,A,N1)	0.09	656	212	6.2	8.93	0.02935(0.1)	0.2016(0.3)	0.04983(0.21)	187.0(9.7)
2)	D(*,A,N1)	0.05	1952	280	8.7	3.05	0.03052(0.1)	0.2250(0.2)	0.05347(0.12)	348.6(5.5)
2)	E(*,TT)	0.14	113	109	4.6	31.20	0.02913(0.5)	0.2005(1.7)	0.04993(1.35)	191.6(63.0)
2)	F(*,TT)	0.16	132	79	3.8	25.00	0.02915(0.4)	0.2002(1.5)	0.04981(1.25)	185.9(58.1)
Long Lake Suite - pink quartz monzonite										
3)	A(*,A,N1)	0.18	4342	301	9.2	1.38	0.02954(0.1)	0.2049(0.1)	0.05030(0.05)	208.8(2.3)
3)	B(*,A,N1)	0.15	6671	346	10.5	0.90	0.02940(0.1)	0.2024(0.1)	0.04993(0.05)	191.8(2.3)
3)	C(*,A,N1)	0.10	2017	304	9.4	2.97	0.03019(0.1)	0.2086(0.1)	0.05012(0.10)	200.3(4.6)
3)	D(*,A,N1)	0.15	5561	375	11.1	1.09	0.02906(0.1)	0.2013(0.1)	0.05025(0.05)	206.7(2.1)
3)	E(*,A,N1)	0.21	7715	337	10.4	0.77	0.02973(0.1)	0.2051(0.1)	0.05003(0.04)	196.3(2.1)
3)	F(*,A,N1)	0.08	1014	325	10.0	5.71	0.02958(0.1)	0.2048(0.2)	0.05023(0.18)	205.7(8.3)
3)	G(*,A,N1)	0.08	3414	359	11.0	1.73	0.02943(0.1)	0.2029(0.2)	0.05000(0.09)	194.8(4.0)

Table 3.1. (continued)

Sample	Fraction ^a	Sample weight (mg)	$\frac{^{206}\text{Pb}}{^{204}\text{Pb}}$ ^b	U (ppm)	Pb (ppm)	Common Pb (%)	$\frac{^{206}\text{Pb}^c}{^{238}\text{U}}$	$\frac{^{207}\text{Pb}^c}{^{235}\text{U}}$	$\frac{^{207}\text{Pb}^c}{^{206}\text{Pb}}$	$\frac{^{207}\text{Pb}}{^{206}\text{Pb}}$ Age ^d (Ma)
Ruby Range Batholith										
4)	A(<75,N1,3)	2.49	109	1116	12.5	4.28	0.01085(0.6)	0.0701(1.0)	0.04685(2.30)	41.5(2.0)
4)	B(N1,3)	3.22	256	401	5.1	8.45	0.01219(0.6)	0.0792(1.0)	0.04716(2.30)	57.5(2.7)
5)	C(<75,N1,3)	3.97	3010	3669	39.3	0.63	0.01088(0.6)	0.0714(1.0)	0.04762(2.30)	80.5(3.8)
5)	D(>75,N1,3)	11.19	1069	1205	13.4	3.26	0.01133(0.6)	0.0745(1.0)	0.04775(2.30)	87.0(4.1)
6)	E(<75,N1,3)	11.27	1360	2756	23.9	2.22	0.00870(0.6)	0.0569(1.0)	0.04749(2.30)	74.0(3.5)
7)	F(<75,N1,3)	10.56	2584	977	12.4	0.80	0.01279(0.6)	0.0895(1.0)	0.05082(2.30)	232.0(10.9)
7)	G(>75,N1,3)	9.29	1280	760	10.4	2.71	0.01368(0.6)	0.1048(1.0)	0.05562(2.30)	440.0(13.0)
8)	H(<75,N1,3)	9.98	1657	1487	15.0	1.56	0.01014(0.6)	0.0697(1.0)	0.04984(2.30)	187.5(8.8)
8)	I(>75,N1,3)	7.27	1528	1194	12.1	1.35	0.01053(0.6)	0.0701(1.0)	0.04829(2.30)	113.5(5.3)
9)	J(<75,N1,3)	8.84	3481	919	8.8	0.10	0.00981(0.6)	0.0658(1.0)	0.04868(2.30)	132.5(6.2)
9)	K(>75,N1,3)	11.04	1100	783	7.6	2.15	0.00974(0.6)	0.0663(1.0)	0.04928(2.30)	161.0(7.5)

a - all analyses are of zircon, except where indicated (TT - titanite); size fractions in μm ; * - sample fractions analyzed at the Geochronology Laboratory of the Geologic Survey of Canada (Ottawa), all other analyses were done at the University of Alberta; A - indicates abrasion; N1 - indicates nonmagnetic zircon separate and the side slope, in degrees, of the Frantz magnetic separator; the composition of Pb (204:206:207:208), from Stacey and Kramer (1975) used for common Pb corrections: 1 is 1:18.40:15.61:38.26; 2 is 1:18.47:15.62:38.36; 3 is 1:18.64:15.62:38.56.

b - measured isotopic ratio.

c - corrected for blank Pb and U and common Pb; errors are quoted at the 1 sigma level in percent.

d - corrected for blank Pb and common Pb; errors are quoted at the 2 sigma level in Ma.

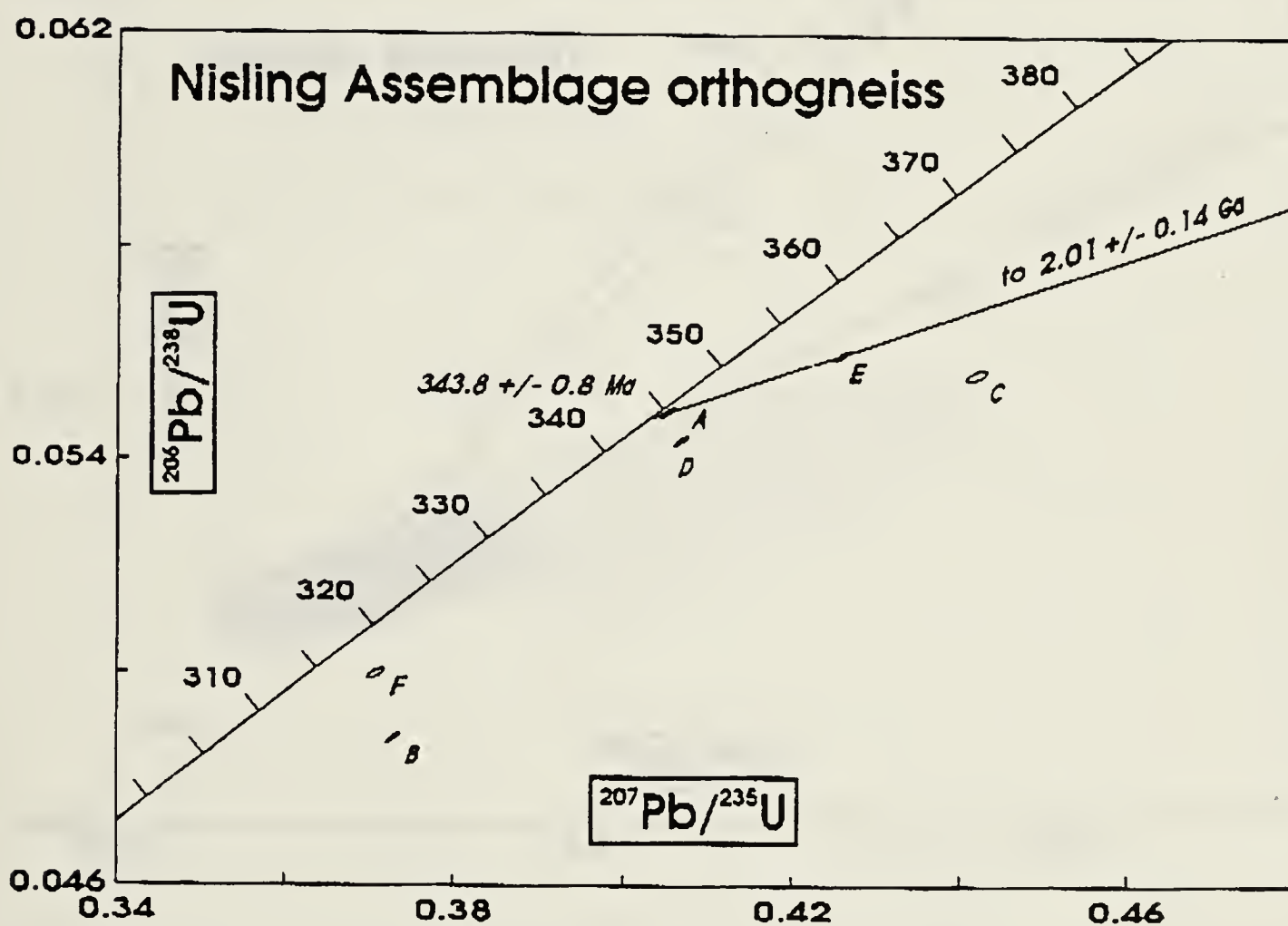


Figure 3.2 U - Pb concordia plot for zircon from two mica orthogneiss of the Nisling Assemblage. Error ellipses are shown at the 2 sigma level. Letter designations correspond with the zircon fractions defined in Table 3.1. A regression line is shown for fractions A and E. See text for discussion.

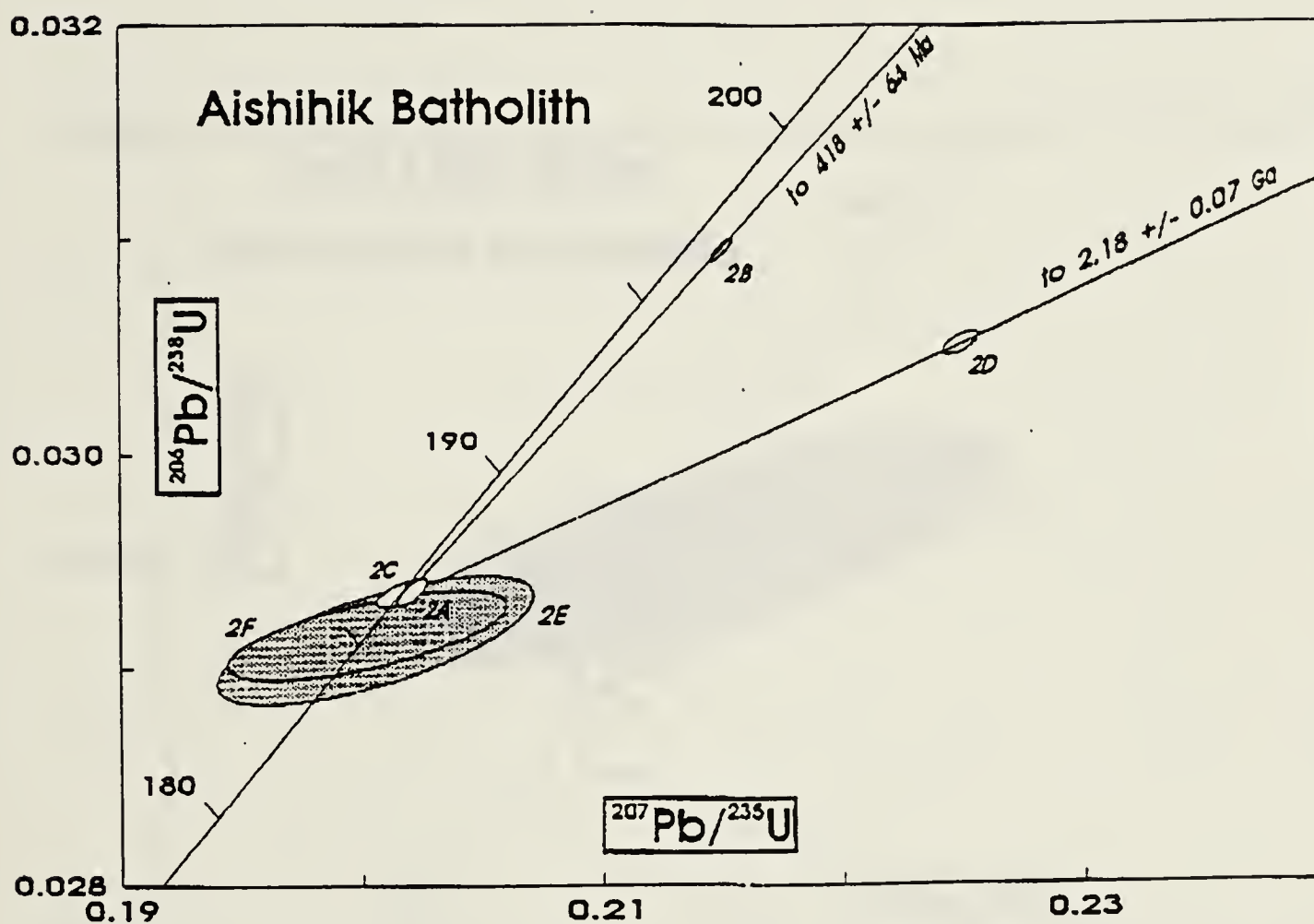


Figure 3.3 U - Pb concordia plots for zircon and titanite fractions from the Aishihik Batholith. Symbols as in Figure 3.2. Titanite fractions (E and F) are shaded. Regression lines for fractions C and B and C and D are shown. See text for discussion.

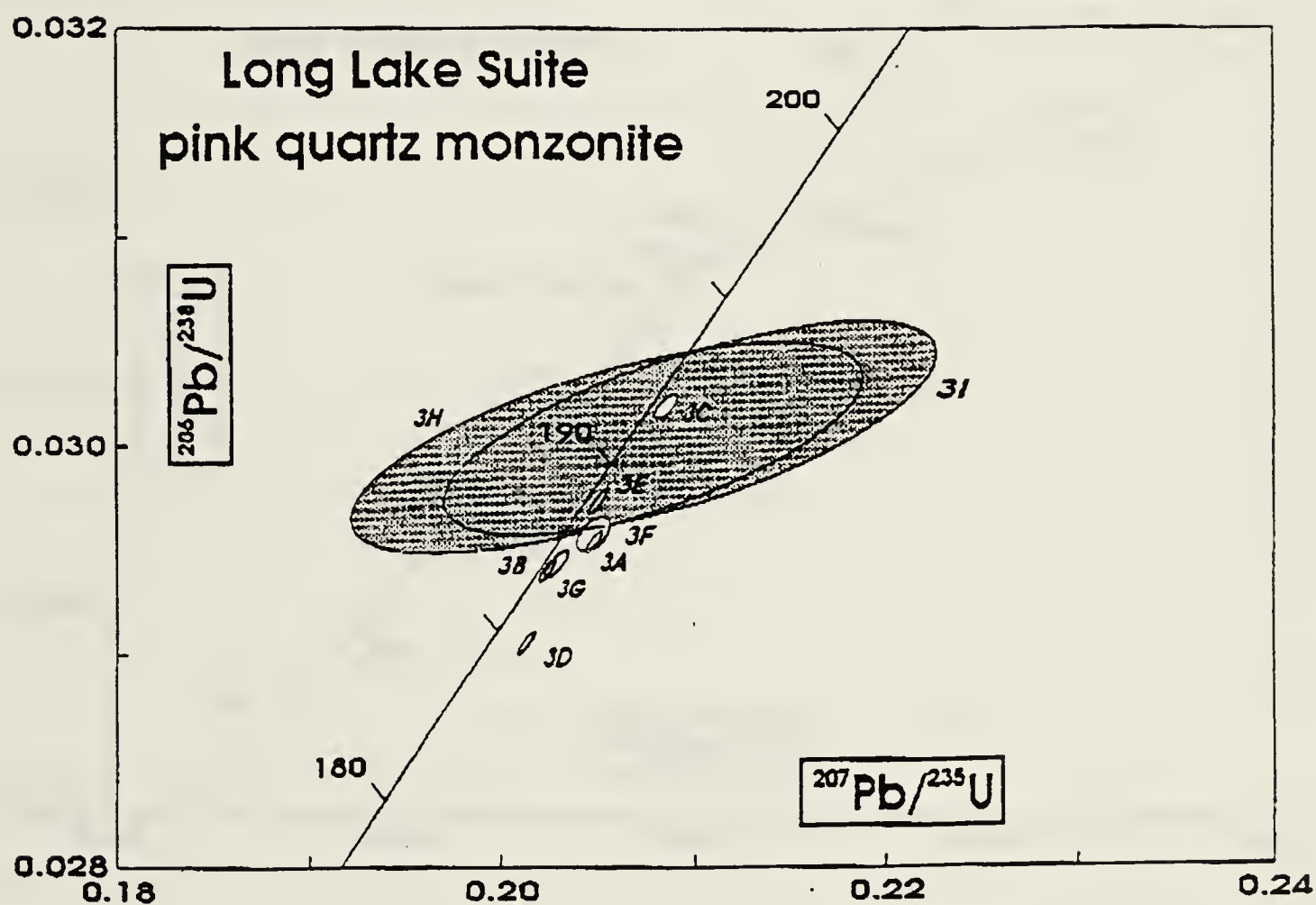


Figure 3.4 U - Pb Concordia plots for zircon and titanite (shaded) from the Long Lake Suite. Symbols as in Figure 3.2. See text for discussion.

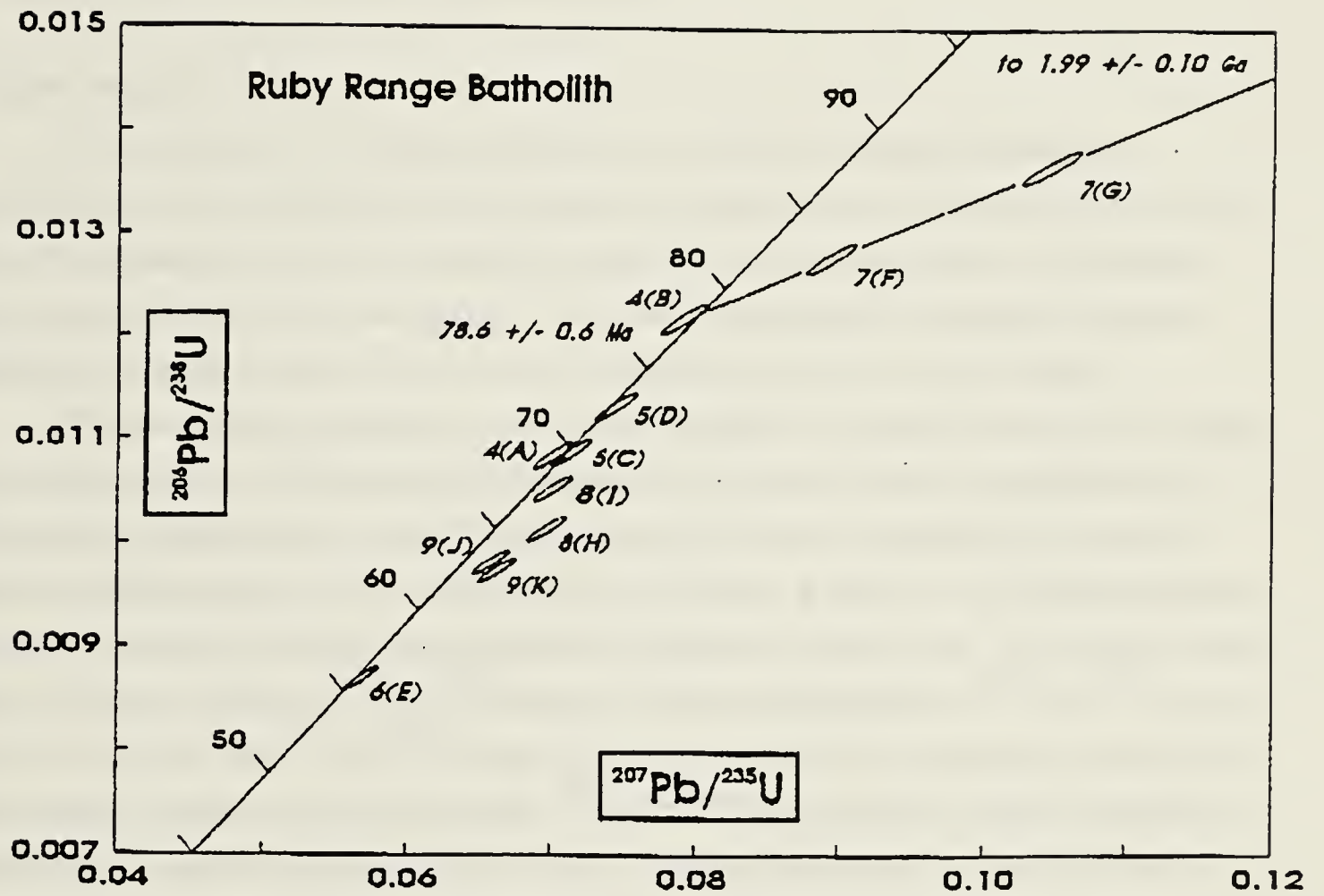


Figure 3.5 U - Pb Concordia plot for zircon from the Ruby Range Batholith. Symbols as in Figure 3.2. A regression line is shown for fractions 4 B and 7 F and G. See text for discussion.

fraction A and the lower intercept of the A - E discordia provides an age range which probably encompasses the age of the granitic protolith to the orthogneiss. Based on these data the emplacement age of the orthogneiss is interpreted as Early Mississippian.

The upper intercept of the A - E discordia suggests that at least some of the inherited zircon component is probably Early Proterozoic or older. This is consistent with the significant inheritance exhibited by fraction C.

Aishihik Batholith (eJab):

Four fractions of abraded zircons from a sample of foliated hornblende granodiorite of the Aishihik Batholith (sample 2; Figure 3.1) were analyzed (Table 3.1). The zircon grains are typically euhedral, translucent, and honey coloured, with aspect ratios ranging from 3 to 8, averaging 4. Two titanite fractions, consisting of broken fragments of clear, medium yellow brown, euhedral grains, were also analyzed.

The data points pertaining to the zircon analyses lie on and beneath the concordia curve between about 186 Ma and 200 Ma and do not form a linear array (Figure 3.3). The scatter is interpreted to result from inheritance of zircon, probably from several sources of different ages. Two of the analyses, fractions A and C, are virtually identical, fall on the concordia, and do not appear to be affected by inheritance. The most precise of these (fraction C) yields a $^{206}\text{Pb}/^{238}\text{U}$ age of 186.5 ± 0.4 Ma and a $^{207}\text{Pb}/^{206}\text{Pb}$ age of $187.0 + 9.7/-9.8$. The $^{207}\text{Pb}/^{206}\text{Pb}$ age provides a conservative estimate of the age of this sample. However, the more precise $^{206}\text{Pb}/^{238}\text{U}$ age provides a better constraint on the minimum age of the sample (186.1 Ma). Together these data suggest that the best interpretation of the age of the sample is $187.0 + 9.7/-0.9$ Ma. This is not, however, necessarily the age of the entire batholith. The large size of the batholith suggests that it developed over a prolonged period lasting perhaps as long as 5 Ma. The analyses presented here provide some constraints on the age of one part of the batholith, but do not preclude the presence of younger and older phases elsewhere in the batholith.

Fractions B and D exhibit significant inheritance, although of two different ages. A two point regression of fractions C and D (Figure 3.3) yields an upper intercept of 2.18 ± 0.07 Ga. This upper intercept age indicates that at least some of the inherited zircon has an Early Proterozoic average age. A regression through fractions C and B yields an upper intercept of 418 ± 64 Ma, suggesting that inherited zircon of Early Paleozoic or late Proterozoic age may also be present. The high degree of scatter in the data, however, precludes placing age(s) on the inherited components.

The two titanite fractions (I and J - both sample 5) yield concordant analyses with

overlapping error envelopes (Figure 3.3). The most precise of these (fraction J) yields a $^{206}\text{Pb}/^{238}\text{U}$ age of 185.2 ± 1.3 Ma. Because the blocking temperature for Pb in titanite is significantly lower than that in zircon (600°C versus $> 800^\circ\text{C}$ (Heaman and Parrish, 1991)) this is interpreted as a cooling age.

Long Lake pink quartz monzonite (eJll):

Six fractions of abraded zircons from a sample of weathered, mildly foliated, medium grained, pink quartz monzonite (sample 3; Figure 3.1) were analyzed (Table 3.1). Zircon grains are typically euhedral, translucent, and honey coloured. Grains range from stubby crystals to elongate prisms; aspect ratios vary from 2 to 12. No visible cores were observed, although clear bubbles and rod shaped inclusions are common. Two titanite fractions, consisting of broken fragments of yellow brown subhedral grains were also analyzed.

The data points pertaining to the zircon analyses lie beneath the concordia curve between 185 Ma and 192 Ma and do not form a linear array (Figure 3.4). The scatter is interpreted to result from inheritance of an older zircon component, compounded by post-crystallization Pb loss. The combination of Pb loss and inheritance of a component of older zircon, together with the lack of concordant data points prevents the assignment of an unequivocal emplacement age for the pink quartz monzonite.

The two titanite fractions, H and I, yield concordant overlapping analyses. The most precise of these (fraction H) yields a $^{206}\text{Pb}/^{238}\text{U}$ age of 189.7 ± 3.3 Ma. These data suggest that the sample of pink quartz monzonite cooled through the Pb blocking temperature for titanite of 600°C (Heamon and Parrish, 1991; and references therein) by 189.7 ± 3.3 Ma.

Although an unequivocal emplacement age for the Long Lake Suite cannot be assigned, these data, together with the age of the Aishihik Batholith, can be used to constrain the age of emplacement. An upper age constraint is provided by the Aishihik Batholith. Plutons of pink quartz monzonite intrude and are therefore clearly younger than the youngest phases of the Aishihik Batholith, limiting their age to less than $187.0 + 9.7/-0.9$ Ma. A lower age constraint is provided by the titanite cooling ages, limiting the age of emplacement to greater than 189.7 ± 3.3 Ma. Plutons of the Long Lake Suite are locally miarolitic (Tempelman-Kluit, 1974; this study), suggesting that the intrusions cooled quickly. This suggests that the U-Pb titanite age should be close to, and not much younger than the age of emplacement of the Long Lake Suite. However, as with the Aishihik Batholith, the large volume and large aerial extent of the Long Lake Suite

suggest that it may have taken several million years to accumulate. The data presented here provide some constraints on the age of part of the Long Lake Suite, but do not preclude the presence of younger phases elsewhere in the suite.

Ruby Range Batholith (KTrr):

Seven samples of the Ruby Range batholith were collected for U - Pb geochronological studies (samples 4 to 9; Figure 3.1). The samples range from medium grained, nebulitic, hornblende biotite granite, from the central part of the batholith, to coarsely crystalline, mafic, hornblende diorite from the margin of the batholith. Eleven bulk unabraded zircon separates were analyzed (Table 3.1). Zircon grains recovered from the samples are typically clear, but vary from fine, euhedral crystals to large blocky fragments. No visible cores and no cloudiness or other alteration of the zircon grains was observed.

The data lie along and beneath the concordia between about 56 and 93 Ma (Figure 3.5). At least some of this scatter is attributable to inheritance of a component of older zircon. This is demonstrated by data from sample 7 (fractions F and G) from the north margin of the batholith. Both fractions lie off of the concordia. The $^{207}\text{Pb}/^{206}\text{Pb}$ ages of the coarse ($> 75 \mu\text{m}$) and fine fractions ($< 75 \mu\text{m}$), G and F respectively, are 440 Ma and 232 Ma. A regression of these data points together with fraction B (sample 4 - also collected from the north margin of the batholith) yields upper and lower intercepts of $1.99 \pm 0.10 \text{ Ga}$ and $78.6 \pm 0.6 \text{ Ma}$. The upper intercept suggests that the inherited zircon component may be, at least in part, Proterozoic.

The significance of the lower intercept is unclear. The age overlaps with the age of the coarse zircon fraction (B) for sample 4 which is concordant and yields a $^{206}\text{Pb}/^{238}\text{U}$ age of $78.1 \pm 1.0 \text{ Ma}$. This may indicate that north margin of the batholith, was emplaced at about 78 Ma. However, this fraction, although concordant, lies largely above the concordia, has a $^{207}\text{Pb}/^{206}\text{Pb}$ age of $57.5 \pm 2.7 \text{ Ma}$. The fine fraction (A) for sample 4 is also concordant, but yields a much younger $^{206}\text{Pb}/^{238}\text{U}$ age of $69.6 \pm 0.9 \text{ Ma}$. This sample also sits mostly above the concordia and yields a $^{207}\text{Pb}/^{206}\text{Pb}$ age of $41.5 \pm 2.0 \text{ Ma}$. Because the coarse and fine fraction zircon fractions yield significantly different, albeit concordant ages, and because both data points lie above the concordia, these data cannot be used to obtain a reliable age of crystallization. In light of these considerations the lower intercept age of $78.6 \pm 0.6 \text{ Ma}$ is interpreted as the maximum possible age of emplacement for the northern part of the batholith. This does not, however, preclude a younger emplacement age.

Tempelman-Kluit and Wanless (1975) reported K-Ar hornblende and biotite ages determinations of 68.3 ± 3.4 Ma and 67.6 ± 2.7 Ma, respectively, for a sample collected close to the sample location of sample 4. These data place a minimum age constraint on the north margin of the batholith of about 68 Ma. K-Ar ages are cooling ages; the closure temperatures, with respect to Ar, for hornblende and biotite are 530 ± 40 °C and 280 ± 40 °C, respectively (Heamon and Parrish, 1991; and references therein). The similarity of the hornblende and biotite cooling ages is indicative of rapid cooling and can be explained by rapid tectonic denudation of an earlier emplaced, deeply seated intrusion. Alternatively, rapid cooling may have resulted from emplacement of the batholith into shallow crustal levels at about 68 Ma. Andalusite and cordierite are present in the metamorphic aureole which encloses the batholith, consistent with intrusion at shallow crustal levels, and lending support to the latter interpretation.

Sample 5 was collected from near the south margin of the batholith. Like sample 4, the coarse and fine zircon fractions yield concordant, but different age determinations. The fine fraction (C) and coarse fraction (D) yield $^{206}\text{Pb}/^{238}\text{U}$ ages of 69.7 ± 0.9 Ma and 72.6 ± 0.9 Ma, and $^{207}\text{Pb}/^{206}\text{Pb}$ ages of 80.5 ± 3.8 Ma and 87.0 ± 4.1 Ma, respectively. These data cannot be used to obtain a reliable age of crystallization. They do, however, suggest that the south margin of the batholith was emplaced sometime between about 69 and 90 Ma.

A fine zircon fraction (E, sample 6), obtained from a sample of the granitic internal part of the batholith is concordant and yields a $^{206}\text{Pb}/^{238}\text{U}$ age of 55.8 ± 0.7 Ma and a $^{207}\text{Pb}/^{206}\text{Pb}$ age of 74.0 ± 3.5 Ma. The sample did not yield enough coarse zircons to analyze. Tempelman-Kluit and Wanless (1975) reported K-Ar hornblende and biotite ages determinations of 53.8 ± 3.2 Ma and 51.6 ± 2.4 Ma, respectively, for a sample collected close to the sample location of sample 6, placing a minimum age constraint on this part of the batholith of about 54 Ma. The similarity of the hornblende and biotite ages requires rapid cooling, either as a result of tectonic unroofing of an earlier emplaced deeply seated intrusion, or due to intrusion at shallow crustal levels. Rapid unroofing of a deeply seated intrusion is inconsistent with K-Ar mineral ages of about 68 Ma for the north margin of the batholith; these data show that parts of the batholith were at shallow crustal levels as early as about 68 Ma, and imply that the central granitic core of the batholith was probably emplaced at shallow crustal levels. It is, therefore, probable that the age of emplacement of the granitic core of the batholith is provided by the $^{206}\text{Pb}/^{238}\text{U}$ age determination of 55.8 ± 0.7 Ma. An older age cannot, however, be ruled out. The lack of resetting of K-Ar mineral systems from the north part of the batholith is consistent with emplacement of

the core of the batholith into a cold supracrustal setting.

Samples 8 and 9 were collected at locations intermediate between the granitic core of the batholith and its more mafic north margin. Age determinations from these samples are discordant, do not define a linear array and cannot be used to constrain the age of the samples.

3.3 Discussion and Conclusions

Nisling Assemblage orthogneiss (PPo):

U - Pb zircon dating indicate that the Early Mississippian plutonic protolith of two mica granitic augen orthogneiss of the Nisling Assemblage lies within the age range established for similar orthogneiss of the Early Mississippian Mink Creek Suite (Mortensen, 1992) of the Yukon - Tanana terrane. This data strongly supports the thesis that the Nisling Assemblage and the Yukon-Tanana terrane are, at least in part, correlative.

Aishihik Batholith (eJab):

The Aishihik Batholith, at least part of which was emplaced at $187.0 \pm 9.7/-0.9$ Ma, appears to be significantly younger than Late Triassic volcanic rocks of the Lewes River Group and cannot, therefore, be their plutonic root. Intrusion in the Early Jurassic is, however, consistent with the emplacement age of other Klotassin Suite intrusions. It seems likely that the Klotassin Suite represents the plutonic roots of the Hazelton volcanic arc, an Early Jurassic arc developed on the Stikine terrane. This arc resulted in the accumulation of marine and non-marine, calc-alkaline andesitic to rhyolitic pyroclastic deposits of the Hazelton Group (Tipper and Richards, 1976).

The presence of a component of inherited zircon thought to be Paleozoic in age may have been derived from orthogneiss of the Nisling Assemblage. The presence of a component of significantly older inherited zircon indicate contamination of the batholith by an Early Proterozoic (average age) crustal source. This is consistent with Rb-Sr mineral - whole rock isochrons for two samples of the batholith which yielded $^{87}\text{Sr}/^{86}\text{Sr}$ initial ratios of 0.706 - 0.707 and which indicate contamination of the batholith by radiogenic strontium from older crust (LeCouteur and Tempelman-Kluit, 1976).

A U-Pb titanite cooling age of 185.2 ± 1.3 Ma suggests that the batholith cooled from greater than 800°C (the Pb closure temperature of zircon (Heamon and Parrish, 1991)) to below 600°C (the Pb closure temperature of titanite (Heamon and Parrish, 1991)) in less than 13 Ma, and probably within about 3 Ma. This corresponds to a cooling

rate of between about 15 and 70 $^{\circ}\text{C}/\text{Ma}$. These results are unexpectedly high given that the batholith was emplaced at moderate to deep crustal levels as indicated by its coarse-grained nature; by the presence of magmatic epidote; by its foliaform contact with schist and gneiss of the adjacent Nisling Assemblage; by the syn-plutonic metamorphic mineral paragenesis developed in the Nisling Assemblage which is consistent with peak metamorphism at pressures of greater than 7 kbar; and by geobarometric studies that suggest syn-plutonic metamorphism of the Nisling Assemblage occurred at pressures of greater than 8 kbar (Chapter V - this study). Rapid cooling is also unexpected given the large size of the batholith, and the addition of heat to the batholith which occurred during this interval as a result of the intrusion of plutons of pink quartz monzonite.

Some (probably most) of the cooling of the batholith was likely accomplished by uplift and erosion. Rapid uplift of the Aishihik Batholith to shallow crustal levels is consistent with the intrusion of the batholith by plutons of pink quartz monzonite of the Long Lake Suite at shallow crustal levels, probably within 10 Ma of the emplacement of the Aishihik Batholith. Emplacement of the plutons of pink quartz monzonite at shallow crustal levels is indicated by the presence of miarolitic cavities in the plutons; by syn-intrusive brittle deformation of the wall rocks, including brecciation; and by the presence of an extensive dyke swarm associated with the intrusions (this study). Assuming a geothermal gradient of 20 $^{\circ}\text{C}/\text{km}$ (i.e. each km of uplift is equivalent to a 20 $^{\circ}\text{C}$ drop in temperature), and assuming that all cooling is the result of uplift, a cooling rate of between 15 and 70 $^{\circ}\text{C}/\text{Ma}$ corresponds to an uplift rate of between 0.075 and 0.35 cm/year. These uplift rates are similar to uplift rates observed in modern collision zones, including Taiwan and the Himalayas (Copeland *et al.*, Wang and Burnett, 1990), and suggest that uplift of the Aishihik Batholith resulted from a collisional tectonic event that involved the Nisling Terrane.

Long Lake pink quartz monzonite (eJII):

Plutons of pink quartz monzonite are younger than $187.0 \pm 9.7/-0.9$ Ma, the age of at least part of the Aishihik Batholith, and are older than 189.7 ± 3.3 Ma, a U-Pb titanite cooling age for a sample of pink quartz monzonite. These data suggest that the Long Lake Plutonic Suite was, at least in part, emplaced within 10 Ma of the emplacement of the Aishihik Batholith. This is consistent with the close spatial relationship between intrusions of the Long Lake Suite and older intrusions of Klotassin Suite foliated hornblende granodiorite evident throughout southwest Yukon (Tempelman-Kluit, 1974).

It is notable that the titanite age determination from the sample of the Aishihik

Batholith (185.2 ± 1.3 Ma) is younger than the titanite age determination for the sample of the Long Lake Plutonic Suite. The Aishihik Batholith sample was collected more than 50 km east of the Long Lake Plutonic Suite sample site. These diachronous titanite cooling ages may indicate that the eastern part of the Aishihik Lake area was uplifted and cooled prior to uplift of the more western parts of the area.

Like samples of the Aishihik Batholith, samples of pink quartz monzonite reveal the presence of a component of inherited zircon. However, the age of the inherited component could not be determined. Sr initial ratios of 0.706 - 0.707 for two samples of the pink quartz monzonite, reported by LeCouteur and Tempelman-Kluit (1976), mimic those reported for the Aishihik Batholith. These data suggest that plutons of the Long Lake Suite may have been contaminated by the same crustal rocks responsible for contamination of the Aishihik Batholith.

Ruby Range Batholith (KTrr):

The north margin of the Ruby Range Batholith was emplaced between about 68 and 78 Ma, while the south margin was emplaced between about 69 and 90 Ma. The core of the batholith appears to have been emplaced at about 55 Ma, although an older emplacement age cannot be ruled out. These data suggest that the batholith is the product of at least two distinct magmatic events. Widespread Eocene sillimanite-grade thermal metamorphism in southwest Yukon (Erdmer, 1989; 1990; 1991; Mortensen and Erdmer, in press) may correspond with the magmatic event responsible for the emplacement of the internal portion of the batholith. The U-Pb zircon data are not, however, unequivocal and further detailed U-Pb isotopic studies of zircon and titanite are required to resolve the magmatic evolution of the batholith.

A component of inherited zircon suggests that the Ruby Range Batholith was contaminated by a crustal source with a Proterozoic average age. Sr initial ratios, reported by LeCouteur and Tempelman-Kluit (1976), range from 0.705 to 0.706 for samples of the batholith, whereas southwest of the batholith Sr initial ratios dip below 0.705. These data are consistent with contamination of the batholith either by rocks of a westward thinning wedge of older crust (possibly the same crust responsible for contamination of the Aishihik Batholith) or by rocks of a heterogeneous block of relatively juvenile crust.

IV. STRUCTURAL GEOLOGY

4.1 Introduction

In the study area the west margin of the Stikine terrane, represented by hornblende granodiorite of Aishihik Batholith, is exposed. Metamorphosed continental clastic, carbonate, and amphibolitic rocks of Nisling Assemblage crop out immediately west of the Stikine terrane (Figures 1.1 and 4.1). Rocks of both Aishihik Batholith and Nisling Assemblage are deformed. Deformation of the batholith is indicated by the development of a penetrative foliation; and by recrystallization (Tempelman-Kluit, 1974). Nisling Assemblage is deformed and is characterized by a penetrative foliation and by a quartz rodding lineation (Tempelman-Kluit, 1974). Foliation is deformed and forms small-scale, asymmetric, west-verging kink folds. A coarse crinkle lineation associated with the small-scale folds is often evident (Tempelman-Kluit, 1974; Erdmer, 1989).

The timing of deformation is poorly constrained. Tempelman-Kluit (1974) suggested that regional shearing and metamorphism post-dated crystallization of the Aishihik Batholith and resulted in the development of foliation in both Nisling Assemblage and in Aishihik Batholith. Erdmer (1989), mapping to the south of the Aishihik Lake area, observed the truncation of Nisling Assemblage foliation and crenulation by foliated granodiorite thought to be correlative with the Aishihik Batholith. The bulk of Nisling Assemblage structures were interpreted to be pre-Early Jurassic, while foliation of the granodiorite was interpreted to indicate post-Early Jurassic, pre-Eocene tectonism. Currie (1992), mapping in northwestern British Columbia, observed that foliated granodiorite of the Hale Mountain Pluton, which is the same age as Aishihik Batholith, is in fault contact with foliated rocks of the Nisling Assemblage. Foliation in the granodiorite and in Nisling Assemblage parallels the contact and is attributed to shearing at lower amphibolite facies conditions between 185 Ma and 170 Ma.

The tectonic significance of these fabrics remains a matter of much conjecture. Tempelman-Kluit (1979) inferred that Nisling Assemblage is the basement of Stikine terrane. Regional deformation and the development of fabric in both the Nisling Assemblage and the Aishihik Batholith was thought to be related to collision with, and overthrusting of, North America by Stikine terrane beginning in the Middle Jurassic. Currie (1992) suggests that Nisling Assemblage and Stikine terrane evolved far removed from one another and that the development of structural fabrics resulted from the Early to Middle Jurassic tectonic juxtaposition of these terranes. Hansen (1990) correlated Nisling Assemblage with the North American continental margin sequence. Structural fabric

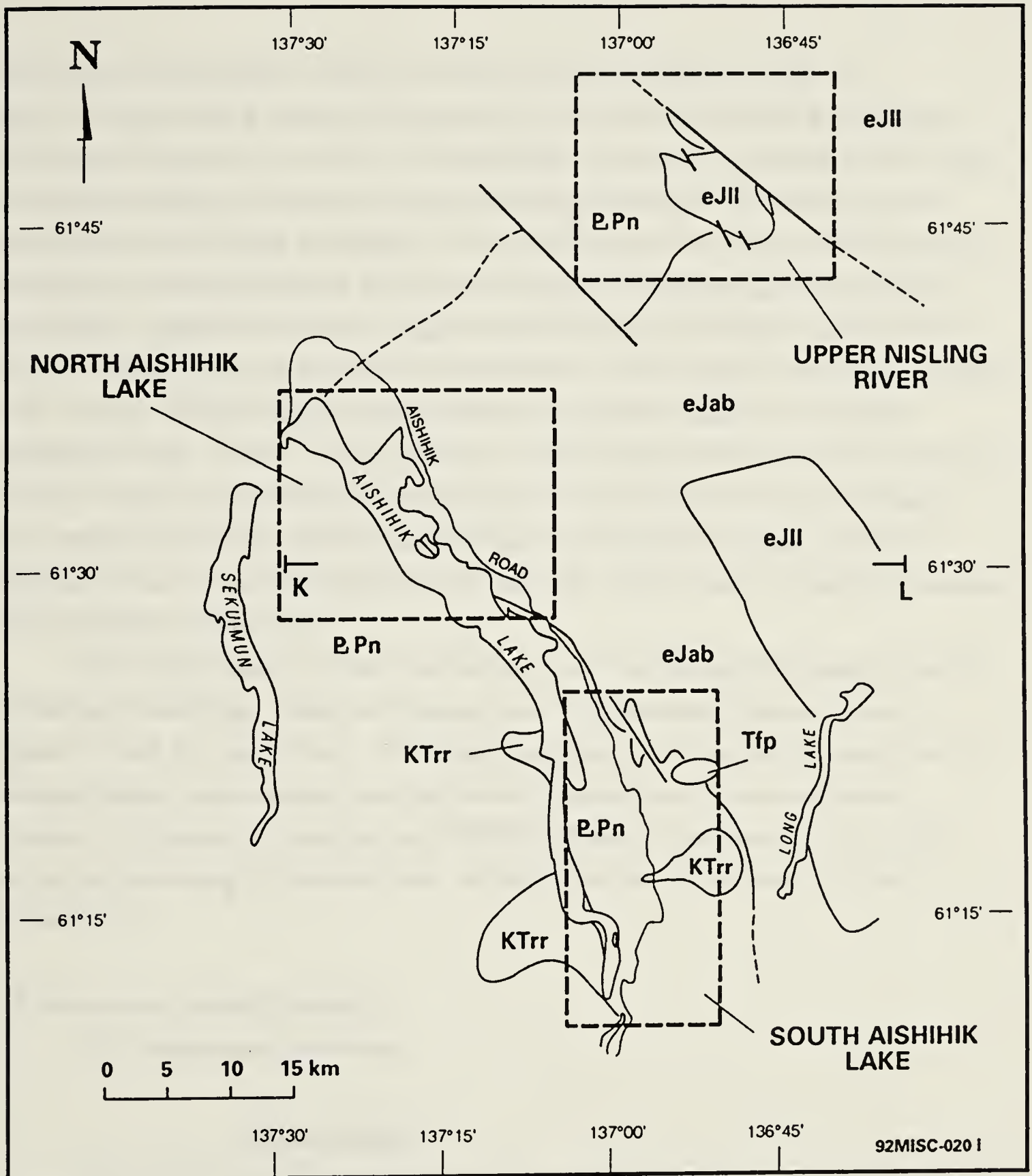


Figure 4.1 General geology of part of the Aishihik Lake map-area, modified after Tempelman-Kluit (1974). PPn - the Nisling Assemblage; eJab - the Aishihik Batholith; eJll - Long Lake Suite intrusions; KTrr - the Ruby Range Batholith; Tfp - Tertiary feldspar porphyry. The boxes indicate the locations of detailed maps shown in Figure 4.2 (a - South Aishihik Lake; b - North Aishihik Lake; and c - Upper Nisling River). Location of cross-section K - L shown in Figure 4.6 is also indicated.

development was thought to reflect two distinct tectonic events including: 1) top-to-the-east shearing during overthrusting of North America (including the Nisling Assemblage) by parts of the Yukon - Tanana terrane in the Early to Middle Jurassic; and 2) significant Middle Cretaceous extension resulting in the uplift and exposure of the tectonically buried Nisling Assemblage. This model implies that rocks of Stikine terrane, including the Aishihik Batholith, have been tectonically juxtaposed against the Nisling Assemblage. Mortensen (in press), suggested that Nisling Assemblage correlates with Yukon - Tanana terrane on the basis of homotaxiality of the Nisling Assemblage and strata of the Yukon - Tanana terrane; broadly similar metamorphic grade; and correlative orthogneiss suites. Yukon - Tanana terrane is characterized by structural fabrics related to pre-Late Triassic but post-Permian mylonitization and penetrative ductile deformation (D₁); regional-scale thrust faulting and imbrication with ophiolitic strata of the Slide Mountain terrane in the Early Jurassic (D₂); and Late Jurassic, Early Cretaceous extension (D₃) (Mortensen, 1990;1992).

This chapter reports on structural fabrics evident in the Aishihik Batholith and in the Nisling Assemblage. Maps and cross-sections with structural data are shown in Figures 4.2 and 4.3, respectively. The relative and absolute timing of the development of structural fabrics is documented and the tectonic implications of structural fabrics discussed. Appendix 4.1 describes the TRIPOD software (Charlesworth *et al.*, 1989) used in the processing of structural data. All structural data are included on a disc in Enclosure 4.1.

4.2 Structure of Aishihik Batholith

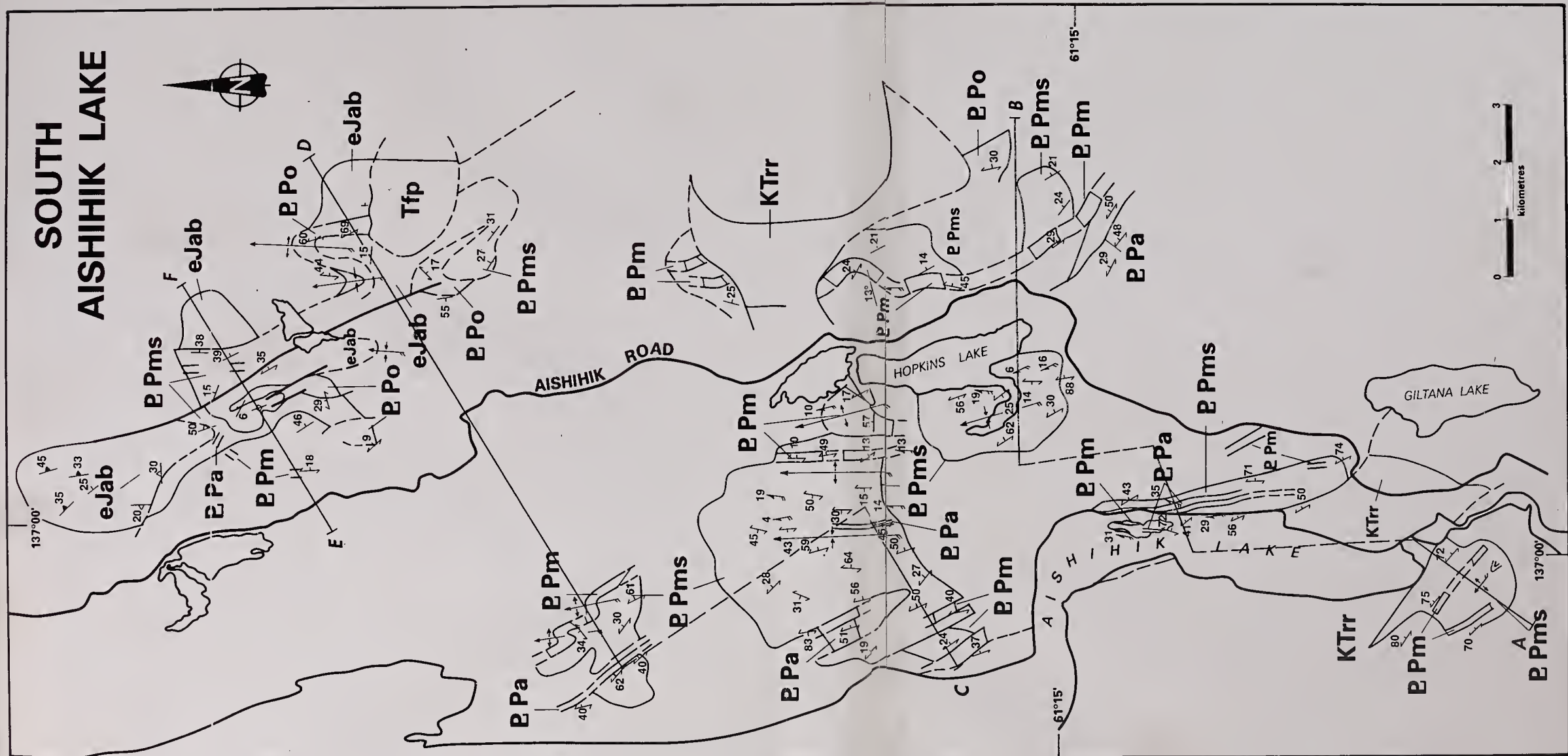
4.2.1 Mesoscopic structures

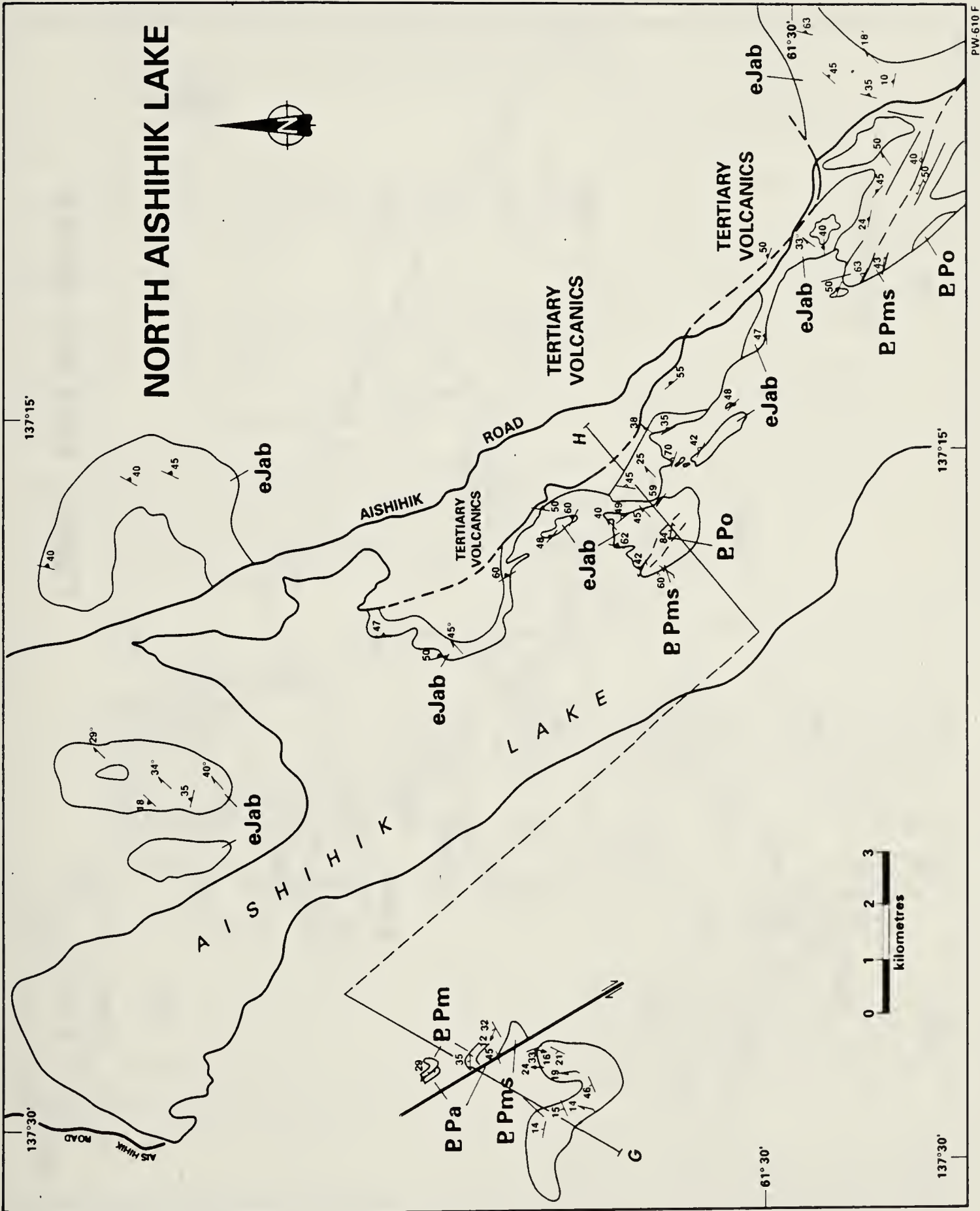
Planar elements

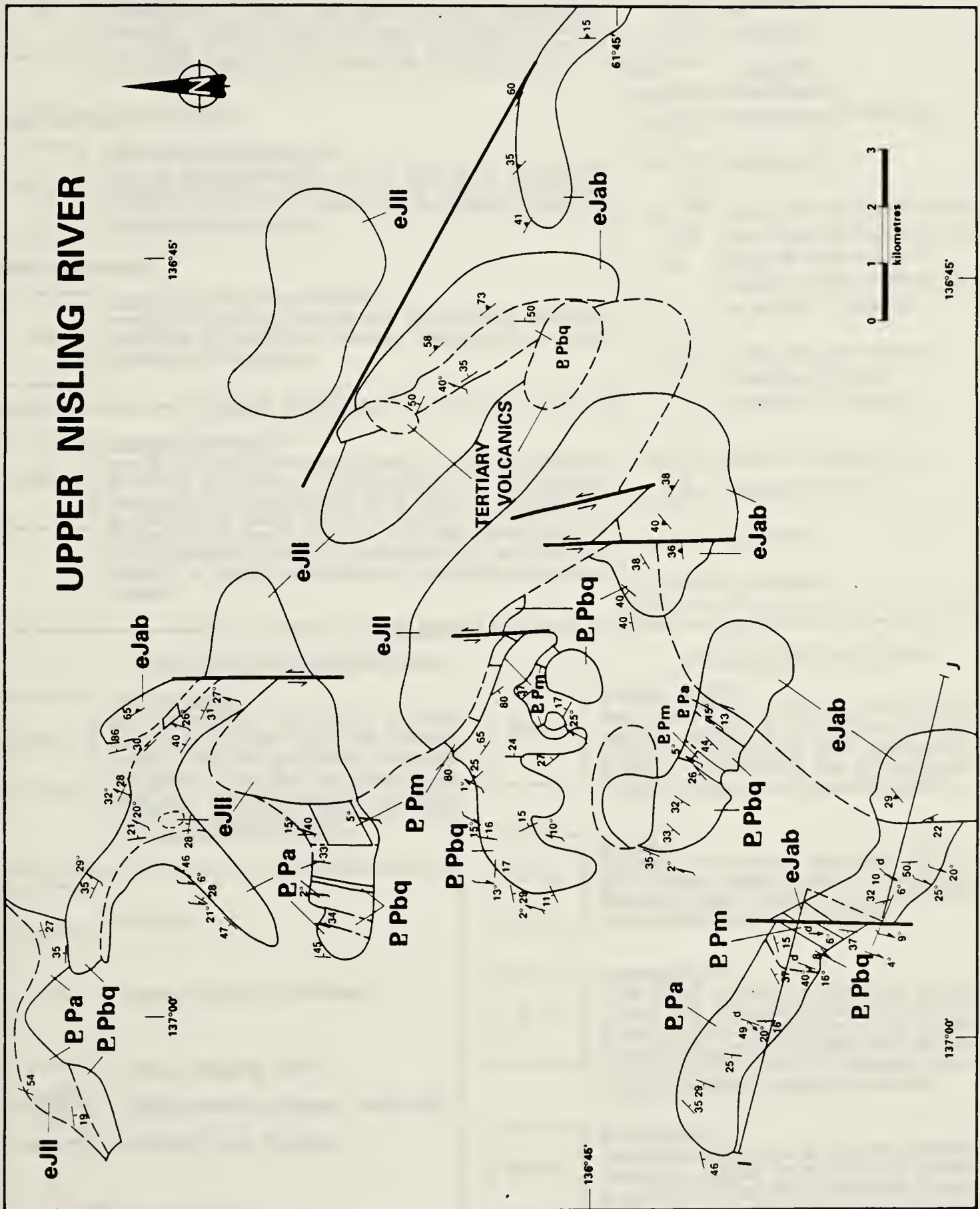
The Aishihik Batholith is characterized by a planar fabric (S_m) which is defined by the parallelism of mineral grains including: euhedral, poikilitic, K-feldspar megacrysts up to 5 cm in length; subhedral to euhedral elongate lathes of chalky white plagioclase up to 1.5 cm in length; subhedral to euhedral elongate prisms of dark green to black hornblende up to 1.5 cm in length (Plate 2.7); and fine- to medium-grained biotite booklets. Finely crystalline, leucocratic aplite veins lie along and parallel the plane of foliation.

S_m is mildly deflected around microgranitoid enclaves. The enclaves are characteristically tabular and consist of leucocratic, finely crystalline granite. Foliation within the enclaves is well developed and parallels the enclave margins and foliation in the

Figure 4.2 Detailed maps showing the distribution of map units and orientation data for each of: a) the South Aishihik Lake area; b) the North Aishihik Lake area; and c) the Upper Nisling River area. The location of these maps is shown in Figure 4.1.







LEGEND

PLUTONIC ROCKS

TERTIARY

**FELDSPAR PORPHYRY**

heterogeneous igneous suite which includes plugs and small plutons of orange and pink weathering, flesh colored, miarolitic, massive, feldspar and quartz - feldspar porphyry; and dykes of brown and dark green weathering, green to buff colored, feldspar and hornblende feldspar porphyry.

CRETACEOUS & TERTIARY

**RUBY RANGE BATHOLITH**

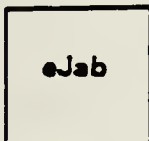
grey to tan weathering, grey to dark grey, medium to coarsely crystalline, massive to mildly foliated, hornblende and biotite hornblende diorite and granodiorite to nebulitic hornblende biotite granite.

EARLY JURASSIC

**LONG LAKE PLUTONIC SUITE**

orange weathering, orange and pink colored, coarsely crystalline to porphyritic, massive, miarolitic, quartz and biotite quartz monzonite.

STIKINE TERRANE

**AISHIHIK BATHOLITH**

grey to light grey weathering, grey to dark grey colored, coarsely crystalline, equigranular to K-feldspar megacrystic, hornblende and biotite hornblende granodiorite to quartz diorite. A foliation, defined by the alignment of mineral grains, is commonly developed. A second foliation, defined by protomylonitic, and gneissic banding, is locally developed and overprints the mineral foliation

METAMORPHIC ROCKS

STRUCTURAL ORIENTATION SYMBOLS
AISHIHIK BATHOLITH

 S_m Foliation

 S₁ Foliation

Lineation

NISLING ASSEMBLAGE

 Compositional Banding (S₁)

 Schistosity (S₂)

 Fold of compositional banding (F₂) with inclined axial surface, plunge of hinges line, and vergence viewed down plunge (S- sinistral, D-Dextral)

 F₂ fold axis and vergence viewed down Plunge (S- sinistral, D-Dextral)

 Folds of schistosity (F₃)

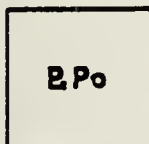
Antiform & Synform

 L₂ Lineation

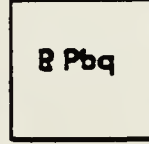
 L₃ Lineation

NISLING ASSEMBLAGE

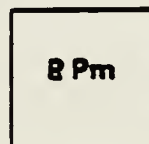
DEVONO-MISSISSIPPIAN

**ORTHOGNEISS**

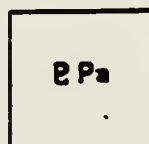
tan weathering, light grey colored, medium to coarsely crystalline, feldspar augan, muscovite and biotite muscovite orthogneiss; and dark grey weathering, dark grey colored, medium grained, hornblende and biotite hornblende diorite and quartz diorite orthogneiss.

**BROWN QTZITE**

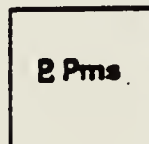
dark to light brown weathering, brown to buff colored, medium to fine grained, locally graphitic, micaceous and feldspathic quartzite. Includes thin and discontinuous marble, amphibolite and micaschist lenses.

**MARBLE**

light grey to light brown weathering, white to grey colored, fetid, coarsely crystalline, laminated calcite marble. Includes minor skarn, amphibolite, and calc-silicate

**AMPHIBOLITE**

dark green to black weathering, green colored, fine to coarsely crystalline, gneissic to well foliated, hornblende and biotite hornblende quartzite, micaschist and marble, and significant amounts of pistachio green, epidote hornblende diopside calc-silicate

**MICASCHIST**

Brown weathering, dark to light grey colored, medium to coarsely crystalline, well foliated to gneissic, migmatitic, muscovite biotite schist with minor grey quartz gneiss and brown weathering, tan colored, medium grained, foliated, micaceous & feldspathic quartzite. Includes minor amphibolite and marble.

PALEOZOIC & OLDER

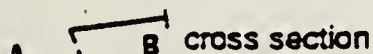
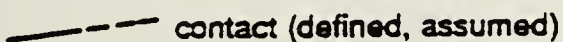
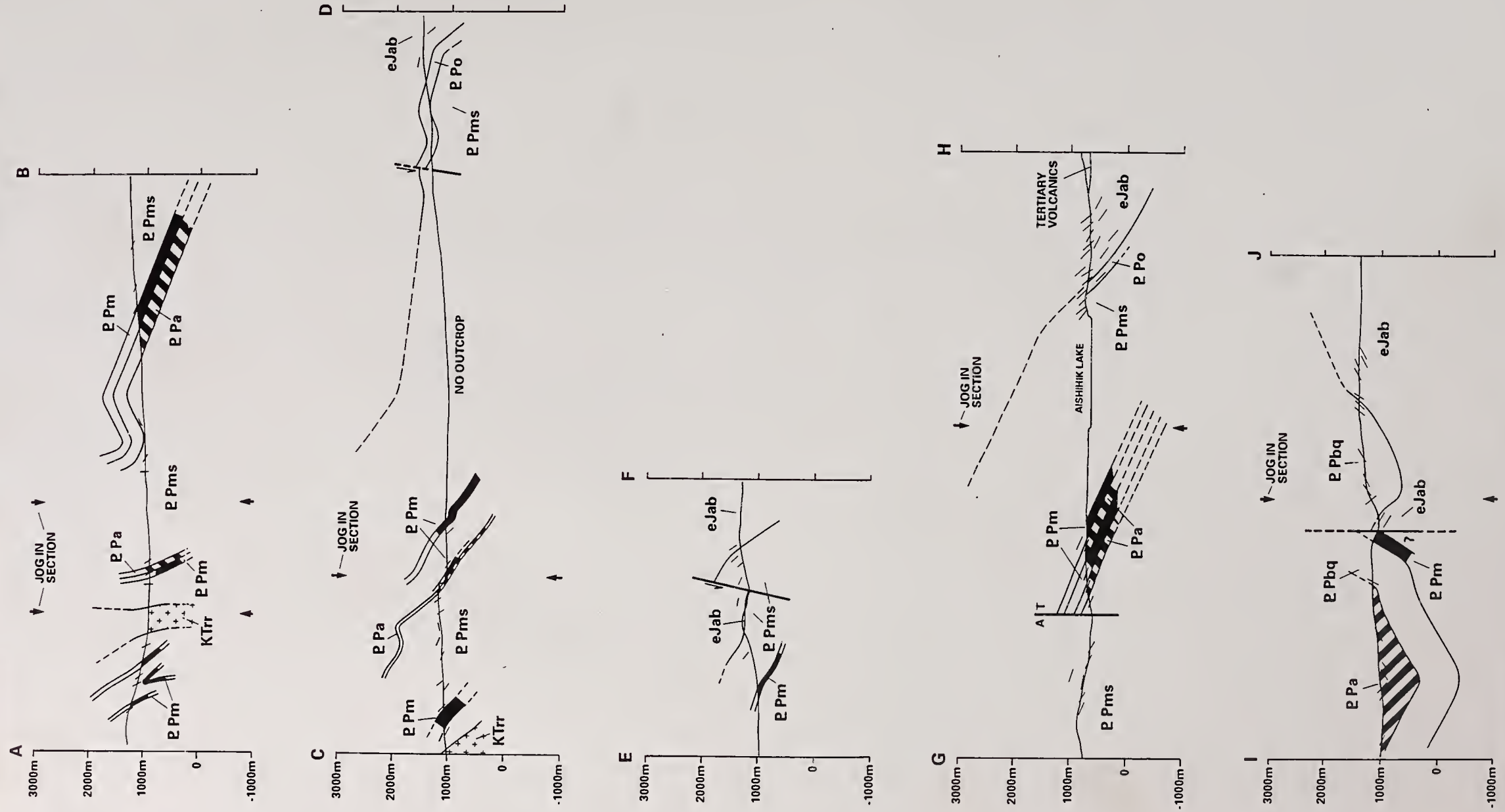


Figure 4.3 Cross-sections, the locations of which are indicated on the maps in Figure 4.2. Symbols are defined in the legend to Figure 4.2. Marble is colored black; amphibolite is indicated by a striped pattern. The apparent dip of foliation is indicated. Data points represent orientation data projected onto the line of section



enclosing granodiorite. Mafic, microdiorite, hornblendite, and hornblende - biotite enclaves occur both as foliaform lenses that extend along the plane of foliation (Plate 4.1) and as discordant bodies whose contacts are oriented at an angle to foliation. Foliation within the enclaves is usually well developed and parallels the foliation in the enclosing granodiorite. Locally foliation in the enclaves intersects foliation in the enclosing granodiorite at a high angle. Foliation is usually poorly developed adjacent to, and exhibits mild deflection about, rare micaschist inclusions (Plate 4.2).

S_m is relatively uniformly developed. It is more obvious in the more mafic, biotitic phases of the batholith. In coarsely crystalline, leucocratic phases, the foliation is poorly defined and only a vague planarity can be discerned. It is thought that the foliation is better developed towards the margin of the batholith, although this cannot be documented (Tempelman-Kluit, 1974). Immediately adjacent to the margin of the batholith the foliation can sometimes be difficult to identify. The central part of the batholith is poorly exposed, is underlain by highly weathered, fissile granodiorite, and is intruded by large volumes of pink quartz monzonite (Figure 4.1).

The grains that together define S_m appear undeformed. K-feldspar megacrysts are sharply defined, euhedral, unbroken and are characterized by detailed internal poikilitic structures which suggest a complex magmatic history (Plate 2.7). Plagioclase and hornblende phenocrysts are similarly pristine. There is no evidence to suggest that these grains are not primary igneous minerals. Quartz occurs as clear, anhedral eyes interstitial to feldspar and hornblende. Locally quartz appears as clear to milky white streaks that mantle and bend around other mineral grains, suggesting that some deformation and recrystallization has occurred.

Veins of coarse pink to white micaceous pegmatite postdate foliation. These veins intrude, truncate, and locally result in offset of, foliated granodiorite (Plate 4.1). Rarely, pegmatite veins are characterized by rafts of foliated granodiorite. Mica within the pegmatite veins show no preferred orientation. Massive andmiarolitic veins and plutons of pink quartz monzonite (Long Lake Suite), which crystallized at about 185 Ma (this study) intrude and truncate foliated hornblende granodiorite of the Aishihik Batholith (Tempelman-Kluit, 1974; this study).

Foliation parallels the margins of the batholith and foliation in the wall rock schists of the Nisling Assemblage (Figures 4.2 a, b, c, and 4.3). Along the west margin of the batholith, the foliated granodiorite overlies schist of the Nisling Assemblage with the contact dipping gently to steeply to the east to northeast (Figure 4.4). Along the north margin of the batholith rocks of the Nisling Assemblage overlie foliated granodiorite that



Plate 4.1 A concordant mafic microdiorite enclave (md) in foliated hornblende granodiorite. A discordant vein of massive pink pegmatite (p) truncates foliation and the enclave. Some offset of the enclave across the vein is evident. The scale bar at lower right represents 5 cm.



Plate 4.2 A well foliated micaceous quartzite inclusion in the Aishihik Batholith observed in the Upper Nisling River area. Hornblende granodiorite that invades the inclusion (indicated by arrows at center) exhibits little or no foliation. The knife at upper left is 4 cm in length.

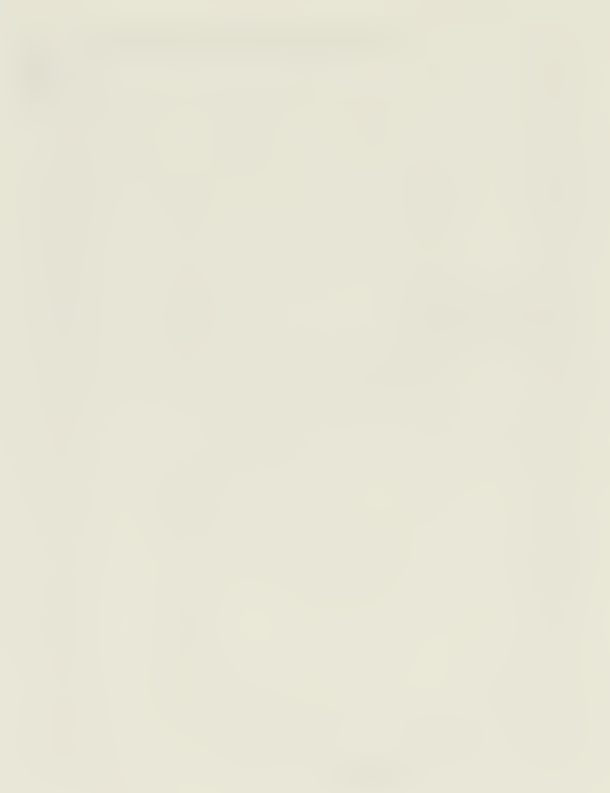
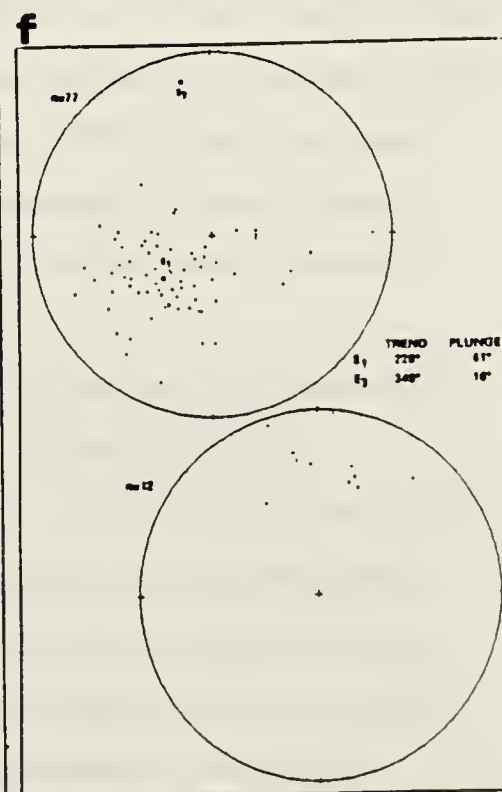
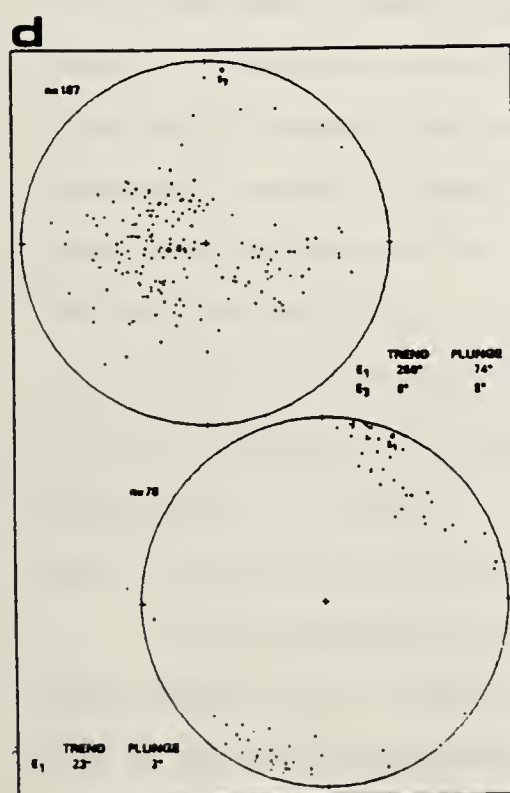
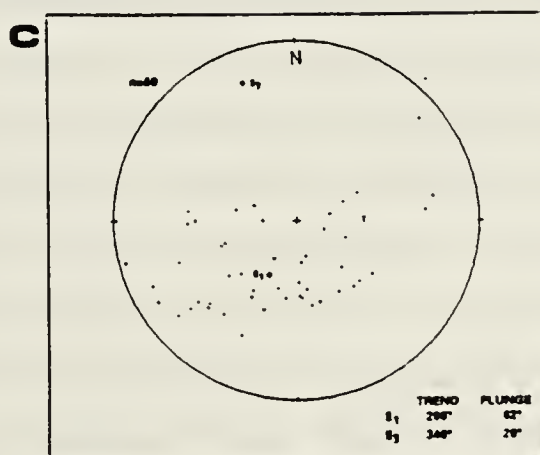
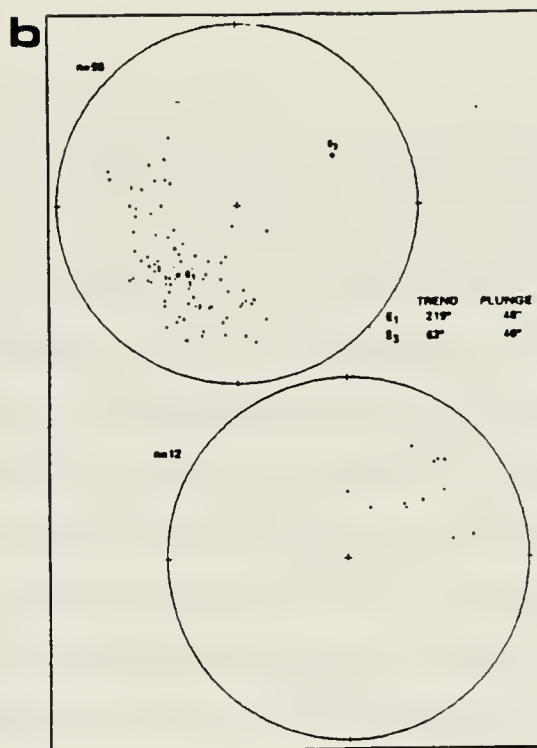
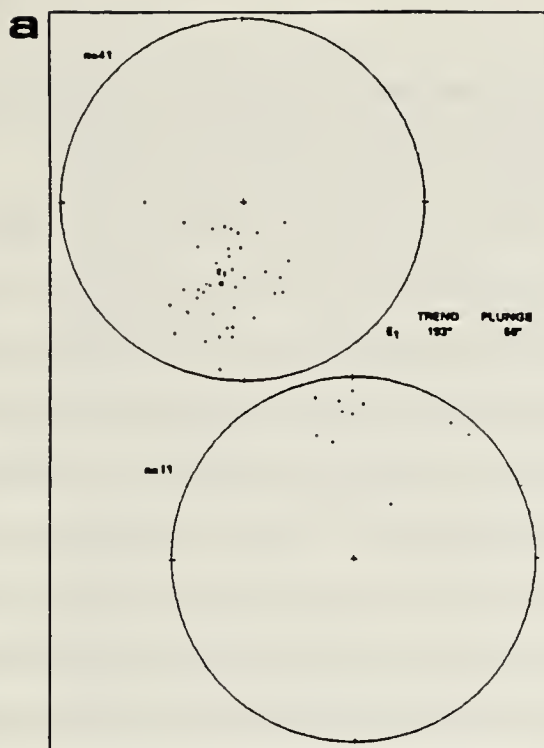


Figure 4.4 Equal area stereo-plots of poles to foliation (upper) and lineations (lower) for: a) Aishihik Batholith in the South Aishihik Lake area; b) Aishihik Batholith in the North Aishihik Lake area; c) Aishihik Batholith in the Upper Nisling River area; d) Nisling Assemblage in the Upper Nisling River area; e) Nisling Assemblage in the South Aishihik Lake area; and f) Nisling Assemblage in the North Aishihik Lake area. In all equal area plots: 1) each cross indicates a data point; 2) the total number of data points for each plot is indicated by n ; 3) the orientation of the E_1 eigenvector indicates the mean orientation of a cluster of data points; and 4) the orientation of the E_3 eigenvector indicates the pole, or fold axis, to a girdle of normals to a folded surface. Where fewer than 15 orientations were collected ($n < 15$) no eigenvectors are calculated. See text for discussion.



dips gently to the north or northwest (Figure 4.4).

A second planar fabric, S_t , is defined by: 1) thin (1 to 500 cm), streaky, finely crystalline to aphanitic, protomylonite bands (Plate 4.3); 2) gneissic banding (Plate 4.4) in which coarsely crystalline, foliated granodiorite is interleaved with finely crystalline bands characterized by recrystallized biotite and by rounded, subhedral to euhedral, fractured K-feldspar augen that lack internal structure; and 3) discrete shears which consist of finely crystalline to aphanitic mylonite and protomylonite and which are commonly characterized by recrystallized biotite. Layering in foliated to gneissic hornblende granodiorite adjacent to the shears bends into and is offset across the shears (Plate 4.5). The shears are commonly discrete, are developed every 5 to 10 cm measured along the S planes, are subhorizontal to west-dipping and intercept foliation at 10° to 30° . Strata above the shears are displaced with a top-to-the-west sense of shear.

The S_t fabric is associated with migmatite of the Aishihik Batholith. Coarsely crystalline to aphanitic, melanocratic and leucocratic phases anastomose with and pass laterally into one another (Plate 4.6). The melanocratic phase is generally more finely crystalline and exhibits more recrystallization of feldspars and biotite. Migmatites were not observed away from the areas in which the S_t fabric was developed.

Development of the S_t fabric is heterogeneous. Thin shear bands alternate with unsheared but foliated granodiorite on a scale of 1 cm to tens of meters. Contacts between sheared granodiorite and foliated but unsheared granodiorite range from sharp, discrete surfaces to broad gradational zones. Sheared granodiorite passes along strike and vertically, with respect to foliation, into unsheared granodiorite. S_t is best developed in a 100 m thick zone, measured perpendicular to foliation, adjacent to the west margin of the batholith. However, along the east shore of the Aishihik Lake, adjacent to the large island in the North Aishihik Lake area the fabric is developed at least 500 m from the contact. Conversely, coarsely crystalline, foliated but unsheared granodiorite is locally present immediately adjacent to the margin of the batholith. S_t is not evident along the north margin of the batholith.

S_t post-dates and overprints S_m . Primary magmatic grains, including potassium feldspar, plagioclase and hornblende, are fractured, broken, and recrystallized. Deformation has resulted in a reduction in grain size. Biotite grains associated with shear bands overprint and have grown at the expense of the pre-existing mineral paragenesis.

The relationship of veins of coarse pink to white micaceous pegmatite to the S_t fabric is equivocal. Locally the veins cross-cut, truncate, and clearly post-date S_t (Plate 4.4). In the southeast corner of the North Aishihik Lake area sheared granodiorite



Plate 4.3 A thin (2 cm in width) protomylonite band, indicated by arrows, in foliated hornblende granodiorite of the Aishihik Batholith, observed near the west margin of the batholith in the South Aishihik Lake area. S_l is parallel with S_m in the overlying granodiorite but cuts across S_m in underlying granodiorite. The knife at lower left is 4 cm in length.



Plate 4.4 Gneissic banding in the Aishihik Batholith, observed along the east shore of Aishihik Lake in the North Aishihik Lake area near the large island. A thick vein of massive micaceous quartz - feldspar pegmatite vein cuts across and clearly post-dates the development of the gneissic banding. A rock hammer, for scale, is evident at lower center.



Plate 4.5 Hornblende granodiorite and diorite gneiss of the Aishihik Batholith, observed on the large island in the North Aishihik Lake area. The photograph was taken looking to the south. A rock hammer, for scale, is evident at lower left. Spaced shear planes are highlighted and dip shallowly to the west. Foliation and gneissic banding are offset down-dip towards the west across the shears, consistent with a top-to-the-west sense of shear.



Plate 4.6 Migmatite observed in the Aishihik Batholith along the east shore of Aishihik Lake near the large island in the North Aishihik Lake area. A thin mafic selvage is evident along the margins of most of the leucocratic (aplite) pods. The knife at lower left is 4 cm in length.

contains boudins of sheared, pink micaceous pegmatite (Plate 4.7). The boudins are elongate, extend along, and lie within, the plane of shearing and are interpreted to represent a once continuous pegmatite vein that was sheared and dismembered during the development of S_t . These mutually contradictory relations suggest that the intrusion of the pegmatite veins and deformation were coeval.

S_t lies parallel to subparallel to S_m fabric (Figures 4.2 a and b). The S_t fabric is, however, irregular. Gneissic and protomylonitic bands are anastomosing, lenticular, and discontinuous. As indicated above, S_t locally consists of two planar elements including discrete shears oriented at small to moderate angles to foliation and gneissosity.

Folds

Deformation of leucocratic aplite veins has produced tight to isoclinal, recumbent to gently inclined, horizontal to gently plunging folds (F_t) (Plate 4.8). The axial surfaces of the folds parallels foliation in the enclosing granodiorite. Symmetric and asymmetric folds with amplitudes of 3 to 100 cm are observed. The geometry of the folds is similar to weakly divergent. Aplite veins are thinned along fold limbs. Locally the veins pinch out, and form discontinuous boudins. In hinges and limbs of the folds, where the veins cut across foliation, significant thickening of the veins is common. Foliation is locally folded parallel with the aplite veins. Elsewhere, foliation passes through the folds unaffected. Locally, symmetric and asymmetric ptigmatic folds of aplite, with amplitudes of 2 to 10 cm, are developed (Plate 4.9). In the North Aishihik Lake area (Figure 4.2 b) near the east shore of the Aishihik Lake adjacent to the large island an outcrop-scale (wavelength = 10 m), inclined fold which affects coarsely crystalline, foliated granodiorite and which closes up-dip towards the west is developed. In the lower limb of the fold significant grain size reduction and shearing has occurred.

F_t folds are rare. They were only observed along the west margin of the batholith in areas where S_t is well-developed. The hinge lines of the F_t folds appears to trend north - south to northeast - southwest, although no direct measurements on the attitudes of the folds were obtained.

Both S_m and S_t are deformed and define small, closed to open, moderately inclined, gently plunging folds (F_{t+1}) (Plate 4.10). The folds have a kink, or chevron shape, with amplitudes of 1 - 2 cm and wavelengths of less than 5 cm, and are characterized by planar limbs and narrow hinge zones. They are strongly asymmetric, are characterized by moderately east-dipping axial surfaces, and verge towards the west.

F_{t+1} folds are rare. They were only observed along the west margin of the



Plate 4.7 Sheared foliated hornblende granodiorite of the Aishihik Batholith observed immediately above the contact with Nisling Assemblage in the southeast corner of the North Aishihik Lake map-area. Boudins of deformed and sheared, coarsely crystalline pink pegmatite (p) are evident at center and at lower left. The knife is 4 cm in length.

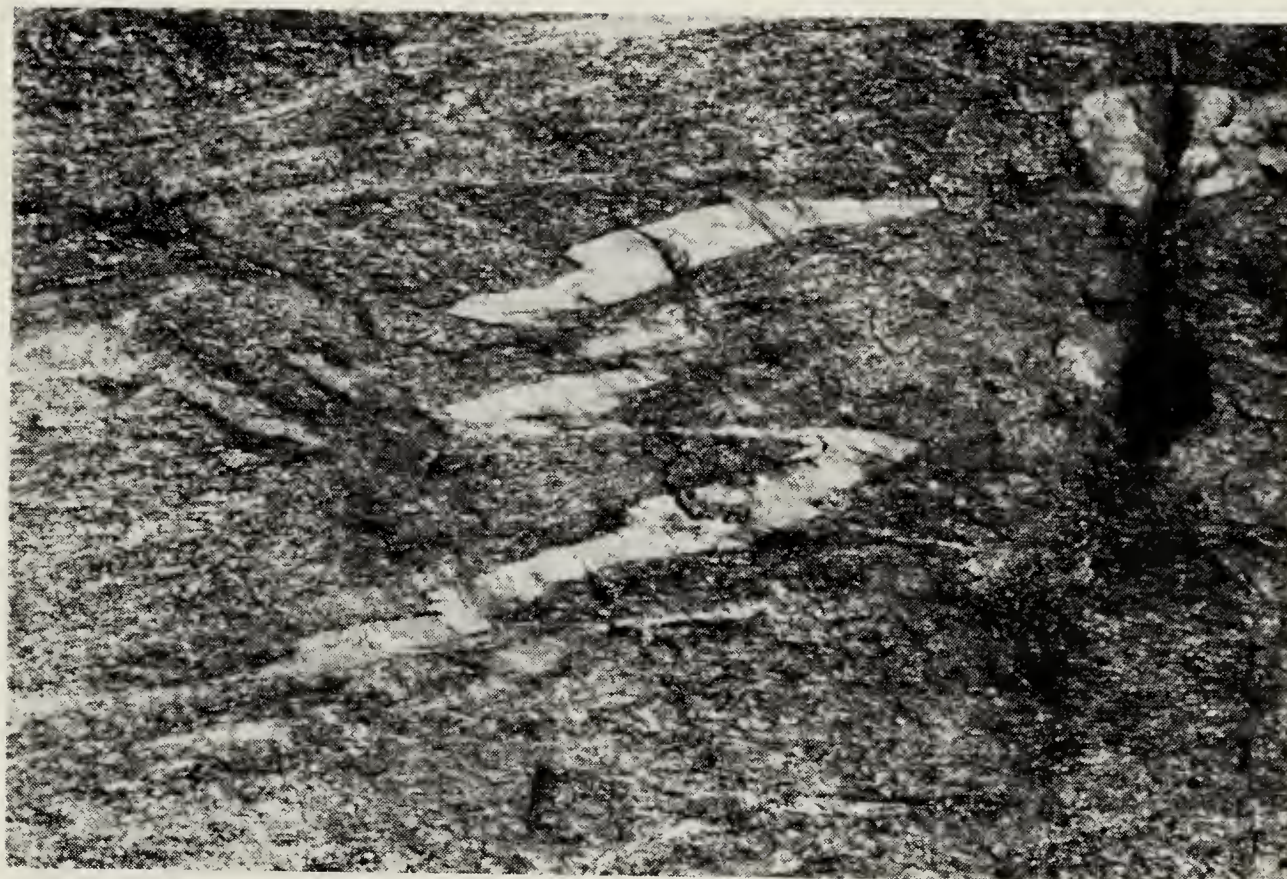


Plate 4.8 A folded vein of finely crystalline aplite observed in Aishihik Batholith in the South Aishihik Lake area. Foliation in the surrounding hornblende granodiorite parallels the axial planes of the folds. The lense cap at right is 6.5 cm in width.



Plate 4.9 Ptygmatic folds of aplite observed in the Aishihik Batholith in the North Aishihik Lake area. The lense cap at lower right is 6.5 cm in width.

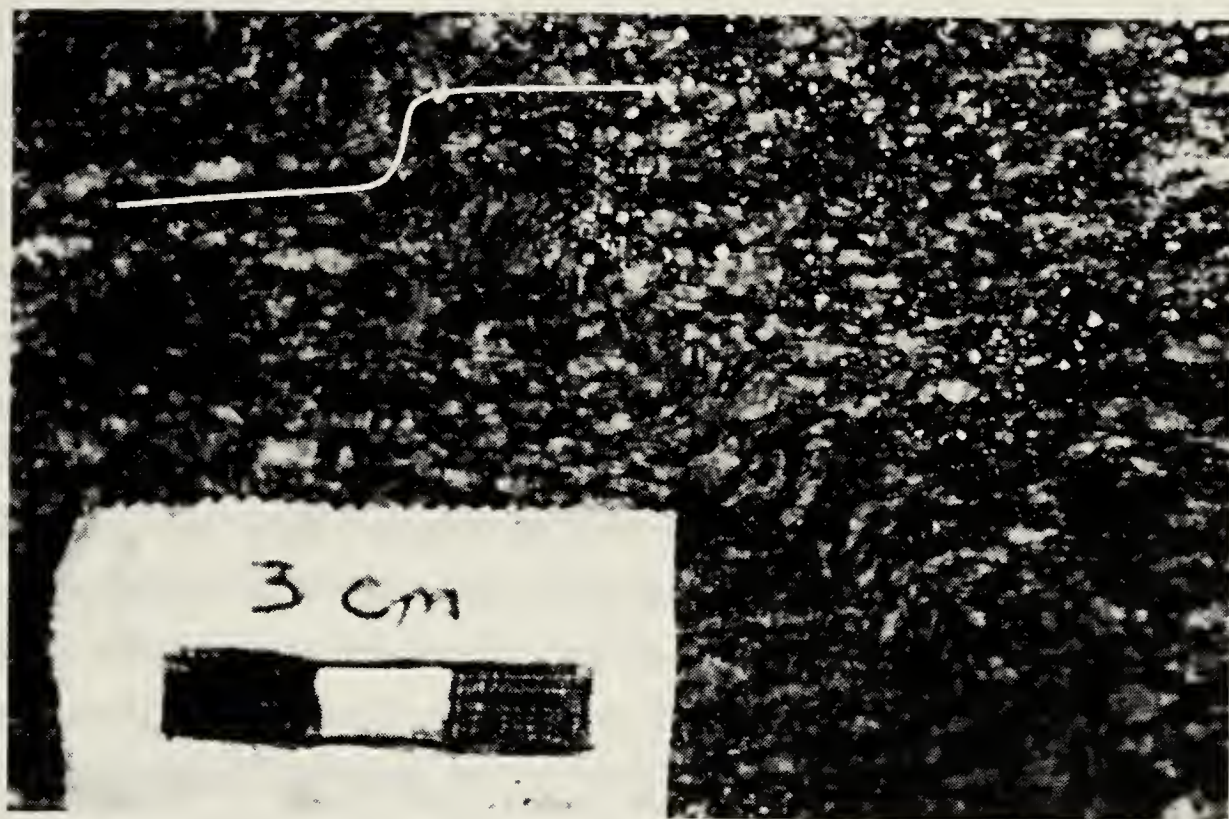


Plate 4.10 An asymmetric kink fold affecting foliated to gneissic hornblende quartz diorite of the Aishihik Batholith. A white line, evident at upper left, parallels foliation and is shown to highlight the geometry of the fold. The photo is taken looking to the north. The fold verges to the west.

batholith close to the contact with the Nisling Assemblage. They overprint and post-date both the S_m and S_t fabrics. The hinge lines of the folds trend north - south to northeast - southwest and are subhorizontal to gently north to northeast plunging.

Map-scale folding of the S_m and S_t fabrics has also occurred (Figures 4.2 a and 4.3). The map-scale folds are upright to steeply inclined, and sub-horizontal to gently north plunging. The folds have rounded to flattened hinge zones and amplitudes and wavelengths of 200 m to 500 m. They are weakly asymmetric, are characterized by vertical to moderately east-dipping axial surfaces, and verge towards the west.

The map-scale folds overprint and post-date both the S_m and S_t fabrics. In addition, they deform the margin of the batholith and the adjacent schists of the Nisling Assemblage. They are best developed along the west margin of the batholith in the region where cross-sections D-D' and E-E' are drawn (Figure 4.2 b). Because the folds affect S_m and S_t , plunge gently to the north, and are west-verging they are interpreted to be large-scale equivalents of the F_{t+1} folds (Figure 4.4).

Linear elements

A lineation (L_m) locally characterizes foliated hornblende granodiorite. It lies within the plane of foliation (S_m) and is defined by the parallel alignment of elongate hornblende prisms and plagioclase laths. A subtle streaking of quartz and potassium feldspar parallels the aligned mineral grains. Locally, the lineation is defined by microcrenulations of biotite. Where leucocratic aplite veins are ptlygmatically folded, isolated aplite rods, thought to represent detached fold hinges, define a strong linear fabric (Plate 4.9).

L_m is poorly developed and is restricted to the west margin of the batholith (Figures 4.2 a and b). Too few orientation measurements were collected to quantitatively assess the orientation of L_m . The data collected however, suggest that L_m is variably oriented plunging shallowly to moderately to the north to east (Figure 4.4).

More than one origin for L_m is probable. The alignment of primary magmatic mineral grains suggests that some lineation is the result of the alignment of mineral grains during magmatic flow. The occurrence of L_m along the west margin of the batholith, where the S_t planar fabric is developed, suggests that the lineation may be due to subsolidus shearing and may reflect elongation within S_t shear zones. This is consistent with the presence of streaky and sheared quartz and feldspar. The crenulation of biotite grains suggest that the lineation may be in part the result of folding of the granodiorite. More detailed fieldwork is necessary to separate out various lineations.

4.2.2 Microscopic structures

S_m foliation is defined in thin section by the parallel alignment of subhedral to euhedral, medium to coarsely crystalline, plagioclase, K-feldspar, hornblende, and, less commonly, biotite grains (Plate 4.11). All grains appear to be primary igneous crystals. Feldspar grains are commonly euhedral. Plagioclase twins parallel the long axis of the plagioclase grains. Plagioclase grains exhibit mild, oscillatory zoning. Poikilitic textures, consisting of concentric growth rings marked by fine grained minerals including hornblende, are observed in K-feldspar megacrysts. Isolated hornblende grains and, more rarely, biotite grains, are aligned parallel with foliation, and are surrounded by feldspar grains which exhibit igneous microstructures.

Quartz occurs as anhedral eyes, interstitial to other grains, which display little or no preferred orientation. Locally, quartz exhibits mild undulatory extinction and the development of elongate subgrains. This suggests that mild solid-state flow, accommodated largely by the deformation of quartz, has occurred.

In samples characterized by S_t , a significantly different microstructural character was observed. S_t is irregular, and consists of isolated, anhedral, fine- to coarsely-crystalline feldspar grains which float in a fine-grained quartzo-feldspathic matrix (Plate 4.12).

Feldspar grains are rounded and equidimensional to oblong. Kink folding, fracturing, and boudinage of feldspar grains is common. Boudin necks and fractures are filled by recrystallized strained and unstrained quartz and mica (Plate 4.13). Plagioclase twins are oriented at a high angle to the long axis of feldspar grains, suggesting that thorough recrystallization has occurred (Plate 4.13).

Quartz occurs as finely crystalline aggregates of equidimensional grains which meet in 120° triple junctions. These aggregates commonly include fine grained feldspar and mica (Plate 4.12). Larger quartz grains are elongate, exhibit undulose extinction and commonly consist of quartz ribbons.

Hornblende is rare to absent in rocks in which the S_t foliation is well developed. Biotite is more common than it is elsewhere and occurs as fine-grained fish with undulose extinction. Biotite also occurs as fine- to medium-grained booklets which are sub-parallel to foliation. These grains are undeformed to mildly strained and often occur in strain shadows adjacent to large feldspar augen (Plate 4.14).

Unannealed mylonitic or cataclastic textures were not observed. All samples are blastomylonitic and recrystallized.

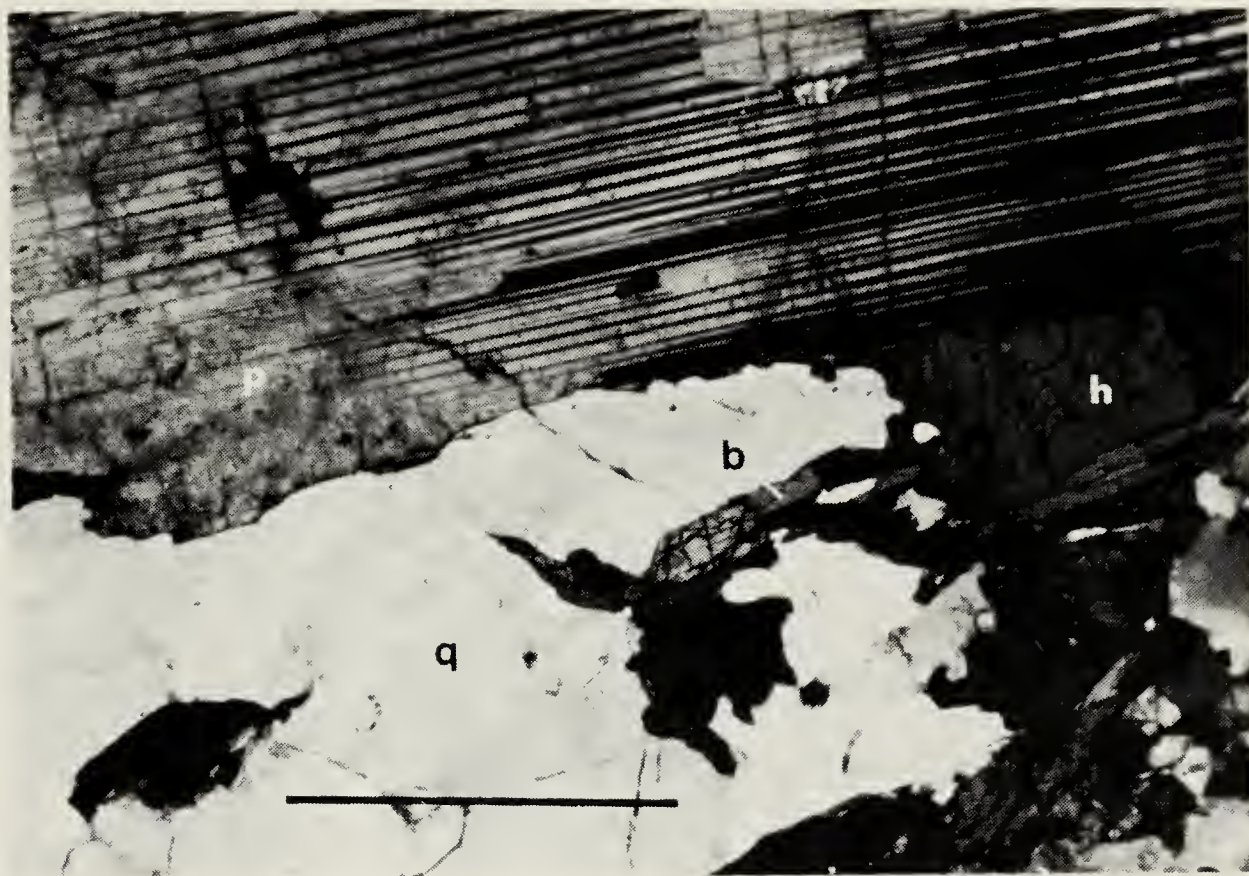


Plate 4.11 A photomicrograph, taken under crossed nicols, of typical, coarsely crystalline foliated hornblende granodiorite of the Aishihik Batholith (sample no. 141). Foliation parallels the top and bottom margins of the photograph and is defined by the parallel alignment of primary magmatic grains p - plagioclase; h - hornblende; q - quartz; b - biotite. The scale bar represents 1 mm.

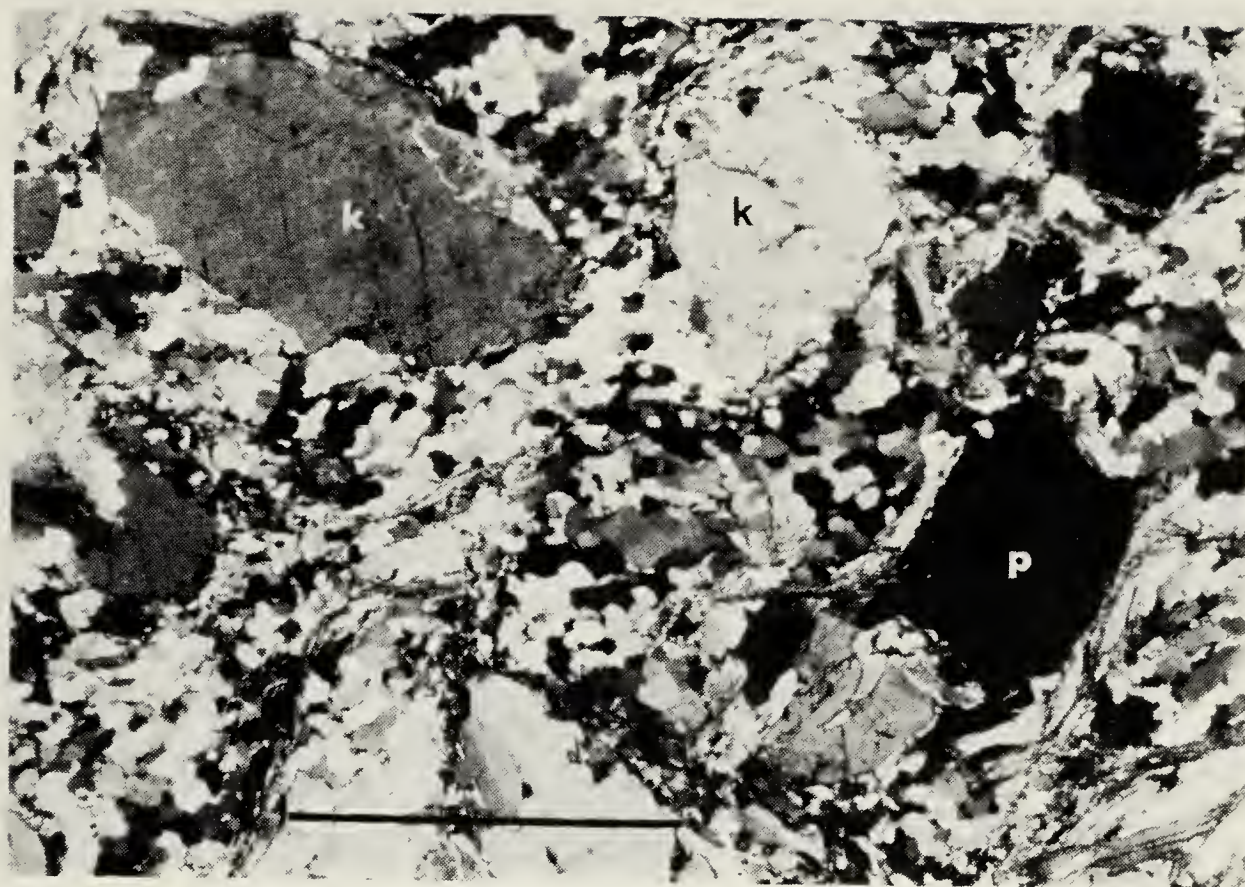


Plate 4.12 A photomicrograph, taken under crossed nicols, of a thermally annealed augen mylonite from near the west margin of the Aishihik Batholith (sample no. 60). Feldspar augen (k - K - feldspar; p - plagioclase) are rounded and anhedral. The augen float in a finely crystalline matrix of recrystallized quartz and mica. The scale bar represents 1 mm.

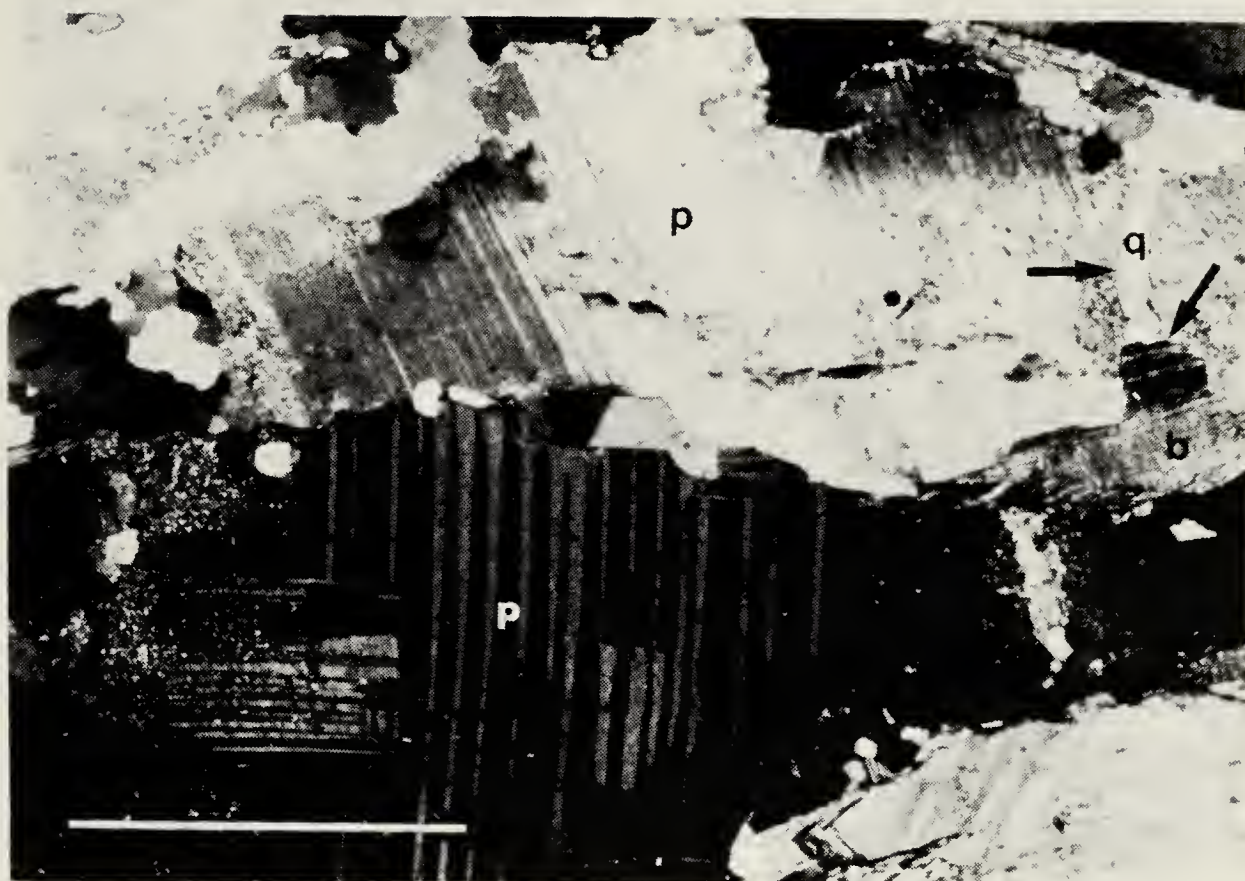


Plate 4.13 A photomicrograph, taken under crossed nicols of sheared hornblende quartz diorite of the Aishihik Batholith (sample no. 6). Twin planes in plagioclase (p) are oriented at a high angle to the long axis of grains, suggesting thorough recrystallization during deformation. Arrows indicate where a fractured feldspar grain has been annealed by undeformed quartz (q) and biotite (b). The scale bar represents 1 mm.

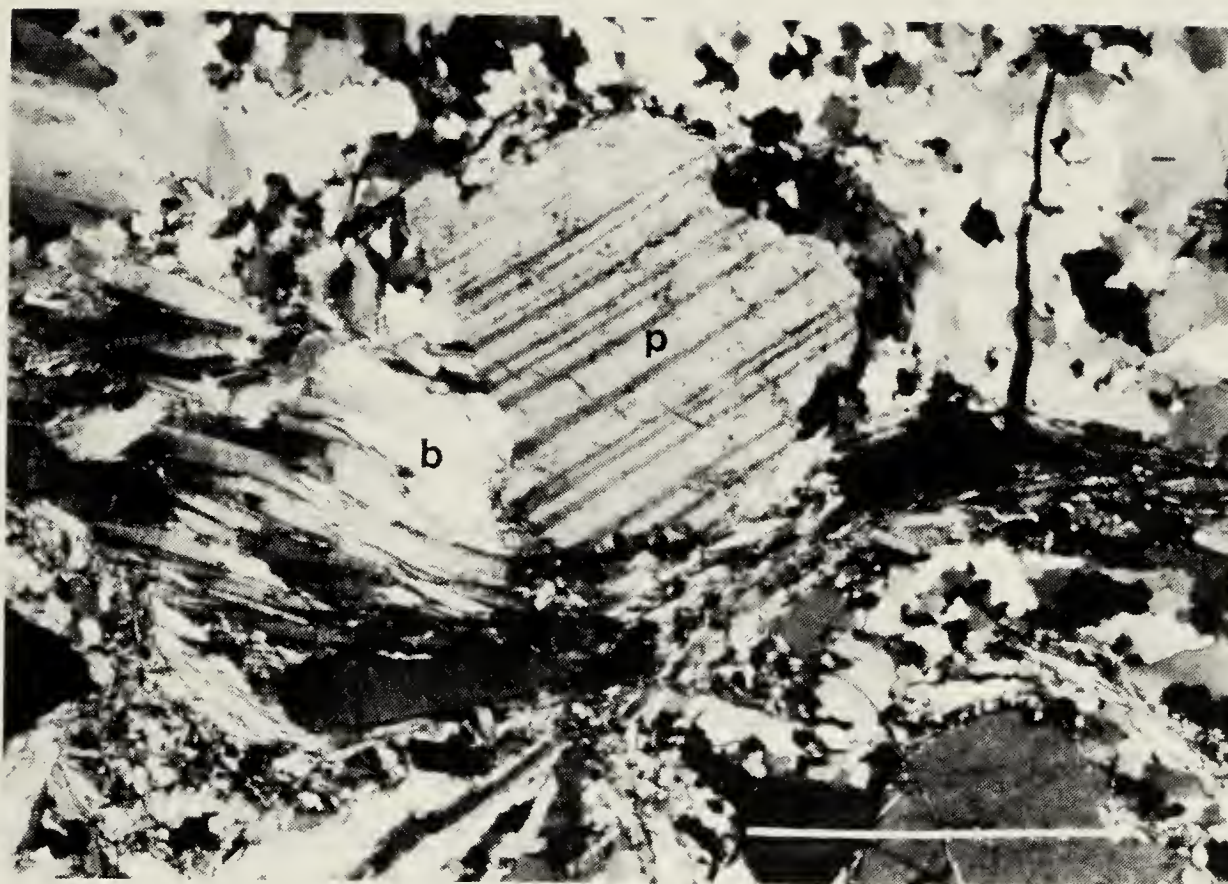


Plate 4.14 A photomicrograph, taken under crossed nicols, of thermally annealed augen mylonite from near the west margin of the Aishihik Batholith (sample no. 60). Biotite (b) has preferentially recrystallized in a strain shadow adjacent to a plagioclase augen (p). The scale bar represents 1 mm.

4.2.3 The nature of S_m and S_t

S_m is interpreted to be the result of magmatic flow during the emplacement of the batholith. This is strongly suggested by the presence of euhedral, primary igneous grains, including feldspar and hornblende, that lie within and define the planar fabric. Other observations that are consistent with a syn-magmatic origin for S_m include: the lack of deformation and fracturing of primary igneous grains; the lack of a preferred orientation of quartz grains; that foliation passes around and not through microgranitoid and microdiorite enclaves and micaschist inclusions; and that foliation is everywhere parallel to the margins of the batholith (*cf.* Paterson *et al.*, 1989).

S_t overprints S_m and is interpreted to be the result of solid-state deformation of the batholith. This is suggested by: folding of aplite veins and, locally, of foliation; the association of folds of foliation with shear zones; the heterogeneous nature of S_t ; the development of mesoscopic shear zones; the plastic deformation of mineral grains; grain size reduction; and the recrystallization of minerals into fine-grained aggregates. Locally, recrystallization of biotite has produced a weakly developed schistosity.

S_t is thought to have formed at elevated temperatures, possibly near the granite solvus. This is suggested by: 1) annealing of mylonitic fabrics; and 2) the association of S_t with migmatite. This suggests that shearing took place at high enough temperatures that local pressure variations, possibly associated with bends in the shear zones, were enough to result in partial melting. Alternatively, shearing may have preferentially developed where pockets of melt were still present, resulting in the development of the compositionally heterogeneous migmatites.

The timing and tectonic significance of the S_t fabric is discussed below.

4.3 Structure of the Nisling Assemblage

4.3.1 Mesoscopic structures

Planar elements

Nisling Assemblage is characterized by a planar fabric (S_0) defined by colour and compositional banding (Plate 4.15). The light and dark coloured bands vary in width from 1 mm to 1 cm and together define a well developed lamination. S_0 is only visible in quartzose rocks where it has not been overgrown and obliterated by younger mica. In addition S_0 can only be distinguished from S_1 where fold hinges affecting S_0 are observed. No orientation data were collected for S_0 .



THESE DOCUMENTS SONT LA PROPRIETE DE LA BIBLIOTHEQUE NATIONALE
DE FRANCE
TOUTES REPRODUCTIONS NON AUTEORISEES
SONT PUNIES PAR LA LOI

Plate 4.15 Deformed quartzite observed in the Upper Nisling River area. A photograph is shown at top and a labeled line drawing of the photograph below. Two phases of folds are evident. Rootless isoclinal folds of compositional banding are labeled F_1 . An L_1 lineation represents the traces of the thickened F_1 fold hinges. Compositional bands and F_1 folds are deformed and define an open fold (F_2). A hammer, evident at lower left, is shown for scale.



A second planar fabric (S_1) is present in quartzose rocks and is defined by colour and compositional banding identical to that described for S_0 (Plates 4.15 and 2.6). A well developed parting, with a spacing of 1 to 50 cm, which parallels S_1 and along which the rocks can be pulled apart is locally developed. Rarely, mica flakes parallel and lie along the plane of parting. Like S_0 , S_1 is not preserved in micaceous rocks where it has been overgrown and obliterated by younger mica.

S_1 is also evident in amphibolite (Plate 2.4) and in marble (Plate 2.5). In amphibolite, S_1 is defined by a plane of parting along which the rock fractures into slabs 10 to 20 cm in width. The plane of parting parallels and is coincident with thin (less than 5 mm) compositional bands which consist largely of epidote. In marble, S_1 consists of fine colour and compositional banding. The colour variations consist of dark grey to brown laminae less than 1 cm thick and spaced at 1 to 20 cm intervals in white marble. Compositional layering consists of alternating bands of coarsely crystalline white calcite 1 cm to greater than 1 m in width, and thin (1 to 2 cm in width) bands of brown weathering, boudinaged chert lenses that extend parallel to the colour banding and which occur at irregular intervals. S_1 can only be distinguished from S_2 in marble where fold hinges affecting S_1 are observed.

Orientation data collected in the Upper Nisling River area in the brown quartzite unit (PPbq) reflects the orientation of the S_1 fabric (Figures 4.2 c and 4.4). Although deformed and folded, the general trend of the foliation parallels S_m and the contact with the Aishihik Batholith (Figures 4.2 c and 4.3). S_1 also parallels and is concordant with the margins of the largest of the intrusions of pink quartz monzonite of the Long Lake Suite, but is discordant with smaller related intrusions (Figure 4.2 c). Dykes of pink quartz monzonite intersect and truncate the S_1 fabric.

Orientation data recorded from the North and South Aishihik Lake areas only locally reflects the orientation of the S_1 fabric as quartzite is less commonly exposed. S_1 was not measured in marble or amphibolite.

A third planar fabric (S_2) is best developed in metapelitic rocks and consists of a coarse and irregular schistosity (Plate 2.1). The schistosity is defined by the subparallel alignment of biotite and muscovite. Migmatite occurs as irregularly shaped lenses that are characterized by corrugated contacts (Plate 2.1). The long axes of the migmatite lenses usually lies within and extends along the plane of foliation. Pinching and swelling of migmatite lenses gives the schistosity a wavy appearance. Rarely, large migmatite lenses are characterized by a planar fabric defined by compositional and colour banding which parallels and is continuous with S_2 in the adjacent schist. In quartzose rocks that are

intimately interfoliated with metapelitic rocks, compositional banding, defined by grey and white gneissic bands 1 to 5 cm in width, parallels the schistosity.

In the Upper Nisling River area, where thick and continuous quartzose rocks of the brown quartzite unit crop out, S_2 is poorly developed to absent. In micaceous laminae, mica locally occurs at an angle to S_1 compositional banding and parallel to the axial plane of folds of S_1 . In amphibolite, S_2 is heterogeneous. In the Upper Nisling River area amphibolite is locally characterized by significant amounts of quartz, and is interfoliated with quartzose rocks. In these areas S_2 is poorly developed. Where amphibolite is quartz-poor and where it occurs in close proximity to marble, the S_2 fabric is generally well developed and is defined by parallelism of hornblende grains and by thin and discontinuous (1 to 5 cm in width) light green and white colour and compositional bands. The light green bands are usually associated with the nearby presence of marble and consist of calc-silicate minerals including diopside and epidote. White bands represent feldspathic horizons. In marble colour and compositional banding, including brown weathering chert bands, parallel the contacts with, and schistosity in, adjacent mica-schist.

Throughout the North and South Aishihik Lake areas S_2 generally dips homoclinally to the east to northeast, and parallels the contact with, and foliation developed within Aishihik Batholith (Figures 4.2 a and b, 4.3, and 4.4).

A fourth planar fabric (S_3), defined by the parallel alignment of finely crystalline mica, overprints the main schistosity (S_2). S_3 is only locally developed and is restricted to micaceous, metapelitic horizons. It is not penetrative, but occurs at intervals of 1 to 5 cm and is associated with crenulations of the S_2 schistosity. The S_3 fabric is not developed in marble, amphibolite, or in quartzose rocks.

An additional planar fabric is defined by: 1) the parallel alignment of mica in schistose bands; 2) compositional banding consisting of alternating bands of fine grained amphibolite up to 20 cm thick and felsic quartzite and felsic metapelite bands from 5 cm to more than 1 m thick (Plate 4.16); 3) anastomosing gneissic bands which appear to represent fully recrystallized shear bands (Plate 4.17); 4) elongate marble boudins up to 50 cm thick and more than 2 m in length; 5) tight to isoclinal overthickened fold hinges. Hinge regions of folds of thin amphibolite horizons (2 cm thick measured along the limbs of the fold) are up to 60 cm thick, measured along the trace of the axial planar surface of the fold (Plate 4.16); 6) discontinuous feldspathic migmatite lenses; 7) the parallel alignment of aplite veins; and 8) the local development of shear bands (Plate 4.18) defined by distinct discrete shears spaced at regular intervals of 5 to 35 cm measured along schistosity and which cut across schistosity at an angle of less than 20° . The shears often



Plate 4.16 Sheared and deformed rocks of the Nisling Assemblage observed immediately beneath the contact with the overlying Aishihik Batholith in the South Aishihik Lake area. Hornblende amphibolite (ha) and migmatitic (white lenses) feldspathic micaschist and quartzite are intimately interfoliated. White and black arrows at lower right indicate the inside and outside edges, respectively, of the hinge zone of a fold. The hinge zone consists of hornblende amphibolite and is 60 cm thick measured along the axial plane of the fold. Hornblende amphibolite in the limbs of the fold is 2 to 3 cm thick.



Plate 4.17 Anastamosing gneissic banding observed immediately beneath the contact with the overlying Aishihik Batholith in the southeast corner of the North Aishihik Lake area. The arrow points to where the anastamosing fabric has truncated earlier developed gneissic bands. The lense cap is 6.5 cm wide.



Plate 4.18 Macroscopic shear bands developed in migmatitic (white lenses) feldspathic micaschist and quartzite of the Nisling Assemblage observed immediately beneath the contact with the overlying Aishihik Batholith in the South Aishihik Lake area. Thin hornblende amphibolite horizons (ha) and aplite veins (indicated by arrows) are also indicated. The photograph was taken looking to the north. Spaced shear planes are highlighted and dip shallowly to the west. Foliation and gneissic banding are offset down-dip towards the west across the shear planes, consistent with a top-to-the-west sense of shear. The field note book at lower right is 12 cm wide.

appear to flatten into micaceous or amphibolitic horizons, while cutting across more feldspathic bands. Rocks above the shears are consistently displaced down-dip towards the west, consistent with their having developed during top-to-the-west shearing.

This fabric is only developed within 30 m of the west margin of the Aishihik Batholith. It was not observed along the north margin of the batholith. The fabric ends up against the overlying contact with granodiorite of the batholith, and is transitional into typical micaschist of the Nisling Assemblage.

The orientation of the fabric, although quite irregular and anastomosing, is subhorizontal to moderately east to northeast dipping, parallel with the overlying contact with the batholith and with the S_2 schistosity in the underlying Nisling Assemblage schists.

Folds

Deformation of compositional banding (S_0) has produced small isoclinal folds (F_1) (Plate 4.15). F_1 folds are characterized by elongate, thin (less than 1 cm) limbs and rare, divergent fold closures which are characterized by thickened hinge zones. Locally, hinge zones are boudinaged and detached. No antiform - synform pairs were observed. S_1 parallels, and is defined by, the elongate limbs of the F_1 folds.

F_1 folds are rare and difficult to recognize. S_0 colour banding is commonly subtle, and subsequent deformation and metamorphism has modified F_1 folds. F_1 folds are best preserved where light and dark banding is well developed in the brown quartzite unit.

F_1 folds, and the associated S_1 axial planar fabric are deformed by isoclinal to open, recumbent to moderately inclined, horizontal to gently plunging folds (F_2). In the majority of the F_2 folds the limbs approach parallelism (isoclinal folds), although not for 1 to 3 m from the hinge line (measured along the axial planar surface). Fold amplitudes vary from less than 1 cm to more than 1 m. Antiform - synform pairs are rare.

Both symmetric (Plate 4.15) and asymmetric folds (Plate 2.6) were observed. In the Upper Nisling River area F_2 folds are weakly to strongly asymmetric, are characterized by gently to moderately north-dipping axial planar surfaces, by subhorizontal north - south to northeast - southwest trending hinge lines, and verge to the east to southeast (Figure 4.2 c). Along Aishihik Lake F_2 folds are less well preserved. Where present they are characterized by subhorizontal to gently northeast- to southeast-dipping axial planar surfaces, and by subhorizontal to gently north- to northeast-plunging hinge lines. No dominant sense of vergence was observed.

F_2 folds are best preserved in quartzose rocks. In micaceous rocks a coarse schistosity (S_2) lies in the axial surface of F_2 folds. Generally, the development of the

schistosity has obliterated the associated folds. In amphibolite open folds of thin compositional bands (S_1) are rare and are generally obliterated by the development of the axial planar gneissosity or schistosity (Plate 2.4). Rare isoclinal folds in marble are characterized by axial planes which parallel the margins of the marble lenses and the schistosity in the adjacent micaschist (Plate 2.5).

S_2 is deformed by small (amplitudes of less than 10 cm, and commonly less than 1 cm) open, moderately inclined, subhorizontal to gently north-plunging kink, or chevron shaped folds (F_3). F_3 folds are asymmetric, characterized by vertical to gently east-dipping axial surfaces, and verge towards the west. The weakly developed S_3 schistosity lies in the axial surface of F_3 folds.

Larger F_3 folds are also developed and are characteristically more rounded. In quartzite F_3 folds are rare, are characteristically outcrop-scale with amplitudes and wavelengths of greater than 5 m (Plate 4.19). Upright, open F_3 folds of marble horizons with amplitudes of 20 m to more than 50 m were observed (Plate 4.20). Upright to steeply inclined, sub-horizontal to gently north-plunging, map-scale folds deform schists of the Nisling Assemblage, and the contact with, and granodiorite of, the Aishihik Batholith (Figures 4.3 a and 4.4). The folds are characterized by rounded to flattened hinge zones, amplitudes and wavelengths of 200 m to 500 m, vertical to moderately east-dipping axial surfaces, and weak westward vergence. F_3 folds are best developed in the South Aishihik Lake area in micaceous rocks. Poles to foliation for the South Aishihik Lake area, when plotted on an equal-area stereonet, define a well developed girdle pattern (Figure 4.4). The girdle pattern is characterized by a pole, reflecting the approximate average orientation of the F_3 fold axis, that plunges gently to the north.

Linear elements

A linear fabric element (L_1), defined by a rippled or wavy appearance apparent on S_1 partings, is weakly developed and is restricted to quartzose rocks in which S_0 and S_1 are present (Plate 4.15). The lineation reflects the thickened and detached hinges of isoclinal F_1 folds which affect S_0 .

A second lineation (L_2) is well developed in quartzose rocks and consists of the penetrative development of parallel quartz rods less than a 5 mm in width (Plate 4.21). The lineation appears to reflect the thickened hinges of small, tight, F_2 folds (Plate 2.3). An intersection lineation is developed in amphibolite where the S_1 and S_2 planar fabrics intersect (Plate 2.4). The lineation is best viewed on the surface of S_1 and consists of the surface trace of a poorly developed parting or jointing. The lineation is non-penetrative



Plate 4.19 Deformed quartzite observed in the Upper Nisling River area. The photograph is taken looking to the north. The arrow indicates the hinge of an F_2 fold, a close up of which was shown in Plate 4.16. The surface traces of a synform - antiform pair of open, asymmetric F_3 folds, which deform the F_2 fold, is also shown. The F_3 folds are characterized by moderately east-dipping axial planes and verge to the west. The outcrop is approximately 7 m high.



Plate 4.20 An F_3 antiform observed in the southern part of the South Aishihik Lake area. The antiform is cored by micaceous quartzite (dark grey) which is overlain by white marble (m). The arrow indicates a back-pack for scale.

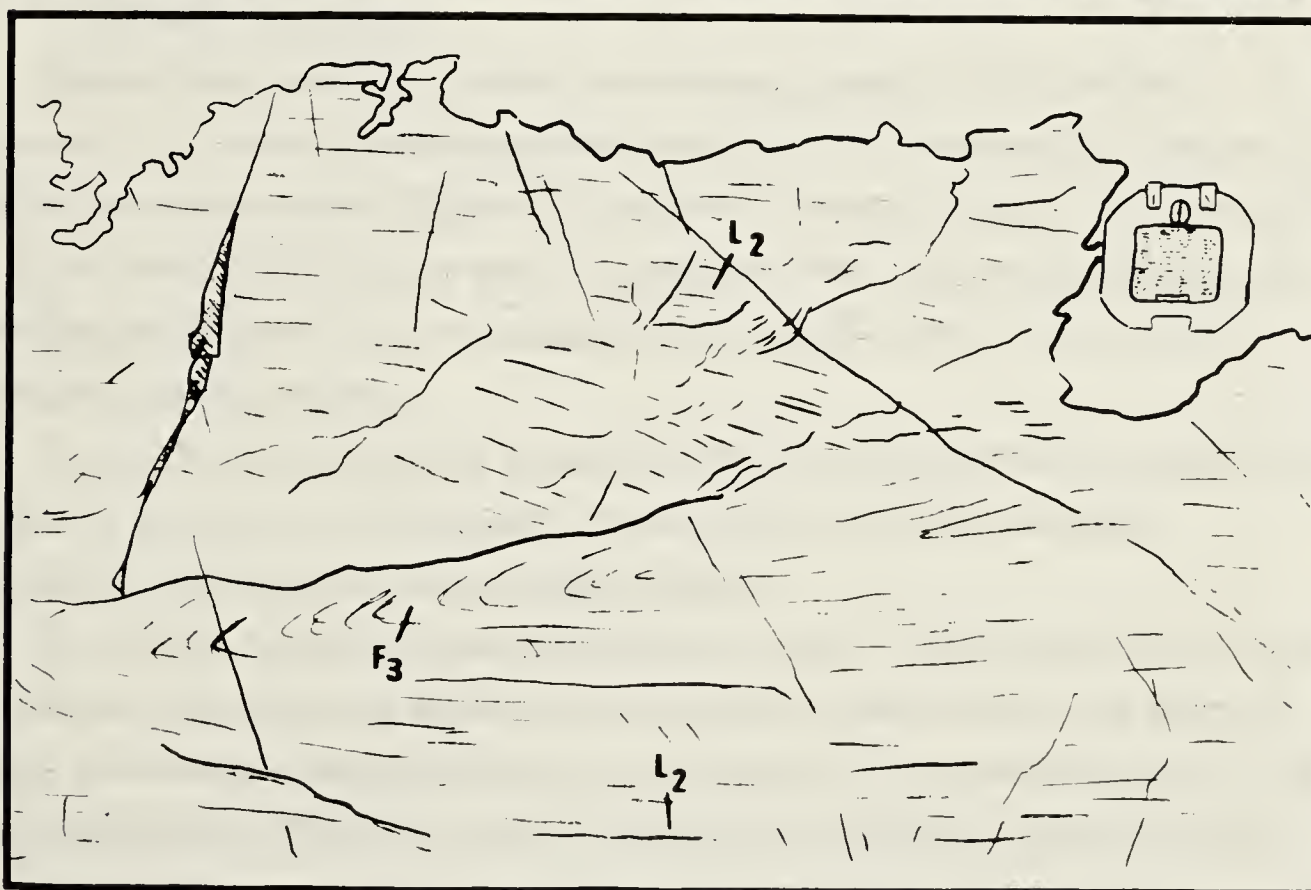
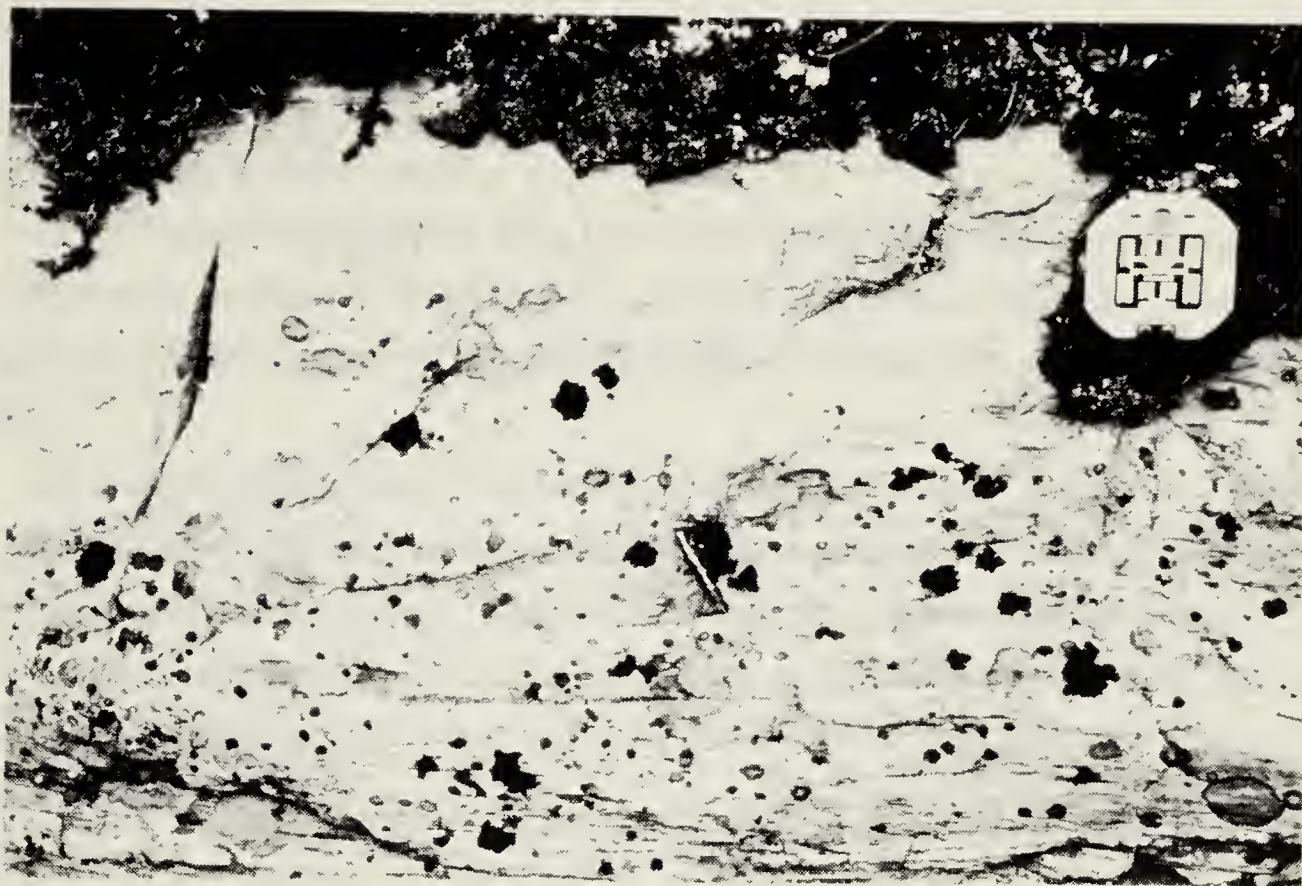


[Faint, illegible text or markings at the bottom of the page, possibly a signature or footer.]



Faint, illegible text or a caption, possibly describing the scene or providing a title.

Plate 4.21 Grey quartz gneiss from the South Aishihik Lake area. A photograph is shown at top and a line drawing of the photograph below. A well developed quartz rodding lineation (L_2) is deformed and folded about an F_3 fold. A brunton compass is shown for scale.



and is not associated with the alignment of any mineral grains. L_2 is not well developed in either of marble or schistose rocks.

In the Upper Nisling River area, L_2 is subhorizontal to moderately plunging and trends northeast - southwest (Figures 4.2 c and 4.4). Along Aishihik Lake, the lineation is poorly developed but appears to be oriented parallel to subparallel with the L_3 crenulation lineation.

L_3 is developed in micaceous rocks and results from small open folds (amplitudes of less than 1 cm) that affect the main schistosity (S_2). L_3 is not well developed in amphibolite, marble, or quartzite. In micaceous quartzites it is weakly developed.

In the South Aishihik Lake area L_3 plunges gently to the north parallel with the hinge lines of F_3 folds and with the pole to the girdle pattern defined by poles to foliation (Figures 4.2 a and 4.4).

4.3.2 Microstructure

Planar fabrics and folds evident at mesoscopic scales, are also visible in thin-section. S_0 , which is indistinguishable from S_1 in the absence of F_1 folds, was only identified in one thin-section (Figure 4.5) cut from a sample collected west of the Aishihik Lake in the North Aishihik Lake area. S_0 consists of thin, finely crystalline, micaceous, quartzofeldspathic bands that are characterized by slightly darker colour than the surrounding quartzitic matrix.

S_0 is deformed and defines an isoclinal fold (F_1) characterized by parallel limbs separated by about 2 mm. Mica grains are not, however, folded, indicating recrystallization during more recent metamorphism.

S_1 , like S_0 , consists of quartzofeldspathic bands. The S_1 bands are up to 1 cm in width and are also defined by micaceous laminae and by subtle colour and grain size banding. In schistose rocks (in which S_2 is pervasive) S_1 is preserved as thin (0.1 mm) iron stained laminae (Plate 4.22) and by discontinuous, quartzite boudins, eyes, and rootless fold hinges.

S_1 is deformed and defines open to tight folds (F_2). Generally, the folds are more open in quartzose rocks and become tighter as the mica content of the rocks increases. Detached tight to isoclinal fold hinges, consisting of medium grained quartz, characterize micaschist. In quartzite, micaceous laminae define tight, parasitic folds which verge towards the hinge of the larger folds.

Traces of S_1 are also preserved in younger mica, garnet, and staurolite porphyroblasts. Mica grains which define the S_2 schistosity are locally characterized by

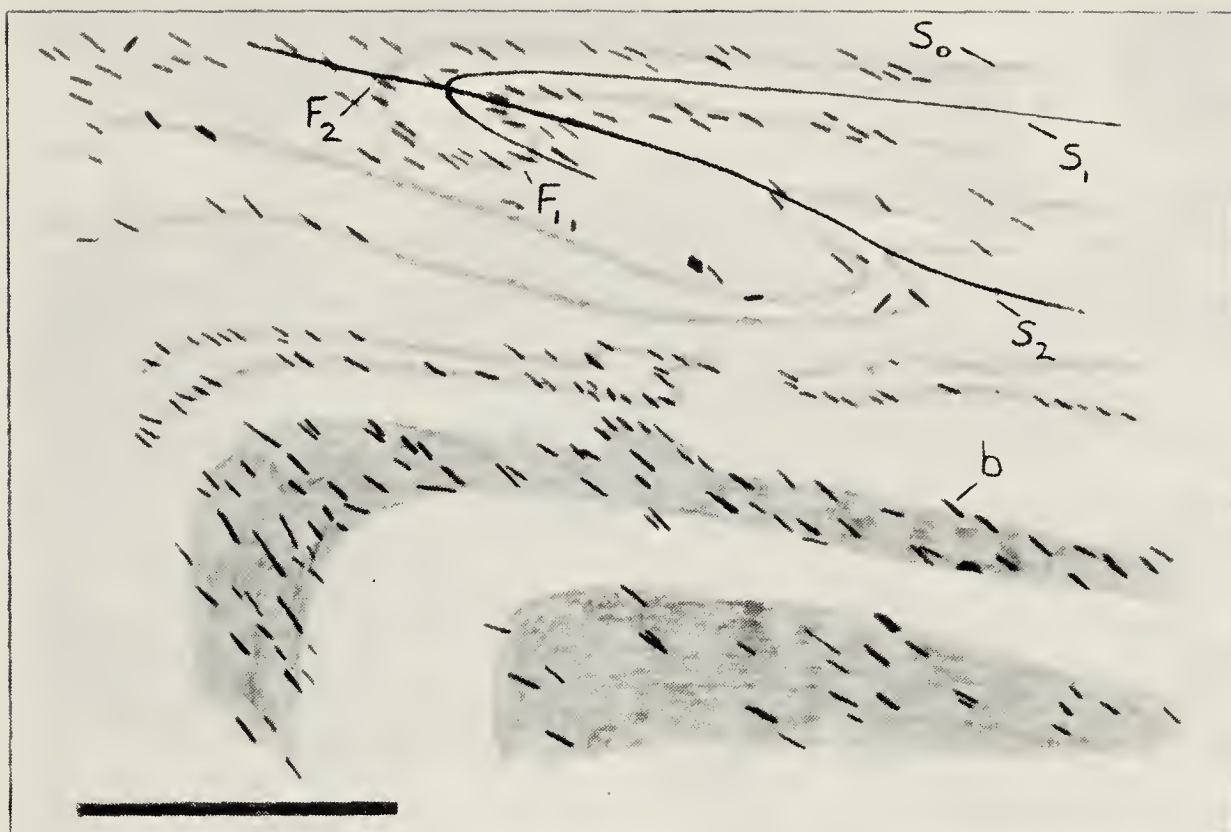


Figure 4.5 A line drawing made from a thin section cut from sample number 211 collected along the west side of Aishihik Lake in the North Aishihik Lake area. The scale bar represents 1 cm. Shaded grey and white bands indicate grain size and compositional banding (grey bands are more micaceous and feldspathic; white bands are clean quartzite; b - biotite porphyroblasts). Also indicated are S_0 - compositional banding; S_1 - the axial plane of folds (F_1) of S_0 ; and S_2 , the axial plane of folds (F_2) of S_1 . Note that biotite porphyroblasts preferentially extend parallel to, and define the S_2 axial planar schistosity.

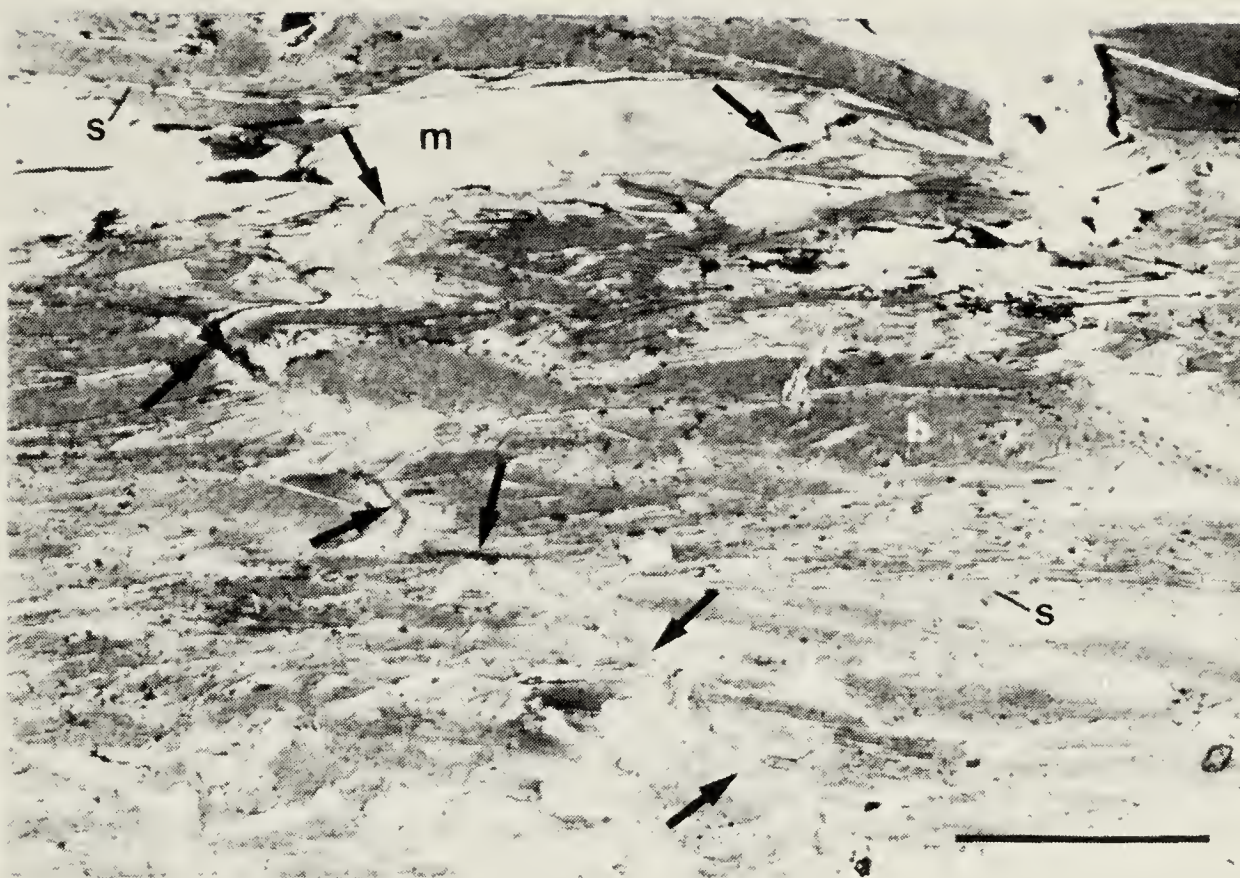


Plate 4.22 A photomicrograph, taken with plane polarized light, of sillimanite schist of the Nisling Assemblage from a sample (no. 87) collected near the contact with the Aishihik Batholith in the South Aishihik Lake area; s - sillimanite, m - muscovite, b - biotite. The arrows point to a thin, deformed horizon, defined by iron staining, which appears to represent an early, now transposed planar fabric (S_1). Mica that define the schistosity (S_2) are axial planar to folds of S_1 . The scale bar represents 250 μm .

fine opaque inclusions thought to be graphite (Plate 4.23). The inclusions define a finely laminated planar fabric that has been deformed and folded. Garnets include grains of quartz, feldspar, mica (usually biotite), fine opaque material (thought to be graphite), and pyrite (Plate 4.24). Inclusions trails define isoclinal to open, symmetric and asymmetric folds. Staurolite exhibits a branching habit extending both subparallel to, and at a high angle to the main schistosity (S_2). Fine opaque inclusions, thought to be graphite, define a planar fabric element (S_1) which is isoclinally folded. The limbs of the isoclinal folds parallels the staurolite branches (Plate 4.25).

Fibrolitic sillimanite defines thin (less than 1 mm in width) and continuous laminae which appear to represent aluminum-rich compositional bands (S_1) (Plate 4.26). The laminae define tight to isoclinal folds which are characterized by narrow, angular hinge zones and by foliation-parallel (S_2) axial planes. Fibrolite needles grow parallel with the lamination. Near the fold hinges fibrolite needles bend gently towards the hinge and exhibit mild undulose extinction. Needles are not, however, continuous around the fold hinges. Fibrolite needles also grow parallel to the trace of the axial planar surfaces of the folds.

S_2 parallels the axial surfaces of F_2 folds. In micaceous quartzite isolated mica grains parallel with the trace of the axial planes of folds of S_1 (Figure 4.5). In schistose rocks, the crystallization of axial planar mica defines a schistosity that has obliterated the associated folds. The schistosity is irregular with multiple generations of mica growing at a slight angle to one another (Plate 4.23). Locally two distinct planar elements, thought to represent a relic S and C fabric, are present (Plate 4.27). The S (flattening) planes consist of stacked, parallel, mica grains. The mica grains are fish-shaped, bend into, and pinch out against the C (shear) planes. The C planes oriented at an angle of about 20° to the S planes. Isolated mica grains locally grow along the C planes. The S and C fabric is rare and poorly preserved.

As indicated above, metamorphic porphyroblasts preserve, primarily in the form of inclusion trails, traces of deformed S_1 . The preservation of pervasively deformed S_1 suggests that the nucleation of porphyroblasts largely post-dated deformation of S_1 . Porphyroblasts are intimately intergrown with mica oriented parallel to the axial planes of folds of S_1 (Plate 4.22; Figure 4.5). The distribution of sillimanite, kyanite, and staurolite defines a series of isograd bound metamorphic zones which extend along the west margin of the Aishihik Batholith and which parallel the S_2 schistosity (Chapter V). These observations indicate that metamorphic porphyroblasts nucleated and grew at the same time as the development of the S_2 schistosity.



Plate 4.23 A photomicrograph, taken with plane polarized light, of micaschist of the Nisling Assemblage from a sample (no. 82) collected in the South Aishihik Lake area; m - mica, b - biotite. A poorly defined foliation parallels the top and bottom margins of the photograph. Several generations of mica, each oriented at a slightly different angle, are evident. Graphitic inclusion trails are interpreted to represent an older, deformed planar fabric which was deformed and overgrown by mica. The scale bar represents 1 mm.

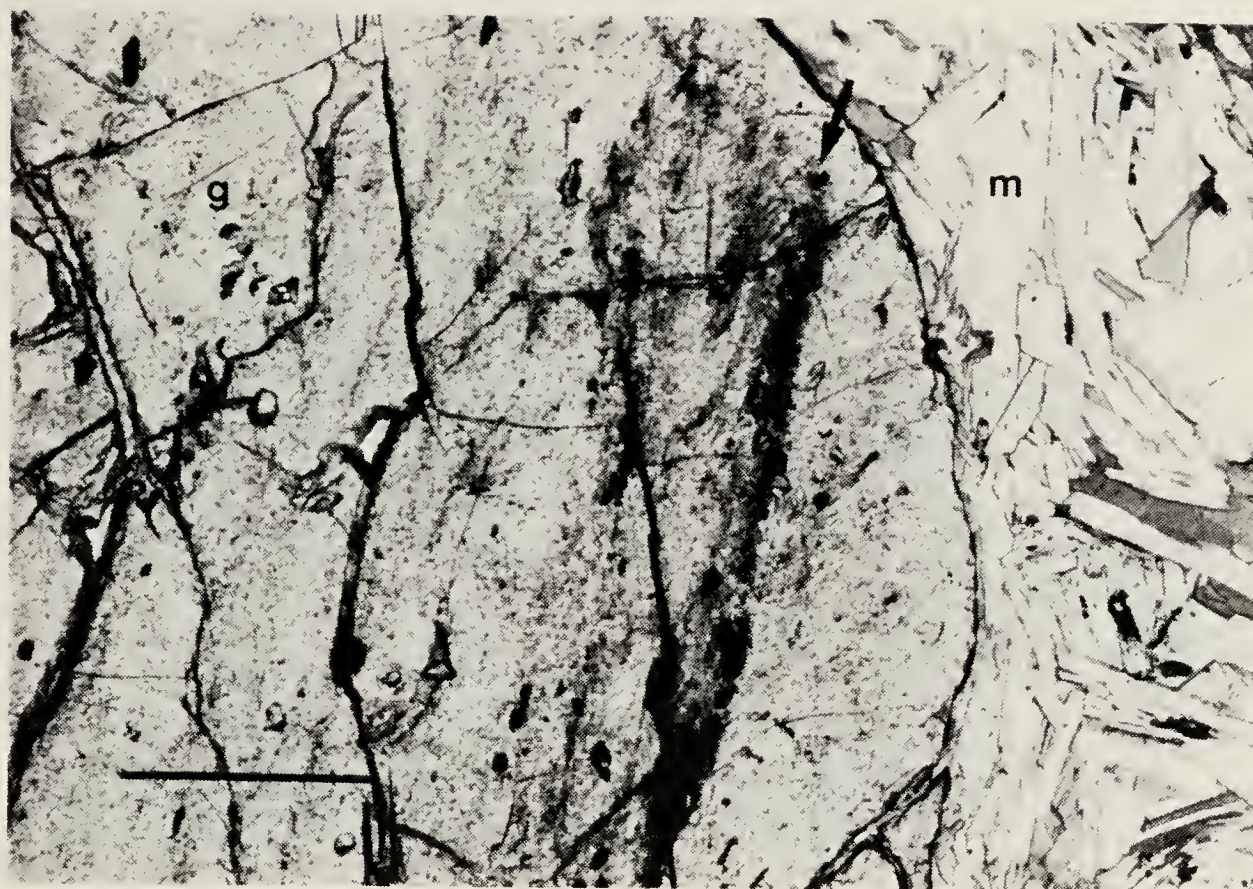


Plate 4.24 A photomicrograph, taken with plane polarized light, of garnet micaschist from a sample (no. 146) collected in the South Aishihik Lake area; g - garnet, m - mica. The garnet porphyroblast is characterized by graphitic inclusion trails which define a tight to isoclinal fold, indicated by the arrow. The scale bar represents 250 μm .

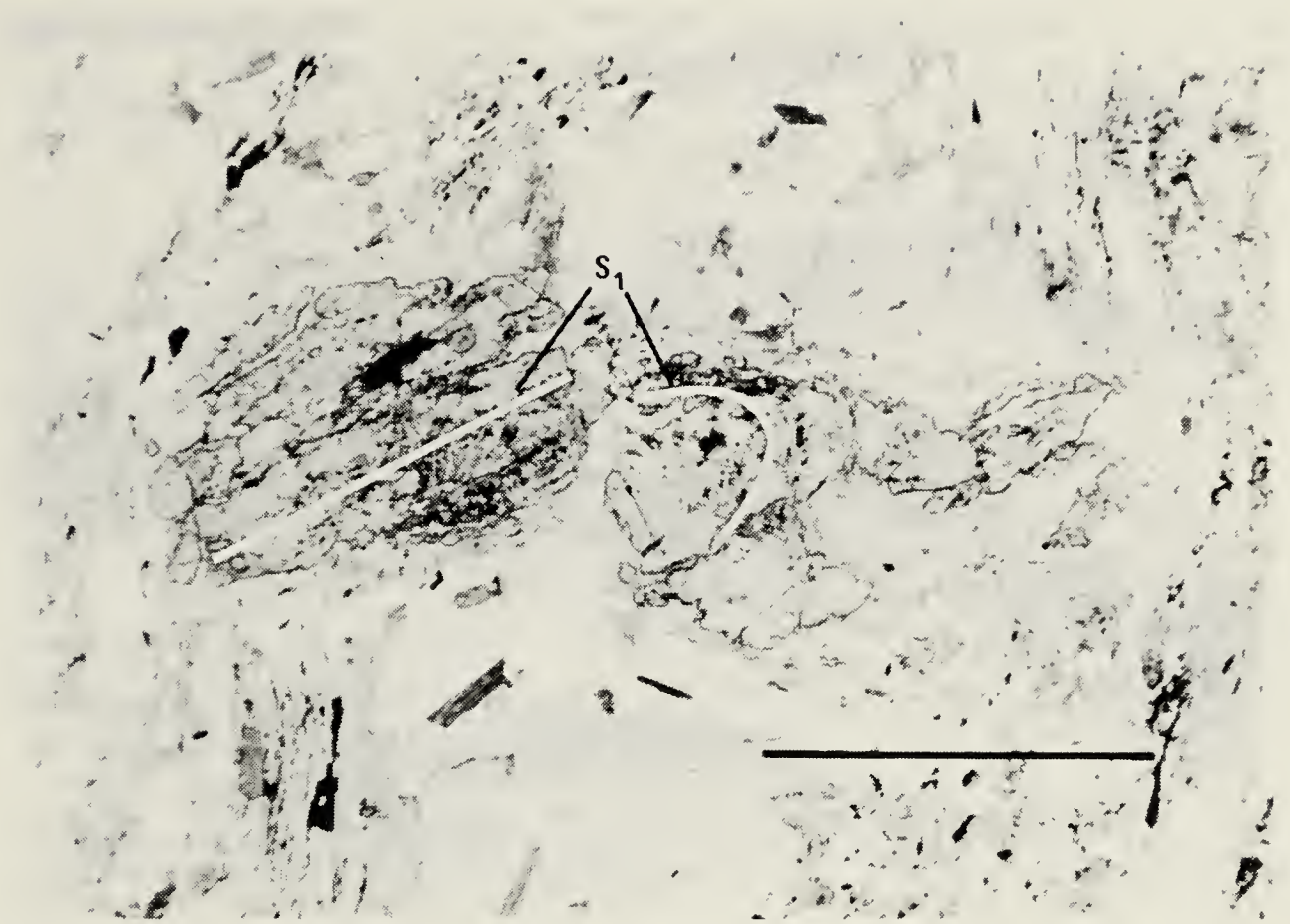


Plate 4.25 A photomicrograph, taken with plane polarized light, of staurolite micaschist from a sample (no. 17) collected in the South Aishihik Lake area. A staurolite porphyroblast, at center, is characterized by graphitic inclusion trails which define a planar fabric (S_1), highlighted in white, which is folded. The scale bar represents 1 mm.

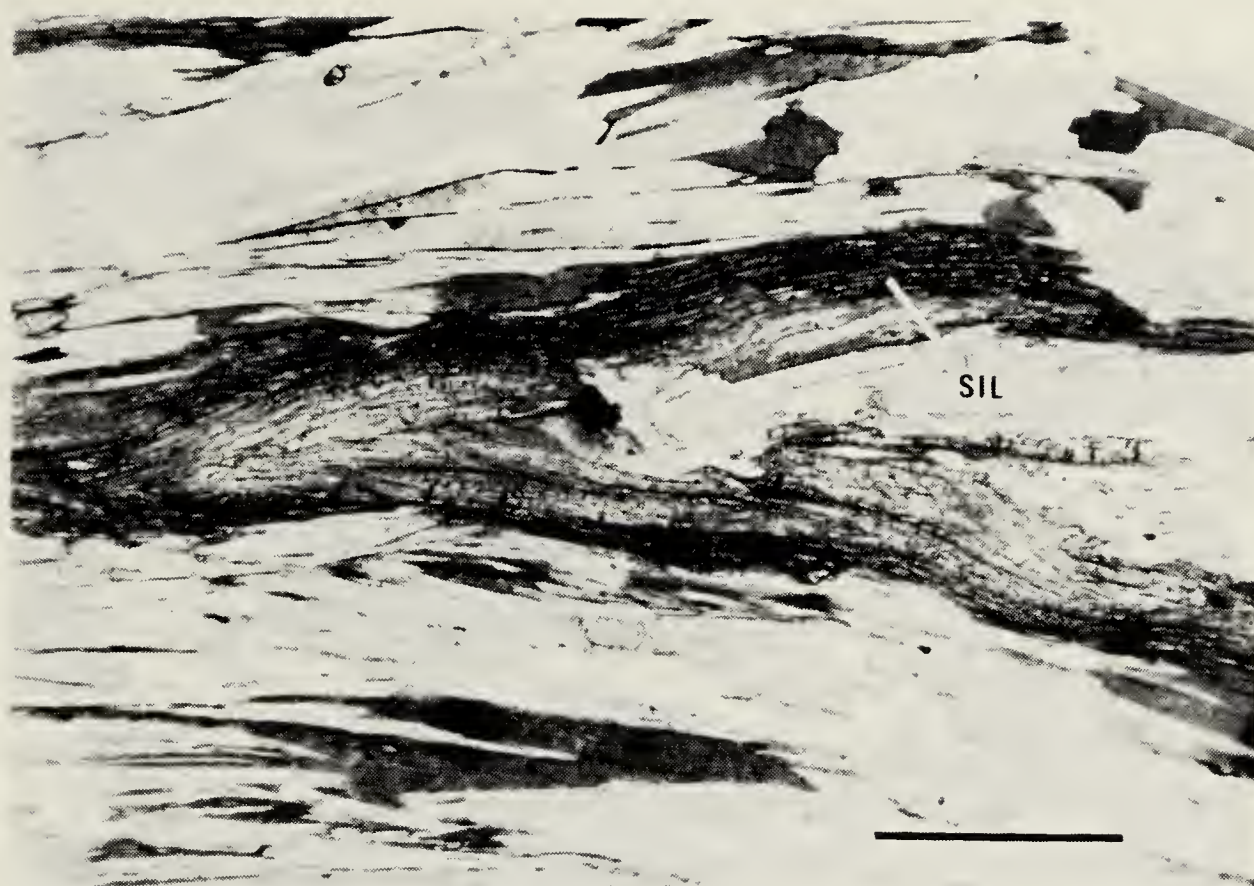


Plate 4.26 A photomicrograph, taken with plane polarized light, of sillimanite micaschist from a sample (no. 69) collected in the Upper Nisling River area; SIL - sillimanite. A sillimanite rich laminae defines a tight, recumbent fold characterized by a schistosity parallel axial plane. Individual sillimanite needles bend gently towards, but are not continuous around, the fold hinge. Fibrolite needles and coarse sillimanite also grow parallel to the axial trace of the fold (indicated just below the SIL label). The scale bar represents 250 μm .



Plate 4.27 A photomicrograph, taken under crossed nicols, of micaschist from a sample (no. 145) collected in the South Aishihik Lake area. A relic, recrystallized S and C fabric is evident. Mica define fish which extend parallel with compositional banding (S planes) and which are bound by planes oriented at about 20° to the S planes and which are thought to represent relic shear planes (C planes). The scale bar represents 250 μm .

The S_2 schistosity is deformed and defines open folds (F_3) (Plate 4.28). The folds are characterized by planar limbs and by narrow, angular hinges. Both symmetric and asymmetric folds occur. When followed up and down section, fold limbs change length and pinch out, resulting in the coalescence of fold axial traces. Rarely, mica grains nucleate and grow along the axial planes of F_3 folds and define a weakly developed S_3 axial planar schistosity.

Samples of sheared micaschist collected from the contact with the Aishihik Batholith, are similar on a microscopic scale to micaschist from elsewhere in the study area (Plate 4.22). Quartzite samples are however, characterized by significant grain size reduction and recrystallization. S and C quartzite mylonites are locally developed (Plate 4.29).

4.3.3 The nature of the planar fabrics

S_0 is the oldest recognized and is deformed and overprinted by the development of all subsequent fabrics. S_0 is not associated with tectonism of any previous fabric, consists of colour and compositional banding, and is inferred to be bedding.

S_1 , F_1 , and L_1 developed during isoclinal folding of bedding (D_1). D_1 fabrics are preserved in quartzite and in younger metamorphic porphyroblasts throughout the South and North Aishihik Lake areas and the Upper Nisling River Area. The wide distribution of D_1 fabric elements suggests that the tectonic event responsible for their development was regional in extent. D_1 tectonism is older than the Aishihik Batholith ($187.0 \pm 9.7/-0.9$ Ma) which is inferred to intrude the Nisling Assemblage but which is not characterized by D_1 structures.

S_2 is best preserved in metapelitic rocks, and parallels the axial surface of open to isoclinal folds (F_2). Small- to microscopic-scale folding has produced a northeast-trending quartz rodding lineation (L_2). F_2 folds are best preserved in quartzite, are asymmetric, and are east to southeast verging. Although F_2 folds are dominantly east-vergent, the north to northeast plunging quartz rodding lineation (L_2) suggests shearing in a north - south direction.

The D_2 tectonic event was regionally extensive. D_2 tectonism resulted in deformation of D_1 fabrics throughout the study area. In quartzose rocks, most folds are attributable to D_2 tectonism. In metapelitic rocks, the schistosity and metamorphic porphyroblasts are attributable to the D_2 event.

The timing of D_2 tectonism is problematic. Regional shearing of the Nisling Assemblage did not result in deformation of the Aishihik Batholith. Except for the

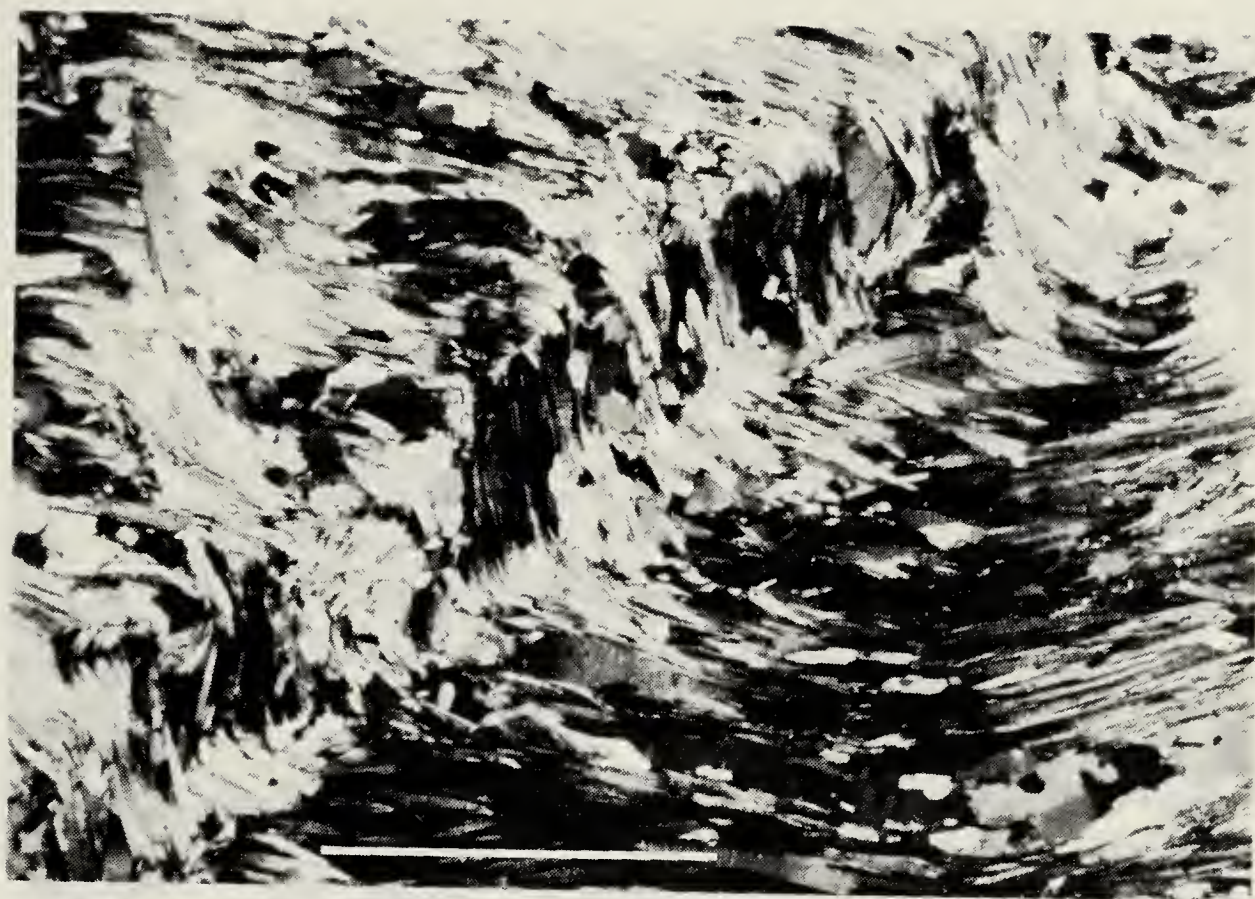


Plate 4.28 A photomicrograph, taken under crossed nicols, of crenulated micaschist from a sample (no. 131) collected in the South Aishihik Lake area. A few grains of recrystallized mica overprint the schistosity and parallel the axial plane of this F_3 fold. The scale bar represents 1 mm.



Plate 4.29 A photomicrograph, taken under crossed nicols, of thermally annealed mylonitic feldspathic quartzite from a sample (no. 62) collected immediately beneath the contact with the Aishihik Batholith in the South Aishihik Lake area. Dynamic recrystallization of quartz has resulted in the development of an S and C fabric. C planes are oriented subparallel with the top and bottom of the photograph and are defined by thin discontinuities which separate elongate composite quartz grains. S planes are oriented at about 25° to the C planes and are defined by the preferred orientation of individual quartz grains. The scale bar represents 1 mm.

restricted development of S_t , which is characterized by top-to-the-west shearing, no regionally extensive, solid-state fabric is developed in the batholith. Neither has the batholith been metamorphosed. Again, except for the restricted development of S_t , no recrystallization of biotite was observed. These observations indicate that D_2 tectonism predates the emplacement of the Aishihik Batholith ($187.0 \pm 9.7/-0.9$ Ma).

However, S_2 parallels the margins of the batholith. The distribution of metamorphic porphyroblasts that nucleated during the development of the schistosity defines a series of isograd-bound metamorphic zones. The isograds and metamorphic zones are sub-parallel to schistosity and with the margin of the batholith and record an increase in metamorphic grade towards the batholith. These observations indicate that metamorphism and the development of the S_2 axial planar schistosity developed during the emplacement of the batholith.

Together, these observations lead to the conclusion that the axial planar schistosity in part post-dates the folds with which it is associated. Several observations are consistent with this premise: 1) in metamorphic porphyroblasts that preserve earlier developed fabrics (S_1) the older fabric is invariably deformed; 2) although the S_2 schistosity is grossly axial planar, it is irregular and defined by multiple generations of mica that overprint one another and that grow at an angle to each other; 3) the margins of migmatite lenses are irregular and corrugated. In addition, migmatites do not exhibit any internal shear fabrics. 4) S_2 -parallel compositional banding locally extends into and is inundated by migmatite; and 5) a relic S and C fabric is locally preserved. Thorough recrystallization and overprinting of the fabric by younger mica has, however, largely obliterated this fabric.

The following sequential geologic history is suggested: 1 - shearing of the Nisling Assemblage prior to the intrusion of the Aishihik Batholith, but after D_1 tectonism; and 2 - the emplacement of the Aishihik Batholith and the thermal enhancement of schistosity and the nucleation of metamorphic porphyroblasts. Intrusion may have occurred shortly prior to the cessation of shearing. The lack of a penetrative solid-state fabric developed throughout the batholith indicates that if intrusion of the batholith did overlap with shearing of the Nisling Assemblage, enough melt was present (greater than 30% melt (van der Molen and Peterson, 1979)) that strain was accommodated without the significant solid-state deformation.

The weakly developed S_3 crenulation schistosity and the L_3 lineation developed in response to open to tight folding of the Nisling Assemblage and the contact with the Aishihik Batholith (D_3). The F_3 folds are weakly to strongly asymmetric, verge to the

west, and indicate top-to-the-west shearing of the Nisling Assemblage and the Aishihik Batholith. D₃ tectonism was regionally extensive; F₃ folds were observed through out the study area. D₃ tectonism was not, however, characterized by significant metamorphism or by the development of a penetrative planar fabric.

The timing of D₃ tectonism is only loosely constrained. F₃ folds deform and are younger than the Aishihik Batholith. The relationship of F₃ folds to the plutons of pink quartz monzonite could not be determined but they are younger than undeformed intrusions of the Ruby Range Batholith (between 90 and 58 Ma).

The planar fabric developed immediately adjacent to the west margin of the Aishihik Batholith is interpreted as the result of intense shearing. This is consistent with the preservation of: anastomosing relic mylonite; tectonically interleaved metapelite, quartzite, marble and amphibolite; and grossly overthickened, rootless fold hinges. When viewed towards the north, rocks above the subhorizontal to gently east dipping C planes are consistently displaced down-dip to the west, indicating top-to-the-west shearing. Shearing is thought to have occurred at high temperatures, as indicated by the ductile nature of deformation, and by the complete annealing of mylonitic fabrics.

The shear fabric in Nisling Assemblage is closely associated with the S_t fabric of the Aishihik Batholith. Both fabrics are developed adjacent to the west margin of the batholith, are not observed elsewhere, and provide a record of top-to-the-west shearing at elevated temperatures. Both fabrics are interpreted to have developed at the same time in response to shearing along the west margin of the batholith. The significance and timing of this shearing is discussed below.

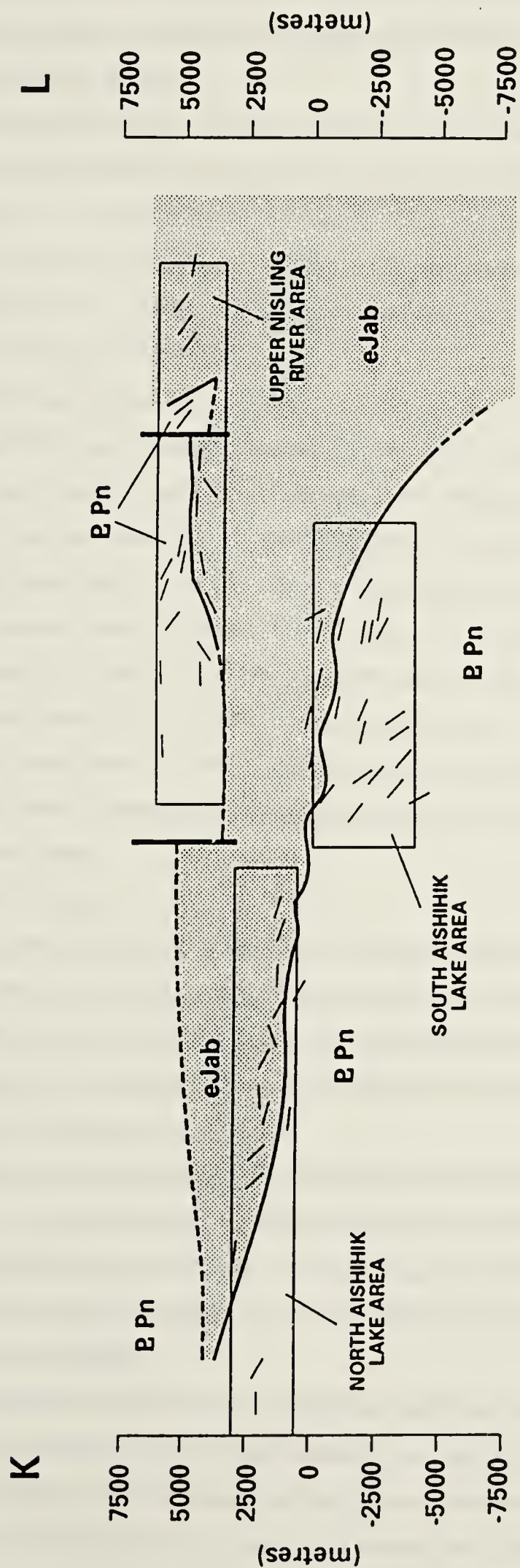
4.4 The shape of the Aishihik Batholith and the nature of the west margin of the batholith

A cross-section, constructed perpendicular to the regional plunge and onto which the Aishihik Batholith - Nisling Assemblage contact has been projected, is shown in Figure 4.6. Intrusions of the Long Lake Suite and the Ruby Range Batholith are not shown. Assuming that the crust underlying the Aishihik Lake region behaved as a solid tabular block that has been tilted 5° to the north, tilting has resulted in the exposure of an approximately 10 km thick section of the crust. Deep structural levels are exposed in the South Aishihik Lake area with progressively shallower crustal levels exposed to the north.

The Aishihik Batholith forms a large overhanging flap. The lower contact, along which the batholith overlies the Nisling Assemblage, crops out along side Aishihik Lake. An abrupt change in the orientation of the batholith - Nisling Assemblage contact occurs near the north end of Aishihik Lake (Figure 4.1). This change in orientation coincides



Figure 4.6 A regional cross-section (K - L), the location of which is indicated in Figure 4.1, showing the geometry of the Nisling Assemblage - Aishihik Batholith contact in profile. Boxes indicate the projections of the North and South Aishihik Lake map areas, and the Upper Nisling River area. Data points represent orientation data projected onto the line of section. Intrusions of the Ruby Range Batholith and the Long Lake Suite are not shown. See text for discussion.



with the pinching out of the batholith to the west. To the north, the roof of the batholith, along which the Nisling Assemblage overlies the batholith, is complicated and deformed by late steeply dipping faults.

S_t is developed along the lower contact of the batholith. A similar shear fabric is developed in metamorphic rocks beneath the contact. Similar tectonic foliations have been attributed to: 1) post-intrusive tectonism (e.g. Page and Bell, 1986); 2) syn-tectonic intrusion (e.g. Gapais and Barbarin, 1986); or 3) ballooning of a diapir (e.g. Sylvester *et al.*, 1978; Bateman *et al.*, 1983). These three models are discussed here in light of the cross-section through the batholith.

1 - Post-intrusive tectonism

The batholith and Nisling Assemblage are deformed by asymmetric west-verging folds (F_3). Some shearing may have resulted from folding. However, although F_3 folds do occur along the north margin of the batholith, no associated S_t fabric development was observed. The shear fabric in the Nisling Assemblage is restricted to the immediate vicinity of the lower contact of the batholith and yet F_3 folds are evident throughout the Nisling Assemblage. Finally, F_3 folds postdate and deform rocks characterized S_t in the batholith and the shear fabric in the Nisling Assemblage. F_3 folds, therefore, post-date S_t .

With the exception of the F_3 folds, no other regionally developed, post-intrusive structures have been observed. This suggests that the S_t fabric is not the result of post-intrusive tectonism.

2 - Syn-tectonic intrusion

Criteria used for the identification of syn-tectonic intrusions include: 1) parallel or subparallel magmatic and high-temperature solid-state foliations in the intrusion; 2) continuity of the solid-state fabric with a regionally developed foliation in the wall rocks; and 3) development of synkinematic porphyroblasts with respect to foliation, in the contact aureole (Paterson *et al.*, 1989).

The fabrics developed along the west margin of the batholith satisfy all of these requirements: 1) S_t in the batholith is a high-temperature solid-state foliation which parallels the magmatic (S_m) foliation; 2) S_t and S_m are parallel to the S_2 schistosity developed in the Nisling Assemblage; and 3) metamorphic porphyroblasts developed at the same time as the schistosity.

However, this model fails to explain the distribution and nature of the tectonic fabrics. Along the north margin of the batholith, no significant shearing either of granodiorite or of the host metamorphic rocks was observed. Shearing is restricted to the west margin of the batholith even though D_2 tectonism affected rocks of the Nisling

Assemblage throughout the study area. In addition, D₂ tectonism resulted in the development of a north-trending quartz rodding lineation, consistent with shearing in a north - south direction. The tectonic fabrics developed along the west margin of the batholith in both the batholith and the adjacent metamorphic rocks is characterized by top-to-the-west shear. These observations suggest that the batholith is not a syn-tectonic intrusive.

3 - Ballooning

Ballooning occurs as a result of the continued emplacement of magma into the core of diapir, the outer portions of which have already solidified (Sylvester *et al.*, 1978; Bateman, 1985). It is however, difficult to separate solid-state foliations that developed in response to ballooning from those that developed in response to post-emplacement tectonism (Paterson *et al.*, 1989). Criteria used for the recognition of ballooning include: 1) a lack of post-emplacement regional deformation of the wall rocks; 2) evidence of high temperature solid-state deformation; 3) evidence of diapirism; 4) the development of an anastomosing foliation in the wallrocks along the contact. Foliation development results from thinning of the wall rocks during pluton expansion and is characterized by the recrystallization of quartz and biotite; and 5) the presence of discontinuities in the intensity of magmatic and solid-state foliations across internal contacts within the intrusion (Sylvester *et al.*, 1978; Bateman, 1985; Paterson *et al.*, 1989).

Post-emplacement regional deformation of the Nisling Assemblage is restricted to the development of west-verging folds (F₃) that also affect the batholith. As shown above, F₃ folds, and an associated axial planar, crenulation schistosity (S₃), deform, overprint, and clearly post-date the development of earlier tectonic fabrics. S_t in the batholith developed at elevated temperatures as indicated by its association with migmatites and by the thorough recrystallization of the shear fabrics. Strong evidence that Aishihik Batholith constitutes a diapir is its profile, shown in Figure 4.6. In addition, a well developed magmatic foliation parallels the margins of the batholith. The shear fabric developed in the wallrock schists is characterized by anastomosing shear zones defined by thorough recrystallization of all mineral grains. Significant thinning of the wall rocks is suggested by the preservation of numerous rootless, thickened fold hinges whose limbs have been thinned and boudinaged. No internal contacts have been identified within the Aishihik Batholith. It remains to be seen whether late stage magmatic pulses can be identified within the core of the Aishihik Batholith.

The development of the tectonic fabrics along the lower contact of the Aishihik Batholith appears to be best explained by ballooning of a diapir. The lack of significant

solid state deformation along the roof of the diapir suggests that ballooning resulted largely in sideways expansion of the intrusion. An analogue for sideways expansion during ballooning of an intrusion, albeit on a smaller scale, may be the Papoose Flats pluton of California (Sylvester *et al.*, 1978). Like the Aishihik Batholith, only one margin of the Papoose Flats intrusion is characterized by a well developed solid-state foliation. Adjacent wallrocks are thinned by up to 90%. Deformation resulted from the sideways expansion of the pluton during the final stages of intrusion in which massive quartz monzonite was emplaced in the core of the intrusion. Paterson *et al.* (1991) have, however, shown that at least some fabric development in the Papoose Flats intrusion is attributable to post-emplacement tectonism.

This model implies that the batholith is largely post-tectonic: metamorphism associated with the emplacement of the Aishihik Batholith is predicted to post-date tectonism responsible for the development of the F₂ folds preserved in the Nisling Assemblage. This is consistent with observations outlined above that suggest that D₂ tectonism is divisible into two stages: 1) shearing of the Nisling Assemblage prior to the intrusion of the Aishihik Batholith but after D₁ tectonism; and 2 - the late to post-tectonic emplacement of the Aishihik Batholith and the development of the schistosity and the metamorphic porphyroblasts at about $187.0 \pm 9.7/0.9$ Ma.

4.5 Steep faults

Late, steep to vertical faults that truncate older structures and fabrics affect the Nisling Assemblage, the Aishihik Batholith, and plutons of pink quartz monzonite of the Long Lake Suite. Faults are poorly exposed and are rarely observed. They are commonly recognized as linear features evident on the ground and on aerial photographs

In the Upper Nisling River area, the displacement of the steeply-dipping margins of an intrusion of pink quartz monzonite across a series of north - south trending lineaments suggests that faulting was characterized by a component of strike-slip motion (Figure 4.2 c). The margins of the pluton are sinistrally offset 100 to 1500 m. A north-northwest trending set of faults is also observed (Figure 4.2 c). The sense of displacement along these faults could not be directly determined. However, mapping immediately to the west of the Upper Nisling River area by Tempelman-Kluit (1974) indicates that the north margin of the Aishihik Batholith is dextrally offset by about 10 km along a north-northwest trending topographic depression (Figure 4.1).

In the North Aishihik Lake area, west of the Aishihik Lake, a linear, north-northwest trending fault zone truncates quartzite, amphibolite and marble of the

Nisling Assemblage (Figure 4.2 b). Foliation in quartzite is deflected in a dextral sense adjacent to the fault, and suggests that faulting was characterized by a component of dextral strike-slip motion (Plate 4.30). Marble in the fault zone is mylonitized (Plate 4.31).

North-northwest trending faults are subparallel to, and appear to be characterized by the same dextral sense of offset as the Denali fault, present 100 km to the southwest (Figure 1.1). 340 km of dextral slip occurred across the Denali fault between 57 Ma and 54 Ma (Eisbacher, 1976). The parallelism of the fault trends, and the matching sense of displacement (dextral strike-slip) suggests that faulting is Eocene and is related to displacement along the Denali fault. North trending faults, which are characterized by a component of sinistral strike-slip offset, probably developed at the same time and would represent a conjugate fault set.

In the South Aishihik Lake area, the Nisling Assemblage - Aishihik Batholith contact is faulted (Figure 4.2 a). The faults strike north to north-northwest. In foliated granodiorite of the batholith individual faults are defined by discrete planar surfaces (Plate 4.32). There is usually some discordance in the orientation of foliation across the faults. In schistose rocks of the Nisling Assemblage, the faults are defined by narrow, recessive zones up to 1 m in width, which are characterized by fault gouge (Plate 4.32). The faults are characterized by predominantly dip-slip displacement. Foliation in rocks in the immediate footwall of one well exposed fault deflects down into the fault. In the hangingwall of faults that cut the Nisling Assemblage - Aishihik Batholith contact, the contact is displaced down-dip 1 to 100 m (Figure 4.3 - cross-section E - F). Both down-dip to the east and down-dip to the west faults were observed.

The timing and tectonic significance of faults characterized by primarily dip-slip motion is not known. There is no evidence to suggest that these faults developed in response to significant extension of the region. Only three faults of minor displacement were identified. No penetrative fabric development is associated with the faults and no fault-related volcanic rocks were observed.

4.6 Discussion

Hornblende granodiorite intrusions of the Klotassin Suite, including the Aishihik Batholith, are characteristically foliated (Tempelman-Kluit, 1974; Woodsworth *et al.*, 1991). It has generally been assumed that the foliation resulted from syn- or post-intrusive deformation and tectonism (Tempelman-Kluit, 1974; 1979; Erdmer, 1989; Currie, 1992). Deformation has been attributed to: 1) Middle Jurassic overthrusting of the North



Plate 4.30 Brown graphitic quartzite next to a steeply dipping, brittle fault zone observed in the North Aishihik Lake area. The fault gouge consists of shattered and broken fragments of brown graphitic quartzite. The knife, which sits atop the fault gouge, is 4 cm long.

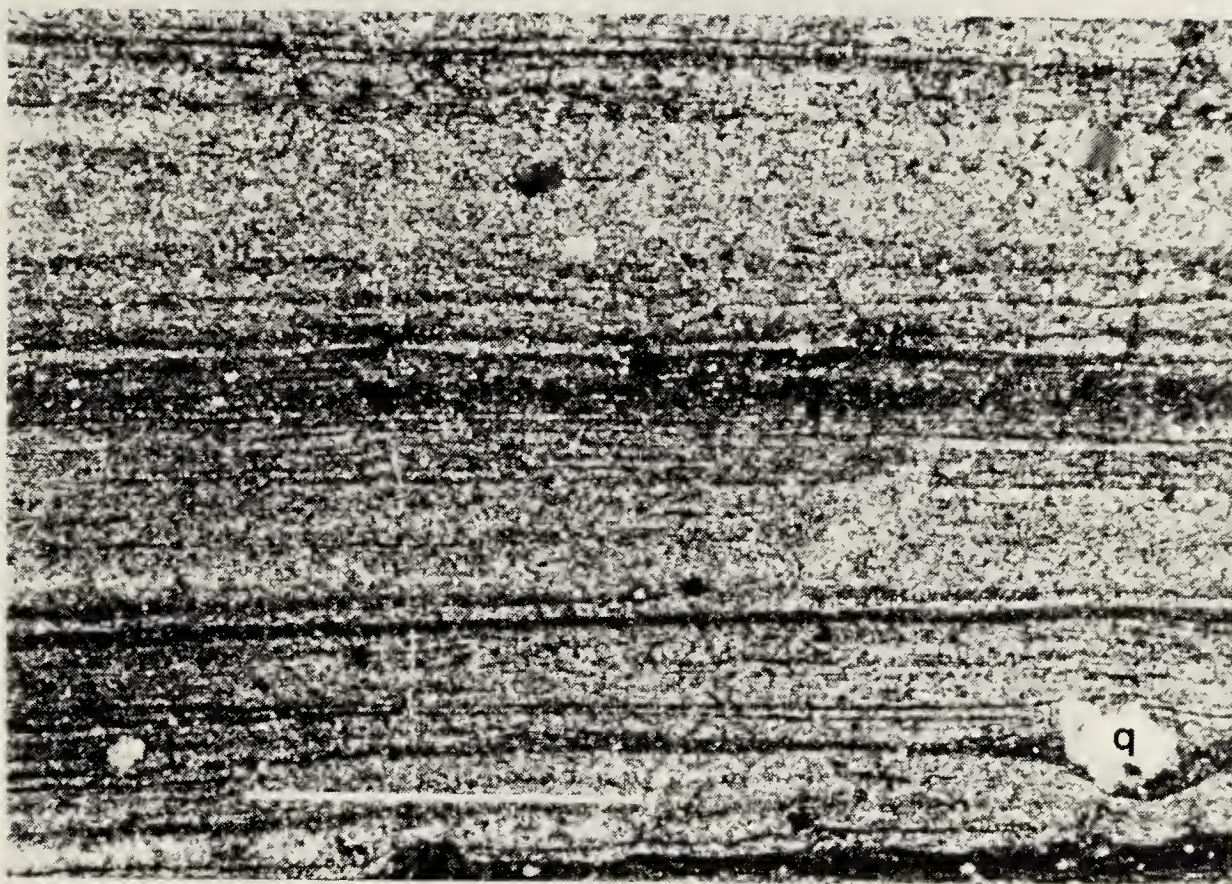


Plate 4.31 A photomicrograph, taken under crossed nicols, of mylonitized marble with characteristic quartz eyes (q). The scale bar represents 1 mm.

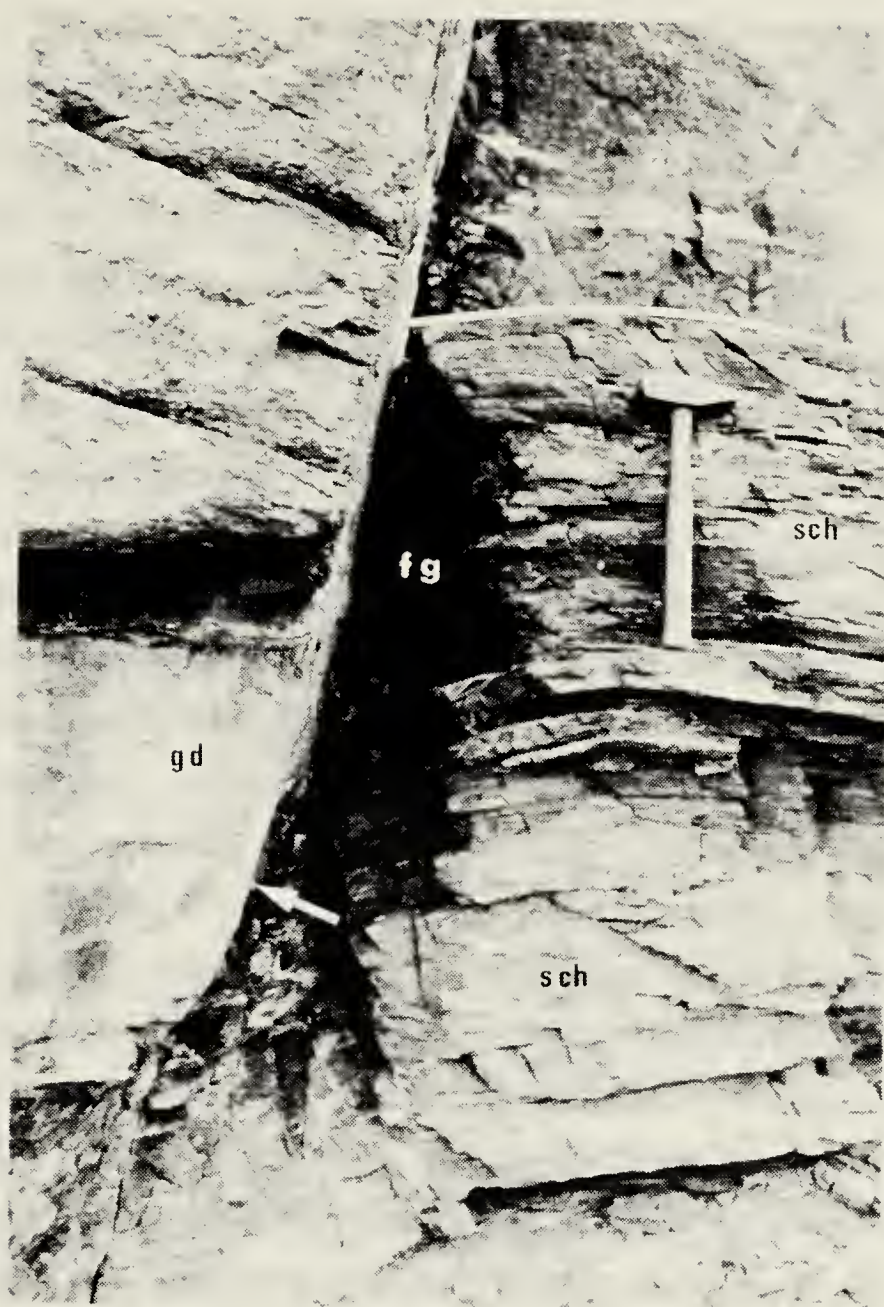


Plate 4.32 A steep fault that offsets the contact of the Aishihik Batholith with underlying schist of the Nisling Assemblage (highlighted with a white line) observed in the South Aishihik Lake area. The fault, indicated by the arrows, consists of a discrete plane in granodiorite (gd) and a narrow, fault gouge zone (fg) in schist (sch). The deflection of foliation in strata adjacent to the fault is consistent with the dip-slip offset of the contact. A hammer is shown for scale.

American continental margin by the Stikine terrane, including the Nisling Assemblage (Tempelman-Kluit, 1979); and 2) the Early to Middle Jurassic tectonic juxtaposition of the Nisling Assemblage with the Stikine terrane (Currie, 1992).

The foliation that characterizes the Aishihik Batholith is inferred largely magmatic and to have developed in response to magmatic flow during the diapiric emplacement of the batholith. A solid-state fabric that characterizes the lower contact of the batholith developed in response to late stage ballooning of the diapir. These relationships indicate that the batholith is post-tectonic and does not provide a record of either of Middle Jurassic overthrusting of the North American continental margin or of Early to Middle Jurassic tectonic juxtaposition of the Nisling Assemblage and the Stikine terrane.

The Nisling Assemblage has been variously interpreted as being: 1) continuous with, and representative of, semi-autochthonous North American continental margin (Hansen, 1990); 2) the basement of the Stikine terrane (Tempelman-Kluit, 1979); or 3) part of the Yukon - Tanana terrane (Mortensen, 1990; in press).

The Nisling Assemblage is inferred to be intruded by the Aishihik Batholith. The batholith constitutes part of the Early Jurassic Klotassin Suite (Tempelman-Kluit, 1974; Woodsworth *et al.*, 1991), which is characteristic of suspect terranes including the Yukon - Tanana and Stikine terranes. Similar plutons are not found intruding the North American continental margin. This suggests that the Nisling Assemblage does not constitute part of, and is not continuous with, the North American continental margin.

Correlation of the Nisling Assemblage with the North American continental margin led Hansen (1990) to suggest that North American rocks are characterized by structural fabrics that developed in response to Early Jurassic top-to-the-east shearing. While the Nisling Assemblage is characterized by east verging folds thought to have developed in the Early Jurassic (F₂), Early Jurassic structures characteristic of top-to-the-east shearing have not been documented for North American rocks and should not be used as a criterion for the recognition of North American strata.

Intrusion of the Nisling Assemblage by the Aishihik Batholith indicates that the Nisling Assemblage was part of Stikinia terrane by 186 Ma. However, pre-Aishihik Batholith, Early Jurassic, shearing in the Nisling Assemblage is not characteristic of Late Triassic and older strata of the Stikine terrane. Late Triassic Lewes River Group strata of the Stikine terrane are relatively undeformed and unmetamorphosed (Tempelman-Kluit, 1974; Wheeler, 1961). The Aishihik Batholith is, therefore, the oldest geologic element that is common to both the Stikine terrane and the Nisling Assemblage. The lack of any significant pre-Aishihik Batholith, shearing of Late Triassic strata suggests that the Stikine

terrane and the Nisling Assemblage constituted separate and distinct tectonic elements prior to the Early Jurassic.

In both the Yukon - Tanana terrane and the Nisling Assemblage the oldest preserved structural fabrics provide a record of ductile deformation of primary bedding (D_1). In the Early Jurassic the Yukon - Tanana terrane was imbricated with ophiolitic strata of the Slide Mountain terrane along regional thrust faults (Mortensen, 1990; in press; Mortensen and Jilson, 1985). Ductile top-to-the-east shearing followed by the intrusion of the Aishihik Batholith characterizes the Nisling Assemblage in the Early Jurassic. Structural fabrics preserved in the Yukon - Tanana terrane and the Nisling Assemblage do not, therefore, preclude the inclusion of the Nisling Assemblage as part of the Yukon - Tanana terrane. They do suggest, however, that the Nisling Assemblage in the Aishihik Lake region was at a deeper structural level in the Early Jurassic than much of the rest of the Yukon - Tanana terrane.

4.7 Conclusions

- 1 - The Aishihik Batholith is inferred to be an asymmetric, post-tectonic diapir which intrudes the Nisling Assemblage.
- 2 - The foliation that characterizes the Aishihik Batholith is largely magmatic and to have developed in response to flow during the emplacement of the batholith.
- 3 - A solid-state fabric that characterizes the lower contact of the Aishihik Batholith developed in response to late stage sideways ballooning of the diapir.
- 4 - The Aishihik Batholith does not provide a record of either of Middle Jurassic overthrusting of North America by the Stikine terrane, or of Early to Middle Jurassic tectonic juxtaposition of the Nisling Assemblage and the Stikine terrane.
- 5 - The Nisling Assemblage records at least three episodes of regional deformation including: D_1 - pre-Early Jurassic isoclinal folding of primary bedding; D_2 - Early Jurassic deformation characterized by the development of asymmetric, east-verging folds; and D_3 - post-Early Jurassic, pre-Late Cretaceous folding. The folds are asymmetric and verge to the west and affect both the Nisling Assemblage and the contact with the Aishihik Batholith.
- 6 - D_2 tectonism is divisible into pre-Aishihik Batholith and syn-Aishihik Batholith phases. Folding and shearing of the Nisling Assemblage preceded the emplacement, and did not result in deformation, of the Aishihik Batholith. The S_2 axial planar schistosity and metamorphic porphyroblasts developed, and provide a record of metamorphism, during the emplacement of the batholith.

7 - The Klotassin Suite plutonic assemblage intrudes Nisling Assemblage, but does not intrude North American strata, suggesting that Nisling Assemblage does not constitute part of, and is not continuous with, the North American continental margin.

8 - The structural evolution of the Nisling Assemblage is similar to and compatible with the structural evolution of the Yukon - Tanana terrane. The Nisling Assemblage in the Aishihik Lake region was, however, at a deeper structural level in the Early Jurassic than much of the rest of the Yukon - Tanana terrane.

9 - Two types of steep faults that are characterized by a component of strike-slip displacement affect rocks in the study area. These include a set of north-northwest trending faults characterized by dextral strike-slip offset and a set of north trending faults characterized by sinistral strike-slip offset. These two sets of faults are inferred to be a conjugate pair that developed in the Eocene at the same time as the Denali fault.

10 - Steeply dipping faults characterized by dip-slip displacement are rare and trend to the north or north-northwest. Both down-dip to the west faults and down-dip to the east faults are developed. Dip-slip faulting is not regionally significant and does not provide a record of significant extension of the Aishihik Lake region.

11 - The crust in the Aishihik Lake region has been regionally tilted more than 5° to the north. Tilting, and subsequent erosion, has resulted in the exposure of an approximately 10 km thick section of the crust. Deep structural levels are exposed near the south end of Aishihik Lake, and progressively shallower structural levels to the north.

V. METAMORPHIC PETROLOGY

5.1 Introduction

The Nisling Assemblage, a heterogeneous package of continental clastic, carbonate, and amphibolitic rocks, that crops out west of the Stikine terrane in southwest Yukon and northwest British Columbia (Figures 1.1 and 1.2), is regionally metamorphosed to upper greenschist to amphibolite grade (Tempelman-Kluit, 1976; Wheeler, 1961; Currie, 1991; Kindle, 1952; Muller, 1967; Way, 1977; Werner, 1977; 1978). Near Aishihik Lake in southwest Yukon metamorphism of the Nisling assemblage is indicated by the schistosity; the presence, in pelitic rocks, of aluminosilicate porphyroblasts including kyanite and sillimanite; and by horizons of amphibolite and marble (Erdmer, 1989; 1990; 1991; Gordey, 1973; Tempelman-Kluit, 1974).

The timing and tectonic significance of metamorphism is, however, poorly understood. Pre-Late Triassic metamorphism is indicated by: 1 - the truncation of metamorphic foliation by undeformed Late Triassic intrusions (Tempelman-Kluit, 1976); 2 - the incorporation of clasts of schistose rocks of the Nisling Assemblage in the Tally Ho Shear Zone, a strike slip fault thought to be active prior to 220 Ma (Hart and Radloff, 1990); 3 - unmetamorphosed sedimentary rocks which include Early Jurassic fossils and which unconformably overlap metamorphosed rocks of the Boundary Ranges Metamorphic Suite, thought to be at least in part correlative with the Nisling Assemblage (Mihalynuk and Rouse, 1988 a and b); and 4 - the incorporation of clasts of schist and gneiss similar to that of the Nisling Assemblage in unmetamorphosed sediments of the Late Triassic Stuhini Group (Currie, 1990). Regional metamorphism may also have occurred as recently as the Early Jurassic, and may have resulted from the intrusion of the Aishihik Batholith at $187.0 \pm 9.7/-0.9$ Ma (this study) as indicated by the regional decrease in metamorphic grade from amphibolite facies in the vicinity of the batholith, to greenschist facies along strike to the south (Tempelman-Kluit, 1974; Wheeler, 1961).

Because so little is known about the nature, timing, and tectonic significance of metamorphism of the Nisling Assemblage, it is difficult to determine the relationship of the assemblage with adjacent terranes. Tempelman-Kluit (1979) interpreted Nisling Assemblage as basement of the Stikine terrane. Hansen (1990) interprets the assemblage as part of the North American continental margin which is exposed in a window through the overlying accreted terranes. Mortensen (1992) has suggested that the Nisling Assemblage is correlative with the Yukon-Tanana terrane. Erdmer (1991) observed that the style and grade of metamorphism recorded in Nisling Assemblage is similar to that of

the Kluane Schist and suggested that the two may be related.

This chapter reports on the metamorphic history of the Nisling Assemblage including an estimate of the pressure and temperature conditions of metamorphism. The timing and tectonic significance of metamorphism and possible terrane correlations of the Nisling Assemblage are examined in light of these data.

5.2 The distribution and morphology of metamorphic minerals and migmatite in pelitic rocks

The distribution of metamorphic indicator minerals is shown in Figures 5.1 a, b, and c, as are the locations of cross-sections included in Figure 5.2. Sample location coordinates and descriptions for each sample are listed in Appendices 5.1. and 5.2, respectively.

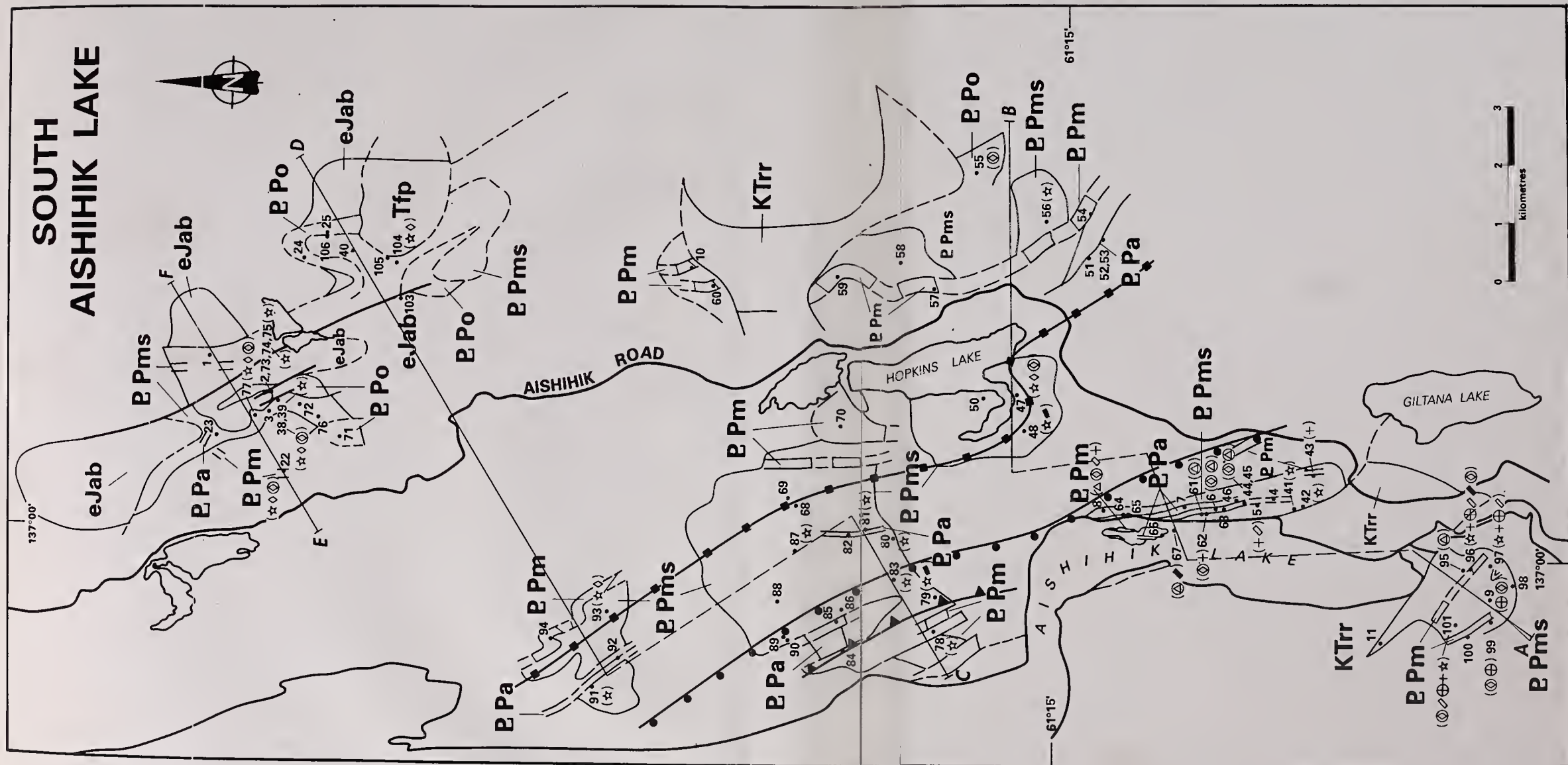
Mica

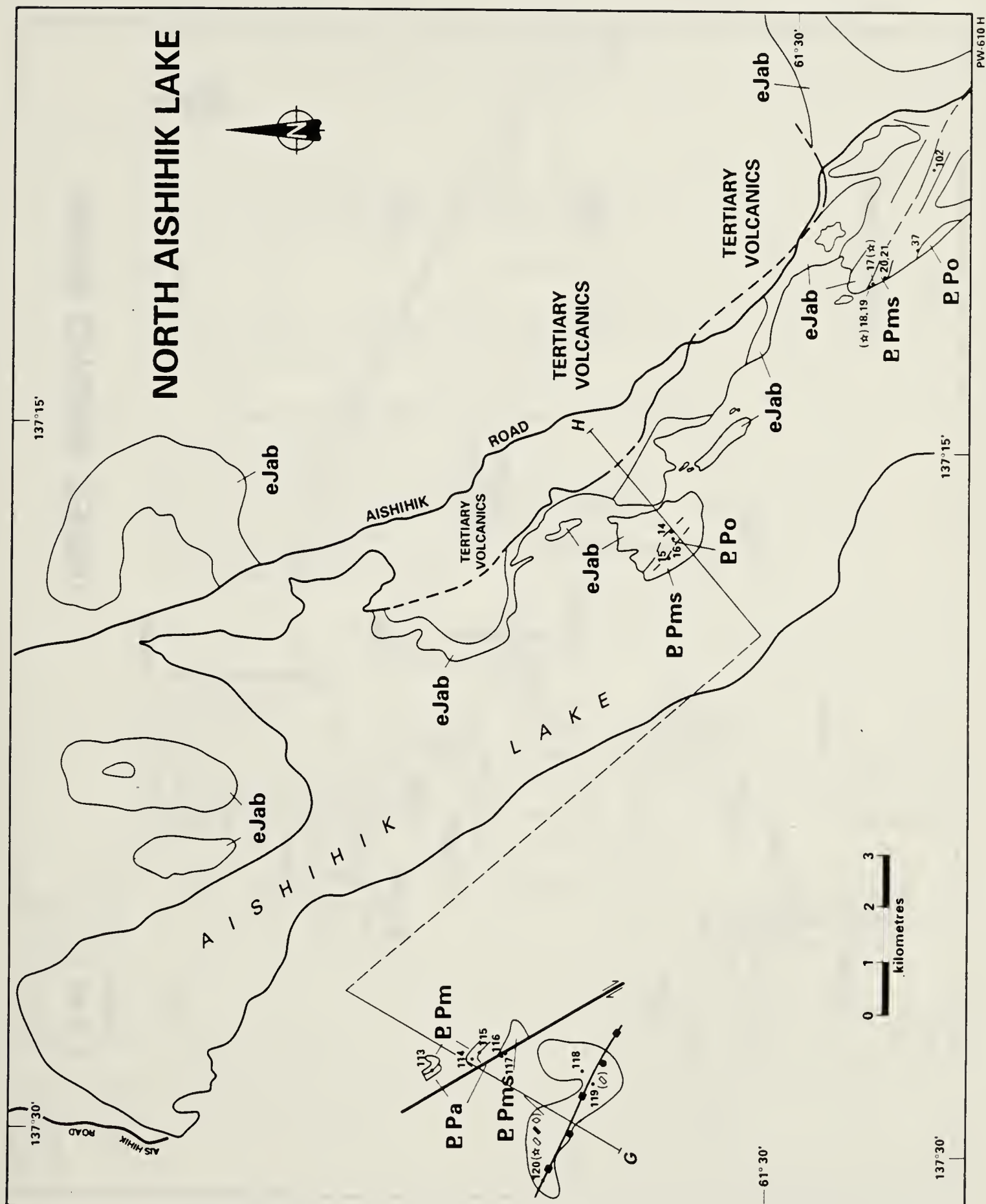
Mica occurs as medium-sized, anhedral grains that define a schistosity (S_2) which is evident throughout much of the study area and which parallels the contact with the Aishihik Batholith. In the hinges of folds of compositional banding mica occurs at an angle to compositional banding and defines an axial planar fabric (Plate 4.24). S_2 is defined by the parallel alignment of both biotite and muscovite. Within mica grains graphitic inclusion trails are locally evident, as are fine rutile needles. Euhedral zircon and tourmaline grains are also included within mica.

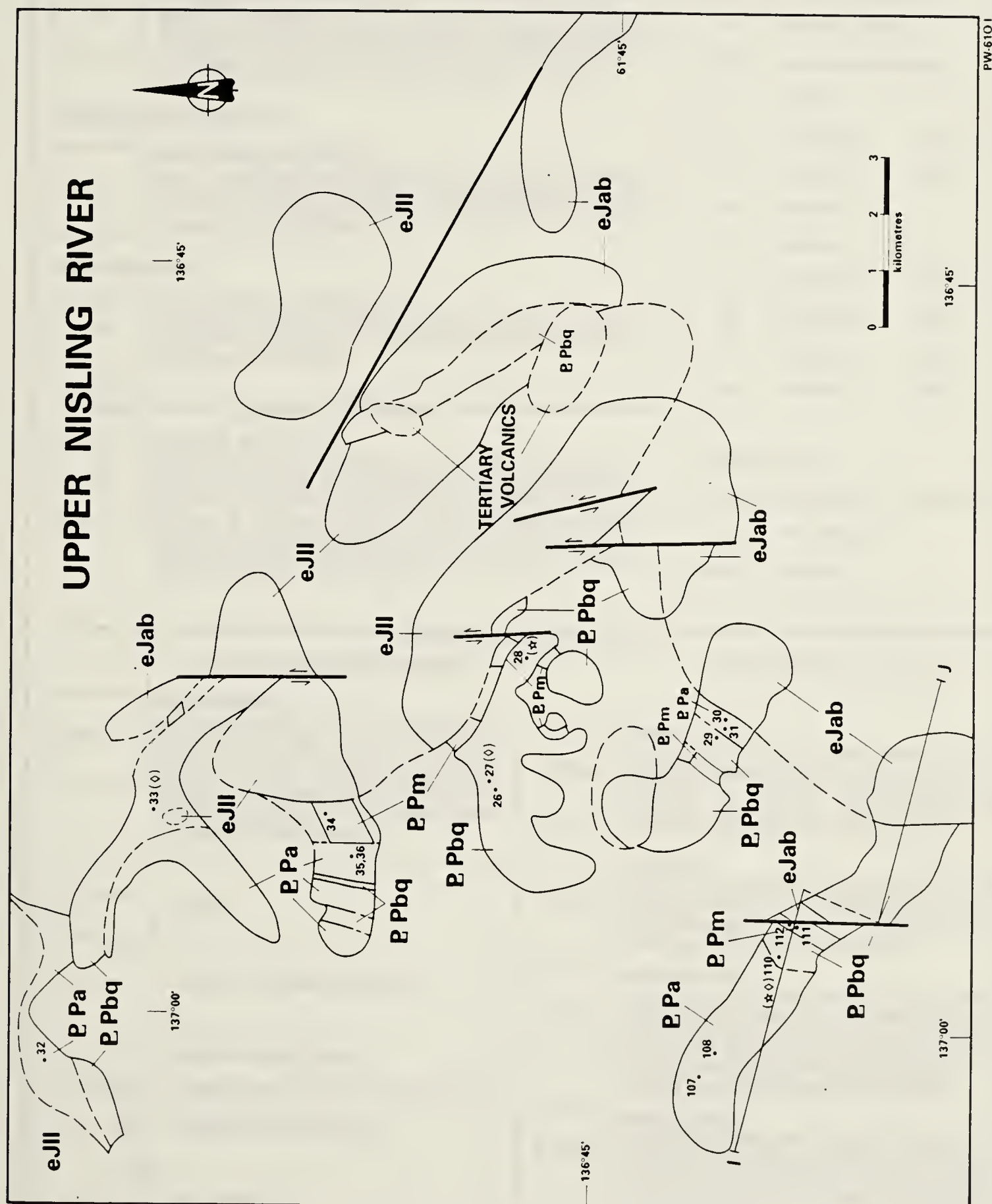
A second schistosity (S_1), defined by fine, anhedral biotite and muscovite grains, is locally evident. S_1 is preserved in a variety of habits including: 1 - within pelitic laminae, where it is characteristically folded and overgrown by foliation-parallel (S_2) mica. These folds are locally well preserved in strain shadows developed adjacent to garnet (Plate 5.1) and have S_2 as its axial planar fabric; 2 - as folded and variably oriented mica within quartz microlithons; 3 - within and adjacent to isolated fold hinges defined by discontinuous quartz horizons; and 4 - parallel to tightly folded compositional banding in micaceous quartzite.

Mica occurs in three other habits: 1 - Biotite overprints and grows at the expense of garnet. Both randomly oriented biotite and foliation subparallel biotite grains are observed, suggesting that garnet replacement occurred late in, and in part postdates, the foliation-forming event. Biotite is, however, affected by, and predates open folding of foliation; 2 - Within pelitic horizons S_2 is locally overgrown by fine-grained mica, usually muscovite, which is axial planar to open folds and crenulations of the main schistosity.

Figure 5.1 Detailed maps showing the distribution of map units, sample locations, the metamorphic mineral paragenesis for metapelitic samples characterized by porphyroblast development, and mineral isograds for each of: a) the South Aishihik Lake area; b) the North Aishihik Lake area; and c) the Upper Nisling River area. The location of these maps is shown in Figure 1.2. See text for explanation and discussion.



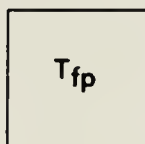




LEGEND

PLUTONIC ROCKS

TERTIARY

**FELDSPAR PORPHYRY**

heterogeneous igneous suite which includes plugs and small plutons of orange and pink weathering, flesh colored, miarolitic, massive, feldspar and quartz - feldspar porphyry; and dykes of brown and dark green weathering, green to buff colored, feldspar and hornblende feldspar porphyry.

CRETACEOUS & TERTIARY

**RUBY RANGE BATHOLITH**

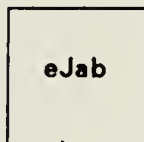
grey to tan weathering, grey to dark grey, medium to coarsely crystalline, massive to mildly foliated, hornblende and biotite hornblende diorite and granodiorite to nebulitic hornblende biotite granite.

EARLY JURASSIC

**LONG LAKE PLUTONIC SUITE**

orange weathering, orange and pink colored, coarsely crystalline to porphyritic, massive, miarolitic, quartz and biotite quartz monzonite.

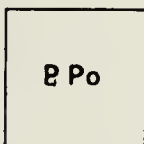
STIKINE TERRANE

**AISHIHIK BATHOLITH**

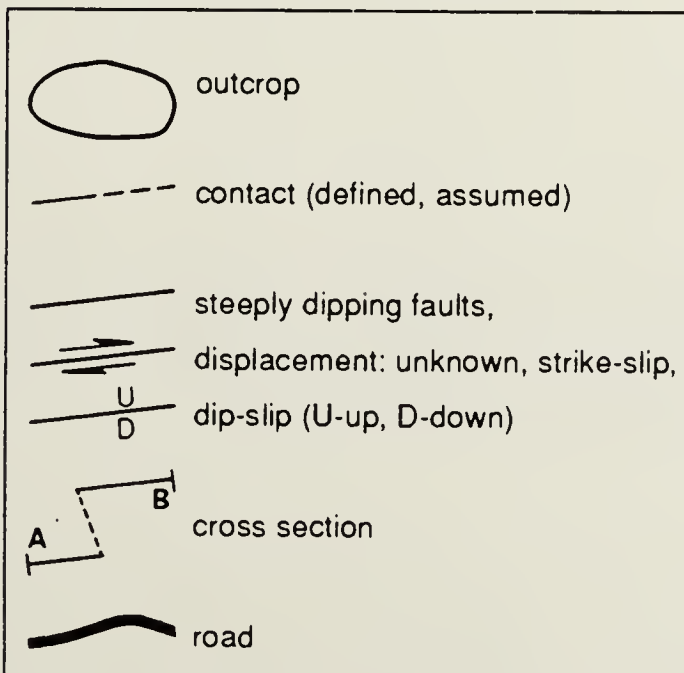
grey to light grey weathering, grey to dark grey colored, coarsely crystalline, equigranular to K-feldspar megacrystic, hornblende and biotite hornblende granodiorite to quartz diorite. A foliation, defined by the alignment of mineral grains, is commonly developed. A second foliation, defined by protomylonitic, and gneissic banding, is locally developed and overprints the mineral foliation.

NISLING ASSEMBLAGE

DEVONO-MISSISSIPPIAN

**ORTHOGNEISS**

tan weathering, light grey colored, medium to coarsely crystalline, feldspar augan, muscovite and biotite muscovite orthogneiss; and dark grey weathering, dark grey colored, medium grained, hornblende and biotite hornblende diorite and quartz diorite orthogneiss.



METAMORPHIC ROCKS

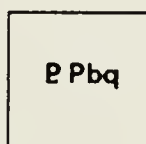
METAMORPHIC SYMBOLS

- Sample Location
- (☆◇) Mineral Assemblage
- ☆ Garnet
- + Andalusite (M₂)
- ⊕ Andalusite (M₄)
- ◇ Staurolite
- ◆ Kyanite
- ◇ Sillimanite (M₂)
- ⊙ Sillimanite (M₄)
- △ Cordierite (M₂)
- ⊙ Cordierite (M₄)

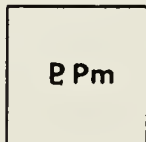
ISOGRADS (M₂)

- Sillimanite In - Kyanite Out
- ▬ Staurolite Out
- ▲ Kyanite In

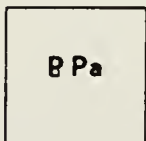
PALEOZOIC & OLDER

**BROWN QTZITE**

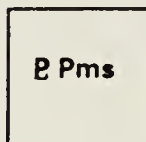
dark to light brown weathering, brown to buff colored, medium to fine grained, locally graphitic, micaceous and feldspathic quartzite. Includes thin and discontinuous marble, amphibolite and micaschist lenses.

**MARBLE**

light grey to light brown weathering, white to grey colored, fetid, coarsely crystalline, laminated calcite marble. Includes minor skarn, amphibolite, and calc-silicate

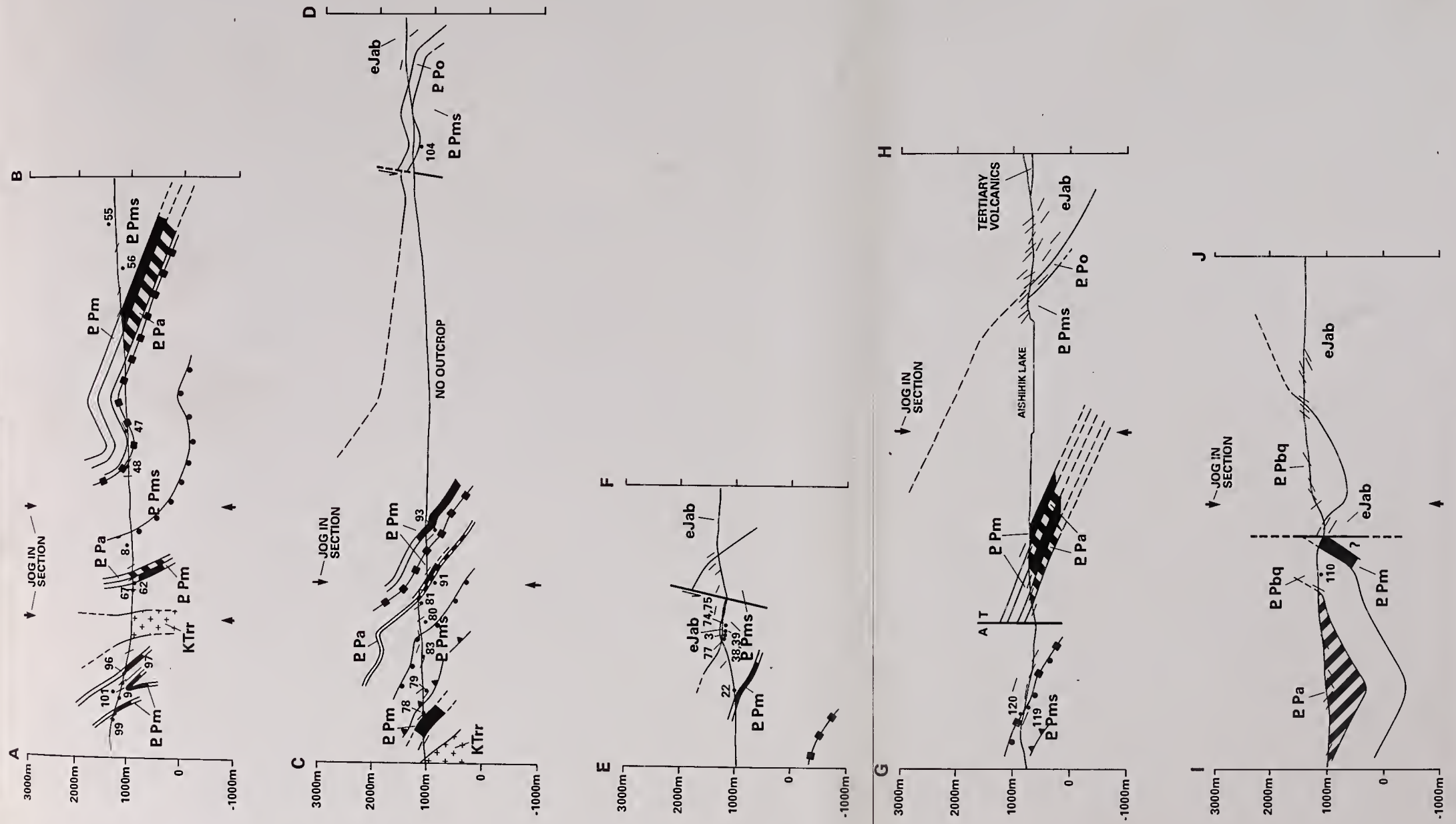
**AMPHIBOLITE**

dark green to black weathering, green colored, fine to coarsely crystalline, gneissic to well foliated, hornblende and biotite hornblende quartzite, micaschist and marble, and significant amounts of pistachio green, epidote hornblende diopside calc-silicate

**MICASCHIST**

Brown weathering, dark to light grey colored, medium to coarsely crystalline, well foliated to gneissic, migmatitic, muscovite biotite schist with minor grey quartz gneiss and brown weathering, tan colored, medium grained, foliated, micaceous & feldspathic quartzite. Includes minor amphibolite and marble.

Figure 5.2 Cross-sections, the locations of which are indicated on the maps in Figure 5.1. Symbols are defined in the legend to Figure 5.1. Marble is colored black; amphibolite is indicated by a striped pattern. The apparent dip of foliation is indicated. Sample locations and mineral isograds are also indicated.



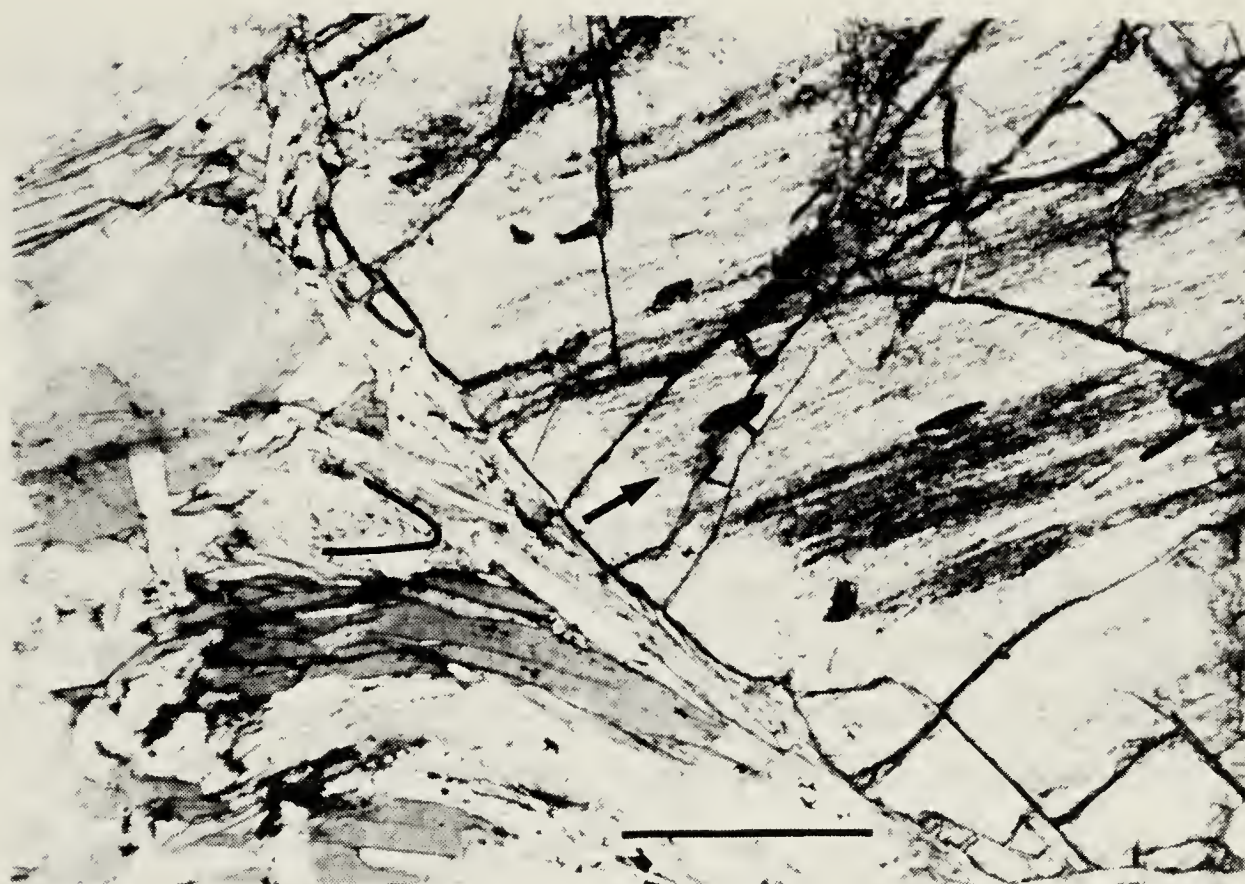


Plate 5.1 A photomicrograph, taken with plane polarized light, of a garnet porphyroblast hosted in micaschist (sample no. 79). The core of the garnet is characterized by a planar fabric (S_1) defined by numerous, fine graphite inclusions. The rim of the garnet is inclusion free. The arrow indicates the abrupt core - rim contact. To the left of the garnet, highlighted by a black line, are fine-grained micas which define a small, tight fold, thought to represent an F2 fold preserved in a pressure shadow adjacent to the garnet. The scale bar represents 250 μm .

These mica define a weakly developed crenulation schistosity (S_3); 3 - In the southern part of the South Aishihik Lake area S_2 is locally overgrown by randomly oriented, anhedral to subhedral, fine- to medium-grained muscovite and biotite porphyroblasts. These mica are most abundant adjacent to the Ruby Range Batholith.

Migmatite

Migmatite, defined as schist hosting an aplitic phase, is common and is present throughout the study area. Aplite occurs as elongate lenses and boudins which extend along foliation, and which are 1 to 20 cm thick and up to 2 m in length. Aplite lenses increase in size and number towards the Aishihik Batholith, but are evident throughout the study area. Foliaform mica and compositional banding wraps about and, rarely is truncated against aplite lenses. Where aplite lenses are abundant, foliation is wavy and irregular, primarily as a result of pinching and swelling of aplite lenses (Plate 2.1). Thin (< 2 mm) fine-grained, aphanitic, mafic selvages which mantle aplite lenses are locally evident. Large aplite lenses locally exhibit an internal curvilinear fabric, defined by coarsely crystalline horizons characterized by abundant K-feldspar augen, which merge with and parallel foliation in the adjacent schist. Larger aplite lenses also locally display a textural asymmetry. The basal surfaces of these asymmetric lenses are planar and define a sharp contact with the adjacent schist. The upper surfaces are, however, diffuse and irregular (Plate 5.2). These 'cauliflower structures' (Burg, 1991) are interpreted as geopetal features that develop in response to the upward migration metamorphic fluid. Upward migration results from a density contrast between the relatively light metamorphic fluid and the relatively heavy melanosome and schist. The presence of cauliflower structures on the top surfaces of aplite lenses suggest that these rocks are, at present, the same way-up as they were during metamorphism and migmatization.

Veins of aplite and granite are also common. Aplite veins are associated with migmatite, locally root in aplite lenses, and trend both along and across foliation. Locally, in metapelitic schist which is interfoliated with thin amphibolite horizons, aplite veins exhibit an asymmetric geometry, preferentially developing along the underside of the thin amphibolite horizons (Plate 4.20). This asymmetric geometry is interpreted as a geopetal feature. Amphibolite horizons are thought to act as impermeable barriers that prevent the upward migration of relatively light metamorphic fluids resulting in their along the undersides of the amphibolite horizons (Burg, 1991a; 1991b). This suggests that these rocks are currently the same way-up as they were during metamorphism and aplite vein development. Lenses of mildly foliated granite that root in migmatitic schist are locally

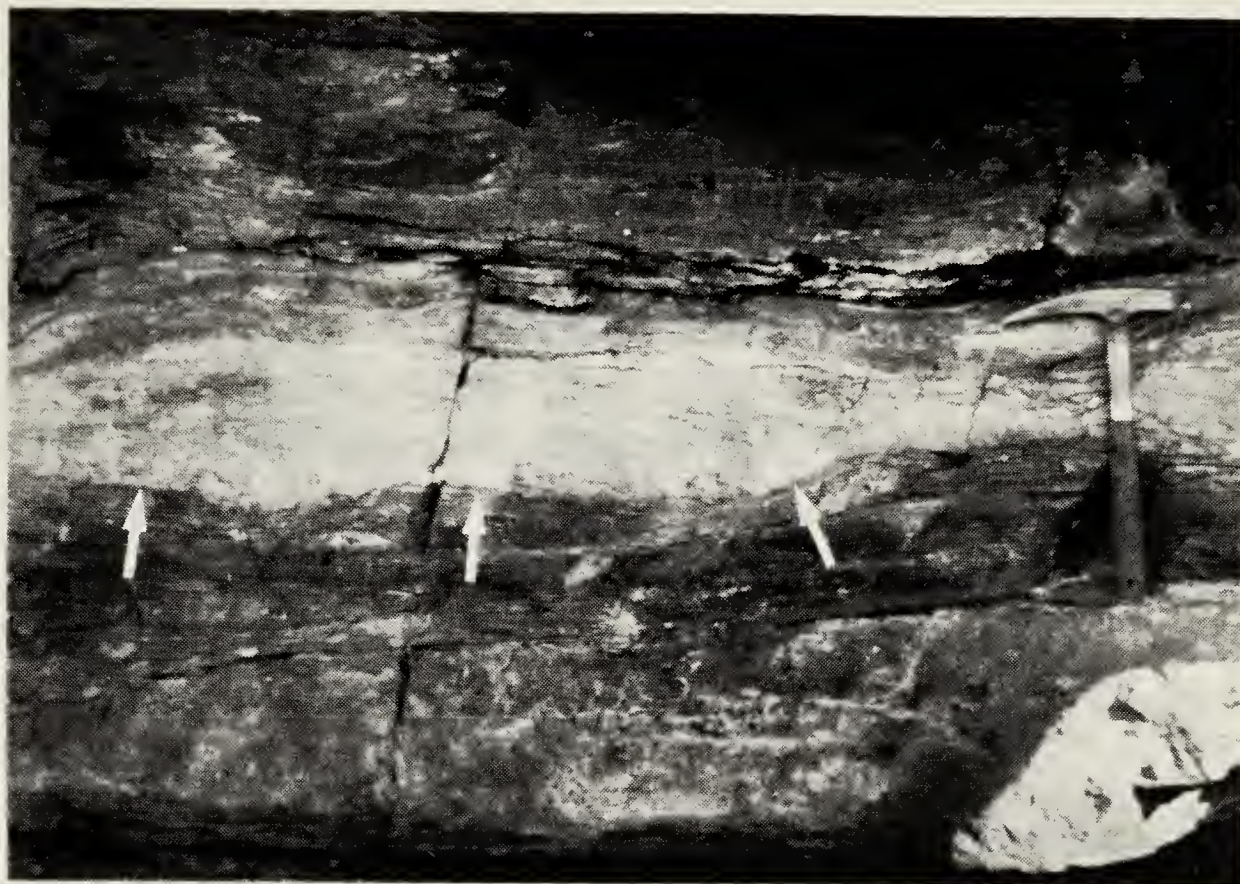


Plate 5.2 A large aplite lense in migmatitic feldspathic micaschist of the Nisling Assemblage observed in the South Aishihik Lake area. The base of the aplite lense is a sharp contact, indicated by the arrows. The top of the lense is a diffuse boundary across which aplite grades into non-migmatitic schist. A rock hammer is shown for scale.



THE UNIVERSITY OF CHICAGO
LIBRARY
540 EAST 57TH STREET
CHICAGO, ILL. 60637
TEL. 773-936-5000
FAX 773-936-5001
WWW.CHICAGO.EDU

evident close to the Aishihik Batholith. Elsewhere intrusions of massive granite truncate schistosity and include rafts of variably oriented schist.

Because aplite occurs as schistosity-parallel lenses and as boudins which are intimately interleaved with and wrapped by foliaform mica migmatite, it is interpreted to have developed contemporaneously with the development of the schistosity (S_2). Although some aplite and granite veins and intrusions are related to syn-schistosity migmatization, the presence of unfoliated granite which truncates the schistosity and which includes variably oriented schist rafts suggests at least one episode of post-schistosity granite intrusion. Unfoliated, cross-cutting granite intrusions are most abundant in the southern part of the South Aishihik Lake area adjacent to the intrusions of the Ruby Range Batholith and is inferred to be directly related to the Ruby Range Batholith (Figure 5.1 a).

Garnet

Garnet, though rare, is found throughout the study area, and occur as pink to dark red, subhedral to anhedral porphyroblasts <1 to 10 mm in diameter, and as fine, disseminated, anhedral grains which extend along the plane of schistosity. Subhedral "spongy" grains of garnet, which consist largely of inclusions within a garnet frame, are common (Plate 5.3). Garnet grains are usually located within pelitic horizons although they do occur in quartz and feldspar. Mica which lies within and defines S_2 wraps around garnet porphyroblasts (Plate 5.3). In almost all samples some replacement of garnet by biotite is evident (see above). Locally garnet porphyroblasts have been entirely replaced by biotite.

Garnets include grains of quartz, feldspar, mica (usually biotite), fine opaque material (thought to be graphite), and pyrite. Inclusions trails generally define a planar fabric that is tightly to isoclinally folded (Plate 4.26) and which is thought to represent an earlier fabric (S_1) which was deformed and subsequently overgrown by garnet. Garnets sometimes exhibit inclusion-free rims (Plate 5.1). Inclusion-free cores were also observed (Plate 5.4).

Garnets are interpreted to have nucleated and grown during the development of the S_2 schistosity as indicated by their preservation, in the form of inclusion trails of an older, deformed planar fabric (S_1) and by their relationship to mica which defines the S_2 schistosity. The presence of inclusion free rims and cores suggests that garnet growth may have resulted from several different reaction mechanisms and that garnet growth was episodic.

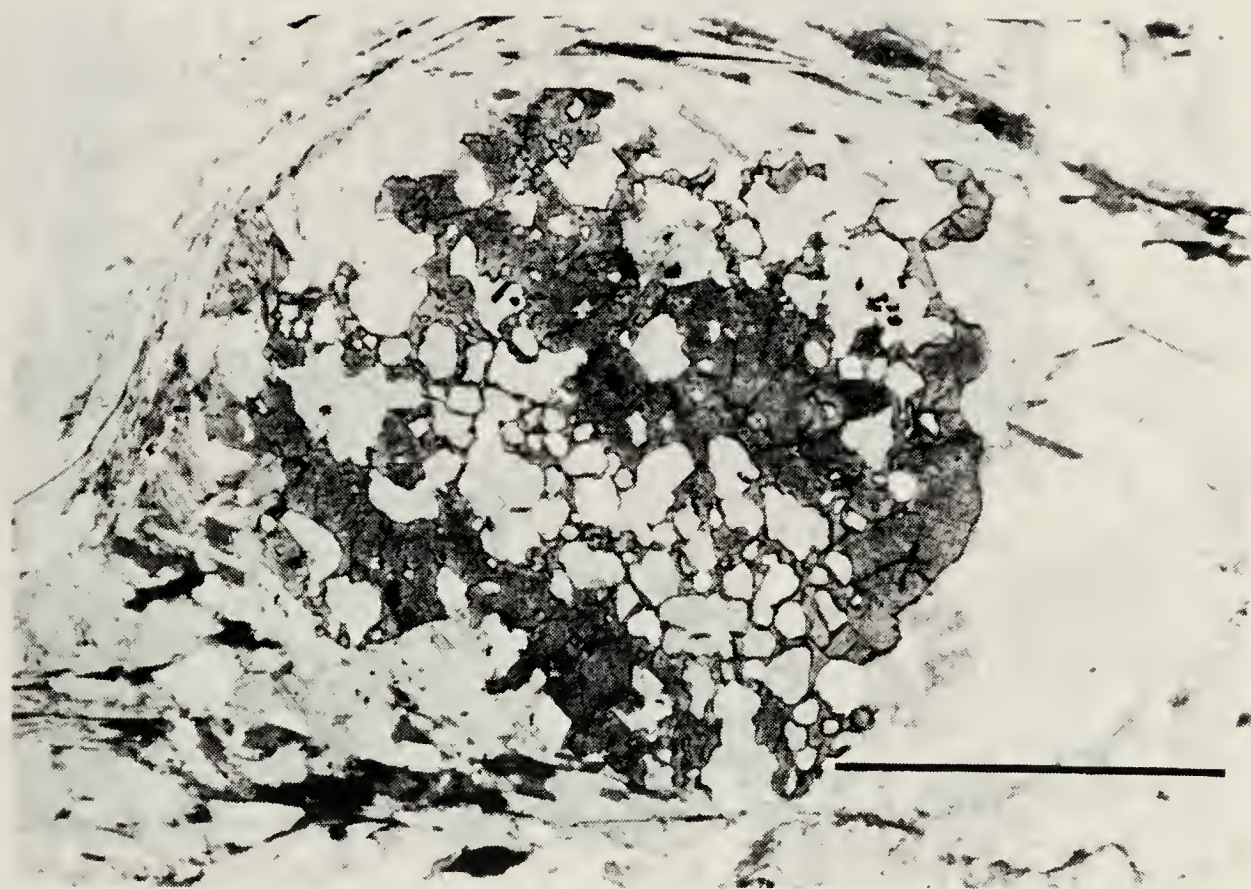


Plate 5.3 A photomicrograph, taken with plane polarized light, of an inclusion rich, spongy garnet in micaceous quartzite of the Nisling Assemblage (sample no. 93). Micas wrap around the garnet porphyroblast at upper left. The scale bar represents 1 mm.

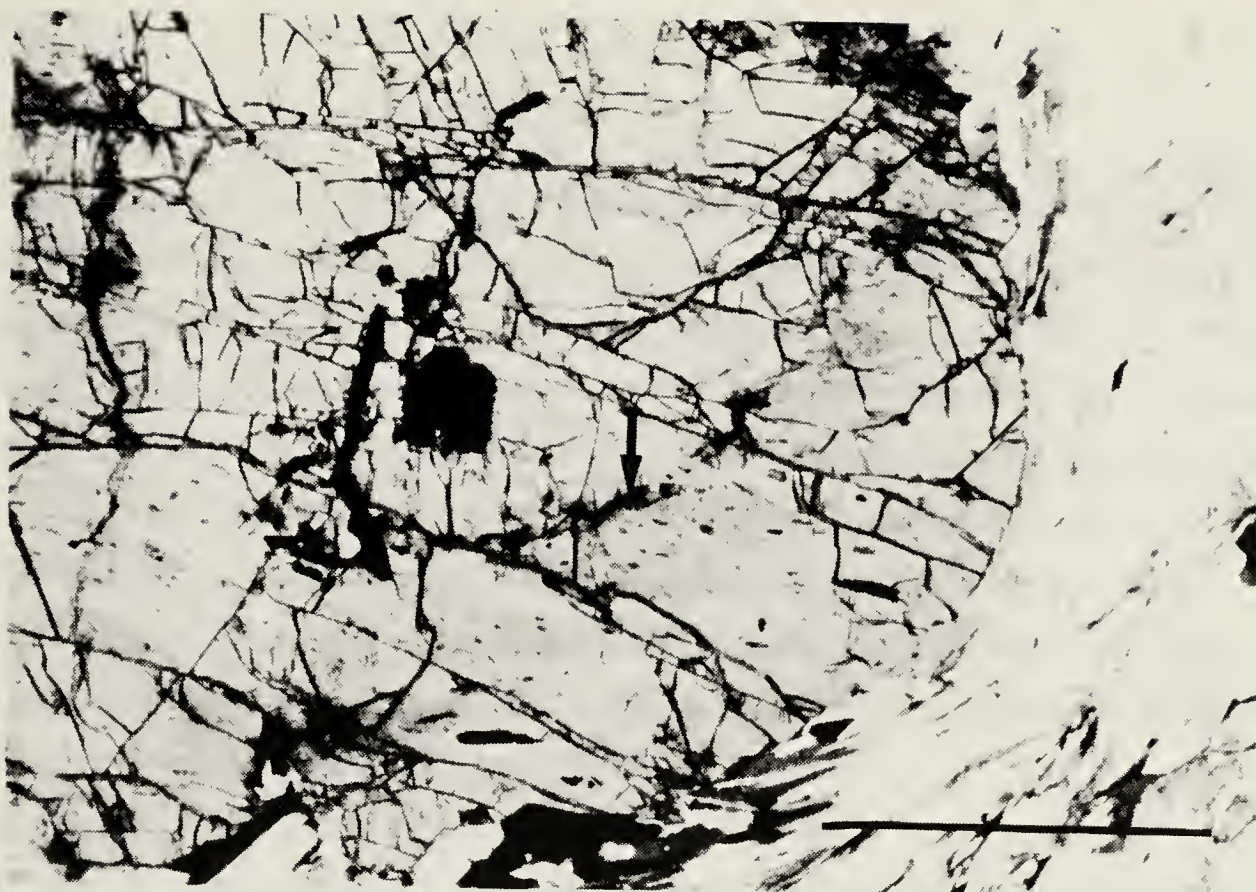


Plate 5.4 A photomicrograph, taken with plane polarized light, of a garnet porphyroblast from a sample of garnet micaschist of the Nisling Assemblage (sample no. 91). The garnet core is characterized by coarse pyrite inclusions but is devoid of graphite inclusions. The outer part of the porphyroblast is characterized by abundant, fine graphite inclusions. The arrow indicates the abrupt core - rim contact. The scale bar represents 1 mm.

Sillimanite

Schistosity-parallel fibrolite and finely crystalline sillimanite occurs intimately intergrown with biotite, and, less commonly, surrounded by quartz and feldspar (Plate 4.24). Locally fibrolitic sillimanite defines thin (less than 1 mm in width) and continuous laminae which define aluminum rich-compositional bands (S_1) (Plate 4.28). The laminae outline tight to isoclinal folds characterized by narrow, angular hinge zones and with S_2 along their axial surface. Fibrolite needles lie parallel to the lamination. Near the fold hinges fibrolite needles bend gently towards the hinge and exhibit mild undulose extinction. Needles are not, however, continuous around the fold hinges. Fibrolite needles also lie parallel to the trace of the axial planar surfaces of the folds. Upright open folds which affect schistosity also affect sillimanite (Plate 5.5).

Sillimanite is restricted to a zone approximately 2 km thick, measured perpendicular to schistosity, which extends out from, and parallels both the contact with the Aishihik Batholith and the S_2 schistosity (Figures 5.1 and 5.2).

As sillimanite is intimately intergrown with foliaform biotite, defines a schistosity-parallel zone, and is most commonly oriented parallel with schistosity, it is interpreted to have developed contemporaneously with the development of schistosity (S_2). However, because sillimanite locally exhibits undulose extinction where it is associated with tight to isoclinally folded S_1 aluminous laminae, it may have, at least in part, developed early during the schistosity-forming event.

A second generation of sillimanite occurs in a variety of habits including: 1 - thin fibrolite veins which parallel and cut across schistosity (Plate 5.6); 2 - randomly oriented fibrolite needles which nucleate in muscovite and along grain boundaries in quartz and feldspar; 3 - fibrolitic clots which pseudomorph and replace staurolite and andalusite; and 4 - fine crystalline sillimanite which fringes and mantles andalusite porphyroblasts. Sillimanite of this variety is not affected by upright open folds of schistosity; clearly post-dates the development of schistosity; is restricted to the South Aishihik Lake area (Figure 5.1 a) and is most abundant adjacent to the Ruby Range Batholith.

Kyanite

Kyanite is evident in five samples and occurs as elongate subhedral to anhedral porphyroblasts 1 to 7 mm in length which are usually oriented subparallel with schistosity (Plate 5.7), and as fine anhedral grains. Kyanite porphyroblasts characteristically include quartz along cleavage planes. Opaque grains and euhedral tourmaline grains also occur as

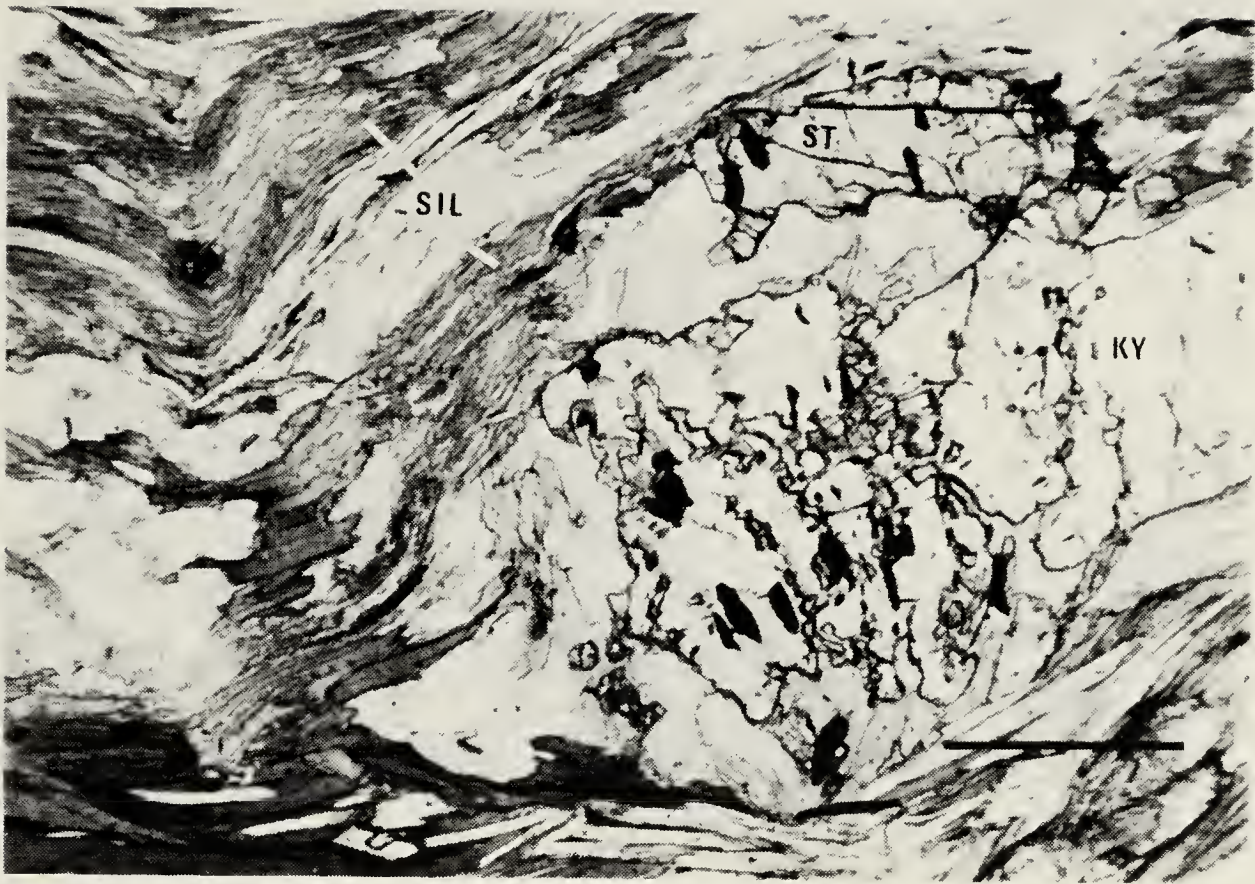


Plate 5.5 A photomicrograph, taken with plane polarized light, of sillimanite (SIL) staurolite (ST) kyanite (KY) schist of the Nisling Assemblage (sample no. 120). A well defined synformal crenulation of schistosity that also affects sillimanite is apparent in the upper left corner of the photograph. The scale bar represents 250 μm .



[Faint, illegible text at the bottom of the page, possibly a footer or a very faded title block.]

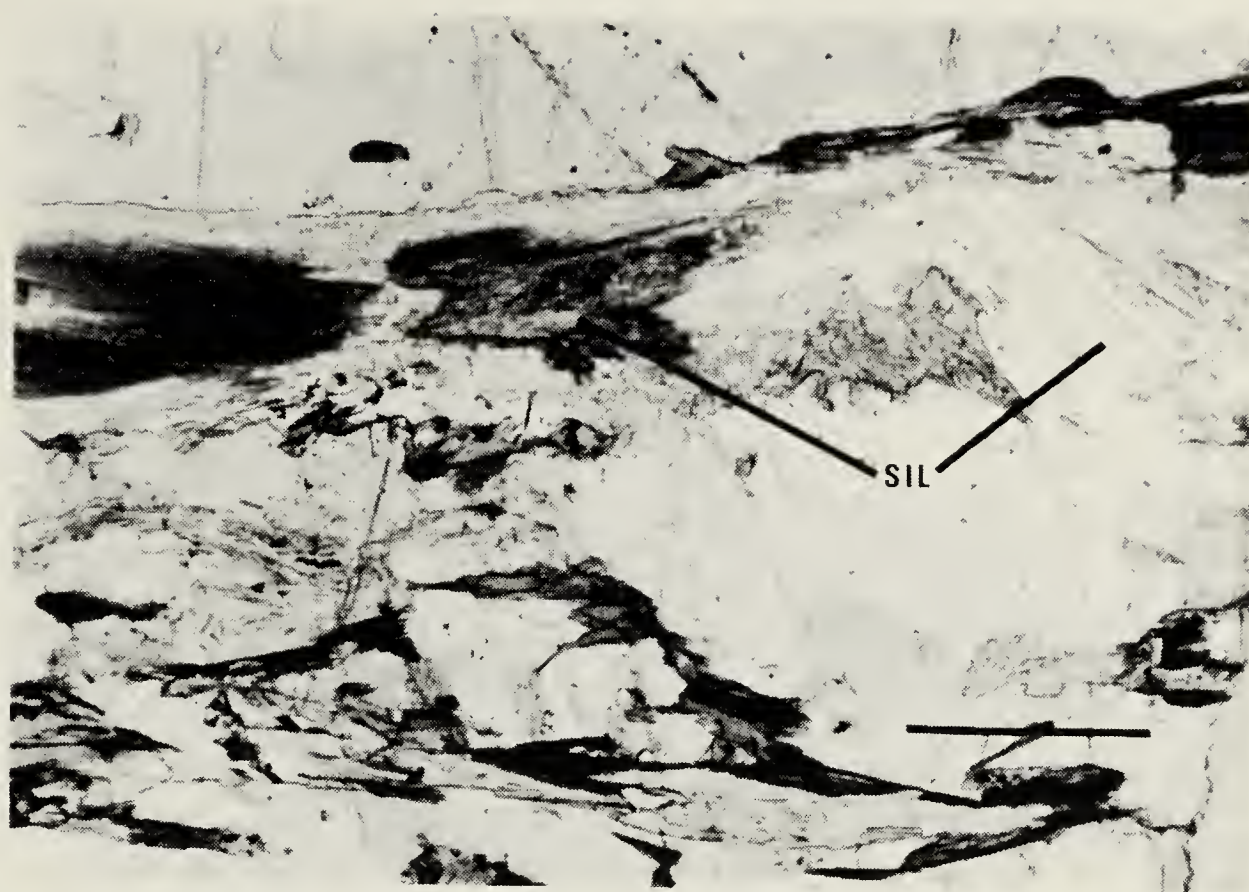


Plate 5.6 A photomicrograph, taken with plane polarized light, of micaceous orthogneiss of the Nisling Assemblage (sample no. 55). A fibrolite vein (SIL) cuts across foliation. Randomly oriented fibrolite needles root in the vein and grow out into the quartz feldspar matrix. The scale bar represents 250 μm .

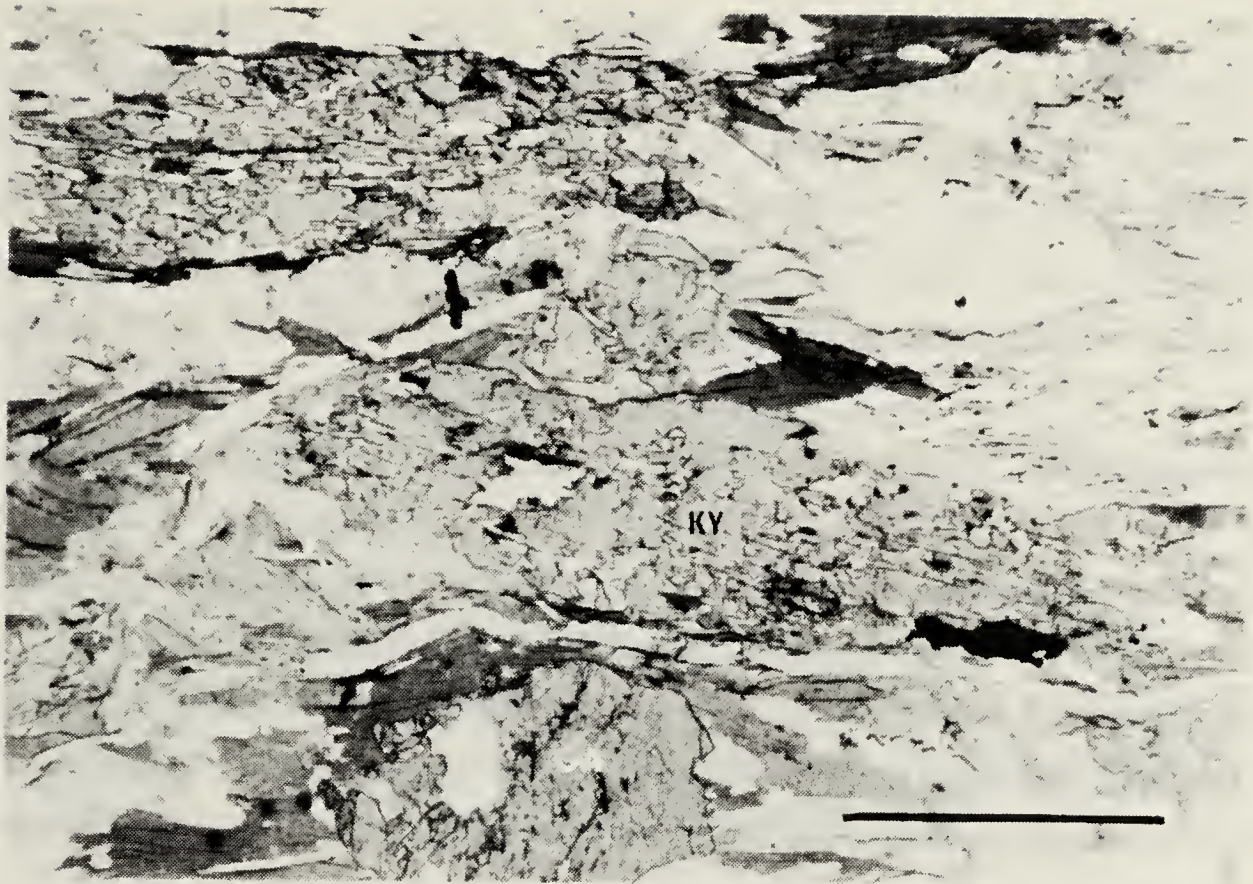


Plate 5.7 A photomicrograph, taken with plane polarized light, of garnet (GA) kyanite (KY) micaschist of the Nisling Assemblage (sample no. 48). The kyanite porphyroblasts lie along the plane of schistosity which parallels the top and bottom of the photograph. The scale bar represents 1 mm.

inclusions. No deflection of schistosity around kyanite porphyroblasts is evident. Where kyanite porphyroblasts are developed adjacent to garnet they are rarely bent, together with foliaform mica, around the garnet. Locally kyanite grains are embayed by and appear to be overgrown and replaced by muscovite. Upright open folds which affect schistosity also affect kyanite (Plate 5.5). Kyanite grains locally exhibit undulose extinction and are visibly folded, rarely resulting in the development of kink bands.

Kyanite is restricted to a 1.5 to 2.5 km thick zone, measured perpendicular to schistosity, which extends the entire length of the Aishihik Lake (Figures 5.1 a, b; and 5.2). The kyanite zone is subparallel with schistosity and with the contact with the Aishihik Batholith, and lies west of and subparallel to the zone in which foliaform sillimanite is developed. In the southern part of the study area the contact between the kyanite and foliaform sillimanite zones is sharp and no overlap is evident. Samples 47 and 48 are located about 200 m apart, measured perpendicular to schistosity, and exhibit well developed fibrolitic sillimanite and kyanite porphyroblasts, respectively (Figure 5.2, cross-section A - B). At the north end of Aishihik Lake, however, some overlap of the kyanite and sillimanite zones exists. Sample no. 120 is characterized by coexisting stable fibrolitic sillimanite and kyanite porphyroblasts (Plate 5.5).

As kyanite coexists with foliaform sillimanite and garnet, as it defines a foliaform zone which trends subparallel with the sillimanite zone, and as it predates the development of upright folds of schistosity, it is interpreted to be contemporaneous with the development of schistosity (S_2).

Staurolite

Staurolite occurs as elongate, anhedral to subhedral porphyroblasts less than 5 mm in length. Staurolite rarely exhibits a branching habit extending both subparallel to, and at a high angle to the S_2 schistosity (Plate 4.27). It also occurs as sigmoidal porphyroblasts which merge with plane of schistosity. Fine opaque inclusions, thought to be graphite, define a planar fabric (S_1) which is tight to isoclinally folded. Staurolite also includes tourmaline grains. Foliaform mica usually exhibits some mild deflection around staurolite porphyroblasts. Open folds of schistosity also affect staurolite grains (Plate 5.5).

Staurolite occurs in an elongate zone which, like the kyanite zone, extends the length of the Aishihik Lake and parallels both schistosity and the contact with the Aishihik Batholith (Figures 5.1 a, b; and 5.2). The staurolite zone lies west of and overlaps with the kyanite zone. Two samples, one collected at the south end of the South Aishihik Lake area (no. 96) and one collected near the north end of Aishihik Lake (no. 120), are

characterized by coexisting staurolite and kyanite. Sample no. 8, in which staurolite is present, was collected about 500 m, measured perpendicular to schistosity, east of sample no. 79, in which kyanite is present, suggesting that the zone of kyanite - staurolite overlap is at least 500 m thick. Sample no. 120, collected in the North Aishihik Lake area (Figure 5.1 b), also contains sillimanite (see above) (Plate 5.5), indicating that, in the North Aishihik Lake area the staurolite zone overlaps with the sillimanite zone. In the south end of the study area the staurolite and sillimanite zones are about 1.5 km apart, measured perpendicular to schistosity. The staurolite zone appears to extend west outside the limit of the study area and is thought to be at least 2 km thick.

As staurolite occurs as porphyroblasts which extend along and preserve an older, deformed fabric (S_1); as schistosity is mildly deflected by staurolite porphyroblasts; as open folds which affect schistosity also affect staurolite grains; and as the zone of staurolite stability extends subparallel to, and overlaps with the kyanite and sillimanite zones; staurolite is interpreted to have developed contemporaneously with the development of schistosity (S_2).

Andalusite

Andalusite occurs as subhedral chiasolitic porphyroblasts 3 - 7 mm in length that extend subparallel to schistosity and include quartz and opaque grains (Plate 5.8). Under crossed polars andalusite porphyroblasts have a felted appearance, consisting of individual "leaves" that extend subparallel to the long axis of the grains. Some deflection of foliaform mica around andalusite porphyroblasts is usually evident. Andalusite also mantles staurolite porphyroblasts. Andalusite appears to postdate and grow at the expense of staurolite as indicated by the presence of isolated, optically continuous staurolite grains within andalusite porphyroblasts (Plate 5.9). Andalusite mantles extend parallel with the long axes of enclosed staurolite grains and are locally sigmoidal, and merge with schistosity. Some deflection of foliaform mica around these composite porphyroblasts is usually evident. Open upright folds affect schistosity in andalusite-bearing rocks, although it is not possible to point to a folded andalusite grain. However, foliaform andalusite porphyroblasts are evident on the planar limbs of open folds of schistosity suggesting that andalusite developed prior to folding.

The area over which andalusite is present is coincident with the staurolite zone (Figure 5.1 a). Both staurolite-mantling andalusite and andalusite porphyroblasts (some of which may represent staurolite porphyroblasts which have been totally replaced by andalusite) are inferred to have developed late in the development of schistosity. This is

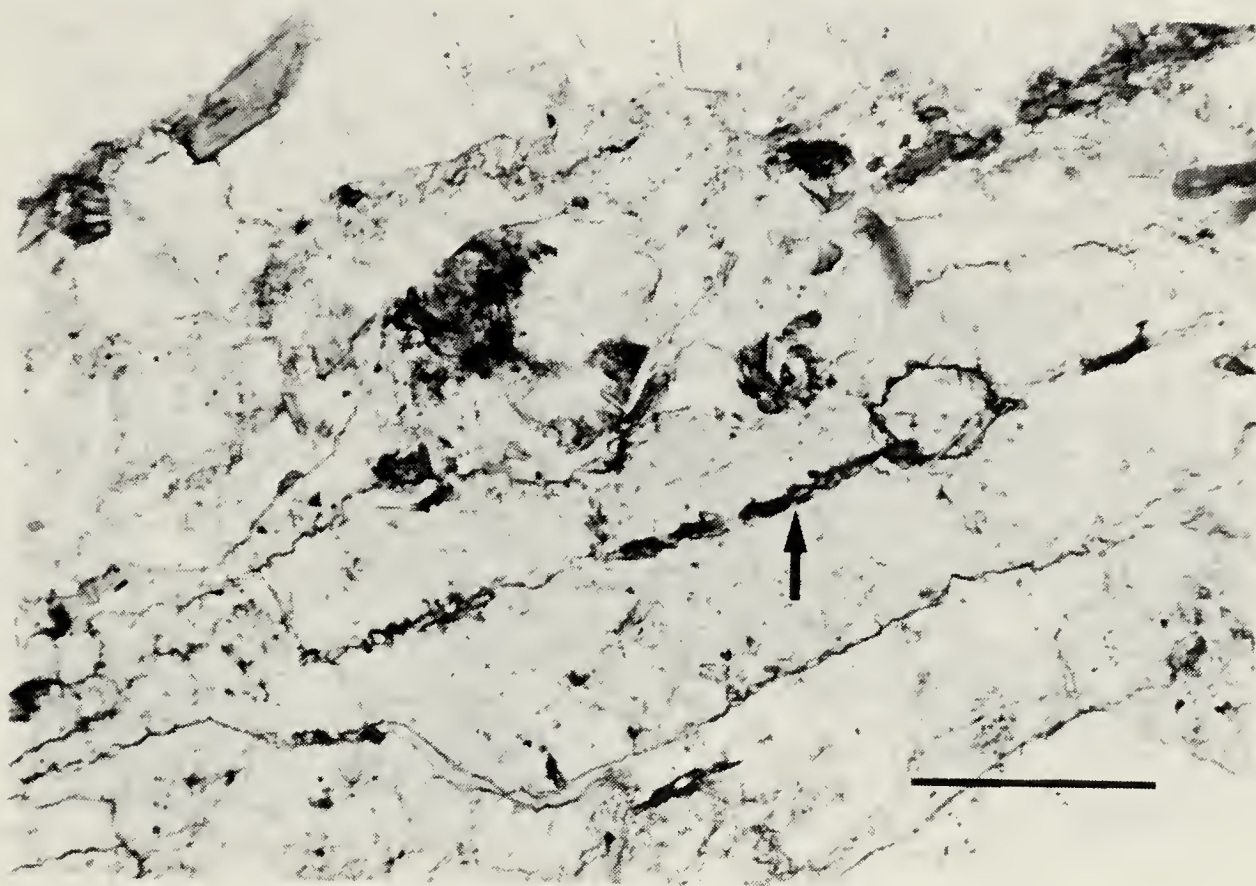


Plate 5.8 A photomicrograph, taken with plane polarized light, of andalusite schist of the Nisling Assemblage (sample no. 43). The arrow indicates the medial inclusion train in a chiastolitic andalusite porphyroblast. The scale bar represents 250 μm .



[Faint, illegible text, possibly a title or header, located in the lower middle section of the page.]

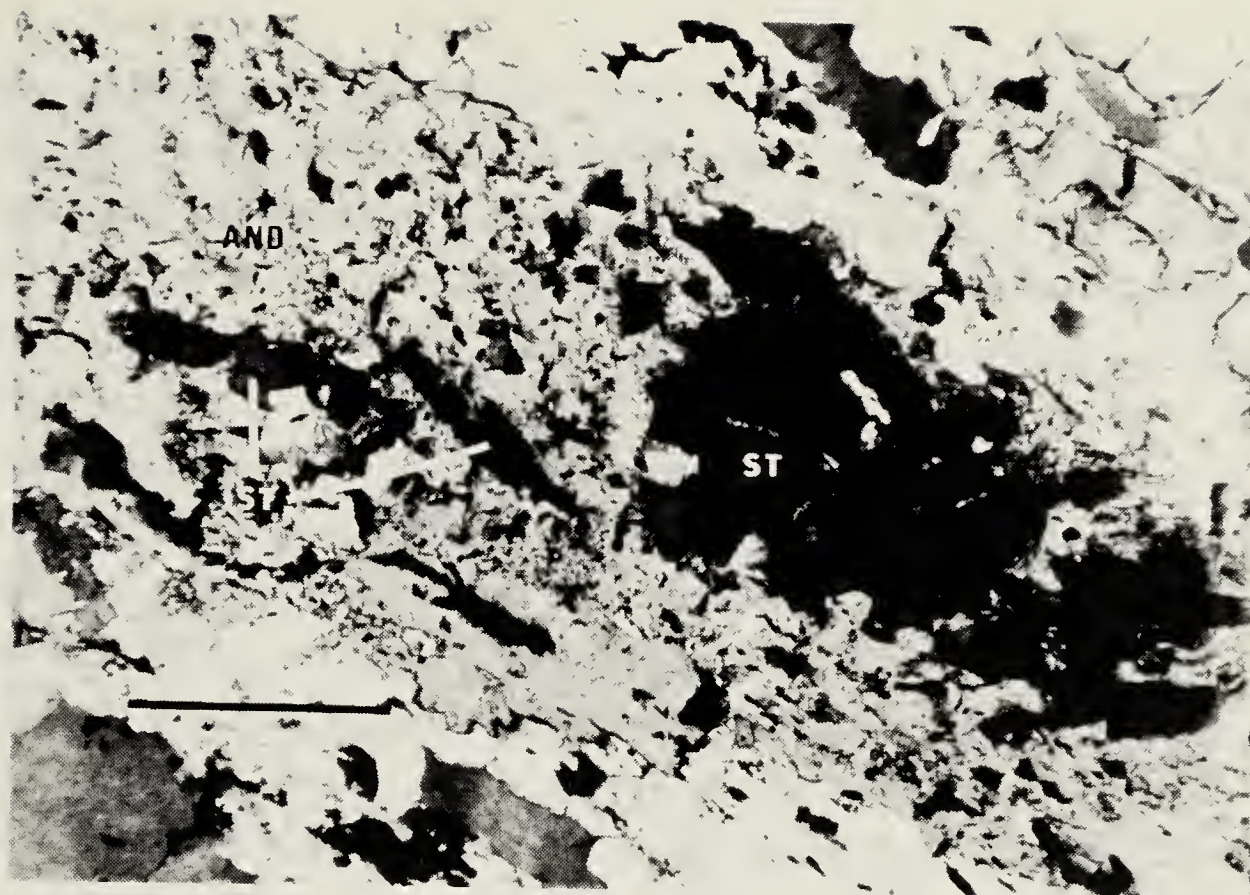


Plate 5.9 A photomicrograph, taken with crossed nicols, of andalusite (AND) staurolite (ST) schist of the Nisling Assemblage (sample no. 8). The andalusite mantles and encloses optically continuous staurolite grains. The scale bar represents 250 μm .

consistent with the alignment of andalusite porphyroblasts along schistosity, with the foliaform geometry of andalusite mantles, with the mild deflection of foliaform mica around both andalusite porphyroblasts and mantles, with the parallelism and overlap of the andalusite zone with the staurolite zone, and with the development of andalusite prior to open folding of schistosity. However, andalusite developed after, and grew at the expense of staurolite.

Andalusite also occurs as subhedral to euhedral (square in cross-section) grains, <1 to 10 mm in diameter, that preferentially nucleate on and grow at the expense of biotite, and that grow across and disrupt foliaform mica (Plate 5.10). This variety of andalusite also includes and grows at the expense of kyanite, garnet, and staurolite. Under crossed polars a few of the larger andalusite porphyroblasts have a felted appearance, consisting of individual "leaves" that radiate out from nucleation points and grain boundaries. Andalusite grows across and postdates open folds of schistosity.

Andalusite of this variety clearly post-dates the development of the S_2 schistosity. It is only observed in a thin zone immediately adjacent to intrusions of the Ruby Range Batholith.

Cordierite

Cordierite occurrence mimics that of andalusite. Cordierite occurs both as small (<5 mm in diameter) porphyroblasts which include graphite and mica grains and which is characterized by intersecting sets of multiple lamellar twins and by yellow, pinitic alteration (Plate 5.11). Inclusions define a planar fabric oriented at a slight angle to schistosity. Some mild deflection of foliaform mica around cordierite porphyroblasts is usually evident. Cordierite also occurs as a thin (<2 mm thick) mantle on foliaform mica and around garnet, kyanite, staurolite, and andalusite, and andalusite-mantled staurolite porphyroblasts. Like the andalusite mantles, cordierite mantles extend parallel with the long axes of enclosed porphyroblasts, are characterized by a sigmoidal geometry, and merge with schistosity. Open upright folds affect schistosity in cordierite-bearing rocks, although it is not possible to point to a folded cordierite grain. However, foliaform cordierite porphyroblasts are evident on the planar limbs of open folds of schistosity suggesting that cordierite developed prior to folding.

The area over which cordierite is present is coincident with the andalusite zone (Figure 5.1 a). Both cordierite mantles and cordierite porphyroblasts are inferred to have developed late in the development of schistosity. This is consistent with the inclusion of a planar fabric, defined by graphite and mica grains, oriented at a slight angle to schistosity,

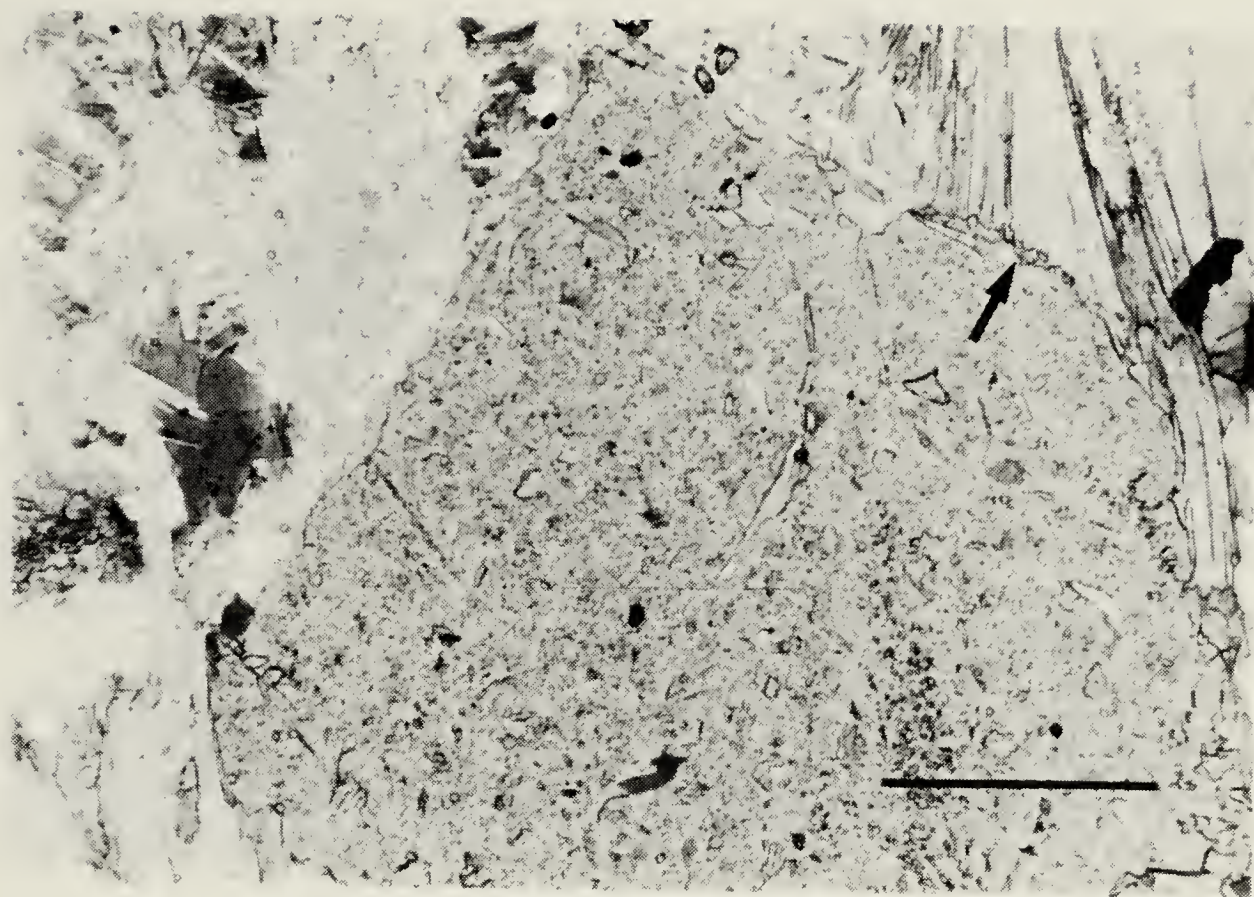


Plate 5.10 A photomicrograph, taken with plane polarized light, of andalusite micaschist of the Nisling Assemblage (sample no. 97). The arrow indicates where a euhedral (square outline) andalusite porphyroblast has overgrown and truncated schistosity parallel mica. The scale bar represents 250 μm .



Plate 5.11 A photomicrograph, taken with plane polarized light, of cordierite micaschist of the Nisling Assemblage (sample no. 8). The arrow indicates the abrupt contact between the core, characterized by abundant fine graphite inclusions, and the inclusion free rim, of a cordierite porphyroblast. The scale bar represents 250 μm .

and with the similarity between cordierite and andalusite morphology and distribution.

Cordierite also occurs as round, anhedral, inclusion free grains that most commonly occur in aggregates of 5 to 10 grains and that exhibit yellow pinitic alteration (Plate 5.12). Locally cordierite is altered to a yellow-brown, amorphous, isotropic substance (pinnite). Cordierite nucleates on and grows across both micaceous and quartzofeldspathic laminae.

Cordierite of this variety post-dates the development of the S_2 schistosity. Like post-schistosity andalusite, cordierite of this variety is only observed in a thin zone immediately adjacent to intrusions of the Ruby Range Batholith.

Feldspar

Potassium and plagioclase feldspar are present throughout the study area. Plagioclase occurs as anhedral to subhedral grains that are intimately intergrown with quartz and K-feldspar and which are locally characterized by curvilinear inclusion trails, consisting of quartz and graphite particles, oriented at a high angle to schistosity. Plagioclase also occurs as subhedral to euhedral porphyroblasts which extend along schistosity, and which include quartz grains and foliaform mica. Quartz lamella accounting for 35% of individual grains, is locally evident. K-feldspar occurs as anhedral to subhedral grains intimately intergrown with plagioclase and quartz and as subhedral porphyroblasts. K-feldspar porphyroblasts extend along schistosity, include quartz grains and foliaform mica, and locally are cored by plagioclase porphyroblasts with quartz exsolution features (Plate 5.13). Upright open folds which affect schistosity also affect plagioclase and K-feldspar grains.

Feldspar development spans the entire schistosity-forming event as indicated by; the preservation of an earlier developed schistosity (S_1) in plagioclase grains; the inclusion of foliaform mica (S_2) in both plagioclase and K-feldspar grains; and by the schistosity-parallel alignment of feldspar porphyroblasts. K-feldspar porphyroblasts are cored by plagioclase porphyroblasts, include mica which parallels the S_2 schistosity, and probably developed late relative to the peak metamorphic paragenesis.

Sericite - Chlorite

Minor sericitic alteration of feldspar is evident throughout the study area. Significant alteration, characterized by the development of dense mats of randomly oriented, anhedral muscovite and sericite grains that preferentially overgrow and replace aluminosilicate porphyroblasts, including kyanite, staurolite, and andalusite (Plate 5.14), is

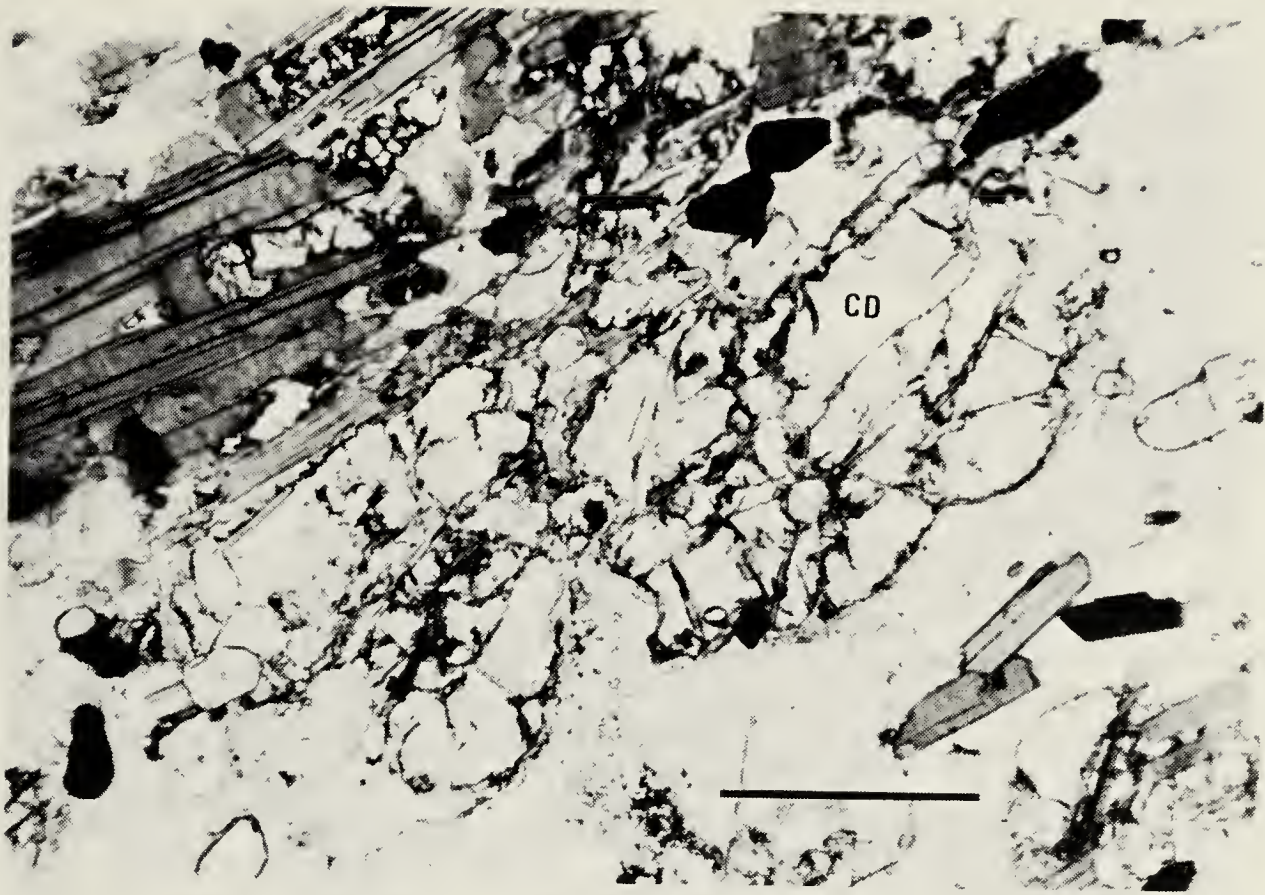


Plate 5.12 A photomicrograph, taken with plane polarized light, of cordierite (CD) micaschist of the Nisling Assemblage (sample no. 42). A cordierite porphyroblast, at center, consists of an aggregate of anhedral, inclusion free grains that overgrow and replace schistosity-parallel biotite. The scale bar represents 250 μm .



[Faint, illegible text, possibly a title or a list of items.]



Plate 5.13 A photomicrograph, taken with crossed nicols, of micaschist of the Nisling Assemblage (sample no. 42). A large inclusions rich K-feldspar porphyroblast occupies much of the field of view. Both the feldspar grain and the inclusions are oriented parallel to the enclosing schistosity. Inclusions include opaque grains, mica, quartz lenses, and (indicated by the arrow) a plagioclase grain that is characterized by quartz lamella. The scale bar represents 1 mm.

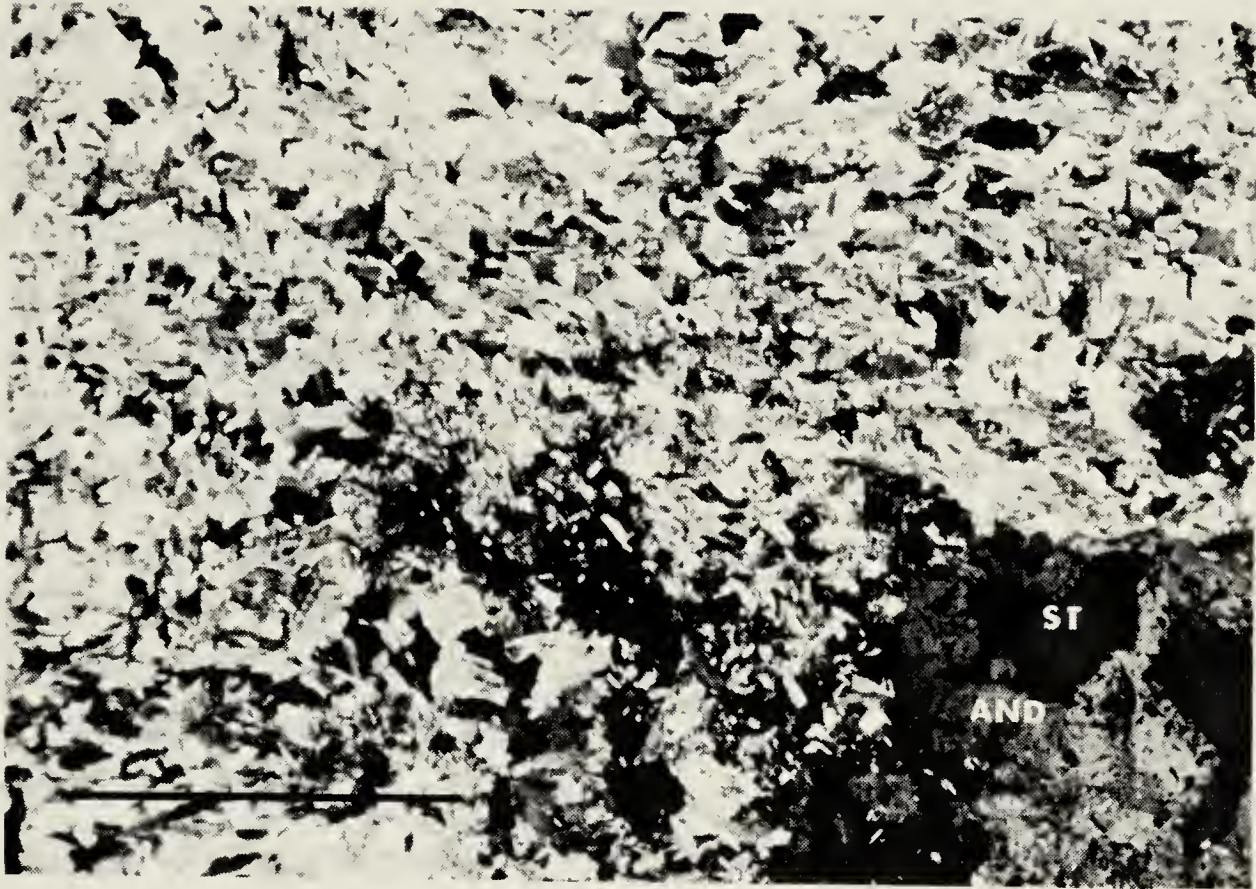


Plate 5.14 A photomicrograph, taken with crossed nicols, of sericitized andalusite (AND) staurolite (ST) micaschist of the Nisling Assemblage (sample no. 5). Intense sericitization has resulted in the almost total replacement of a composite andalusite - staurolite porphyroblast, some of which is evident at lower right, by fine-grained, randomly oriented, mica. The scale bar represents 1 mm.

only observed in the South Aishihik Lake area (Figure 5.1 a) adjacent to the Ruby Range Batholith. Sericitic alteration postdates and is not affected by open folds of schistosity.

Chlorite is widely distributed in the study area and occurs as randomly oriented anhedral to subhedral grains and preferentially replaces mica and garnet. Chlorite is also present along fractures and locally overgrows and totally replaces schistosity. Chlorite grains postdate and are not affected by open folds of schistosity.

Like sericite, chlorite alteration is most significant in the southern part of the study area adjacent to the Ruby Range Batholith.

5.3 Mineral isograds

Textural relationships and the areal distribution of metamorphic indicator minerals (Figure 5.1 a, b, and c) suggests that rocks of the Nisling Assemblage have been subjected to four metamorphic events (Figure 5.3). Evidence of the earliest metamorphic event (M_1) consists of a locally preserved micaceous schistosity (S_1) that has been deformed and overgrown during subsequent tectonism. This early schistosity is also preserved as inclusion trails in various porphyroblasts including mica, garnet, staurolite, and plagioclase. Staurolite porphyroblasts exhibit a branching habit that mimics an earlier developed schistosity.

Most metamorphic minerals, including mica (which defines a schistosity - S_2 - evident throughout the study area), garnet, sillimanite, kyanite, staurolite, andalusite, and cordierite, postdate and overprint S_1 , and record a younger metamorphic event, M_2 (Figure 5.3). Significant amounts of migmatite developed during this event. The distribution of sillimanite, kyanite, and staurolite define a series of isograd-bound metamorphic zones (Figure 5.1). Isograds are well defined in the South Aishihik Lake area and are more loosely defined to the north. In the Upper Nisling River area (Figure 5.1 c) only sillimanite was observed. West of the Aishihik Batholith sillimanite (in), kyanite (out and in), and staurolite (out) isograds are oriented sub-parallel with the S_2 schistosity and with the contact with the Aishihik Batholith, and dip east beneath the batholith (Figure 5.2). Mineral isograds truncate to the south against the Ruby Range Batholith. The regional distribution of M_2 isograds and metamorphic zones is shown in Figure 5.4, a map of the study area. Andalusite and cordierite post-date peak M_2 metamorphism and cannot be used to define isograds. This is discussed further below.

Of the four metamorphic events, M_3 is the least significant. During folding and crenulation of the S_2 schistosity small mica grains (mostly muscovite) nucleated and grew subparallel with the axial planes of the crenulations. S_3 mica are rare and are not



Figure 5.3 The relative timing of metamorphic mineral nucleation and growth. Four metamorphic events are recognized. See text for discussion. Ga - garnet; Bi - biotite; St - staurolite; Ad - andalusite.



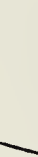
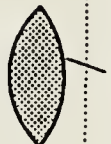





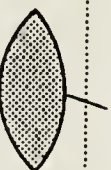
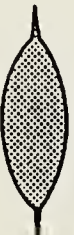

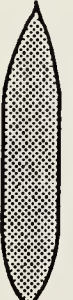
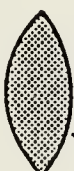
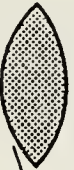


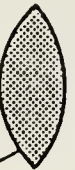

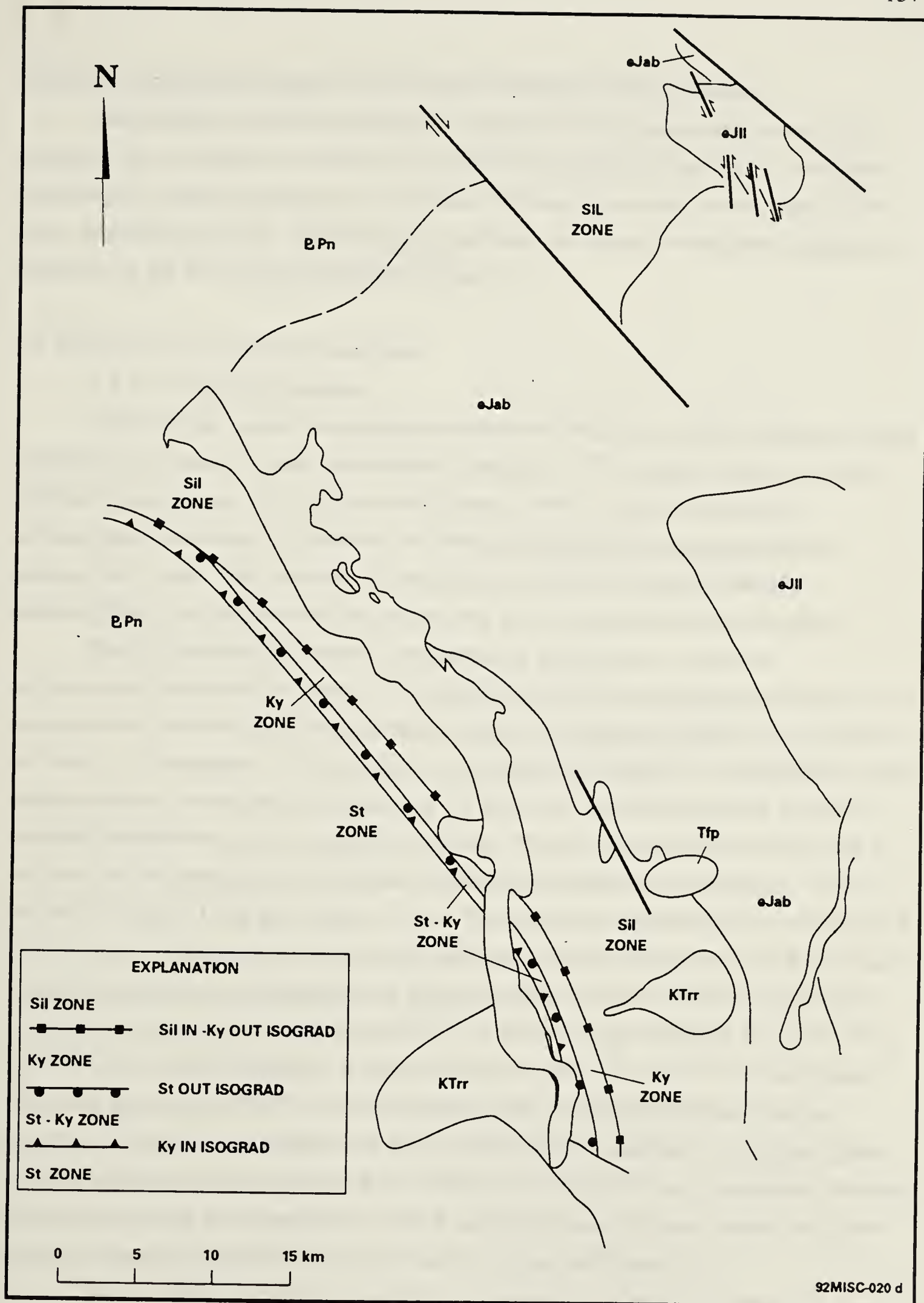
	M1	PEAK	POST-PEAK	M3	M4
MICA (Mu & Bi)			 CONSUMPTION OF GA BY Bi (?)	 POORLY DEVELOPED CRENULATION CLEAVAGE	 RANDOMLY ORIENTED PORPHYROBLASTS
GARNET			 EPISODIC GA GROWTH (?)		
MIGMATITE					
SILLIMANITE					 FRINGES AND POST DATES AD PORPHYROBLASTS
KYANITE					
STAUROLITE	 PRESERVATION OF S1 BY BRANCHING ST				
ANDALUSITE			 OVERGROWS AND DISRUPTS PREVIOUSLY DEVELOPED FOLIATION		
CORDIERITE		 MANTLES AND REPLACES PREVIOUSLY DEVELOPED PORPHYROBLASTS			
SERICITE					 POTASSIC METASOMATISM



Figure 5.4 A map of the Aishihik Lake area showing the distribution of isograd-bound metamorphic mineral zones that reflect the peak M_2 metamorphic mineral paragenesis. Map units follow from Figure 1.2. Sil - sillimanite; Ky - kyanite; St - staurolite.



associated with the development of any other metamorphic porphyroblasts.

Metamorphic minerals attributable to the most recent metamorphic event, M₄, including mica, andalusite, cordierite and sillimanite, overprint all previously developed metamorphic mineral parageneses. Discordant sillimanite is evident across much of the South Aishihik Lake area. Andalusite and cordierite are evident immediately adjacent to intrusions of the Ruby Range Batholith (Figure 5.1 a).

5.4 Estimate of metamorphic conditions

5.4.1 Petrogenetic relations

Metamorphic mineral assemblages and mineral textures in pelitic rocks can be used to provide an estimate of peak metamorphic conditions. This analysis makes use of the calibrated petrogenetic grid of Spear and Cheney (1989). Too little of the M₁ metamorphic parageneses is preserved to allow any quantitative analysis of the M₁ metamorphic event. The presence of a micaceous schistosity suggests that M₁ metamorphism was characterized by, at the very least, greenschist facies conditions.

The M₂ metamorphic mineral paragenesis is divisible into a series of isograd-bound metamorphic zones. The isograds, which are based upon continuous and discontinuous reactions, and characteristic mineral assemblages for each zone, are shown in Table 5.1. Petrogenetic relationships are summarized in Figure 5.5, a petrogenetic grid. Metamorphism is restricted to pressures of 7.5 kbars; the minimum pressure at which staurolite breaks down and is replaced by kyanite. Pressure may decrease to the north as indicated by the coexistence of staurolite, kyanite, and sillimanite in sample no. 120 from the North Aishihik Lake area (Figure 5.1 b). Temperatures are restricted to a minimum of 600 °C by the widespread occurrence of migmatite (assumes that boron, which can cause a significant decrease in temperature of the wet solidus, was not present in significant quantities). Temperatures range from 600 °C to 650 °C in the staurolite zone; 650 °C to 680 °C in the zone of staurolite - kyanite coexistence; 680 °C to 720 °C in the kyanite zone; and greater than 720 °C in the sillimanite zone. These mineral zones dip east beneath the batholith and define a hot side up metamorphic sequence - the highest grade rocks (sillimanite zone) are present at the shallowest structural levels (immediately beneath the batholith) while lower grade rocks (the kyanite and staurolite zone, respectively) are present at deeper structural levels away from the batholith (Figure 5.2).

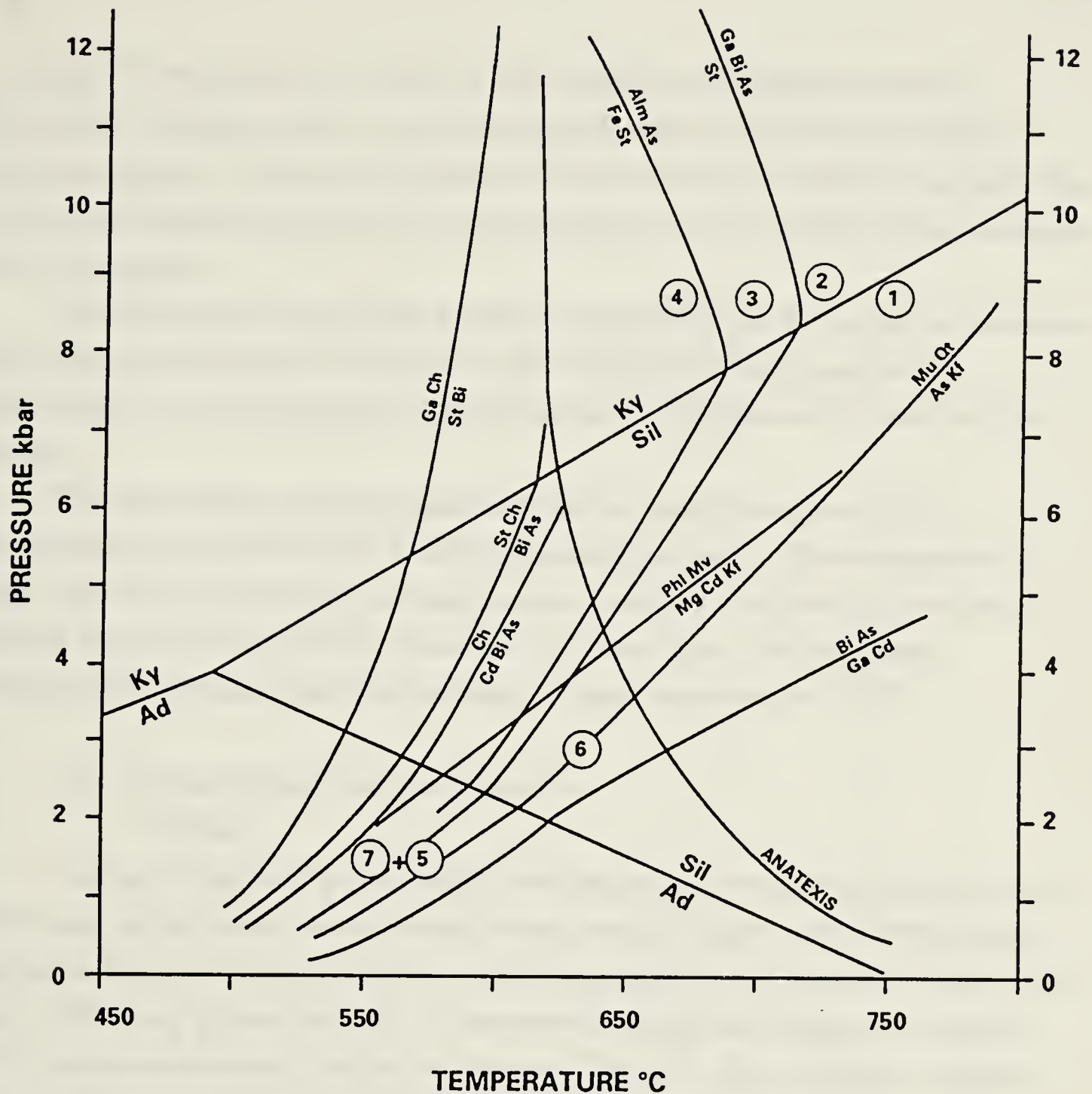
The mantling of staurolite by andalusite and cordierite and the presence of andalusite and cordierite porphyroblasts in the staurolite zone presents a significant dilemma. The andalusite - cordierite paragenesis suggests temperatures of between 550

TABLE 5.1. Characteristic mineral paragenesis for M2 mineral zones.
See text for discussion.

Zone	Bounding isograds and/or related mineral equilibria
M ₂ peak metamorphic mineral paragenesis	
1) Sillimanite zone	Kyanite out - sillimanite in isograd reflecting the discontinuous equilibria $KY = SIL$
2) Kyanite zone	Staurolite out isograd reflecting the discontinuous equilibria $ST + QT = KY + BI + H_2O$
3) Kyanite - Staurolite zone	Kyanite in isograd reflecting the continuous equilibria represented by shifting of the ST - GA - ALSI sub-triangle to the right on a Thompson projection
4) Staurolite zone	
Note that migmatite, quartz, biotite, muscovite, feldspar, and garnet are present throughout each of these zones.	
M ₂ post-peak metamorphic mineral paragenesis	
5) Andalusite - Cordierite zone	AD reflects the continuous equilibria represented by shifting of the ST - GA - ALSI sub-triangle to the right on a Thompson projection. CD reflects the continuous equilibria represented by shifting of the BI - CD - ALSI subtriangle to the left on a Thompson projection.

TABLE 5.1. (continued)

Zone	Bounding isograds and/or related mineral equilibria
M ₄ metamorphism	
6) Sillimanite zone	Reflects the discontinuous equilibria $MU + QT = SIL + KF + H_2O$
7) Andalusite - Cordierite zone	Continuous reactions (?) reflecting breakdown of the pre-existing metamorphic mineral paragenesis



92MISC-020c

Figure 5.5 A calibrated petrogenetic Pressure - Temperature grid after Spear and Cheney (1989) showing metamorphic reactions in metapelitic rocks of the Nisling Assemblage. The numbers refer to metamorphic zones as defined in Table 5.1. Alm - almandine garnet; As - Aluminosilicate (And - andalusite; Ky - kyanite; Sil - sillimanite); Bi - biotite; Cd - cordierite (MgCd - Magnesium end member cordierite); Ch - chlorite; Kf - potassium feldspar; Mu - muscovite; Phl - phlogopite; Qt - quartz; St - staurolite (FeSt - iron end member staurolite).

$^{\circ}\text{C}$ and 600°C and pressures of 2 kbar or less, and point to a significant change in metamorphic conditions relative to the pressures indicated by the peak metamorphic mineral paragenesis. This calls into question the interpretation of andalusite and cordierite as having developed late during the M₂ metamorphic event. This will be further discussed later in this chapter.

The nucleation of a negligible number of mica grains, and the lack of the nucleation of any other porphyroblasts during the M₃ metamorphic event suggests that M₃ metamorphism was characterized by sub-greenschist temperatures and by relatively low pressures.

The metamorphic mineral paragenesis that developed in response to M₄ metamorphism are consistent with a thermal metamorphic event. The development of narrow andalusite and cordierite aureoles, present immediately adjacent to intrusions of the Ruby Range Batholith, restricts pressure to 2 kbar or less. The widespread development of sillimanite indicates that peak temperatures exceeded 550°C .

5.4.2 Geothermometry and geobarometry

Methods

Analyses of grains of garnet, biotite, and plagioclase, thought to represent part of the M₂ mineral paragenesis, were obtained using an eight-channel ARL SEMQ electron microprobe at the University of Calgary (operating conditions are described in Nichols and Stout, 1988), using silicate standards. Characteristic mineral assemblages for samples used in geothermobarometry studies are shown in Table 5.2. Data reduction, using the method of Bence and Albee (1968), was accomplished using online computer programs modified from Nicholls *et al.* (1977). Analytical data are shown in Table 5.3.

Mineral Chemistry

garnet - All analyzed garnets are almandine rich and exhibit an increase in grossular content in grain cores. Almandine content increases from core to rim in garnets obtained from samples collected in the foliaform sillimanite zone. Most samples show some spessartine enrichment in the rims suggesting some retrogressive re-equilibration of garnets with matrix minerals.

biotite - Mild zonation is evident in most of the analyzed biotite grains. All but one of the biotite grains analyzed are characterized by a phlogopite enriched core relative to rim compositions. This is consistent with retrogressive enrichment of biotite in Fe.

plagioclase - Analyzed plagioclase grains range from 65 mole% to 80 mole% albite

Table 5.2. Characteristic mineral assemblage for samples used in geothermobarometry studies.

SAMPLE	QT	PL	KF	BI	MU	GT	AS	ST	OP ^a	AM	EP	CA	CL ^b	SC ^b
48	x	x	x	x	x	x	KY	-	x	-	-	-	x	x
77	x	x	x	x	x	x	SI	-	x	-	-	-	x	-
79	x	x	x	x	x	x	KY	-	x	-	-	-	x	-
81	x	x	x	x	x	x	-	-	x	-	-	-	x	x
91	x	x	x	x	x	x	-	-	x	-	-	-	x	x
93	x	x	x	x	x	x	SI	-	x	-	-	-	x	x
101	x	x	x	x	x	x	SI,AD ^c	x	x	-	-	x	x	x
104	x	x	x	x	x	x	SI	-	x	-	-	-	x	x
110	x	x	x	x	x	x	SI	-	x	-	-	-	x	x
120	x	x	x	x	x	x	SI,KY	x	x	-	-	-	x	x

Notes:

x - present in the sample. Mineral abbreviations QT - quartz, PL - plagioclase, KF - potassium feldspar, BI - biotite, MU - muscovite, GT - garnet, AS - aluminosilicate, ST - staurolite, OP - opaques, AM - amphibolite, EP - epidote, CC - calcite, CL - chlorite, SC - sericite, KY - kyanite, SI - sillimanite, AD - andalusite.

a - opaque minerals include graphite, pyrite, and ilmenite.

b - both chlorite and sericite are retrogressive phases.

c - andalusite postdates, and is not part of, the peak metamorphic mineral paragenesis. See text for discussion.

Table 5.3. Data used in the calculation of paleotemperatures and paleopressures.

Sample ^a	garnet			biotite			garnet			plagioclase				
	Mg	Fe	Fe	Fe		Fe	Ca	Mn	X _{Ca}	Ca	Na	K	X _{Ca}	AS ^B
				Mg+Fe	Mg									
48-C	0.34	4.68	0.93	2.04	3.04	0.60	-2.22	1.12	0.06	0.18	0.99	2.01	0.03	KY
48-R	0.52	4.74	0.90	2.00	3.13	0.61	-1.76	0.86	0.12	0.14	1.02	1.98	0.03	KY
77-C	0.84	4.32	0.84	1.96	2.80	0.59	-1.29	0.34	0.64	0.05	0.87	2.10	0.03	SI
77-R	0.48	4.10	0.89	1.93	2.77	0.59	-1.78	0.30	1.24	0.05	0.72	2.19	0.03	SI
79-C	0.36	4.16	0.92	2.47	2.53	0.51	-2.44	0.94	0.78	0.15	0.57	2.37	0.03	KY
79-R	0.58	4.46	0.88	2.45	2.65	0.52	-1.96	0.86	0.30	0.14	0.72	2.22	0.03	KY
81-C	0.58	4.46	0.88	2.44	3.10	0.56	-1.71	0.86	0.30	0.14				KY
81-R	0.80	4.88	0.86	2.33	3.10	0.57	-1.53	0.46	0.02	0.08				
91-C	0.22	4.50	0.95	1.77	3.25	0.65	-2.41	0.98	0.38	0.16				
91-R	0.50	4.96	0.91	1.90	3.63	0.66	-1.63	0.54	0.06	0.09				
93-C	0.50	4.54	0.90	1.81	3.21	0.64	-1.64	0.78	0.28	0.13	0.96	2.04	0.03	SI
93-R	0.54	4.78	0.90	1.77	3.15	0.64	-1.60	0.52	0.24	0.08	0.93	2.04	0.03	SI
101-C	0.56	4.76	0.89	2.00	3.08	0.61	-1.70	0.90	0.02	0.14	0.81	2.19	0.00	SI,AD ^C
101-R	0.58	4.64	0.89	1.97	3.07	0.61	-1.63	0.68	0.22	0.11	0.81	2.19	0.00	SI,AD ^C
104-C	0.60	4.66	0.89	1.85	3.16	0.63	-1.51	0.32	0.50	0.05	0.90	2.07	0.03	SI
104-R	0.50	4.72	0.90	1.80	3.31	0.65	-1.63	0.32	0.52	0.05	0.63	2.01	0.21	SI
110-C	0.64	4.60	0.88	1.88	3.07	0.62	-1.48	0.40	0.48	0.07	1.02	1.98	0.03	SI
110-R	0.42	4.66	0.92	1.88	3.16	0.63	-1.87	0.36	0.68	0.06	1.02	1.98	0.03	SI
120-C	0.26	4.54	0.95	1.87	3.12	0.63	-2.37	1.12	0.16	0.18	0.60	2.34	0.03	SI,KY ^D
120-R	0.46	4.68	0.91	1.57	3.31	0.68	-1.56	0.74	0.20	0.12	0.60	2.34	0.03	SI,KY ^D

Notes:

a) C - grain core analysis; R - grain rim analysis.

b) Mineral abbreviations; KY - kyanite; SI - sillimanite; AD - andalusite.

c) Andalusite is post-peak metamorphism. See text for discussion.

d) Sillimanite and kyanite are both stable.

(oligoclase - andesine). Mild zonation (both normal and reverse) is common. No systematic variation in plagioclase composition is apparent either on the scale of individual grains or on a map scale.

Garnet - biotite geothermometry

The applicability of garnet - biotite geothermometry to analysis of the M₂ metamorphic event is severely restricted by the paucity of garnet; by complex zonation of the garnets; by the uncertain relationship of some andalusite and cordierite to the peak M₂ metamorphic mineral paragenesis; by alteration of the M₂ metamorphic mineral paragenesis during M₄ thermal metamorphism including the widespread development of retrogressive chloritic alteration of both biotite and garnet. Retrogressive alteration is also indicated by the presence of spessartine enriched garnet rims and phlogopite enriched biotite cores.

Garnet - biotite pairs from ten samples, in which only minor retrogressive alteration was apparent, were analyzed. Only biotite grains in contact with garnet were analyzed. Core (garnet and biotite grain cores) and rim (rims of adjacent garnet and biotite grains) temperatures were calculated for each sample. Core temperatures are suspect as there is no way to show that the garnet core and the biotite core were ever in equilibrium with one another. Rim temperatures are assumed to provide minimum estimates of peak temperature as retrogressive re-equilibration of garnet - biotite pairs is common. Error bars on absolute temperatures are at least 50 °C (Ferry and Spear, 1978) and, because of microprobe analytical error, are likely larger. Because of the paucity of suitable garnet - biotite pairs it was not possible to analyze multiple garnet - biotite pairs for each sample and determine a sample specific standard deviation. Based on a review of recent papers which employed garnet - biotite geothermometry on similar rocks (i.e. McClelland *et al.*, 1991) it is assumed that there is an error of 80 °C on absolute temperatures.

Results are shown in Table 5.4. Sample 101, collected from within the staurolite - kyanite zone immediately adjacent to the Ruby Range Batholith, is characterized by relatively high garnet - biotite temperatures (678 °C to 713 °C) relative to other samples collected in the staurolite - kyanite zone. These anomalous results are thought to be attributable to thermal metamorphism (M₄) associated with the intrusion of the Ruby Range Batholith. Rim temperatures for samples 77 and 110 are low relative to core temperatures for the same samples. Both samples are characterized by chloritization of garnet rims. For these reasons core and rim temperatures for sample 101 and rim

Table 5.4. Temperature and pressure estimates.

Sample	Core Temperature (°C)	Core Pressure (kbar)	Rim temperature (°C)	Rim Pressure (kbar)
48	439	2.7	639	9.0
77	766	7.6	563	6.6
79	475	8.4	580	9.4
81	624		713	
91	502		668	
93	680	10.0	674	7.5
101	678	11.1	713	10.8
104	673	5.6	622	5.6
110	684	6.8	553	3.7
120	477	6.55	751	13.8

Notes: Pressure and temperature estimates were calculated using the PTAX function of GEOCALC (Berman *et al.*, 1987), a program for the calculation of mineral equilibria. In all cases the Berman (1988) garnet, McMullin and Berman (1988) biotite, and the Fuhrman and Lindsley (1988) plagioclase solution models were used to account for the effects of non-ideal mixing in the respective solid-solution phases. No corrections were made for the presence of additional components including Mn and Fe⁺⁺⁺ in garnet and Ti in biotite. Where plagioclase grains were not present, temperatures were calculated assuming P = 8 kbar. Minimum errors on calculated temperatures and pressures are estimated to be 80 °C and 1.6 kbar, respectively.

temperatures for samples 77 and 110 are not further considered here. Core temperatures average 656 °C in the sillimanite zone, 521 °C in the kyanite zone, and 475 °C in the staurolite - kyanite zone. Rim temperatures provide slightly higher temperature estimates, averaging 682 °C in sillimanite zone, 673 °C in the kyanite zone, and 580 °C in the staurolite - kyanite zone (Figure 5.6). These results are consistent with the decrease in metamorphic grade away from the batholith suggested by the metamorphic mineral paragenesis. Temperatures are, however, lower than (although within error of) temperatures suggested by the peak metamorphic mineral paragenesis. This may reflect disequilibrium resulting from younger thermal overprinting.

Garnet - Al_2SiO_5 - plagioclase (GASP) geobarometry

Restrictions on the use of garnet - biotite geothermometry, outlined above, are also applicable to GASP geobarometry. Only six samples were suitable for GASP geobarometry. Matrix plagioclase were analyzed - plagioclase in contact with biotite and garnet was not observed. Sericitic alteration of plagioclase is common and care was taken to avoid affected grains. Core and rim pressures were calculated for each sample. Errors associated with the calculation of temperature propagate through the calculation of pressure. Error bars on absolute pressures are at least 1.6 kbar (Ghent *et al.*, 1979).

Results are shown in Table 5.4. Pressure estimates for sample 101 and rim pressure estimates for samples 77 and 110 are not considered here as their associated temperature estimates are considered unreliable (see above). Core and rim pressure estimates average 6.8 and 9.0 kbar, respectively. However, a core pressure estimate of 2.7 kbar for sample 48 is inconsistent with the presence of kyanite in that sample. A rim pressure estimate of 13.8 kbar for sample 120 is inconsistent with the absence of eclogite in mafic rocks which crop out a short distance from where sample 120 was collected. Discarding these two data points results in core and rim average pressures of 7.5 and 7.9, respectively. These results are within error of each other and are similar to the pressure suggested by the peak metamorphic mineral paragenesis.

5.5 The nature of the metamorphic events

At least four metamorphic events have affected rocks of the Nisling Assemblage (Figure 5.3).

M₁ - The mineral paragenesis attributable to the M₁ metamorphic event are the most ancient preserved within the study area. As a result, these minerals have been largely obliterated, overgrown, and deformed during subsequent metamorphism and deformation.

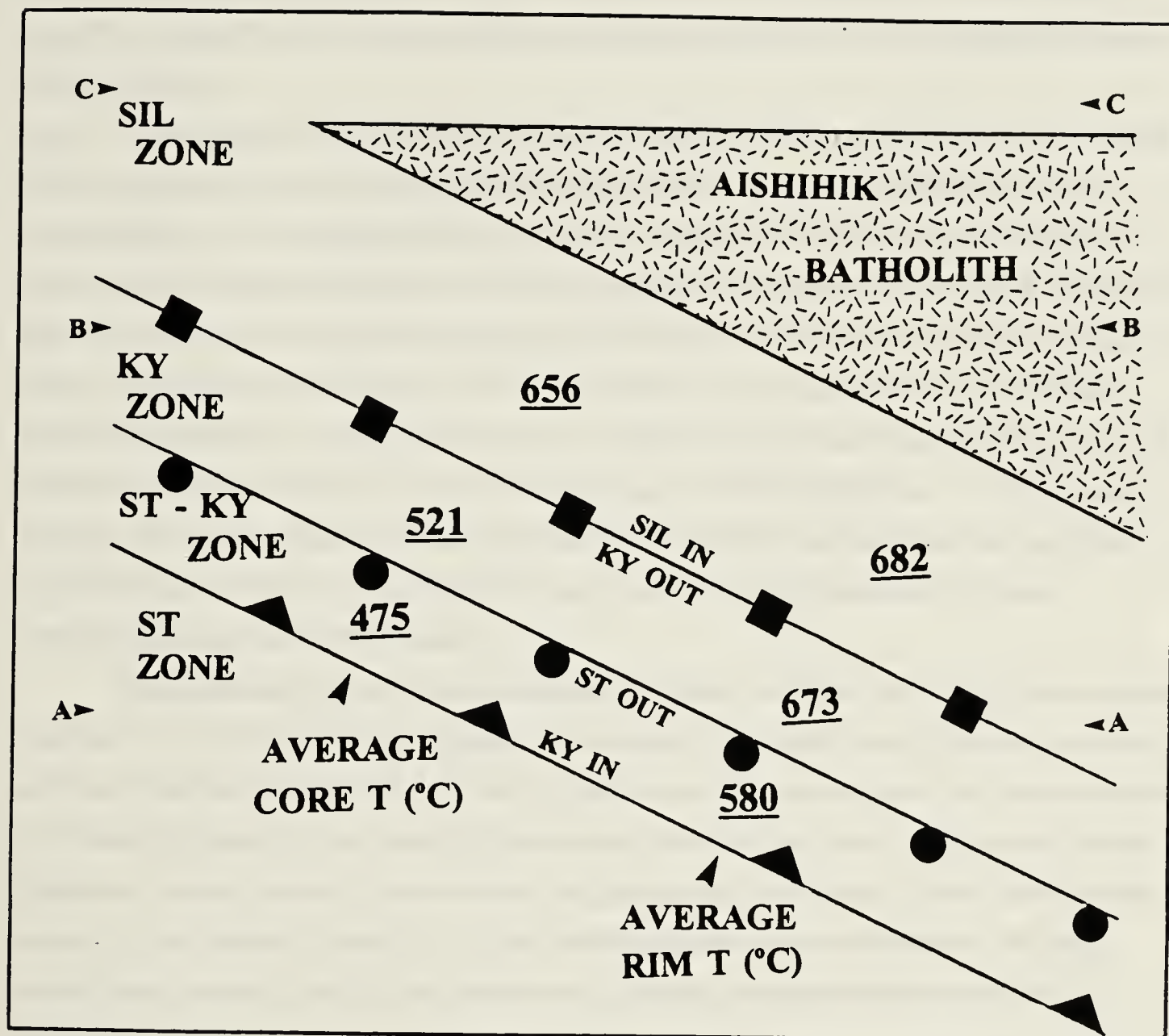


Figure 5.6 A schematic cross-section showing the geometry of the metamorphic aureole developed in Nisling Assemblage adjacent to the west margin of Aishihik Batholith. Average core and rim temperatures, based on garnet-biotite geothermometry, are shown, as are the kyanite (KY) in, staurolite (ST) out, and kyanite out - sillimanite (SIL) in isograds. A - A, B - B, and C - C indicates the approximate level of exposure in each of the South Aishihik Lake, North Aishihik Lake, and Upper Nisling River areas, respectively. See text for discussion.

M₁ appears to have been a regional event, as indicated by the widespread distribution of minerals and fabrics attributable to M₁ metamorphism. The presence of biotite and muscovite suggests that metamorphism was characterized by at least greenschist facies metamorphism.

M₂ - The dominant metamorphic event to have affected the assemblage, M₂, resulted in the development of mineral paragenesis characteristic of upper amphibolite grade metamorphism. Syn-metamorphic mica define a schistosity (S₂) which parallels the margin of the Aishihik Batholith. Isograds parallel the margin of the Aishihik Batholith and define an increase in metamorphic grade (temperature) towards the batholith. Results of garnet - biotite geothermometry are also consistent with an increase in temperature towards the batholith. These observations indicate that regional metamorphism is directly related to, and resulted from, the intrusion of the Aishihik Batholith. U - Pb isotopic analyses of zircon separates from samples of the batholith indicate that the batholith crystallized at 187.0 ± 9.7/-0.9 Ma (this study) and restricts the timing of peak metamorphism to the Early Jurassic.

The metamorphic mineral paragenesis together with geobarometric data indicate that deep crustal levels (25 to 30 km) are exposed in the study area. This is consistent with the distribution of isograds, which define a hot-side-up metamorphic aureole beneath the Aishihik Batholith, and implies that erosion has removed much of the overlying rocks. Moderate to deep crustal levels are also suggested by the coarse-grained equigranular nature of the Aishihik Batholith; by the foliaform nature of the batholith - Nisling Assemblage contact; and by the presence of primary magmatic epidote within the batholith.

The andalusite - cordierite problem

Foliaform andalusite and cordierite mantles (on staurolite) and porphyroblasts are interpreted to have developed late during M₂, post-dating peak metamorphism. Their presence requires rapid uplift of the Nisling Assemblage and the Aishihik Batholith to shallow crustal levels (P = 2 kbar) during the waning stages of M₂. The development of foliaform andalusite and cordierite as a result of rapid uplift of a still hot metamorphic terrain is, however, problematic. Andalusite is not thought to be stable under rapidly changing pressure and temperature conditions. If the entire terrain was subjected to rapid uplift, why is it that andalusite and cordierite porphyroblasts appear to be restricted to the staurolite zone? Andalusite and cordierite should, according to this model, be present throughout the Nisling Assemblage.

Two possible explanations are suggested: 1) M₂ andalusite and cordierite record a

metamorphic event which significantly post-dates regional (M₂) metamorphism. This hypothesis explains the juxtaposition of high and low-pressure metamorphic mineral paragenesis. However, it does not address the limited distribution of andalusite and cordierite (within the staurolite zone) or the morphology of these minerals (lying within schistosity and preserving, in the form of inclusion trails, traces of the S₁ planar fabric);

2) The high-pressure metamorphic parageneses predates the intrusion of the batholith. In this scenario a pre-intrusive, hot-side-down metamorphic package may have been dragged into a hot-side-up orientation by the diapiric emplacement of the batholith at shallow crustal depths. Andalusite and cordierite record metamorphism associated with intrusion. This model fails, however, on several counts. It does not explain why andalusite and cordierite do not overprint the kyanite and sillimanite zones. Metamorphic geopetal features, including cauliflower structures and asymmetric vein clusters, suggest that the Nisling Assemblage is, at present, the same way-up as it was during metamorphism and migmatization. Finally, the style of intrusion of the batholith, in addition to the presence of magmatic epidote, indicate that the batholith was intruded at deep crustal levels.

Three lines of evidence are consistent with the development of andalusite and cordierite as a result of rapid post-peak-metamorphism uplift of the Nisling Assemblage and the Aishihik Batholith: 1 - Plutons of the Long Lake Suite that intrude and truncate schistosity in both the Aishihik Batholith and the Nisling Terrane appear to have been emplaced at shallow crustal levels. The plutons are characterized by the presence of miarolitic cavities; by syn-intrusive brittle deformation of the wall rocks, including brecciation; and by the presence of an extensive dyke swarm (this study). U - Pb isotopic studies of zircon separates from samples of the Pink Quartz Monzonite plutons indicate that these plutons crystallized within about 1 Ma of crystallization of the Aishihik Batholith (189.0 +9.7/-0.9 Ma) (this study); 2 - K - Ar hornblende, U - Pb titanite, and U - Pb zircon isotopic studies of samples from the Aishihik Batholith yield overlapping age determinations consistent with rapid cooling of the batholith. Rapid cooling of the batholith is unexpected, given that the batholith was intruded at moderate to deep crustal levels and suggest rapid, post-crystallization uplift of the batholith; and 3 - Blocks of foliated hornblende granodiorite, similar to that of the Aishihik Batholith, and micaschist, similar to that of the Nisling Assemblage, are incorporated in unmetamorphosed conglomerates of the Early Jurassic Laberge Group. Laberge Group conglomerates crop out a short distance to the east of the study area, within the Whitehorse Trough. This stratigraphic relationship requires unroofing of the Nisling Assemblage and the Aishihik Batholith soon after metamorphism. These observations support the hypothesis that

andalusite and cordierite developed in response to the rapid uplift of the still hot metamorphic terrain.

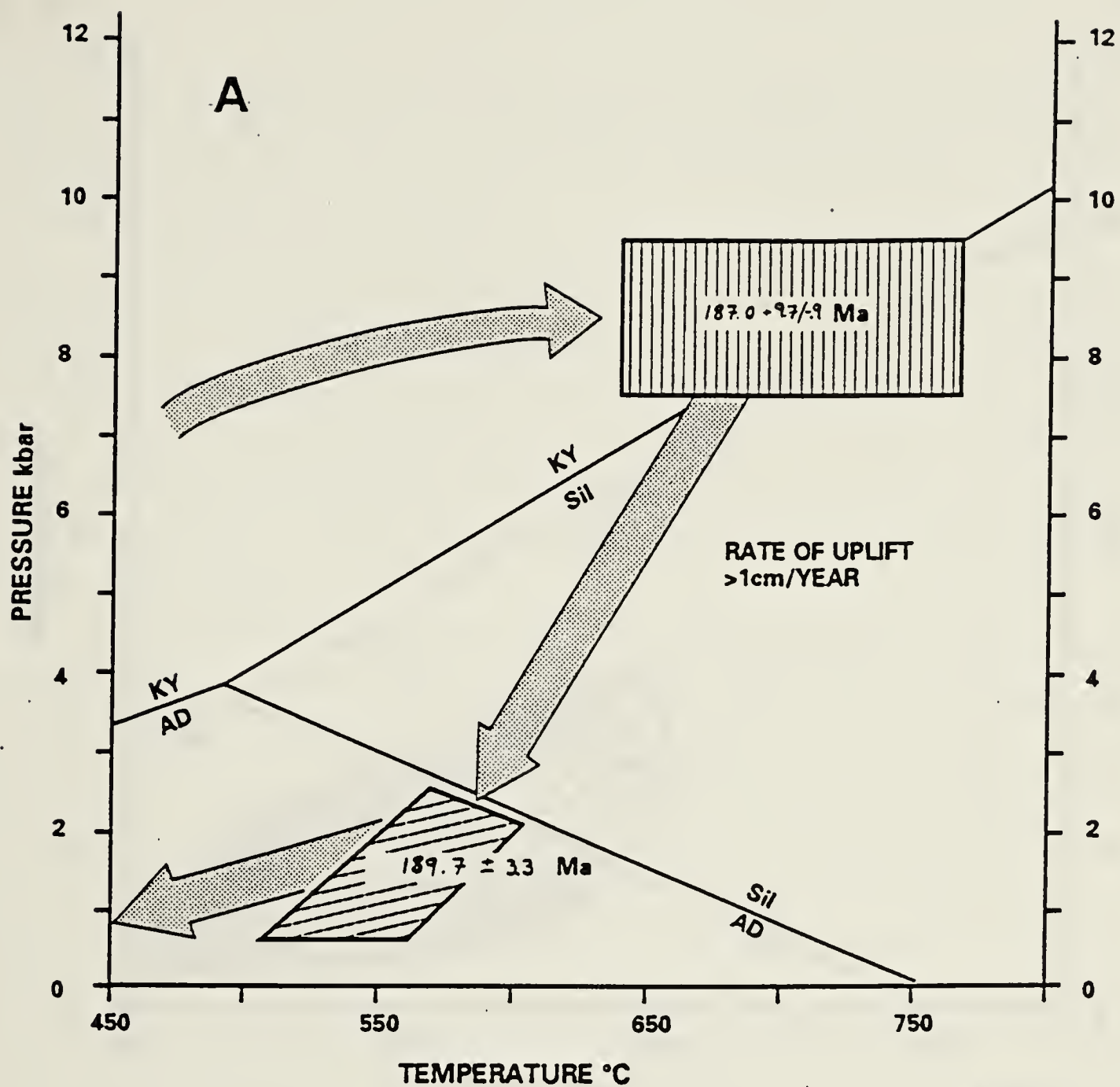
M₃ - The close association of mica that nucleated during the M₃ metamorphic event with crenulations of the S₂ schistosity (M₃ mica grows along the axial planes of the crenulations) indicates that M₃ metamorphism was associated with folding of the Nisling Assemblage. The timing of folding is poorly constrained. The folds affect and are younger than the S₂ schistosity, but are older than the Late Cretaceous to Tertiary Ruby Range Batholith: crenulated micaschist is truncated by granitic intrusions of the Ruby Range Batholith.

M₄ - The final metamorphic event to affect rocks of the Nisling Assemblage is characterized by thermal overprinting of the previously developed metamorphic paragenesis. Metamorphism is restricted to the South Aishihik Lake area (Figure 5.1 a). Andalusite - cordierite aureoles developed immediately adjacent to intrusions of the Ruby Range Batholith. Sillimanite is more widespread and post-dates the andalusite - cordierite aureoles: fine-grained sillimanite and fibrolitic sillimanite replaces, nucleates on, and mantles andalusite. Potassic metasomatism, characterized by sericitization, increases towards the Ruby Range Batholith and is, locally, pervasive immediately adjacent to the batholith. These observations indicate that thermal metamorphism is related to the intrusion of the Ruby Range Batholith. U - Pb zircon geochronology indicate that Ruby Range plutonism probably ranged from between 68 and 90 Ma to 58 Ma.

5.6 Pressure - temperature - time displacement

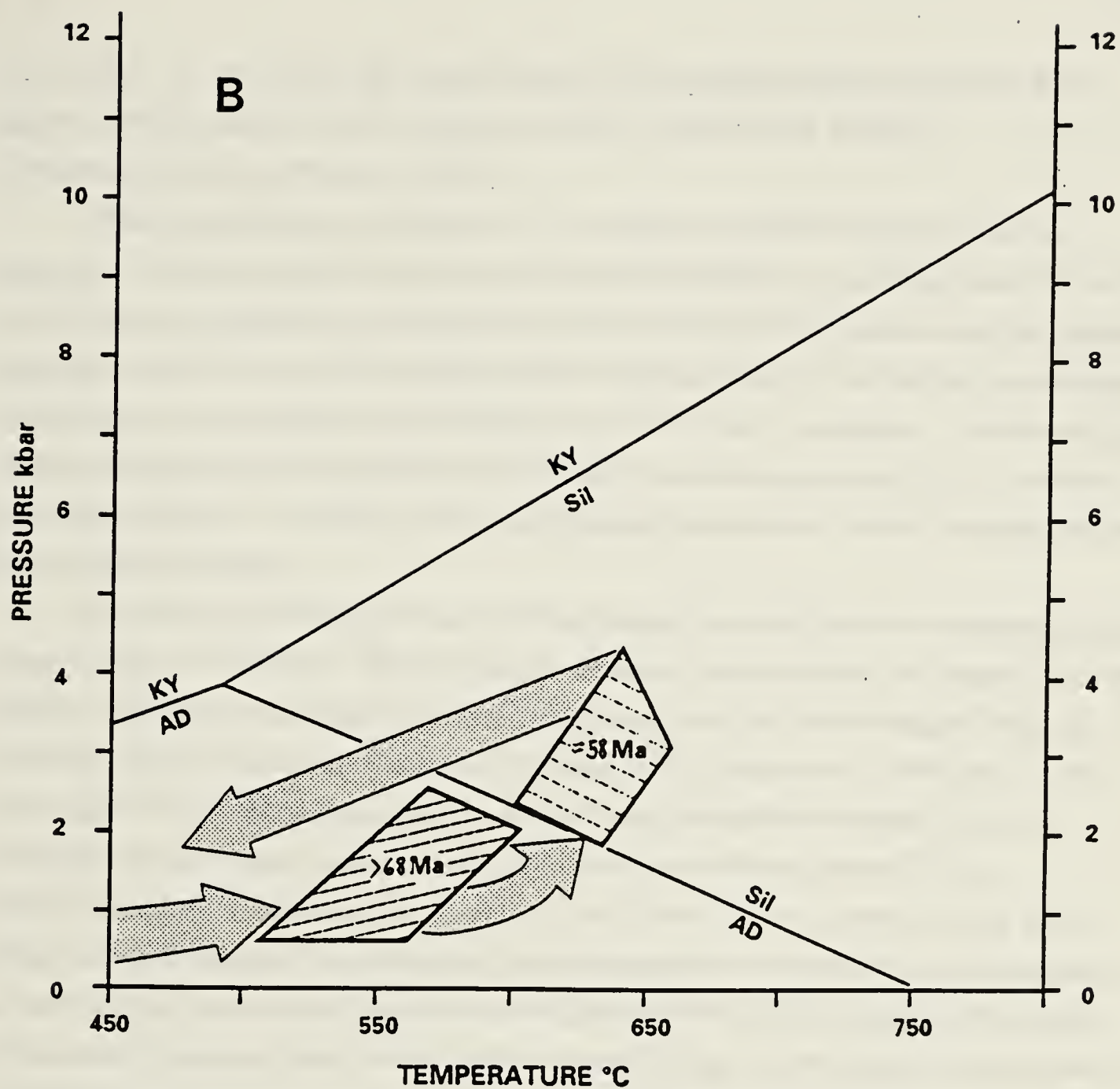
Geochronologic data, together with pressure and temperature determinations, define a pressure - temperature - time (P - T - t) evolution for the Nisling Assemblage (Figure 5.7 a and b). Only the M₂ and M₄ metamorphic events are considered here. Too little is known about the M₁ and M₃ metamorphic events to include them in this discussion.

During the M₂ event rocks of the Nisling Assemblage were metamorphosed at moderate to high P - T conditions. Metamorphism was directly attributable to the intrusion of the Aishihik Batholith and resulted in the overprinting of the folded S₁ planar fabric. The batholith and metamorphosed rocks of the Nisling Assemblage were then rapidly uplifted and unroofed prior to the intrusion of the Long Lake Suite of post-tectonic plutons. Andalusite and cordierite developed at this time. Sediments of the Early Jurassic Laberge Group, preserved within the Whitehorse Trough just east of the study area, consist of immature clastic rocks derived from the west and provide a record



32MISC-0206

Figure 5.7 Pressure - temperature - time displacement diagrams for the Nisling Assemblage. Arrows indicate the relative order of crustal conditions experienced by the Nisling Assemblage as indicated by metamorphic mineral parageneses. A - M_2 metamorphism; B - M_4 metamorphism. See text for discussion.



92MISC-020a

of this uplift. K - Ar biotite age determinations from samples of the Long Lake Suite suggests that the terrain cooled through the 300 °C isotherm by 150 Ma (Tempelman-Kluit and Wanless, 1975).

These data define a clockwise P - T - t evolution which is divisible into four segments: 1) initial tectonic burial of the Nisling Assemblage to crustal depths of 25 to 30 km. The time of initiation of tectonic burial is not constrained; 2) intrusion of the Aishihik Batholith at 189.0 +9.7/-0.9 Ma and associated metamorphism of the Nisling Assemblage; 3) rapid uplift and unroofing of the batholith and the Nisling Assemblage. Geochronologic constraints suggest that more than 20 km of uplift occurred in less than 2 Ma - a rate of uplift of greater than 1 cm/year; and 4) a prolonged post-tectonic period characterized by relative tectonic stability.

During M4 metamorphism rocks of the Nisling Assemblage were metamorphosed at low P, high T conditions. Metamorphism, potassic metasomatism, and alteration of the Nisling Assemblage was directly related to the intrusion of the Ruby Range Batholith. K - Ar mineral ages (Tempelman-Kluit and Wanless, 1975; Farrar *et al.*, 1988) and U - Pb zircon ages (this study) indicate that the Ruby Range Batholith developed during a prolonged period of plutonism extending from at least 68 Ma to about 58 Ma. Geochronologic and metamorphic studies of the Kluane Schist southwest of the Ruby Range batholith indicate that widespread sillimanite-grade metamorphism of those rocks occurred during the Eocene (Mortensen and Erdmer, 1992). This suggests that similar widespread sillimanite-grade metamorphism of the Nisling Assemblage developed late in the Ruby Range plutonic event and is consistent with the presence of mantles of fine-grained sillimanite on andalusite.

These relationships define a linear P - T - t path that is divisible into three segments: 1) initiation of Ruby Range plutonism before 68 Ma and associated development of andalusite - cordierite aureoles; 2) continued plutonism and crustal heating, culminating at about 58 Ma (?) with the widespread development of sillimanite; 3) cessation of Ruby Range plutonism and associated metamorphism. No constraints are available on the rate of post-Ruby Range cooling of the Nisling Assemblage.

5.7 Discussion

The metamorphic evolution of a package of rocks can be used to constrain the terrane affinities of those rocks. Three terrane correlations have been proposed for Nisling Assemblage. These are: 1 - North America (Hansen, 1990 a and b); 2 - Yukon-Tanana terrane (Mortensen, 1992); and 3 - Stikine terrane (Tempelman-Kluit,

1979).

North America - Hansen (1990 a and b) defined North America on the basis of structural position and time of unroofing. North American rocks are present at structurally deep levels, having been overthrust by Stikine terrane (?) in the Early Jurassic, and were not unroofed until the Middle Cretaceous when crustal extension and granite plutonism affected large areas of southwest Yukon and Alaska. Nisling Assemblage rocks were correlated with North America as they were thought to record a similar metamorphic history.

Like North American rocks, rocks of Nisling Assemblage that underlie the study area were overthrust and tectonically buried in the Early Jurassic or earlier. Nisling Assemblage rocks were, however, unroofed in the Early Jurassic. No structures attributable to Middle Cretaceous extension of the Nisling Assemblage in the vicinity of Aishihik Lake have been identified (Tempelman-Kluit, 1974; this study), although Middle Cretaceous plutons of the Whitehorse - Coffee Cr. Suite (Woodsworth *et al.*, 1991) intrude the Nisling Assemblage northwest of Aishihik Lake (Tempelman-Kluit, 1974).

North American and Nisling Assemblage rocks, therefore, share a similar Early Jurassic tectonic history. However, the post-Early Jurassic histories of these terranes are significantly different.

Yukon-Tanana terrane - Mortensen (1992), suggested that Nisling Assemblage is similar to, and should be included as part of, the Yukon-Tanana terrane. The similarities include homotaxiality of the Nisling Assemblage and strata of the Yukon-Tanana terrane; broadly similar metamorphic grade; and correlative orthogneiss suites. The Yukon-Tanana terrane is characterized by: 1) fabrics and metamorphic mineral parageneses related to pre-Late Triassic but post-Permian mylonitization and regional metamorphism (D₁); 2) regional scale thrust faulting and imbrication with ophiolitic strata of the Slide Mountain terrane in the Early Jurassic (D₂). Tectonism was not accompanied by regional metamorphism; and 3) extension and localized contact metamorphism associated with extensive Middle Cretaceous granite plutonism (D₃) (Mortensen, 1992; 1990).

The M₁ metamorphic event recorded by rocks of the Nisling Assemblage may be correlative with D₁ metamorphism of the Yukon-Tanana terrane. There is, however, little to substantiate this correlation. Early Jurassic tectonism resulted in moderate to high P - T metamorphism of Nisling Assemblage while Yukon-Tanana terrane experienced regional-scale imbrication at shallow crustal levels.

These data do not rule out correlation of Yukon-Tanana terrane and Nisling Assemblage. They do, however, indicate that Yukon-Tanana terrane and Nisling

Assemblage were at different structural levels in the Early Jurassic.

Stikine terrane - The Nisling Assemblage has been suggested as the possible basement for Stikine terrane based on the assumption that the Aishihik Batholith represented the plutonic root of the Late Triassic Lewes River volcanic arc (Tempelman-Kluit, 1979).

However, the Aishihik Batholith crystallized in the Early Jurassic (this study). Late Triassic and older strata of the Stikine terrane do not record significant regional metamorphism of Early Jurassic or pre-Early Jurassic age. This suggests that the Nisling Assemblage and the Stikine terrane constituted separate tectonic elements until at least the Early Jurassic and that the Nisling Assemblage is not basement to Late Triassic rocks of Stikine terrane.

Post-tectonic plutons of the Long Lake Suite intrude metamorphosed rocks of the Nisling Assemblage, the Aishihik Batholith and unmetamorphosed mafic volcanic rocks of the Stikine terrane (Tempelman-Kluit, 1974; Wheeler, 1961). These plutons define an overlap assemblage that stitches together the Nisling Assemblage and the Stikine terrane by 189.7 ± 3.3 Ma (this study). These relationships suggest that M₂ metamorphism of the Nisling Assemblage is closely associated with the amalgamation of the Nisling Assemblage and the Stikine terrane.

5.8 Conclusions

1. Rocks of the Nisling Assemblage record four metamorphic events. These are, in order of occurrence:

M₁ - Pre - Early Jurassic regional greenschist to amphibolite grade (?) metamorphism, signs of which have now been largely obliterated by more recent metamorphism;

M₂ - Early Jurassic region, syn- to post-kinematic, moderate to high P - T metamorphism directly attributable to the intrusion of the Aishihik Batholith;

M₃ - Post - Early Jurassic but pre - Late Cretaceous sub-greenschist facies metamorphism related to folding of the Nisling Assemblage and the development of crenulations of the S₂ schistosity;

M₄ - Late Cretaceous to Tertiary low P - high T thermal metamorphism associated with the Ruby Range Batholith.

2. Nisling Assemblage rocks that underlie the study area were tectonically buried to depths of 25 to 30 km depth (corresponding to a pressure of 8 to 9 kbar) in the Early Jurassic as indicated by the development of staurolite - migmatite schist. The exposure of

deep crustal levels at the present erosion surface is consistent with the results of geothermobarometry studies and with the distribution of mineral isograds: mineral isograds define a hot side up metamorphic aureole developed beneath the overlying Aishihik Batholith.

3. Immediately after intrusion of the Aishihik Batholith, the Nisling Assemblage and the batholith were rapidly uplifted (uplift rates of over 1 cm/year for two million years) and unroofed. Uplift is indicated by: 1 - the development of andalusite and cordierite mantles on staurolite; and 2 - by the intrusion of metamorphosed rocks of the Nisling Assemblage and the Aishihik Batholith by discordant, shallow level, miarolitic dykes and plutons of the Long Lake Suite at about 189.7 ± 3.3 Ma.
4. Thermal metamorphism associated with the Ruby Range Batholith is divisible into two distinct phases. An initial phase is characterized by the development of andalusite - cordierite aureoles in the wall rocks immediately adjacent to intrusions of the Ruby Range Batholith. A second phase, associated with the final stages of intrusion of the Ruby Range Batholith and of probable Eocene age, is characterized by the widespread development of sillimanite.
5. It is difficult to reconcile any of the terrane correlations suggested for the Nisling Assemblage, although the following can be said: The Nisling Assemblage does not constitute the basement of the Stikine terrane; rocks of the Nisling Assemblage and the Yukon-Tanana terrane both record Early Jurassic and pre-Early Jurassic tectonic events, although the Nisling Assemblage was at structurally deep levels in the Early Jurassic while the Yukon-Tanana terrane was at shallow structural levels; rocks of the Nisling Assemblage and North America were overthrust and tectonically buried in the Early Jurassic, although the Nisling Assemblage was unroofed in the Early Jurassic, while North American rocks were not unroofed until the Middle Cretaceous.

VI. DISCUSSION

6.1 Towards a tectonic model

Observations made in the Aishihik Lake map-area can be used to constrain models of the early- to mid-Mesozoic tectonic evolution of the Northern Cordillera. Presented here are: 1) criteria used to constrain the tectonic evolution of Nisling Assemblage in the Aishihik Lake area; and 2) a suggested model of terrane interaction.

Constraining criteria:

1) Nisling Assemblage consists of a structurally thickened and metamorphosed quartzose clastic shelf sequence more than 10 km thick. The nature of the basement onto which this shelf sequence was deposited remains unknown. Plutons that intrude Nisling Assemblage are characterized by initial strontium ratios in excess of .706 (LeCouteur and Tempelman-Kluit, 1976) and by the presence of a component of inherited zircon of early Proterozoic age consistent with the presence of a crystalline basement beneath Nisling Assemblage. Nisling Assemblage plunges to the north throughout the Aishihik Lake area, resulting in the exposure of the structurally deepest part of the terrane in the region south of Aishihik Lake. If basement to Nisling Assemblage is exposed in Yukon it may be in this region. Further mapping is necessary to investigate this possibility.

Interfoliated with quartzose rocks is a 4 km thick amphibolite-marble sequence and orthogneiss. These rocks provide a record of volcanism, carbonate deposition and intrusion which define an apparent volcanic arc sequence of mid-Paleozoic age. Middle Paleozoic volcanic arc sequences are present in Yukon-Tanana Terrane and Stikinia and intimates a Paleozoic link between these terranes (L Currie, pers.comm. 1992; Mortensen, 1992).

Yukon-Tanana Terrane consists of a Paleozoic and older pericratonic succession similar to that of Nisling Assemblage and an inferred volcanic arc sequence that consists of Devonian-Mississippian orthogneiss (the Mink Cr. and Selwyn gneisses), metavolcanics, and marble (Mortensen, 1990; 1992). Like Nisling Assemblage, plutons that intrude Yukon-Tanana Terrane are characterized by initial strontium ratios in excess of .706 (LeCouteur and Tempelman-Kluit, 1976) and by the presence of a component of inherited zircon of early Proterozoic age (Mortensen, 1990; 1992) suggesting that the basement beneath Nisling Assemblage is continuous beneath Yukon-Tanana Terrane.

Stikinia includes the Devonian to Middle Triassic Stikine Assemblage which consists of arc-related volcanic and volcanoclastic strata, and carbonate rocks (Monger, 1977; Brown et al., 1991). The nature of the basement beneath the Stikine Assemblage

remains unknown. However, younger volcanics deposited on Stikine Assemblage are characterized by juvenile Nd isotopic values and have not been significantly contaminated by evolved crystalline crust (Samson *et al.*, 1989).

Because of temporally and lithologically similar mid-Paleozoic volcanic arc sequences, Nisling Assemblage, Yukon-Tanana Terrane, and Stikinia are interpreted to have formed a coherent microcontinent through much of the Paleozoic (J. Mortensen, pers. comm, 1992; Mortensen, 1992). The apparent lack of crystalline basement beneath Stikinia suggests that crystalline basement beneath Nisling Assemblage is discontinuous to the south.

2) Nisling Assemblage was regionally deformed twice between the middle Paleozoic and the Early Jurassic. Little is known about the nature of D₁ deformation as fabrics attributable to the earlier event have been largely obliterated during younger metamorphism and deformation. D₂ deformation is characterized by tight to isoclinal folding (F₂) of a previously developed tectonic fabric (S₁), and by the development of a north-trending quartz-rodging lineation (L₂). Deformation had largely ceased by 186 Ma as Aishihik Batholith, which intrudes Nisling Assemblage, was not significantly deformed. F₂ folds in Nisling Assemblage are characterized by an axial planar schistosity which parallels the margin of the batholith, suggesting that the batholith may have intruded during the final stages of deformation.

D₂ tectonism resulted in the tectonic burial of Nisling Assemblage to moderate to deep crustal levels. Evidence for tectonic burial of Nisling Assemblage comes primarily from the metamorphic mineral paragenesis which characterizes the metamorphic aureole around the late- to post-kinematic Aishihik Batholith. The aureole includes staurolite migmatite but not eclogite, limiting pressure to between 8 kbar and 10 kbar. Sparse geobarometry data are consistent with metamorphism at pressures in excess of 8 kbar. Mineral isograds define a hot-side-up metamorphic aureole developed beneath the overlying Aishihik Batholith, consistent with the exposure of deep crustal levels at the present erosion surface. In the batholith late stage magma reacted with plagioclase and hornblende to produce epidote and biotite, a process indicative of pressures of about 8 kbar (Zen, 1989; Zen and Hammerstrom, 1984).

Yukon-Tanana Terrane is characterized by similar high-pressure-moderate-temperature metamorphism associated with post-Middle Permian but pre-Early Jurassic deformation (Mortensen, 1992; Dusel-Bacon and Douglass, 1990). This is strong evidence in favour of continued correlation of Yukon-Tanana Terrane and Nisling Assemblage (Mortensen, 1992). There is, however, no record of Triassic (?) high-

pressure-moderate-temperature metamorphism in Stikinia. Instead Stikinia is characterized in the Late Triassic by the development of a volcanic arc as indicated by volcanic rocks of the Stuhini Group. Because Nisling Assemblage was buried to moderate crustal depths synchronously with the development of a volcanic arc on Stikinia, Stikinia is inferred to have been a tectonic element distinct from Nisling Assemblage by the Late Triassic.

3) The Aishihik Batholith crystallized at $187.0 \pm 9.7/-0.9$ Ma and intrudes Nisling Assemblage. The batholith is characterized by rare micaschist inclusions similar to micaschist of Nisling Assemblage, and by a margin-parallel foliation, defined by the alignment of primary magmatic grains. Solid-state deformation, characterized by top-to-the-west shearing of the west margin of the batholith, is thought to reflect late magmatic ballooning. Intrusion resulted in metamorphism of Nisling Assemblage; isograds are parallel to the margin of the batholith and define an increase in grade towards the batholith. Sparse geothermometric data are consistent with an increase in temperature towards the batholith.

The batholith is part of the Klotassin Plutonic Suite (Tempelman-Kluit, 1974; 1979) which ranges in age from 210 Ma to 185 Ma (LeCouteur and Tempelman-Kluit, 1976; Tempelman-Kluit and Wanless, 1980; this study) and which is intrusive into both Nisling Assemblage (Tempelman-Kluit, 1974; this study) and Yukon-Tanana Terrane (Mortensen, 1992). Lithologically similar intrusions of the same age are also present in Stikinia (the Texas Creek and Topley suites) and in the Slide Mountain and Cache Creek terranes (Gabrielse and Reesor, 1974; Woodsworth et al., 1991). Magmatism was synchronous with the development of the Hazelton volcanic arc in Stikinia.

4) Rapid uplift of Nisling Assemblage occurred after intrusion of Aishihik Batholith and before, or during, the intrusion of the Long Lake Suite. Plutons of the suite post-date the batholith and crystallized by about 189.7 ± 3.3 Ma at shallow crustal levels and are characterized by miarolitic cavities and discordant contacts. Dyke swarms that consist of pink quartz monzonite and that are spatially associated with plutons of the Long Lake Suite are common. Geochronological data indicate rapid cooling (between $100^\circ\text{C}/\text{Ma}$ and $45^\circ\text{C}/\text{Ma}$) of Aishihik Batholith, consistent with rates of uplift in excess of 2 cm/year. The preservation of unaltered magmatic epidote in Aishihik Batholith requires quenching by rapid uplift and cooling (Zen, 1989; Zen and Hammerstrom, 1984). Staurolite grains in staurolite migmatite schist are mantled by andalusite and cordierite, requiring that pressure dropped from 8 kbar during peak metamorphic conditions, to less than 3 kbar. West-verging folds of Nisling Assemblage and Aishihik Batholith may have

developed at this time. Modern analogues suggest that rapid uplift of the order inferred for Nisling Assemblage and Aishihik Batholith can be associated with collision (Copeland *et al.*, 1988; Wang and Burnett, 1990).

In Yukon-Tanana Terrane intrusion of the Klotassin Plutonic Suite was followed by imbrication of the terrane along regional scale thrust faults. Thrust faults are characterized by slices mafic and ultramafic rock thought to represent ophiolite of the Slide Mountain Terrane (Mortensen, 1990). In Stikinia Hazelton arc volcanism began to wane by about 187 Ma (Marsden and Thorkelson, 1992) although contraction, during which Cache Creek Terrane was thrust westward over Stikinia along the Nahlin and King Salmon thrust faults, did not occur until the Middle Jurassic.

A tectonic model for Nisling Assemblage :

These criteria are consistent with a tectonic model (Figure 6.1) in which Nisling Assemblage: 1) formed part of a microcontinent which included Yukon-Tanana Terrane and Stikinia through much of the Paleozoic; 2) collided with and was subducted beneath another terrane in the Late Triassic; 3) was the site of Early Jurassic magmatic arc development; and 4) collided with and was thrust above another terrane in the middle to late Early Jurassic.

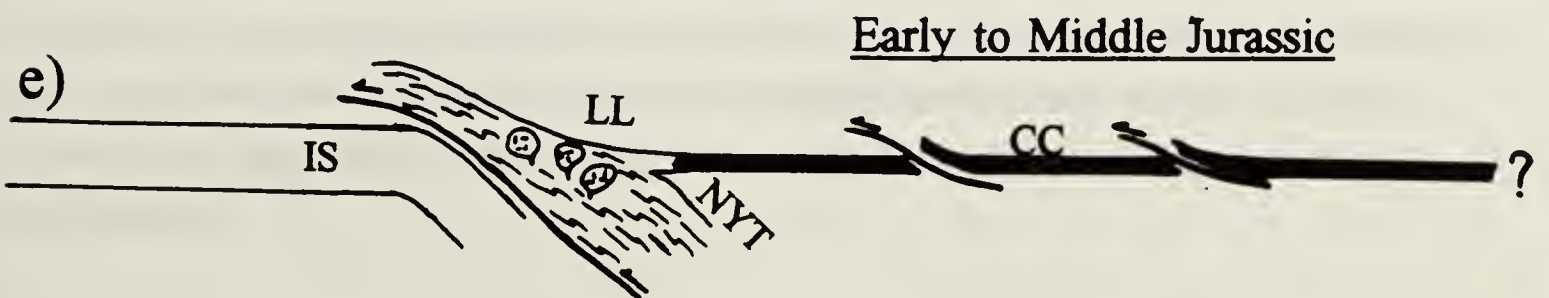
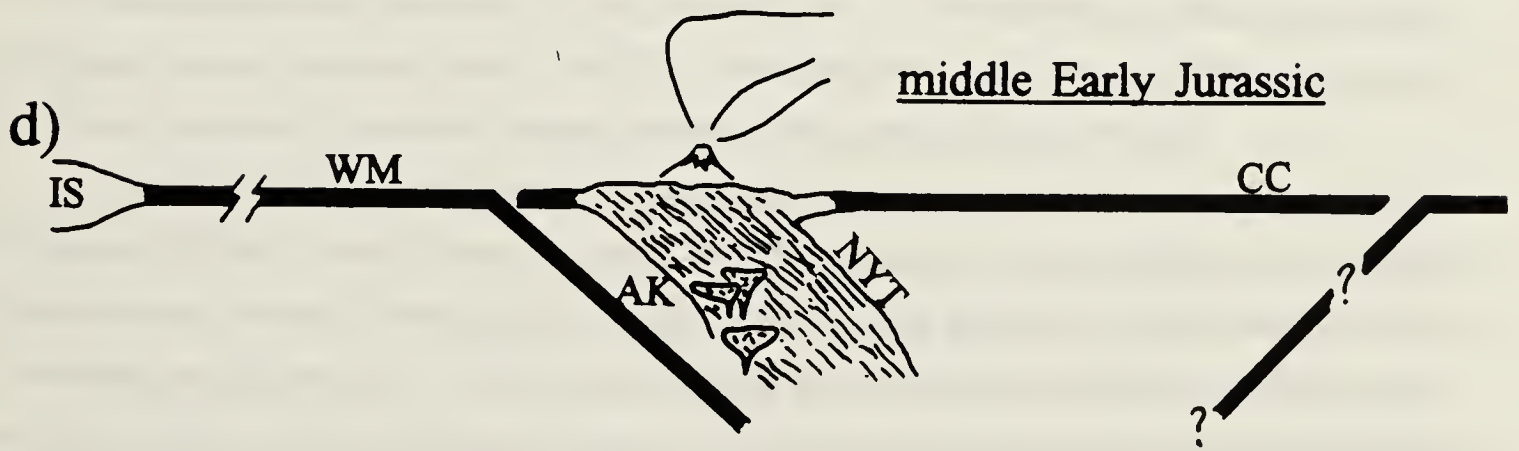
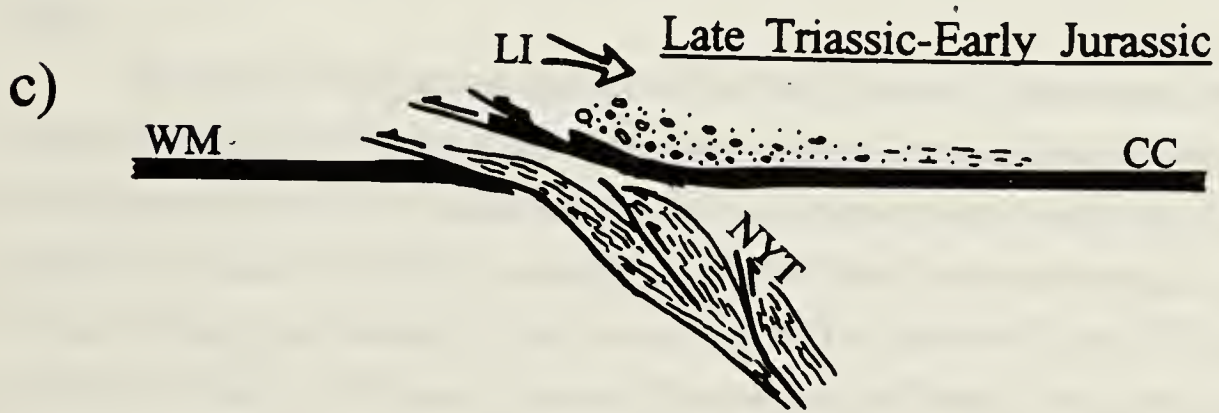
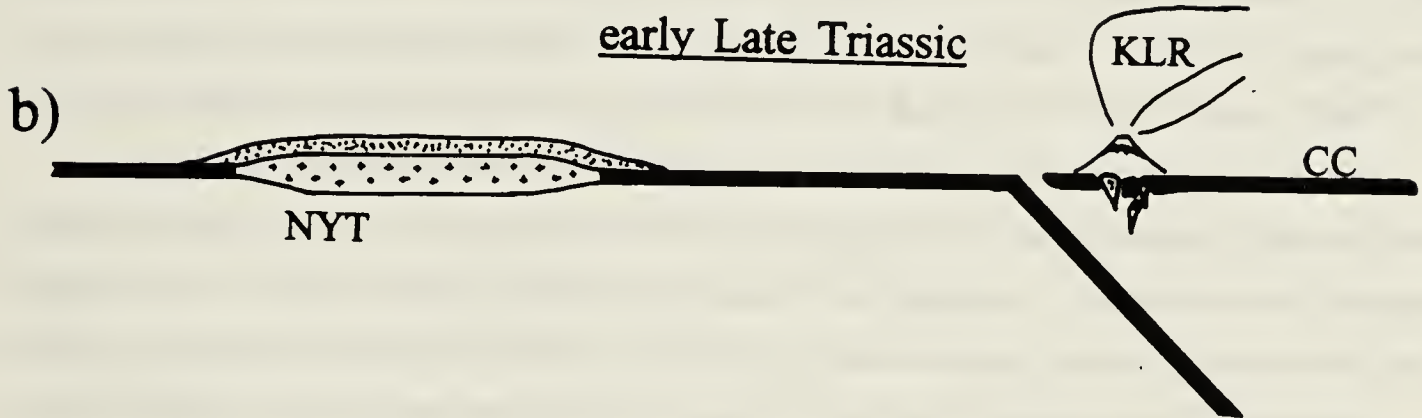
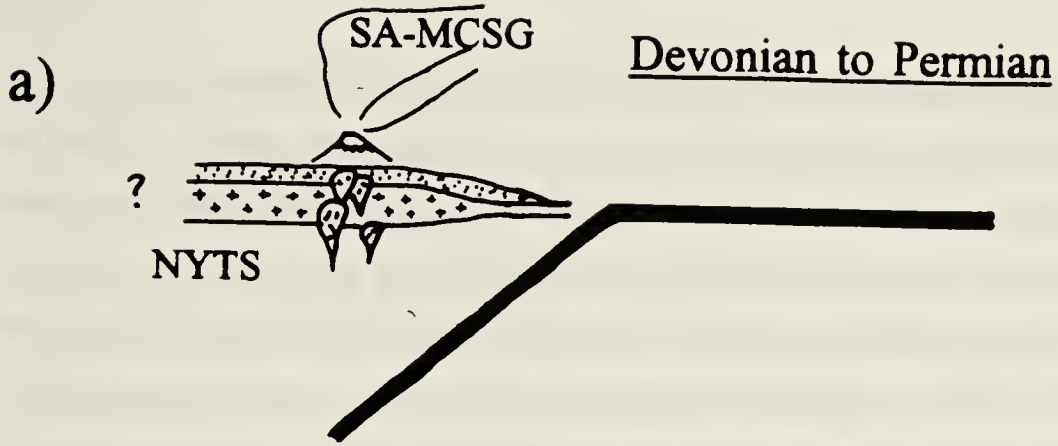
The model begins with the Devonian-Mississippian development of volcanic arc sequences in Nisling Assemblage, Stikinia and Yukon-Tanana Terrane, consistent with mid-Paleozoic subduction beneath a Nisling-Yukon-Tanana-Stikinia microcontinent (Figure 6.1a). Permian volcanic arc sequences occur in both Stikinia (Monger, 1977) and Yukon-Tanana Terrane (Mortensen, 1992; 1990), but have not been recognized in Nisling Assemblage. Further field mapping and geochronological studies of Nisling Assemblage are necessary to determine if this arc sequence is absent from Nisling Assemblage.

Subsequent to Permian subduction beneath part or all of the Nisling-Yukon-Tanana-Stikinia microcontinent, Nisling Assemblage and Yukon-Tanana Terrane collided with and were underthrust beneath another terrane (Figure 6.1b and c). Stikinia was characterized by volcanic arc sequence, represented by volcanic rocks of the Stuhini Group, and constituted a tectonic element distinct from Nisling Assemblage and Yukon-Tanana Terrane. Pre-Stuhini Group deformation of Stikinia - the Tahltanian Orogeny (Monger, 1977) - may provide a record of separation of Stikinia from Nisling Assemblage, although the significance of this event remains a matter of conjecture.

The landmass beneath which Nisling Assemblage was underthrust is likely to be Cache Creek Terrane. Cache Creek Terrane is characterized by a structural and



Figure 6.1 A model of the tectonic evolution of Nisling Assemblage. See text for discussion. Terranes: NYTS - Nisling Assemblage-Yukon-Tanana-Stikinia microcontinent; NYT - Nisling Assemblage-Yukon-Tanana microcontinent; CC - Cache Creek; WM; Windy-McKinley; IS - Insular SuperTerrane. Plutonic, volcanic, and sedimentary suites: SA-MCSG - Stikine Assemblage-Mink Cr. - Selwyn Gneiss; KLR - Kutcho-Lewes River groups; LI - Laberge Group-Inklin Formation (with arrow indicating sedimentary transport direction); AK - Aishihik-Klotassin Plutonic Suite; LL - Long Lake Plutonic Suite.



stratigraphic record of Late Triassic collision with a terrane of continental affinity, including: 1) the cessation arc volcanism of the Kutcho and Lewes River groups; 2) shearing of rocks of the Lewes River Group in the Tally-Ho shear zone along the west margin of Whitehorse Trough (Hart and Radloff, 1990); 3) the development of southwest verging folds which affect 218 Ma to 211 Ma blueschists (Paterson, 1974) but which are deformed by earliest Late Jurassic structures (Monger, 1977); and 4) the deposition of a thick blanket of molasse, including the Laberge Group and the Inklin formation. Collision with a terrane of continental affinity is suggested by the presence of clasts of quartzite and quartz mica schist in the molasse sequence (Hart and Radloff, 1990; Wheeler, 1960).

Subduction beneath the tectonically buried Nisling Assemblage began in the earliest Jurassic and was responsible for the development of the Klotassin Plutonic Suite (Figure 6.1d). Early Jurassic plutons and volcanic sequences, in particular the Hazelton Group, are present across the entire width of the Intermontane Belt consistent with the inward-dipping subduction beneath both sides of the belt (Marsden and Thorkelson, 1992).

The bulk of the plutons that constitute the Klotassin Suite occur along the southwest margin of Nisling Assemblage and Yukon-Tanana Terrane consistent with their development above crust subducting to the east (present day coordinates) beneath the ancient west coast of Nisling Assemblage. The White River Assemblage, which crops out west of Nisling Assemblage in southwest Yukon (Tempelman-Kluit, 1974) and which is included in Windy-McKinley Terrane (Wheeler and McFeely, 1991), may constitute a relic of the ocean subducted beneath Nisling Assemblage. The assemblage consists of marine Paleozoic rocks, including cherty argillite, chert, phyllite, and Devonian limestone, and mafic and ultramafic rocks of oceanic affinity (Tempelman-Kluit, 1974).

In this model post-Aishihik Batholith tectonism is attributed to the closure of the Windy-McKinley ocean closed by about 187 Ma. Buoyant crust, probably of the Insular Superterrane, entered the subduction zone colliding with and being thrust beneath Nisling Assemblage (Figure 6.1e). Nisling Assemblage and Aishihik Batholith were folded and rapidly uplifted. Yukon-Tanana Terrane was imbricated along regional scale thrust faults. Deep-seated intrusions of foliated hornblende granodiorite of the Klotassin Suite were succeeded by shallow-level emplacement of massive leucocratic pink quartz monzonite of the Long Lake Suite. Accretion of the more westerly Insular Superterrane may have begun in the Early Jurassic (van der Heyden, 1990; Currie, 1991), consistent with this interpretation.

The demise of the Windy-McKinley ocean coincided with intra- and inter-terrane contractional tectonism, and a cessation of Early Jurassic arc volcanism. Inboard and outboard subduction beneath Stikinia ceased (Marsden and Thorkelson, 1992). Cache Creek was thrust west over Stikinia along the King Salmon and Nahlin thrust faults. Internal imbrication of Cache Creek terrane also occurred at this time (Gabrielse, 1991) and molasse shed from the emergent terrane was deposited on Stikinia forming Bowser Basin.

This model explains the Late Triassic-Early Jurassic tectonic evolution of the Northern Cordillera in terms of two collisional events. Late Triassic tectonic burial of Nisling Assemblage resulted from the closure of an ocean by subduction beneath Cache Creek Terrane. Subsequent closure of the Windy-McKinley ocean by subduction beneath Nisling Assemblage resulted in the Early Jurassic accretion of Insular Superterrane to the ancient outboard margin of Nisling Assemblage.

6.2 Conclusions

To elucidate the relationship between Stikinia and Nisling Assemblage, this study examined the contact between Aishihik Batholith, an intrusion previously considered to be part of Stikinia, and a metamorphosed package of quartzose clastic rocks, marble, amphibolite and orthogneiss, constituting Nisling Assemblage. The evidence presented here indicates that: 1) Aishihik Batholith crystallized at about 186 Ma and belongs to the Klotassin Plutonic Suite; and 2) that the batholith intrudes Nisling Assemblage.

These findings, together with other recent research in the northern Cordillera, indicate that there is a profound misunderstanding of northern Stikinia. The origin of this misunderstanding is twofold, and includes: 1) the assumption that the Klotassin Suite represents the plutonic root of Late Triassic volcanic rocks of the Lewes River Group (Tempelman-Kluit, 1979); and 2) an initial correlation of Nisling Assemblage with Stikinia (Tempelman-Kluit, 1979). Because Klotassin Suite appeared to intrude "Stikinia" (now Nisling Assemblage) and because the Klotassin Suite was thought to be related to the volcanic rocks of the Lewes River Group, the Lewes River Group was inferred to have been deposited on Stikinia. By 1981 Nisling Assemblage was considered as part of a terrane distinct from Stikinia (Tempelman-Kluit, 1981). This reinterpretation did not, however, result in a re-evaluation of the terrane affinity of the Lewes River arc. Indeed it was the continued inclusion of the Lewes River arc, including the Lewes River Group and the Klotassin Suite, in Stikinia which suggested that the Klotassin Suite was allochthonous with respect to Nisling Assemblage. Even the subsequent realization that the Klotassin

Suite was too young to represent the plutonic root of the Lewes River arc did not result in a re-assignment of the terrane affinity of the Lewes River Group. Thus on recent terrane maps (Wheeler and McFeely, 1991) the Lewes River succession is considered as part of Stikinia despite the fact that the two initial assumptions which led to its inclusion in Stikinia (Klotassin Suite related to Lewes River Group and Nisling Assemblage equivalent to Stikinia) had been discarded. The only remaining basis for the inclusion of the Lewes River Group in Stikinia is the lithological similarity of the Lewes River and Stuhini groups. However, the lithological similarity of two successions is not in itself sufficient evidence that they belong to the same terrane.

This confusion over what constitutes northern Stikinia has hindered the development of ideas concerning the tectonic evolution of the northern Cordillera. To address this problem I suggest that the current terrane nomenclature of the Cordillera be changed such that neither the Lewes River Group nor the Klotassin Suite are included in, or are used to define, Stikinia.

If the Lewes River Group and the Klotassin Suite are not part of Stikinia, what then is their terrane affinity? In Whitehorse Trough Lewes River Group strata unconformably overlie fragments of former oceanic crust thought to be correlative with nearby Cache Creek Terrane. This relationship suggests that the Whitehorse Trough, including the Lewes River Group, should be included in Cache Creek Terrane. In northern British Columbia Gabrielse (1991) has included Whitehorse Trough strata carried in the hangingwall of the King Salmon fault in the Cache Creek Terrane, consistent with this interpretation. The inclusion of Lewes River Group in Cache Creek Terrane is strong evidence in support of the suggestion that a volcanic arc developed on Cache Creek in the Late Triassic (Thorstad and Gabrielse, 1986). The Klotassin Suite should not be accorded terrane status. The suite post-dates tectonism related to the collision of Nisling Assemblage with another terrane, probably Cache Creek, and constitutes part of a pan-Intermontane magmatic-volcanic sequence.

Nisling Assemblage, Yukon-Tanana Terrane and Stikinia are inferred to have formed a Paleozoic microcontinent that fragmented in the Triassic. These correlations and suggested terrane relations await testing by further comparative mapping, geochronological, and geochemical studies of these tectonic assemblages.

REFERENCES

- Baadsgaard, H., and Lerbekmo, J.F., 1983. Rb - Sr and U - Pb dating of bentonites. *Can. J. Earth Sci.*, 20, p. 1282-1290.
- Barbarin, B., 1988. Field evidence for successive mixing and mingling between the Piolard Diorite and the Saint-Julien-LaVetre Monzogranite (Nord-Forez, Massif Central, France). *Can. J. Earth Sci.*, p. 49-59.
- Bateman, P.C., Busacca, A.J., and Sawka, W.N., 1983. Cretaceous deformation in the western foothills of the Sierra Nevada, California. *Bull. Geol. Soc. Amer.*, 94, p. 30-42.
- Bateman, R., 1985. Aureole deformation by flattening around a diapir during in situ ballooning: the Cannibal Creek granite. *J. Geol.*, 93, p. 293-310.
- Bence, A.E., and Albee, A.L., 1968. Empirical correction factors of the electron microanalysis of silicates and oxides. *J. Geol.*, 76, p. 382-403.
- Berman, R.G., 1988. Internally-consistent thermodynamic data for minerals in the system NaO-KO-CaO-MgO-FeO-FeO-AlO-SiO-TiO-HO-CO. *J. Petrol.*, 29, p. 445-522.
- Berman, R.G., Brown, T.H., and Greenwood, H.J., 1987. GEOCALC: Software for calculation and display of P-T-X phase diagrams. *Amer. Mineral.*, 72, p. 861-862.
- Brew, D.A., and Morrell, R.P., 1983. Intrusive rocks and plutonic belts of southeastern Alaska, U.S.A. in Roddick, J.A. (ed.), *Circum-Pacific Plutonic Terranes*, Geol. Soc. America, Mem. 159, p. 171-193.
- Brown, D.A., Logan, J.M., Gunning, M.H., Orchard, M.J., and Bamber, W.E., 1991. *Can. J. Earth Sci.*, 28, p. 958-972.
- Bultman, T.R., 1979. Geology and tectonic history of the Whitehorse Trough west of Atlin, British Columbia. Yale University, unpublished Ph.D. thesis, 284 p.
- Burg, J.-P., 1991. Syn-migmatization way-up criteria. *J. Structural Geol.*, 13.
- Burg, J.-P., and Philippot, P., 1991. Asymmetric compositional layering of syntectonic metamorphic veins as way-up criterion. *Geology*, 19, p. 1112-1115.

- Charlesworth, H.A.K., Guidos, J., Gold, C., and Wynne, D., 1989. TRIPOD 3.0, a microcomputer program for storing, retrieving, displaying and analysing orientation, stratigraphic and positional data from drillholes, outcrops and seismic lines. University of Alberta, unpublished manual, 80 p.
- Cockfield, W.E., 1927. Aishihik Lake District, Yukon. Geol. Surv. Can., Sum. Rept. 1926, p. 1-13, reprinted in Bostock, H.S., 1957, Selected field reports of the Geological Survey of Canada, 1898-1933. Geol. Surv. Can., Mem. 284, p. 558-569.
- Copeland, P., Hodges, K.V., Harrison, T.M., LeFort, P., and Pecher, A., 1988. Rapid Pliocene uplift associated with the Main Boundary thrust, central Nepal: Geol. Soc. America., Abstracts with Programs, 20, p. A321.
- Currie, L.D., 1992. Jurassic accretion of Nisling Terrane along the western margin of Stikinia, Coast Mountains, northwestern British Columbia (abstract). in Southern Cordillera Transect Workshop (Report no. 24) and Cordilleran Tectonics Workshop, Program and Abstracts, p. 89.
- Currie, L.D., 1991. Geology of the Tagish Lake area, northern Coast Mountains, northwestern British Columbia. in Geol. Surv. Canada, Paper 91-1A, Current Research, Part A, Cordillera and Pacific margin, p. 147-154.
- Cushing, G., Foster, H.L., and Garrison, T.M., 1984. Mesozoic age of metamorphism and thrusting in the eastern part of east-central Alaska (abstract). Trans. AGU, 65, p. 290-291.
- Dickie, J.R., and Hein, F.J., 1990. A Pliensbachian submarine slope and conglomeratic gully-fill succession: Richtofen to Conglomerate Formation Transition (Laberge Group), Brute Mountain, Yukon. in Yukon Geology, 3, Indian and Northern Affairs Canada, Yukon Region, Whitehorse. p.
- Dickie, J.R., and Hein, F.J., 1988. Facies and depositional setting of Laberge Conglomerates (Jurassic), Whitehorse Trough. in Yukon Geology, 2, Exploration and Geological services division, Yukon, Indian and Northern Affairs Canada, p. 26-32.
- Dusel-Bacon, C., and Foster, H.L., 1990. New thermobarometric evidence for high pressure, medium temperature metamorphism of two subterranees of the Yukon Tanana composite terrane (YTT) in easternmost Alaska (Abstract). Geol. Assoc. Can. Program with Abstracts, 15, p. A35.

- Eisbacher, G.H., 1976. Sedimentology of the Dezadeash flysch and its implications for strike-slip faulting along the Denali fault, Yukon Territory and Alaska. *Can. J. Earth Sci.*, 13, p. 1495-1513.
- Erdmer, P.E., 1991. Metamorphic terrane east of Denali fault between Kluane Lake and Kusawa Lake, Yukon Territory. in *Current Research, Part E, Geol. Surv. Can. Pap 90-1E*, p. 107-111.
- Erdmer, P.E., 1990. Studies of the Kluane and Nisling assemblages in Kluane and Dezadeash map areas, Yukon. in *Current Research, Part E, Geol. Surv. Can. Pap 90-1E*, p. 107-111.
- Erdmer, P.E., and 21 others, 1989. Lithoprobe transect proposal, unpublished, 25 p.
- Evenchick, C.A., 1991. Geometry, evolution, and tectonic framework of the Skeena Fold Belt, north-central British Columbia. *Tectonics*, 10, p. 527-546.
- Farrar, E., Clark, A.H., Archibald, D.A., and Way, D.C., 1988. Potassium-Argon age of granitoid plutonic rocks, southwest Yukon territory, Canada. *Isochron/West*, 51, p. 19-23.
- Ferry, J.M., and Spear, F.S., 1978. Experimental calibration of the partitioning of Fe and Mg between biotite and garnet. *Contributions to Mineralogy and Petrology*, 66, p. 113-114.
- Fuhrman, M.L., and Lindsley, D.H., 1988. Ternary-feldspar modeling and thermometry. *Amer. Mineral.*, 73, p. 201-215.
- Gabrielse, H., 1991. Late Paleozoic and Mesozoic terrane interactions in north-central British Columbia, *Can. J. Earth Sci.*, 28, p. 947-957.
- Gabrielse, H., and Reesor, J.E., 1974. The nature and setting of granitic plutonism in the central and eastern parts of the Canadian Cordillera. *Pacific Geology*, 8, p. 109-138.
- Ganguly, J., and Saxena, S.K., 1984. Mixing properties of aluminosilicate garnets: Constraints from natural and experimental data, and applications to geothermobarometry. *American Mineralogist*, 69, p. 88-97.
- Gapais, D., and Barbarin, B., 1986. Quartz fabric transition in a cooling syntectonic granite (Hermitage Massif, France). *Tectonophysics*, 125, p. 357-370.

- Gehrels, G.E., McClelland, W.C., Samson, S.D., Patchett, P.J., and Jackson, J.L., 1990. Ancient continental margin assemblage in the Coast Mountains, southeast Alaska and northwest Canada. *Geology*, 18, p. 208-211.
- Gehrels, G.E., McClelland, W.C., Jackson, J.L., Samson, S.D., and Patchett, J., 1989. Nisling terrane, a Proterozoic - Lower Paleozoic (?) continental margin assemblage, in and adjacent to the northern Coast Mountains Batholith. *in* Program and Abstracts, 1989 Cordilleran Tectonics Workshop, p. 2.
- Ghent, E.K., Robbins, D.B., and Stout, M.Z., 1979. Geothermometry, geobarometry and fluid compositions of metamorphosed calc-silicates and pelites, Mica Creek, British Columbia. *American Mineralogist*, 64, p. 874-885.
- Gordey, S.L., 1973. Petrology and structural relations of volcanic and basement rocks on the west side of Aishihik Lake Yukon Territory. Unpublished B.Sc. thesis, University of British Columbia, 69 p.
- Hansen, V.L., Yukon-Tanana Terrane: a partial acquittal. *Geology*, 18, p. 365-369.
- Hansen, V.L., Mortensen, J.K., and Armstrong, R.L., 1989. Pre-Jurassic ductile deformation and synchronous metamorphism of the Yukon-Tanana Terrane: geochronologic constraints from the Teslin suture zone, Yukon. *Can. J. Earth Sci.*, 26, p. 2224-2235.
- Harland, W.B., Armstrong, R.L., Cox, A.V., Craig, L.E., Smith, A.G., and Smith, D.G., 1990. A geologic time scale 1989. Cambridge University Press, Cambridge, 263 p.
- Hart, C.J.R., and Radloff, J.K., 1990. Geology of Whitehorse, Alligator Lake, Fenwick Creek, Carcross and part of Robinson map areas (105D/11, 6, 3, 2, and 7). Indian and Northern Affairs Canada, Open File 1990-4, 113 p.
- Heaman, L., and Parrish, R., 1991. U-Pb geochronology of accessory minerals. *in* Heaman, L., and Ludden, J.N. (eds.), G.A.C. short course handbook on applications of radiogenic isotope systems to problems in geology, p. 59-102.
- Hodges, K.V., and Spear, F.S., 1982. Geothermometry, geobarometry and the Al_2SiO_5 triple point at Mt. Moosilauke, New Hampshire. *Amer. Min.*, 67, p. 1118-1134.
- Hutchison, W.W., 1970. Metamorphic framework and plutonic styles in the Prince Rupert region of the central Coast Mountains. *Can. J. Earth Sci.*, 7, 376-405.

- Jackson, J.L., Gehrels, G.E., Patchett, P.J., and Mihalynuk, M.G., 1991. Stratigraphic and isotopic link between the northern Stikine terrane and an ancient continental margin assemblage, Canadian Cordillera. *Geology*, 19, p. 1177-1180.
- Kindle, E.D., 1952. Dezadeash map-area, Yukon Territory. *Geol. Surv. Canada. Mem.*, 364, 68 p.
- Krogh, T.E., 1982. Improved accuracy of U-Pb zircon ages by the creation of more concordant systems using an air abrasion technique. *Geochim. Cosmochim. Acta*, 46, p. 631-649.
- Lanphere, M.A., 1978. Displacement history of the Denali fault system, Alaska and Canada. *Can. J. Earth Sci.*, 15, p. 817-822.
- Le Couteur, P.C., and Tempelman-Kluit, D.J., 1976. Rb/Sr ages and a profile of initial $^{87}\text{Sr}/^{86}\text{Sr}$ ratios for plutonic rocks across the Yukon Crystalline terrane. *Can. J. Earth Sci.*, 13, p. 319-330.
- Lynch, G.V., Pride, C., and Watson, P.I., 1983. Petrology and geochemistry of the Pattison Alaskite pluton. *in* Yukon Exploration and Geology 1982, Dept. Indian North. Affairs, Whitehorse, Yukon, p. 38-49.
- Ludwig, K.R., 1980. Calculation of uncertainties of U-Pb isotope data. *Earth Planet. Sci. Lett.*, 46, p. 212-220.
- Marsden, H., and Thorkelson, D.J., 1992. Geology of the Hazelton volcanic belt in British Columbia: implications for the early to middle Jurassic evolution of Stikinia. *Tectonics*, in press.
- McClelland, W.C., Anovitz, L.M., and Gehrels, G.E., 1991. Thermobarometric constraints on the structural evolution of the Coast Mountains batholith, central southeastern Alaska. *Can. J. Earth Sci.*, 28, p. 912-928.
- Mihalynuk, M.G., and Rouse, J.N., 1987. Preliminary geology of the Tutshi Lake area, northwestern British Columbia (104M/15). *in* British Columbia Ministry of Energy, Mines and Petroleum Resources, Geological Fieldwork, Pap. 1988-1, p. 217-231.
- Monger, J.W.H., 1989. Overview of Cordilleran Geology. *in* Ricketts, B.D. (ed.), Western Canada Sedimentary Basin: a case history. *Can. Soc. Petrol. Geol.*, Calgary, p. 9-32.

- Monger, J.W.H., 1977. Upper Paleozoic rocks of northwestern British Columbia. in Report of activities, part A. Geol. Surv. Can. Pap., 77-1A, p. 255-261.
- Monger, J.W.H., 1975. Upper Paleozoic rocks of the Atlin Terrane, northwestern B.C. and southcentral Yukon. Geol. Surv. Canada., Pap. 74-47, 63 p.
- Monger, J.W.H., 1974. Paleozoic rocks of the Atlin terrane, northwestern British Columbia and south-central Yukon. Geol. Surv. Can. Pap., 74-47, 63 p.
- Monger, J.W.H., and Berg, H.C., 1987. Lithotectonic terrane map of western Canada and southeastern Alaska. U.S. Geol. Surv. Misc. Field Stud. map, MF 1874-B.
- Monger, J.W.H., and Church, B.N., 1977. Revised stratigraphy of the Takla Group, north-central British Columbia, Can. J. Earth Sci., 14, p. 318-326.
- Monger, J.W.H., Price, R.A., and Tempelman-Kluit, D.J., 1982. Tectonic accretion and the origin of the two major metamorphic and plutonic welts in the Canadian Cordillera. Geology, 10, p. 70-75.
- Morin, J.A., 1981. Geology and Mineralization of the Hopkins lake area, 115 H 2, 3, 6, 7. in Geology and Exploration, 1979-80., Dept. Indian Northern Affairs, Whitehorse, Yukon, p. 98-104.
- Mortensen, J.K., 1992. Pre-mid-Mesozoic tectonic evolution of the Yukon-Tanana Terrane, Yukon and Alaska. Tectonics, 11, 4, p. 836-853.
- Mortensen, J.K., 1990. Geology and U-Pb geochronology of the Klondike District, west-central Yukon Territory. Can. J. Earth Sci., 27, p. 903-914.
- Mortensen, J.K., and Jilson, G.A., 1985. Evolution of the Yukon-Tanana terrane: Evidence from southeastern Yukon Territory. Geology, 13, p. 806-810.
- Muller, J.E., 1967. Kluane Lake map area, Yukon Territory (115G, 115F(E1/2)). Geol. Surv. Can. Mem., 340, 137 p.
- Nicholls, J., and Stout, M.Z., 1988. Picritic melts in Kilauea: Evidence from the 1967-1968 Halemaumau and Hilaka eruptions. J. Petrology, 29, p. 1031-1057.
- Nokleberg, W.J., Jones, D.L., and Silberling, N.J., 1985. Origin and tectonic evolution of the Maclaren and Wrangellia terranes, eastern Alaska Range, Alaska. G.S.A. Bull., 96, p. 1251-1270.
- Page, R.W., and Bell, T.H., 1986. Isotopic and structural responses of granite to successive deformation and metamorphism. J. Geol., 94, p. 365-379.

- Parrish, R.R., Roddick, J.C., Loveridge, W.D., and Sullivan, R.W., 1987. Uranium lead analytical techniques at the geochronology laboratory, Geological Survey of Canada. *Geol. Surv. Can. Pap.*, 87-2, p. 3-7.
- Paterson, I.A., 1974. Geology of the Cache Cr. Group and Mesozoic rocks at the north end of the Stuart Lake Belt, central British Columbia. *Geol. Surv. Canada Pap.*, 74-1B, p. 31-42.
- Paterson, S.R., Vernon, R.H., and Tobisch, O.T., 1989. A review of criteria for the identification of magmatic and tectonic foliations in granitoids. *J. Structural Geol.*, 11, p. 349-363.
- Roddick, J.C., 1987. Generalized numerical error analysis with applications to geochronology and thermodynamics. *Geochim. Cosmochim. Acta*, 51, p. 2129-2135.
- Roddick, J.A., and Hutchison, W.W., 1974. Setting of the Coast Plutonic Complex, British Columbia. *Pacific Geology*, 8, p. 91-108.
- Samson, S.D., McClelland, W.C., Patchett, P.J., Gehrels, G.E., and Anderson, R.G., 1989. Evidence from Nd isotopes for mantle contributions to Phanerozoic crustal genesis in the Canadian Cordillera. *Nature*, 337, p. 705-709.
- Souther, J.G., 1971. Geology and mineral deposits of Tulsequah map area, British Columbia (104K). *Geol. Surv. Can. Mem.*, 362, 84 p.
- Spear, F.S., and Cheney, J.T., 1989. A petrogenetic grid for pelitic schists in the system $\text{SiO}_2\text{-Al}_2\text{O}_3\text{-FeO-MgO-K}_2\text{O-H}_2\text{O}$. *Contrib. Min. Pet.*, 1989.
- Stanley, W.D., Labson, V.F., Nokleberg, W.J., Csejtey, B. Jr., and Fisher, M.A., 1990. The Denali fault system and Alaska Range of Alaska: Evidence for underplated Mesozoic flysch from magnetotelluric surveys. *G.S.A. Bull.*, 102, p. 160-173.
- Steiger, R.H., and Jager, E., 1977. Subcommittee on geochronology: Conventions on the use of decay constants in geo- and cosmochronology. *Earth Planet. Sci. Lett.*, 36, p. 359-362.
- Sylvester, A.G., Oertel, G., Nelson, C.A., and Christie, J.M., 1978. Papoose Flat pluton: a granite blister in the Inyo Mountains, eastern California. *Bull. geol. Soc. Amer.*, 89, p. 1205-1219.

- Tempelman-Kluit, D.J., 1981. Geology and mineral deposits of southern Yukon. *in* Yukon Geology and Exploration 1979-80. Dept. Indian Northern Affairs, Whitehorse, Yukon, p. 7-31.
- Tempelman-Kluit, D.J., 1979. Transported cataclasite, ophiolite and granodiorite in Yukon: Evidence of arc-continent collision. Geol. Surv. Can., Pap. 79-14, 27 p.
- Tempelman-Kluit, D.J., 1977b. Quiet Lake (105F) and Finlayson Lake (105G) map-areas, Yukon. Geol. Surv. Canada, Open File 486.
- Tempelman-Kluit, D.J., 1976. The Yukon Crystalline Terrane: Enigma in the Canadian Cordillera. Geol. Soc. America Bull., 87, p. 1343-1357.
- Tempelman-Kluit, D.J., 1974. Reconnaissance geology of Aishihik Lake, Snag and part of Stewart River map-areas, west-central Yukon Territory. Geol. Surv. Can., Pap. 73-14, 93 p.
- Tempelman-Kluit, D.J., and Wanless, R.K., 1980. Zircon ages for the Pelly Gneiss and Klotassin granodiorite in western Yukon; Can. J. Earth Sci., 17, p. 297-306.
- Tempelman-Kluit, D.J., and Wanless, R.K., 1975. Potassium - argon age determinations of metamorphic and plutonic rocks in the Yukon Crystalline terrane. Can. J. Earth Sci., 12, p. 1895-1909.
- Thorstad, L.E., and Gabrielse, H., 1986. The Upper Triassic Kutcho Formation, Cassiar Mountains, north-central British Columbia. Geol. Surv. Can. Pap., 86 16, 53 p.
- Tipper, H.W., and Richards, T.A., 1976. Jurassic stratigraphy and history of north central British Columbia. Geol. Surv. Can. Bull., 270, 58 p.
- van der Heyden, P., 1990. Preliminary U-Pb dates and field observations from the eastern Coast Belt near 52°N, British Columbia. *in* Current Research, Part A, Geol. Surv. Can. Pap., 91-1A, p. 79-84.
- van der Molen, I., and Peterson, M.S., 1979. Experimental deformation of partly melted granite. Contrib. Min. Pet., 70, p. 299-318.
- Wang, C.-H., and Burnett, W.C., 1990. Holocene mean uplift rates across an active plate-collision boundary in Taiwan. Science, 248, p. 204-206.
- Way, D.C., 1977. A reconnaissance study of granitoid plutonism in southwestern Yukon Territory. Queen's University, M.Sc. thesis, Kingston, Ontario, 177 p.

- Werner, L.J., 1978. Metamorphic Terrane, Northern Coast Mountains west of Atlin Lake, British Columbia. *in* Current Research, Part A, Geol. Surv. Canada, Pap. 78-1A, p. 69-70.
- Werner, L.J., 1977. Metamorphic Terrane, Northern Coast Mountains west of Atlin Lake, British Columbia. *in* Report of Activities, Part A, Geol. Surv. Canada, Pap. 77-1A, p. 267-269.
- Wheeler, J.O., 1961. Whitehorse map-area, Yukon Territory (105D). Geological Survey of Canada, Memoir 312, 156 p.
- Wheeler, J.O., and McFeely, P., 1991. Tectonic Assemblage map of the Canadian Cordillera and adjacent parts of the United States of America. *in* Gabrielse, H. and Yorath, C.J. (editors), Geology of Canada no. 4: Geology of the Cordilleran Orogen in Canada.
- Woodsworth, G.J., Anderson, R.G., and Armstrong, R.L., 1991. Plutonic Regimes in the Canadian Cordillera. *in* Gabrielse, H. and Yorath, C.J. (editors), Geology of Canada no. 4: Geology of the Cordilleran Orogen in Canada, p. 491 - 532.
- Zen, E., 1989. Plumbing the depths of batholiths. *Amer. J. Sci.*, 289, p. 1137-1157.
- Zen, E., and Hammarstrom, J.M., 1984. Magmatic epidote and its petrologic significance. *Geology*, 12, p. 515-518.

THE UNIVERSITY OF CHICAGO
DEPARTMENT OF THE HISTORY OF ARTS
CHICAGO, ILLINOIS

THE UNIVERSITY OF CHICAGO
DEPARTMENT OF THE HISTORY OF ARTS
CHICAGO, ILLINOIS

THE UNIVERSITY OF CHICAGO
DEPARTMENT OF THE HISTORY OF ARTS
CHICAGO, ILLINOIS

THE UNIVERSITY OF CHICAGO
DEPARTMENT OF THE HISTORY OF ARTS
CHICAGO, ILLINOIS

THE UNIVERSITY OF CHICAGO
DEPARTMENT OF THE HISTORY OF ARTS
CHICAGO, ILLINOIS

THE UNIVERSITY OF CHICAGO
DEPARTMENT OF THE HISTORY OF ARTS
CHICAGO, ILLINOIS

APPENDIX 2.1

Locations of all samples

SAMPLE no.	id	EASTING (m)	NORTHING (m)	LONGITUDE	LATITUDE	ELEV (masl)	UNIT
UTM grid zone - 8V							
1	85-1	379436	6825036	61°32'30.6"N	137°16'05.1"W	944	eJab
2	85-2	379100	6825072	61°32'31.3"N	137°16'27.9"W	917	eJab
3	85-3	379569	6823716	61°31'48.1"N	137°15'53.0"W	915	eJab
4	85-4	380038	6822564	61°31'11.4"N	137°15'18.6"W	915	eJab
5	85-5	393282	6806972	61°23'01.8"N	136°59'50.7"W	1015	Tfp
6	85-6	394842	6806912	61°23'01.4"N	136°58'05.5"W	1264	eJab
7	85-7	395301	6806042	61°22'33.8"N	136°57'32.8"W	1264	eJab
8	85-8	395930	6805978	61°22'32.3"N	136°56'50.4"W	1219	eJab
9	85-9	395953	6806322	61°22'43.4"N	136°56'49.5"W	1234	PPm
10	85-10	395349	6805542	61°22'17.7"N	136°57'28.6"W	1203	PPo
11	85-11	395168	6805458	61°22'14.8"N	136°57'40.6"W	1188	PPo
12	85-12	395168	6805458	61°22'14.8"N	136°57'40.6"W	1219	Tfp
13	85-13	393551	6788195	61°12'55.6"N	136°58'54.2"W	917	PPms
14	85-14	393438	6788454	61°13'03.9"N	136°59'02.3"W	917	PPms
15	85-15	393364	6789172	61°13'27.0"N	136°59'08.7"W	917	PPms
16	85-16	393418	6789694	61°13'43.9"N	136°59'06.1"W	917	PPm
17	85-17	393364	6791063	61°14'28.1"N	136°59'12.5"W	917	PPms

18	86-1	392550	6785500	61°11'27.6"N	136°59'55.7"W	930	Tfp
19	86-2	391830	6784551	61°10'56.2"N	137°00'41.9"W	1097	PPms
20	86-3	397506	6798053	61°18'17.8"N	136°54'48.6"W	1295	PPm
21	86-4	391081	6786401	61°11'55.2"N	137°01'35.9"W	1204	PPa
22	86-5	378007	6834112	61°37'22.0"N	137°18'03.5"W	1036	eJab
23	86-6	378643	6829061	61°34'39.6"N	137°17'08.3"W	960	Tv
24	86-7	373692	6831411	61°35'49.8"N	137°22'49.5"W	1128	eJab
25	86-8	374107	6832935	61°36'39.5"N	137°22'25.1"W	1234	Tv
26	86-9	376300	6826831	61°33'25.0"N	137°19'41.6"W	914	eJab
27	86-10	386810	6818988	61°29'23.3"N	137°07'32.8"W	1006	eJab
28	86-11	387152	6819524	61°29'41.0"N	137°07'10.9"W	1090	eJab
29	86-12	387152	6819524	61°29'41.0"N	137°07'10.9"W	1090	eJab
29	86-13	384239	6819627	61°29'41.2"N	137°10'27.9"W	930	eJab
30	86-14	385597	6817779	61°28'43.0"N	137°08'52.0"W	983	eJab
31	86-15	385633	6817856	61°28'45.5"N	137°08'49.8"W	1006	eJab
32	86-16	391175	6813180	61°26'20.2"N	137°02'25.6"W	1059	PPms
33	86-17	390560	6813110	61°26'17.3"N	137°03'06.9"W	1052	PPms
34	86-18	377722	6827974	61°34'03.5"N	137°18'08.1"W	922	Tv
35	86-19	376703	6827838	61°33'57.9"N	137°19'16.8"W	914	eJab
36	86-20	377292	6825440	61°32'41.2"N	137°18'31.1"W	922	eJab
37	86-21	378902	6822562	61°31'10.1"N	137°16'35.4"W	960	eJab
38	86-22	378902	6822562	61°31'10.1"N	137°16'35.4"W	960	eJab
39	86-23	378827	6822608	61°31'11.5"N	137°16'40.6"W	960	Tfp
40	86-24	378843	6822707	61°31'14.7"N	137°16'39.7"W	975	PPo
41	86-25	378697	6823490	61°31'39.8"N	137°16'51.5"W	945	eJab
42	86-26	378377	6823409	61°31'36.8"N	137°17'12.9"W	983	Tfp
43	86-27	378262	6823220	61°31'30.6"N	137°17'20.2"W	937	eJab
44	86-28	378094	6823184	61°31'29.2"N	137°17'31.5"W	945	eJab
45	86-29	377931	6822721	61°31'14.1"N	137°17'41.4"W	922	Tfp
46	86-30	378434	6822862	61°31'19.2"N	137°17'07.8"W	968	PPms

47	86-31	378622	6822602	61°31'11.0"N	137°16'54.4"W	960	PPo
48	86-32	379471	6823332	61°31'35.6"N	137°15'58.7"W	975	eJab
49	86-33	380614	6822791	61°31'19.4"N	137°14'40.2"W	960	eJab
50	86-34	380025	6822256	61°31'01.5"N	137°15'18.8"W	922	eJab
51	86-35	379926	6822318	61°31'03.3"N	137°15'25.6"W	922	eJab
52	86-36	383487	6818782	61°29'13.1"N	137°11'16.8"W	922	PPms
53	86-37	378615	6824631	61°32'16.6"N	137°16'59.7"W	917	Tfp
54	86-38	383448	6818811	61°29'14.0"N	137°11'19.5"W	922	PPms
55	86-39	383448	6818811	61°29'14.0"N	137°11'19.5"W	922	PPms
56	86-40	383545	6818646	61°29'08.7"N	137°11'12.6"W	922	PPo
57	86-41	383545	6818646	61°29'08.7"N	137°11'12.6"W	922	PPo
58	86-42	393963	6805012	61°21'59.2"N	136°59'00.8"W	1059	PPm
59	86-43	394594	6806180	61°22'37.5"N	136°58'20.7"W	1181	PPms
60	86-44	394626	6806943	61°23'02.2"N	136°58'20.1"W	1234	eJab
61	86-45	395396	6805570	61°22'18.6"N	136°57'25.5"W	1311	eJab
62	86-46	397438	6804735	61°21'53.6"N	136°55'06.4"W	1311	Q
63	86-47	397523	6804425	61°21'43.7"N	136°55'00.1"W	1471	eJab
64	86-48	398075	6804303	61°21'40.2"N	136°54'22.7"W	1562	PPo
65	86-49	404482	6851517	61°47'11.2"N	136°48'39.9"W	1341	eJll
66	86-50	402894	6851929	61°47'23.0"N	136°50'29.0"W	1402	eJll
67	86-51	410390	6848748	61°45'46.9"N	136°41'51.9"W	1364	eJab
68	86-52	398314	6849368	61°45'56.0"N	136°55'36.3"W	1402	Q
69	86-53	398460	6849473	61°45'59.5"N	136°55'26.6"W	1402	Q
70	86-54	400617	6848820	61°45'40.5"N	136°52'58.2"W	1425	Q
71	86-55	397926	6846919	61°44'36.5"N	136°55'57.8"W	1250	eJll
72	86-56	399272	6845466	61°43'50.9"N	136°54'23.2"W	1433	Q
73	86-57	399623	6845349	61°43'47.5"N	136°53'59.1"W	1425	PPo
74	86-58	399516	6845355	61°43'47.5"N	136°54'06.4"W	1440	PPo
75	86-59	342000	6856550	61°48'39.0"N	137°59'55.1"W	1181	eJll
76	86-60	393500	6857250	61°50'05.9"N	137°01'21.2"W	1227	PPa

77	86-61	397922	6855329	61°49'08.2"N	136°56'15.1"W	1219	PPms
78	86-62	399263	6853023	61°47'55.0"N	136°54'38.9"W	1521	eJll
79	86-63	397855	6852328	61°47'31.2"N	136°56'13.6"W	1288	PPm
80	86-64	397363	6851898	61°47'16.8"N	136°56'46.3"W	1314	PPa
81	86-65	397363	6851898	61°47'16.8"N	136°56'46.3"W	1314	PPa
82	86-66	398670	6842153	61°42'03.3"N	136°54'57.5"W	1417	eJab
83	86-67	398511	6842060	61°42'00.2"N	136°55'08.2"W	1394	eJab
84	86-68	385507	6819989	61°29'54.2"N	137°09'03.0"W	1005	eJab
85	86-69	376167	6835456	61°38'03.3"N	137°20'11.6"W	1005	eJab
86	86-74	384052	6818033	61°28'49.5"N	137°10'36.9"W	914	PPo
87	86-75	391650	6784348	61°10'49.5"N	137°00'53.6"W	1219	PPms
88	86-76	391410	6784425	61°10'51.7"N	137°01'09.8"W	1249	PPms
89	86-78	393959	6809569	61°24'26.4"N	136°59'10.4"W	1082	eJab
90	86-79	392783	6786205	61°11'50.6"N	136°59'41.6"W	922	KTrr
91	86-80	379949	6822362	61°31'04.8"N	137°15'24.1"W	915	eJab
92	86-82	376329	6826868	61°33'26.2"N	137°19'39.8"W	914	eJab
93	86-83	397926	6803613	61°21'17.8"N	136°54'31.3"W	1539	Tfp
94	86-84	397775	6803837	61°21'24.9"N	136°54'41.9"W	1532	PPa
95	86-85	397459	6804255	61°21'38.1"N	136°55'04.0"W	1433	eJab

96	87-1	393339	6787829	61°12'43.6"N	136°59'07.6"W	975	Q
97	87-2	393385	6787692	61°12'39.2"N	136°59'04.3"W	983	PPms
98	87-3	393530	6787465	61°12'32.0"N	136°58'54.1"W	1006	Tfp
99	87-4	393812	6787450	61°12'31.8"N	136°58'35.2"W	1021	KTrr
100	87-5	393941	6787519	61°12'34.2"N	136°58'26.7"W	1021	PPms
101	87-6	394196	6788340	61°13'00.9"N	136°58'11.3"W	975	Tfp
102	87-7	393481	6788688	61°13'11.5"N	136°58'59.9"W	983	PPm
103	87-8	393481	6788688	61°13'11.5"N	136°58'59.9"W	983	PPm
104	87-9	393511	6788810	61°13'15.4"N	136°58'58.1"W	975	PPms

105	87-10	395327	6792516	61°15'16.9"N	136°57'03.9"W	991	PPms
106	87-11	394693	6792384	61°15'12.0"N	136°57'46.1"W	1006	Q
107	87-12	394693	6792384	61°15'12.0"N	136°57'46.1"W	1006	Q
108	87-13	395261	6793073	61°15'34.8"N	136°57'09.4"W	1006	Q
109	87-14	397661	6791312	61°14'40.2"N	136°54'25.0"W	1067	PPa
110	87-15	397987	6791083	61°14'33.1"N	136°54'02.7"W	1219	PPa
111	87-16	397987	6791083	61°14'33.1"N	136°54'02.7"W	1219	PPa
112	87-17	397987	6791083	61°14'33.1"N	136°54'02.7"W	1219	Tfp
113	87-18	398437	6791264	61°14'39.4"N	136°53'32.9"W	1234	PPm
114	87-19	399128	6793184	61°15'42.1"N	136°52'50.3"W	1387	Q
115	87-20	399043	6793505	61°15'52.4"N	136°52'56.6"W	1394	KTrr
116	87-21	398300	6792000	61°15'03.1"N	136°53'43.5"W	1181	PPms
117	87-22	397140	6793906	61°16'03.5"N	136°55'05.0"W	1052	PPm
118	87-23	397592	6794468	61°16'22.1"N	136°54'35.8"W	1189	PPms
119	87-24	397369	6795560	61°16'57.2"N	136°54'52.9"W	1303	PPm
120	87-25	397354	6796374	61°17'23.4"N	136°54'55.5"W	1372	KTrr
121	87-26	397188	6797678	61°18'05.4"N	136°55'09.3"W	1341	PPm
122	87-27	393282	6789389	61°13'33.9"N	136°59'14.6"W	922	PPms
123	87-28	393289	6789335	61°13'32.2"N	136°59'14.1"W	922	PPms
124	87-29	393357	6789023	61°13'22.2"N	136°59'08.9"W	922	PPm
125	87-30	393280	6790736	61°14'17.4"N	136°59'17.5"W	922	PPms
126	87-31	393280	6790668	61°14'15.2"N	136°59'17.4"W	922	PPm
127	87-32	393317	6790561	61°14'11.8"N	136°59'14.7"W	922	Tfp
128	87-33	392927	6790068	61°13'55.5"N	136°59'39.8"W	922	PPa
129	87-34	393002	6789869	61°13'49.1"N	136°59'34.4"W	922	PPms
130	87-35	394855	6795485	61°16'52.3"N	136°57'41.5"W	1234	Tfp
131	87-37	393439	6796226	61°17'14.9"N	136°59'18.1"W	1158	Q
132	87-38	393563	6796375	61°17'19.8"N	136°59'10.0"W	1158	PPa
133	87-39	394802	6795493	61°16'52.5"N	136°57'45.1"W	1219	PPm
134	87-40	388278	6765137	61°00'25.6"N	137°03'58.5"W	762	KTrr

135	87-42	392422	6773358	61°04'55.3"N	136°59'39.5"W	914	KTrr
136	87-43	394569	6804046	61°21'28.6"N	136°58'18.1"W	1120	PPo
137	87-44	395106	6804739	61°21'51.5"N	136°57'43.3"W	1204	PPo
138	87-45	395452	6805442	61°22'14.5"N	136°57'21.5"W	1273	PPo
139	87-46	395328	6805530	61°22'17.2"N	136°57'30.0"W	1295	PPms
140	87-47	395359	6805508	61°22'16.6"N	136°57'27.9"W	1295	PPms
141	87-48	394750	6807000	61°23'04.2"N	136°58'11.9"W	1280	eJab
142	87-49	394750	6807000	61°23'04.2"N	136°58'11.9"W	1280	eJab
143	87-50	394902	6804413	61°21'40.8"N	136°57'56.4"W	1196	PPms
144	87-51	395104	6805639	61°22'20.5"N	136°57'45.3"W	1219	PPms
145	87-52	391289	6793934	61°15'58.7"N	137°01'37.6"W	1029	Q
146	87-53	391859	6793898	61°15'58.1"N	137°00'59.3"W	1036	PPms
147	87-54	392877	6794601	61°16'21.8"N	136°59'52.4"W	1151	Q
148	87-55	393007	6795100	61°16'38.1"N	136°59'44.7"W	1196	PPms
149	87-56	392951	6795322	61°16'45.2"N	136°59'49.0"W	1196	PPa
150	87-57	392140	6794625	61°16'21.9"N	137°00'41.9"W	1097	PPms
151	87-58	390970	6795435	61°16'46.9"N	137°02'02.1"W	945	PPa
152	87-59	391465	6795536	61°16'50.6"N	137°01'29.1"W	975	PPm
153	87-60	391662	6795458	61°16'48.3"N	137°01'15.7"W	1006	Q
154	87-61	392257	6795688	61°16'56.3"N	137°00'36.3"W	1128	Tfp
155	87-62	392688	6796253	61°17'15.0"N	137°00'08.5"W	1219	Q
156	87-63	391787	6796528	61°17'23.0"N	137°01'09.6"W	1143	PPm
157	87-64	391178	6796421	61°17'18.9"N	137°01'50.2"W	1021	PPms
158	87-65	391147	6796368	61°17'17.2"N	137°01'52.2"W	1029	PPms
159	87-66	390315	6799690	61°19'03.7"N	137°02'55.0"W	991	Q
160	87-67	390789	6799245	61°18'49.8"N	137°02'22.3"W	1021	PPm
161	87-68	391580	6799457	61°18'57.4"N	137°01'29.6"W	1166	PPms
162	87-69	391112	6800403	61°19'27.5"N	137°02'03.0"W	1082	PPm
163	87-70	389889	6800302	61°19'23.0"N	137°03'25.0"W	968	KTrr
164	87-71	392313	6785057	61°11'13.0"N	137°00'10.7"W	945	Tfp

165	87-72	392319	6784989	61°11'10.8"N	137°00'10.1"W	945	PPm
166	87-73	392347	6784874	61°11'07.2"N	137°00'08.0"W	975	PPms
167	87-74	392377	6784539	61°10'56.4"N	137°00'05.3"W	1067	PPms
168	87-75	392064	6784166	61°10'44.0"N	137°00'25.5"W	1143	PPm
169	87-76	391442	6784530	61°10'55.1"N	137°01'07.8"W	1257	PPms
170	87-77	391207	6784915	61°11'07.3"N	137°01'24.4"W	1250	PPm
171	87-78	391395	6785139	61°11'14.8"N	137°01'12.2"W	1189	PPms
172	87-79	385963	6817767	61°28'43.0"N	137°08'27.3"W	975	eJab
173	87-80	385538	6817623	61°28'37.9"N	137°08'55.7"W	975	PPms
174	87-81	400118	6795707	61°17'04.5"N	136°51'48.7"W	1554	KTrr
175	87-82	392945	6778026	61°07'26.6"N	136°59'14.1"W	1066	KTrr
176	87-83	393292	6775798	61°06'14.9"N	136°58'46.4"W	1036	KTrr
177	87-84	396952	6803014	61°20'57.5"N	136°55'35.7"W	1280	PPo
178	87-85	397552	6803092	61°21'00.6"N	136°54'55.5"W	1334	PPo
179	87-86	397639	6803254	61°21'05.9"N	136°54'49.9"W	1417	PPo
180	87-88	398029	6804301	61°21'40.1"N	136°54'25.8"W	1570	PPo
181	87-90	432727	6842178	61°42'31.1"N	136°16'20.2"W	822	eJll
182	87-91	432727	6842178	61°42'31.1"N	136°16'20.2"W	822	TJgk
183	87-92	432693	6841067	61°41'55.2"N	136°16'21.0"W	777	eJll
184	87-93	431369	6839011	61°40'47.9"N	136°17'48.3"W	899	TJgk
185	87-94	431110	6838463	61°40'30.0"N	136°18'05.2"W	822	TJgk
186	87-95	430516	6838628	61°40'35.0"N	136°18'45.8"W	777	TJgk
187	87-96	430087	6838801	61°40'40.3"N	136°19'15.2"W	792	TJgk
188	87-97	429696	6839350	61°40'57.8"N	136°19'42.5"W	853	eJll
189	87-98	431223	6835865	61°39'06.2"N	136°17'54.0"W	1319	eJll
190	87-99	426970	6831220	61°36'33.3"N	136°22'36.2"W	1374	eJll
191	87-100	393243	6845769	61°43'54.8"N	137°01'14.3"W	1394	PPa
192	87-101	393548	6845557	61°43'48.0"N	137°00'53.1"W	1364	PPi
193	87-102	393670	6845497	61°43'46.5"N	137°00'44.7"W	1341	PPa
194	87-103	393670	6845497	61°43'46.5"N	137°00'44.7"W	1341	PPa

195	87-104	395537	6844285	61°43'09.2"N	136°58'35.1"W	1349	PPms
196	87-105	395979	6844199	61°43'06.8"N	136°58'04.8"W	1173	PPm
197	87-106	396123	6844216	61°43'07.5"N	136°57'55.0"W	1143	PPm
198	87-107	397900	6841489	61°41'41.1"N	136°55'48.6"W	1371	eJab
199	87-108	399144	6842358	61°42'10.4"N	136°54'25.7"W	1371	eJab
200	87-109	400545	6845058	61°43'38.9"N	136°52'55.7"W	1371	eJab
201	87-110	400955	6849576	61°46'05.2"N	136°52'36.7"W	1432	eJll
202	87-111	403746	6851632	61°47'14.2"N	136°49'30.3"W	1463	eJll
203	87-112	406922	6852929	61°47'58.9"N	136°45'56.1"W	1310	eJll
204	87-113	406597	6863509	61°53'40.4"N	136°46'38.0"W	1676	eJll
205	87-114	368565	6827037	61°33'22.4"N	137°28'25.7"W	1212	PPa
206	87-115	368772	6826275	61°32'58.0"N	137°28'09.7"W	1227	PPm
207	87-116	368892	6826153	61°32'54.3"N	137°28'01.3"W	1234	PPa
208	87-117	368836	6825728	61°32'40.5"N	137°28'04.0"W	1219	Q
209	87-118	368873	6825674	61°32'38.8"N	137°28'01.4"W	1219	Q
210	87-119	368560	6824234	61°31'51.9"N	137°28'18.8"W	1371	PPms
211	87-120	368749	6824338	61°31'55.5"N	137°28'06.3"W	1311	Tfp
212	87-121	368320	6824014	61°31'44.5"N	137°28'34.5"W	1402	PPms
213	87-122	366500	6824930	61°32'11.8"N	137°30'40.0"W	1420	PPms

APPENDIX 2.2 - SAMPLE DESCRIPTIONS

Sample		Description
no.	field id ^a	
1	85-1	unit ^b : eJab name: foliated to gneissic hornblende biotite granodiorite maj. ^c : qt, pl ₍₃₀₎ min.: hbl, bi, ks, op, chl, ep, cc, sc acc.: tt
2	85-2	unit: eJab name: foliated hornblende granodiorite maj.: hbl, pl ₍₃₃₎ , qt min.: bi, ks, op, chl, ep, cc, sc acc.: al, ep, ap, tt, zi
3	85-3	unit: eJab name: leucocratic, foliated quartz monzonite maj.: pl ₍₂₅₎ , ks min.: hlb, bi, qt, op, chl, cc, ep, sc acc.: al, ep
4	85-4	unit: eJab name: foliated hornblende granodiorite maj.: hbl, pl, qt min.: ks, sc, op acc.:
5	85-5	unit: Tfp name: massive, dark green, ultramafic maj.: pl, ol, py min.: tr, op acc.:
6	85-6	unit: eJab name: foliated biotite hornblende quartz diorite maj.: hbl, plag ₍₄₀₎ min.: bi, qt, op, sc, ep acc.: tt

THE HISTORY OF THE

CHAPTER I	
1700	1700
1701	1701
1702	1702
1703	1703
1704	1704
1705	1705
1706	1706
1707	1707
1708	1708
1709	1709
1710	1710
1711	1711
1712	1712
1713	1713
1714	1714
1715	1715
1716	1716
1717	1717
1718	1718
1719	1719
1720	1720
1721	1721
1722	1722
1723	1723
1724	1724
1725	1725
1726	1726
1727	1727
1728	1728
1729	1729
1730	1730
1731	1731
1732	1732
1733	1733
1734	1734
1735	1735
1736	1736
1737	1737
1738	1738
1739	1739
1740	1740
1741	1741
1742	1742
1743	1743
1744	1744
1745	1745
1746	1746
1747	1747
1748	1748
1749	1749
1750	1750
1751	1751
1752	1752
1753	1753
1754	1754
1755	1755
1756	1756
1757	1757
1758	1758
1759	1759
1760	1760
1761	1761
1762	1762
1763	1763
1764	1764
1765	1765
1766	1766
1767	1767
1768	1768
1769	1769
1770	1770
1771	1771
1772	1772
1773	1773
1774	1774
1775	1775
1776	1776
1777	1777
1778	1778
1779	1779
1780	1780
1781	1781
1782	1782
1783	1783
1784	1784
1785	1785
1786	1786
1787	1787
1788	1788
1789	1789
1790	1790
1791	1791
1792	1792
1793	1793
1794	1794
1795	1795
1796	1796
1797	1797
1798	1798
1799	1799
1800	1800

- 7 85-7 unit: eJab
 name: foliated biotite hornblende quartz diorite
 maj.: qt, pl₍₃₅₎
 min.: hbl, bi, op, sc, ep
 acc.: tt
- 8 85-8 unit: eJab
 name: foliated biotite granodiorite
 maj.: pl₍₂₅₎, qt
 min.: ks, bi, op, chl, ep, sc, cc
 acc.: al, ep
- 9 85-9 unit: PPm
 name: coarsely crystalline banded fetid tremolite diopside marble
 maj.: cc, di
 min.: tr, ep, qt, fs, sc, op
 acc.: tt
- 10 85-10 unit: PPO
 name: biotite augan granodiorite orthogneiss
 maj.: qt, pl₍₃₀₎, ks
 min.: bi, chl, sc, cc, gt, op
 acc.: zi
- 11 85-11 unit: PPO
 name: biotite hornblende granodiorite orthogneiss
 maj.: qt, pl, ks
 min.: hbl, bi, chl, op
 acc.: zi, ap
- 12 85-12 unit: Tfp
 name: chloritized feldspar hornblende porphyry
 maj.: fs, qt, hbl
 min.: chl, op
 acc.: zi, tt, ap
- 13 85-13 unit: PPms
 name: mica schist
 maj.: qt, bi_{1,2}, mu_{1,2}, pl₍₃₅₎
 min.: chl, sc, op
 acc.: zi, to, ap
- 14 85-14 unit: PPms

- name: andalusite staurolite mica schist
 maj.: qt, bi_{1,2}, mu_{1,2}, fs
 min.: ad₂, st, op, chl, sc
 acc.: ap
- 15 85-15 unit: PPms
 name: quartzose sillimanite mica schist
 maj.: qt
 min.: bi_{1,2}, mu_{1,2}, sil₄, fs, op, chl, sc
 acc.: rt
- 16 85-16 unit: PPM
 name: chloritized diopside marble
 maj.: cc
 min.: di, chl, op
 acc.:
- 17 85-17 unit: PPms
 name: andalusite cordierite staurolite sillimanite mica schist
 maj.: qt
 min.: fs, bi₂, mu₂, op, gt, st, sil₄, ad₂, cd₂, sc
 acc.: tt, zi
- 18 86-1 unit: KTrr
 name: quartz porphyritic biotite hornblende granodiorite
 maj.: qt, fs
 min.: bi, hbl, op, sc
 acc.:
- 19 86-2 unit: PPms
 name: sillimanite andalusite mica schist
 maj.: qt, bi
 min.: mu, fs, op, ad₄, sil₄
 acc.:
- 20 86-3 unit: PPM
 name: garnet diopside magnetite skarn
 maj.: gt, di, mt
 min.:
 acc.:
- 21 86-4 unit: PPa

- name: chloritized amphibolite breccia hosted in leucocratic pegmatite
maj.: hbl, chl, fs
min.: qt, bi, op, sc, ep
acc.: ap, tt
- 22 86-5 unit: eJab
name: weakly foliated hornblende granodiorite
maj.: hbl, fs, qz
min.: bi, op, chl
acc.: tt
- 23 86-6 unit: Tertiary volcanics
name: brown weathering, dark olive brown finely crystalline volcanics
maj.: hbl, fs
min.:
acc.:
- 24 86-7 unit: eJab
name: foliated and altered hornblende granodiorite
maj.: hbl, qt, fs
min.: chl, ep, sc, op
acc.: ap, tt
- 25 86-8 unit: Tfp
name: finely crystalline, leucocratic, brown weathering, vesicular,
flow banded, rhyolitic volcanic
maj.: qt, fs
min.: op, sc, ep
acc.:
- 26 86-9 unit: eJab
name: K-feldspar megacrystic, foliated hornblende granodiorite
maj.: pl, qt, hbl
min.: ks, op, chl, sc, ep
acc.: tt, ap
- 27 86-10 unit: eJab
name: coarsely crystalline, pink and white micaceous pegmatite
maj.: ks, pl₍₃₀₎, qt
min.: mu, chl
acc.:
- 28 86-11 unit: eJab
name: sheared hornblende biotite granodiorite

- maj.: bi, qt, fs
 min.: hbl, fs, op, ep, sc, chl
 acc.: ap, zi, ep, al, tt
- 29 86-12 unit: eJab
 name: mafic hornblende biotite granodiorite
 maj.: bi, qt, fs
 min.: hbl, op, chl, sc
 acc.: tt, ap, , ep, al
- 29 86-13 unit: eJab
 name: chloritized foliated biotite hornblende granodiorite
 maj.: hbl, qt, fs
 min.: chl, bi, sc, op
 acc.: tt, ap, ep, al
- 30 86-14 unit: eJab
 name: leucocratic coarsely crystalline micaceous pegmatite
 maj.: qt, fs
 min.: bi, chl, sc, ep, sp, op
 acc.:
- 31 86-15 unit: eJab
 name: heavily altered foliated hornblende granodiorite
 maj.: qt, fs, bi
 min.: chl, cc, ep, sc
 acc.:
- 32 86-16 unit: PPO
 name: biotite granite orthogneiss
 maj.: qt, pl₍₃₀₎
 min.: bi, ks, op
 acc.: al, tt, to
- 33 86-17 unit: PPO
 name: biotite granite orthogneiss
 maj.: qt, fs
 min.: bi, op
 acc.: al, ap
- 34 86-18 unit: Tfp
 name: dark green, amygdoloidal feldspar porphyry
 maj.: hbl, pl
 min.: chl, qt

acc.:

- 35 86-19 unit: eJab
 name: fissile, foliated chloritized biotite granodiorite
 maj.: bi, pl, qt
 min.: ks, chl, cc
 acc.:
- 36 86-20 unit: ?
 name: pink weathering, medium grained, equicrystalline hornblende
 granite
 maj.: ks, qt, pl
 min.: hbl
 acc.:
- 37 86-21 unit: eJab
 name: well foliated hornblende granodiorite
 maj.: hbl, fs, qt
 min.: bi, op, chl
 acc.:
- 38 86-22 unit: eJab
 name: hornblende biotite foliated to gneissic granodiorite
 maj.: hbl, qt, fs
 min.: bi, op, chl, sc
 acc.: al, ep, zi, ap, tt
- 39 86-23 unit: Tfp
 name: leucocratic, finely crystalline, siliceous dyke
 maj.: qt, fs
 min.: op, cc, sc, chl
 acc.:
- 40 86-24 unit: PPO
 name: fine grained quartzo-feldspathic biotite schist / biotite granite
 orthogneiss
 maj.: bi, qt, fs
 min.:
 acc.: ap
- 41 86-25 unit: eJab
 name: gneissic hornblende granodiorite
 maj.: bhl, qt, fs
 min.: bi, op, chl, sc, cc, ep

acc.: tt, ap, al, ep

- | | | |
|----|-------|---|
| 42 | 86-26 | unit: Tfp
name: fractured and altered diabase dyke
maj.:
min.:
acc.: |
| 43 | 86-27 | unit: eJab
name: finely crystalline mafic, biotite microdiorite enclave
maj.: bi, fs
min.: qt, op, sc, ep, chl
acc.: al, ep, tt, ap, zi |
| 44 | 86-28 | unit: eJab
name: blastomylonitic micaceous quartz hornblende schist
maj.: qt, hbl, fs
min.: bi, cc, sc, chl
acc.: tt, ap |
| 45 | 86-29 | unit: Tfp
name: dark green weathering, phenocrystic, diabase dyke
maj.: hbl, pl, op
min.: cc
acc.: |
| 46 | 86-30 | unit: PPo
name: biotite hornblende granite orthogneiss
maj.: qt, pl ₍₃₀₎ , ks, hbl
min.: bi, op, sc
acc.: al, ep, ap, tt |
| 47 | 86-31 | unit: PPo
name: hornblende granodiorite orthogneiss
maj.: hb, fs
min.: qt, bi, op, ep, cc, chl, sc
acc.: ap |
| 48 | 86-32 | unit: eJab
name: amphibolitic quartz diorite gneiss
maj.: hbl, fs
min.: qt, bi, chl, sc, cc
acc.: al, ep, tt, ap, zi |

- 49 86-33 unit: eJab
 name: gneissic, mafic, hornblende granodiorite with folded leucocratic
 aplite veins
 maj.: hbl, qt, fs
 min.: bi, op, sc, chl, cc
 acc.: tt, ap, al, ep
- 50 86-34 unit: eJab
 name: migmatic hornblende orthogneiss
 maj.: hbl, qt, fs
 min.: bi, op, ep, chl
 acc.: tt, ap, al, ep
- 51 86-35 unit: eJab
 name: banded green and red calc-silicate (inclusion)
 maj.: ga, ep, qt
 min.: di, fs, cc, sc
 acc.:
- 52 86-36 unit: PPO
 name: blastomylonitic feldspar augan gneiss
 maj.: qt, fs
 min.: bi, op, gt, mu, sc
 acc.: ap
- 53 86-37 unit: Tfp
 name: fractured and heavily jointed diabase dyke
 maj.: pl
 min.: chl, hbl
 acc.:
- 54 86-38 unit: PPO
 name: blastomylonitic feldspar augan gneiss
 maj.: qt, pl₍₃₆₎, ks
 min.: bi, op, chl, sc
 acc.: al, tt
- 55 86-39 unit: PPO
 name: blastomylonitic feldspar augan gneiss
 maj.: qt, fs
 min.: bi, op, gt, mu
 acc.:
- 56 86-40 unit: PPO

- name: altered hornblende granodiorite orthogneiss
maj.: hbl, fs, ep, qt
min.: bi, op, chl
acc.: ap
- 57 86-41 unit: PPO
name: hornblende granodiorite orthogneiss
maj.: hbl, fs, qt
min.: bi, ep, cc, chl, sc
acc.: zi, ap
- 58 86-42 unit: PPms
name: migmatitic sillimanite garnet mica schist
maj.: qt, bi₂
min.: sil_{2,4}, pl₍₃₂₎, op, gt, mu, ep, chl, sc
acc.: tt, to, ap
- 59 86-43 unit: PPO
name: garnetiferous hornblende granodiorite orthogneiss
maj.: fs, hbl, qt
min.: bi, gt
acc.:
- 60 86-44 unit: eJab
name: glassy, siliceous, finely laminated mylonite
maj.: qt, ks, pl
min.: bi, mu, sc, chl, ep
acc.:
- 61 86-45 unit: eJab
name: brown, feldspathic garnetiferous micaceous gneiss
maj.: pl₍₂₈₎, qt, ks
min.: bi, op, gt, cc, chl, sc
acc.:
- 62 86-46 unit: PPqtz
name: finely banded orthoquartzite
maj.: qt
min.: fs, op, ap, sc
acc.:
- 63 86-47 unit: eJab
name: heavily altered, megacrystic granodiorite
maj.: qt, fs

- min.: sc, mu, op, ep
acc.: ap
- 64 86-48 unit: PPO
name: finely crystalline hornblende biotite granite orthogneiss
maj.: qt, gs, hb, bi
min.: op, ch, sc
acc.:
- 65 86-49 unit: ejll
name: orange weathering, finely crystalline, equigranular quartz monzonite
maj.: ks, pl, qt
min.: sc
acc.:
- 66 86-50 unit: eJll
name: equigranular, medium grained, well foliated, biotite quartz monzonite
maj.: pl, ks, qt
min.: bi, chl, sc, op
acc.:
- 67 86-51 unit: eJll
name: equigranular, orange weathering, pink quartz monzonite
maj.: fs, qt
min.: sc
acc.:
- 68 86-52 unit: PPms
name: micaceous quartzite
maj.: qt
min.: bi, pl₍₂₈₎, ks, op, mu, chl, sc
acc.: zi, to, ap
- 69 86-53 unit: PPms
name: sillimanite mica schist
maj.: bi, mu, qt
min.: qt, fs, gt, op, sil₂, sc
acc.: zi, ap
- 70 86-54 unit: PPms
name: quartzose garnet sillimanite mica schist
maj.: qt, bi

- min.: mu, fs, op, sil, sc
acc.:
- 71 86-55 unit: eJll
name: highly altered pink weathering, miarolitic, finely crystalline
leucocratic quartz monzonite
maj.: fs, qt
min.: sc, op
acc.:
- 72 86-56 unit: PPa
name: banded hornblende amphibolite
maj.: hbl
min.: bi, fs, qt, chl
acc.: tt, ap
- 73 86-57 unit: PPa
name: leucocratic hornblende biotite gneiss
maj.: qt, fs
min.: hbl, bi, gt, ep, chl
acc.: tt, zi ap
- 74 86-58 unit: PPa
name: leucocratic hornblende biotite gneiss
maj.: qt, fs
min.: hbl, bi, ep, sc
acc.: zi, ap, al
- 75 86-59 unit: eJll
name: orange weathering, finely crystalline, well foliated biotite
quartz monzonite
maj.: qt, pl_(>10), ks
min.: bi, op, chl, sc
acc.: zi
- 76 86-60 unit: PPa
name: weakly foliated hornblende amphibolite
maj.: hbl, pl₍₅₄₎
min.: ks, op, sc
acc.: ap
- 77 86-61 unit: PPms
name: crenulated sillimanite mica schist
maj.: bi₂, qt, mu₂

- min.: fs, op, sil₂
acc.: to
- 78 86-62 unit: eJll
name: massive, orange weathering, quartz monzonite
maj.: fs, qt
min.:
acc.:
- 79 86-63 unit: PPm
name: diopside marble / skarn
maj.: di
min.: cc, tr, op
acc.:
- 80 86-64 unit: PPa
name: leucocratic, finely crystalline, quartz porphyritic meta-tuff
maj.: qt, fs
min.: hbl, ep, cc
acc.: ap
- 81 86-65 unit: PPa
name: augite hornblende amphibolite
maj.: hbl, ag
min.: chl
acc.: tt, ap
- 82 86-66 unit: eJab
name: leucocratic white to pink hornblende granodiorite
maj.: qt, fs
min.: hbl, sc, op
acc.:
- 83 86-67 unit: eJab
name: gneissic biotite hornblende granodiorite
maj.: qt, fs, hbl
min.: bi, op, chl, sc, cc
acc.: tt, ap, ep, al
- 84 86-68 unit: eJab
name: foliated biotite hornblende quartz diorite to granodiorite
maj.: hbl, fs, qt
min.: bi, op, chl, sc
acc.: zi, tt, ap

- 85 86-69 unit: eJab
 name: weathered and chloritized foliated biotite hornblende
 granodiorite
 maj.: hbl, fs, qt
 min.: bi, op, chl, cc, sc
 acc.: zi, tt, ap
- 86 86-74 unit: PPo
 name: two mica banded augan granite orthogneiss
 maj.: qt, fs
 min.: bi, mu, gt, sc
 acc.:
- 87 86-75 unit: PPms
 name: sillimanite garnet mica schist
 maj.: bi_{1,2}, mu_{1,2}, qt, pl₍₃₃₎
 min.: ks, gt, op, sil_{2,4}, chl, sc
 acc.:
- 88 86-76 unit: PPms
 name: quartzose garnet biotite schist
 maj.: qt, fs
 min.: bi, op, gt, chl, sc
 acc.: zi, ap
- 89 86-78 unit: eJab
 name: leucocratic hornblende granodiorite
 maj.: hbl, fs, qt
 min.: op
 acc.: zi, tt, ap
- 90 86-79 unit: KTrr
 name: massive to mildly foliated mafic hornblende quartz diorite
 maj.: hbl, fs, qt
 min.: op, bi
 acc.: zi, tt, ap
- 91 86-80 unit: eJab
 name: migmatitic hornblende granodiorite with mafic hornblendite
 enclaves
 maj.: hbl, fs, qt
 min.: op, chl, sc
 acc.: zi, tt, ap

- 92 86-82 unit: eJab
 name: foliated K-spar megacrystic hornblende granodiorite
 maj.: hbl, fs, qt
 min.: op, chl, sc, ep
 acc.: zi, tt, ap
- 93 86-83 unit: Tfp
 name: flesh colored, feldspar and quartz porphyry
 maj.: ks, qt
 min.: sc
 acc.:
- 94 86-84 unit: PPa
 name: mafic biotite hornblende amphibolite
 maj.: hbl, bi
 min.: pl, op, ep, chl, sc
 acc.: tt
- 95 86-85 unit: eJab
 name: feldspathic augan gneiss
 maj.: fs, qt,
 min.: bi, op, gt
 acc.:
- 96 87-1 unit: PPms
 name: micaceous garnetiferous grey quartz gneiss
 maj.: qt
 min.: bi, fs, gt, op, chl
 acc.: zi, ap
- 97 87-2 unit: PPms
 name: migmatitic garnet biotite schist
 maj.: qt, fs, bi_{1,2}
 min.: gt, chl, sc
 acc.: ap, al
- 98 87-3 unit: Tfp
 name: finely crystalline biotite feldspar porphyry
 maj.: fs
 min.: bi, qt, op
 acc.:

- 99 87-4 unit: KTrr?
name: coarsely crystalline hornblende feldspar porphyry
maj.: hbl, pl
min.:
acc.:
- 100 87-5 unit: PPms
name: andalusite biotite schist
maj.: bi_{2,3}, pl₍₂₈₎, qt
min.: op, ad₂, ks, chl, sc
acc.:
- 101 87-6 unit: Tfp
name: finely crystalline asicular hornblende porphyry
maj.: hbl, fs
min.: bi, op, qt, op
acc.: tt
- 102 87-7 unit: PPms
name: sillimanite (?) mica schist
maj.: qt, fs, bi_{1,2}
min.: mu_{1,2}, sil₄, chl, sc
acc.: zi, to, ap, tt
- 103 87-8 unit: PPa
name: hornblende amphibolite gneiss
maj.: hbl
min.: bi, pl, qt, ep, cc, chl, sc
acc.: tt
- 104 87-9 unit: PPms
name: migmatitic mica schist
maj.: qt, fl
min.: bi_{1,2}, mu_{1,2}, chl, sc
acc.: zi, to
- 105 87-10 unit: PPms
name: quartzose sillimanite garnet mica schist
maj.: qt, mu, bi
min.: fs, op, gt, sil_{2,4}, chl, sc
acc.: zi, to, ap
- 106 87-11 unit: PPms

- name: quartzose kyanite garnet mica schist
maj.: qt, bi, mu
min.: fl, op, gt, ky, ch, sc
acc.:
- 107 87-12 unit: PPa
name: garnetiferous diopside calc-silicate
maj.: cc, di
min.: gt, ep, tr, chl
acc.: tt
- 108 87-13 unit: PPa
name: hornblende amphibolite gneiss
maj.: hbl
min.: pl, bi, qt, op, py, chl, sc
acc.: tt, zi, ap
- 109 87-14 unit: PPa
name: hornblende amphibolite gneiss
maj.: hbl
min.: bi, fs, qt, op, chl, sc
acc.: al, ap
- 110 87-15 unit: PPa
name: blastomylonitic hornblende amphibolite
maj.: hbl
min.: bi, fs, qt, op, ep, cc, chl, sc
acc.: ap
- 111 87-16 unit: PPa
name: hornblende amphibolite with biotite schist laminae
maj.: qt, fs, bi, hbl
min.: op, ep, sc
acc.: tt, zi, ap
- 112 87-17 unit: Tfp
name: hornblende feldspar porphyry
maj.: fs, hbl
min.: cc, chl, ep
acc.:
- 113 87-18 unit: PPm
name: banded fetid tremolite marble
maj.: cc

- min.: tr, qt, fs, op, chl, sc
acc.: tt
- 114 87-19 unit: PPms
name: micaceous grey sillimanite quartz gneiss
maj.: qt, fs
min.: bi_{2,4}, mu_{2,4}, sil₄, chl, sc
acc.:
- 115 87-20 unit: Tfp?
name: coarsely crystalline hornblende gabbro
maj.: hbl, py, pl
min.: op
acc.:
- 116 87-21 unit: PPms
name: quartzose garnet mica schist
maj.: qt
min.: bi, fs, op, gt, mu, chl, sc
acc.: tt, zi
- 117 87-22 unit: PPm
name: tremolite diopside calc-silicate
maj.: di, tr, qt
min.: cc, fs, sc
acc.: tt
- 118 87-23 unit: PPms
name: tourmaline mica schist
maj.: bi_{1,2}, qt
min.: pl₍₄₆₎, ks, op, mu_{1,2}, chl, sc
acc.: zi, to, ap
- 119 87-24 unit: PPm
name: banded garnet diopside skarn
maj.: gt, di, qt, fs
min.: tr, chl sc,
acc.: tt
- 120 87-25 unit: KTrr
name: biotite granodiorite
maj.: bi, qt, fs
min.:
acc.:

- 121 87-26 unit: PPm
 name: garnet tremolite diopside calc-silicate
 maj.: di
 min.: phl, fs, qt, gt, tr, chl, sc
 acc.: tt
- 122 87-27 unit: PPms
 name: biotite schist
 maj.: bi_{1,2,4}
 min.: qt, fs, gt, cd_{2?}, chl, sc, op
 acc.: zi, ap
- 123 87-28 unit: PPms
 name: andalusite mica schist
 maj.: qt, bi
 min.: pl₍₃₄₎, ks, op, mu, ad_{2?}, sil₄, chl, sc
 acc.: zi, ap
- 124 87-29 unit: PPm
 name: coarsely crystalline banded diopside marble
 maj.: cc
 min.: phl, qt, tr, di, chl, sc
 acc.:
- 125 87-30 unit: PPms
 name: mica schist
 maj.: bi_{1,2}, mu_{1,2}, qt
 min.: pl₍₃₂₎, ks, op, sc
 acc.: zi, to, ap
- 126 87-31 unit: PPm
 name: tremolite diopside calc-silicate
 maj.: qt, tr, di
 min.: fs, ep, cc, chl, sc
 acc.: tt
- 127 87-32 unit: Tfp
 name: hornblende porphyry
 maj.: hbl, fs
 min.:
 acc.:
- 128 87-33 unit: PPa

- name: fine grained hornblende amphibolite
maj.: hbl, fs
min.: bi, qt, chl, sc
acc.: ap
- 129 87-34 unit: PPms
name: kyanite mica schist
maj.: bi, qt, fs
min.: pl₍₃₄₎, ks, mu, st, ky, cd_{2?}, sc
acc.: rt
- 130 87-35 unit: Tfp
name: quartz feldspar porphyry
maj.: fs, qt
min.:
acc.:
- 131 87-37 unit: PPms
name: crenulated mica schist
maj.: qt, mu_{2,3}
min.: bi₂, fs, op, chl, sc
acc.: tt
- 132 87-38 unit: PPa
name: banded hornblende amphibolite
maj.: hbl
min.: bi, pl, qt, op, ep, chl, sc
acc.: tt
- 133 87-39 unit: PPM
name: altered diopside marble
maj.: cc
min.: qt, di, sc, chl
acc.:
- 134 87-40 unit: KTrr
name: finely crystalline hornblende biotite granodiorite
maj.: bi, pl₍₁₂₎, qt
min.: hbl, ks, op, sc
acc.: zi, tt, ap
- 135 87-42 unit: KTrr
name: nebulitic biotite granite with minor mafic biotite rich
enclaves

- maj.: bi, fs, qt
 min.: sc
 acc.: zi, tt, ap
- 136 87-43 unit: PPo
 name: biotite muscovite granite orthogneiss
 maj.: qt, fs
 min.: mu, bi, op, sc, chl, cc
 acc.: ap, zi
- 137 87-44 unit: PPo
 name: leucocratic two mica granite orthogneiss
 maj.: qt, fs
 min.: bi, mu, op, sc
 acc.:
- 138 87-45 unit: PPo
 name: chloritized biotite feldspar orthogneiss
 maj.: qt, fs
 min.: bi, chl, op, chl
 acc.:
- 139 87-46 unit: PPms
 name: garnet amphibolite schist
 maj.: hbl, qt, fs
 min.: op, gt, chl, sc
 acc.: tt, zi, ap
- 140 87-47 unit: PPms
 name: mica schist with thin amphibolite laminae
 maj.: qt, fs, bi
 min.: hbl, op, gt, mu
 acc.:
- 141 87-48 unit: eJab
 name: heavily altered finely crystalline, biotite hornblende
 granodiorite
 maj.: hbl, qt, fs
 min.: bi, chl, sc, ep, cc
 acc.:
- 142 87-49 unit: eJab
 name: gneissic, finely crystalline, biotite hornblende granodiorite
 maj.: hbl, qt, fsp

- min.: bi, op, sc, sch
acc.: ap, al, ep
- 143 87-50 unit: PPa
name: calc-silicate gneiss
maj.: di, cc, qt
min.: bi, hbl, op, fs, sc, chl, ep
acc.: tt, ap, zi
- 144 87-51 unit: PPms
name: sillimanite garnet mica schist
maj.: bi, fs, qt
min.: mu, op, gt, sil_{2,4}, chl
acc.: zi, to
- 145 87-52 unit: PPms
name: garnet mica schist
maj.: bi, qt
min.: fs, op, mu, gt
acc.: zi, to, ap
- 146 87-53 unit: PPms
name: kyanite garnet mica schist
maj.: bi_{1,2,3}, qt, mu_{1,2,3}
min.: fs, op, gt, ky, chl
acc.: zi, to, ap
- 147 87-54 unit: PPms
name: interfoliated garnet mica schist and amphibolite
maj.: qt, bi, hbl, fs
min.: op, gt, ep, chl, sc
acc.: tt, zi, ap
- 148 87-55 unit: PPms
name: garnet biotite schist
maj.: bi, qt, gt
min.: fs, op, chl, sc
acc.: zi, to
- 149 87-56 unit: PPa
name: banded amphibolite gneiss
maj.: hbl, qt
min.: fs, bi, op, ep, chl, sc
acc.: tt, ap

- 150 87-57 unit: PPms
 name: garnet mica schist
 maj.: qt, fs
 min.: bi, gt, mu, op, ep, chl, sc
 acc.: zi, ap
- 151 87-58 unit: PPa
 name: dark green garnetiferous calc-silicate skarn
 maj.: ga, di
 min.: qt, op, fs, sc, ep, cc
 acc.: tt
- 152 87-59 unit: PPM
 name: coarsely crystalline banded grey and white marble
 maj.: cc
 min.: qt, op, di(?), sc
 acc.:
- 153 87-60 unit:
 name: PPms
 maj.: micaceous quartzite
 min.: qt
 acc.: fs, mu, chl
- 154 87-61 unit: Tfp
 name: chloritized hornblende porphyry
 maj.: hbl, pl
 min.: chl, op
 acc.:
- 155 87-62 unit: PPms
 name: garnet mica quartzite
 maj.: qt
 min.: bi, fs, op, mu, gt, chl, sc
 acc.: zi, to, ap
- 156 87-63 unit: PPM
 name: gneissic diopside hornblende marble - calc silicate
 maj.: hbl, qt, di
 min.: ph, ep, cc, chl, sc
 acc.: tt, zi, ap
- 157 87-64 unit: PPms

- name: micaceous quartzite
maj.: qt, mu
min.: bi, fs, op
acc.: zi
- 158 87-65 unit: PPms
name: andalusite mica schist
maj.: qt, fs, mu_{2,3}, bi₂
min.: op, ad₂₇, ep, sc
acc.: zi, to
- 159 87-66 unit: PPms
name: garnet mica schist
maj.: qt, mu_{1,2}
min.: bi_{1,2}, fs, op, gt, chl, sc
acc.: zi, to, ap
- 160 87-67 unit: PPM
name: interfoliated hornblende amphibolite and marble
maj.: hbl, cc
min.: qt, fs, chl, sc
acc.:
- 161 87-68 unit: PPms
name: quartzose sillimanite garnet mica schist
maj.: qt
min.: bi, pl₍₃₄₎, ks, op, mu, gt, sil₂, chl, sc
acc.: zi, to, ap
- 162 87-69 unit: PPM
name: coarsely crystalline banded white and grey tremolite marble
maj.: cc
min.: qt, tr, ph
acc.: tt
- 163 87-70 unit: KTrr
name: hornblende granodiorite with mafic enclaves
maj.: hbl, fs, qt
min.: op, chl, sc
acc.: zi, tt, ap
- 164 87-71 unit: Tfp
name: hornblende feldspar porphyry
maj.: hbl, fs

- min.: chl, ep, op
acc.:
- 165 87-72 unit: PPm
name: coarsely crystalline banded green and white tremolite diopside marble
maj.: cc
min.: fs, qt, tr, di, sc
acc.: tt
- 166 87-73 unit: PPms
name: andalusite staurolite kyanite sillimanite garnet mica schist
maj.: qt, mu_{2,4}
min.: bi_{2,4}, fs, op, gt, st, ky, ad_{2,4}, sil₄, chl, sc
acc.: zi, to
- 167 87-74 unit: PPms
name: andalusite staurolite garnet mica schist
maj.: qt, fs, mu
min.: bi, op, gt, st, ad_{2,4}, chl, sc
acc.:
- 168 87-75 unit: PPms
name: crenulated sericitized porphyroblastic mica schist
maj.: qt, fs, mu
min.: bi, chl, sc
acc.: to, ap
- 169 87-76 unit: PPms
name: sericitized andalusite mica schist
maj.: qt
min.: bi, fs, mu, sil₄?, ad, chl, sc
acc.: tt, zi, to
- 170 87-77 unit: PPm
name: coarsely crystalline banded garnet tremolite diopside marble
maj.: cc
min.: qt, fs, gt, tr, di, chl, sc
acc.: tt
- 171 87-78 unit: PPms
name: andalusite staurolite sillimanite garnet mica schist
maj.: qt, mu
min.: bi, fs, op, gt, st, ad_{2,4}, sil₄, chl, sc

- acc.: tt, zi, to, ap
- 172 87-79 unit: eJab
name: amphibolite schist
maj.: hbl, qt, fs
min.: bi, op, sc, chl
acc.: al, ep, ap, tt
- 173 87-80 unit: PPms
name: mica schist
maj.: qt,
min.: pl₍₃₈₎, ks, bi, mu, wp, gt, chl, sc
acc.:
- 174 87-81 unit: KTrr
name: biotite hornblende quartz diorite
maj.: pl
min.: hbl, bi, qt
acc.: zi, ap, chl, sc
- 175 87-82 unit: KTrr
name: hornblende granodiorite
maj.: hbl, fs, qt
min.: op, bi
acc.: zi, tt, ap
- 176 87-83 unit: KTrr
name: hornblende granodiorite
maj.: hbl, fs, qt
min.: op, bi
acc.: zi, tt, ap
- 177 87-84 unit: PPa
name: massive hornblende amphibolite
maj.: hbl, fs
min.: qt, op, ep, chl, sc
acc.:
- 178 87-85 unit: PPms
name: sillimanite garnet mica schist
maj.: qt, fs
min.: bi, mu, gt, op, sil₂, chl, sc
acc.:

- 179 87-86 unit: PPm
 name: banded calcite marble and garnet diopside hornblende calc
 silicate
 maj.: cc, hbl
 min.: fs, qt, gt, ep, cc, tr, di, chl, sc
 acc.:
- 180 87-88 unit: PPa
 name: sericitized feldspar amphibolite gneiss
 maj.: hbl, fs, sc
 min.: qt, bi, chl
 acc.:
- 181 87-90 unit: eJll
 name: pink orange weathering, coarsely crystalline granite
 maj.: qt, ks
 min.: pl, ep, cc, sc
 acc.:
- 182 87-91 unit: Trgk?
 name: dark green micaceous feldspar porphyry
 maj.: pl, qt
 min.: hbl, bi
 acc.:
- 183 87-92 unit: eJll
 name: orange weathering massive K-spar megacrystic biotite
 monzonite
 maj.: fs
 min.: bi, qt, op, sc
 acc.: zi, tt, ap
- 184 87-93 unit: Trgk
 name: augite porphyritic volcanic breccia
 maj.: ag, pl
 min.: hbl, ep
 acc.:
- 185 87-94 unit: Trgk
 name: hornblende feldspar andesite breccia
 maj.: ag, pl
 min.: hbl, chl, op
 acc.:

- 186 87-95 unit: Trgk
 name: heavily altered dark green andesite
 maj.: pl, ag
 min.: hbl, ep
 acc.:
- 187 87-96 unit: Trgk
 name: pl, ag
 maj.: hbl
 min.:
 acc.:
- 188 87-97 unit: eJll
 name: orange weathering massive K-spar megacrystic biotite quartz
 monzonite
 maj.: fs, qt
 min.: bi, op, sc
 acc.: zi, tt, ap
- 189 87-98 unit: Trgk
 name: dark green andesite
 maj.: pl, ag
 min.: hbl
 acc.:
- 190 87-99 unit: Trgk
 name: dark green andesite
 maj.: pl, ag
 min.: hbl
 acc.:
- 191 87-100 unit: PPa
 name: biotite amphibolite gneiss
 maj.: hbl, fs, qt
 min.: bi, cc, sc
 acc.: tt, ap
- 192 87-101 unit:
 name: finely crystalline white to grey biotite hornblende granite
 maj.: qt, pl, ks
 min.: bi, hbl, op, chl
 acc.: ap
- 193 87-102 unit: PPa

- name: garnet biotite hornblende amphibolite
 maj.: hbl, fs
 min.: qt, bi, op, gt, chl, sc
 acc.:
- 194 87-103 unit: PPa
 name: feldspar augan hornblende amphibolite
 maj.: hlb, fs
 min.: qt, op, chl, sc
 acc.:
- 195 87-104 unit: PPms
 name: sillimanite garnet mica schist
 maj.: qt, mu
 min.: bi, fs, op, sil₄, chl, sc
 acc.: tt, zi to
- 196 87-105 unit: PPM
 name: brown weathering diopside marble breccia
 maj.: cc
 min.: di, op, ep, chl
 acc.:
- 197 87-106 unit: PPM
 name: diopside marble
 maj.: cc, di
 min.: ph, fs, qt, op, ep, tr, sc
 acc.: tt, ap
- 198 87-107 unit: eJab
 name: foliated to gneissic biotite hornblende granodiorite to
 hornblende quartz diorite
 maj.: hbl, fs, qt
 min.: bi, op, chl, sc
 acc.: zi, tt, ap,
- 199 87-108 unit: eJab
 name: foliated to gneissic biotite hornblende granodiorite to
 hornblende quartz diorite
 maj.: hbl, fs, qt
 min.: bi, op, sc
 acc.: zi, tt, ap,
- 200 87-109 unit: eJab

- name: foliated to gneissic biotite hornblende granodiorite to
hornblende quartz diorite
maj.: hbl, fs, qt
min.: bi, op, chl, sc, cc
acc.: zi, tt, ap,
- 201 87-110 unit: eJll
name: orange weathering massive feldspar porphyritic quartz
monzonite
maj.: pl₍₉₎, ks, qt
min.: op, bi, sc
acc.: zi, tt, ap
- 202 87-111 unit: eJll
name: orange weathering massive feldspar porphyritic quartz
monzonite
maj.: fs, qt
min.: op, sc
acc.: zi, tt, ap
- 203 87-112 unit: eJll
name: orange weathering massive feldspar porphyritic quartz
monzonite
maj.: fs, qt
min.: op, bi, sc
acc.: zi, tt, ap
- 204 87-113 unit: eJll
name: orange weathering massive feldspar porphyritic quartz
monzonite
maj.: fs, qt
min.: op, bi, sc
acc.: zi, tt, ap
- 205 87-114 unit: PPa
name: leucocratic micaceous augan mylonite
maj.: qt, fs
min.: bi, mu, op, chl, sc
acc.:
- 206 87-115 unit: PPM
name: mylonitized calcite marble
maj.: cc
min.: qt

THE UNIVERSITY OF CHICAGO
DIVISION OF THE PHYSICAL SCIENCES
DEPARTMENT OF CHEMISTRY
530 SOUTH EAST ASIAN AVENUE
CHICAGO, ILLINOIS 60607

RECEIVED
JAN 10 1964
FROM
J. H. DUNN
TO
J. H. DUNN

RECEIVED
JAN 10 1964
FROM
J. H. DUNN
TO
J. H. DUNN

RECEIVED
JAN 10 1964
FROM
J. H. DUNN
TO
J. H. DUNN

RECEIVED
JAN 10 1964
FROM
J. H. DUNN
TO
J. H. DUNN

RECEIVED
JAN 10 1964
FROM
J. H. DUNN
TO
J. H. DUNN

RECEIVED
JAN 10 1964
FROM
J. H. DUNN
TO
J. H. DUNN

acc.:

- 207 87-116 unit: PPa
 name: biotite hornblende blastomylonite
 maj.: hbl, fs, qt
 min.: bi, op, ep, cc, chl, sc
 acc.: tt, ap
- 208 87-117 unit: PPms
 name: brown graphitic quartzite
 maj.: qt
 min.: bi_{1,2}, fs, op
 acc.:
- 209 87-118 unit: PPms
 name: micaceous brown graphitic quartzite
 maj.: qt
 min.: bi, fs, qp, mu, chl, sc
 acc.:
- 210 87-119 unit: PPms
 name: sericitized and altered mica schist
 maj.: qt, sc
 min.: bi, fs, chl
 acc.: to
- 211 87-120 unit: Tfp
 name: flesh colored quartz feldspar porphyry
 maj.: qt, fs
 min.: sc
 acc.:
- 212 87-121 unit: PPms
 name: quartzose staurolite mica schist
 maj.: qt
 min.: bi, fs, op, st, chl, sc
 acc.:
- 213 87-122 unit: PPms
 name: crenulated sillimanite staurolite kyanite garnet mica schist
 maj.: bi, mu, qt
 min.: fs, op, gt, st, sil₄, ky, chl, sc
 acc.: zi, to

Name		Address		City	
Mr. J. H. Smith		123 Main St.		New York	
Mrs. A. B. Jones		456 Elm St.		Chicago	
Mr. C. D. Brown		789 Oak St.		Los Angeles	
Mrs. E. F. Green		101 Pine St.		San Francisco	
Mr. G. H. White		202 Cedar St.		Boston	
Mrs. I. J. Black		303 Birch St.		Philadelphia	
Mr. K. L. Gray		404 Spruce St.		Portland	
Mrs. M. N. Hall		505 Willow St.		Seattle	
Mr. O. P. Young		606 Ash St.		Denver	
Mrs. Q. R. King		707 Hickory St.		Nashville	
Mr. S. T. Lee		808 Sycamore St.		Indianapolis	
Mrs. U. V. Scott		909 Magnolia St.		Columbus	
Mr. W. X. Adams		1010 Dogwood St.		Savannah	
Mrs. Y. Z. Baker		1111 Redwood St.		San Jose	
Mr. A. B. Carter		1212 Cypress St.		Fresno	
Mrs. C. D. Evans		1313 Juniper St.		Sacramento	
Mr. E. F. Harris		1414 Fir St.		Stockton	
Mrs. G. H. Clark		1515 Laurel St.		Modesto	
Mr. I. J. Lewis		1616 Alder St.		Yuba City	
Mrs. K. L. Walker		1717 Hawthorn St.		Wichita	
Mr. M. N. Hall		1818 Boxwood St.		Topeka	
Mrs. O. P. Young		1919 Yew St.		Lawrence	
Mr. Q. R. King		2020 Rose St.		Haskell	
Mrs. S. T. Lee		2121 Violet St.		Tulsa	
Mr. U. V. Scott		2222 Iris St.		Oklahoma City	
Mrs. W. X. Adams		2323 Pansy St.		Norman	
Mr. Y. Z. Baker		2424 Dandelion St.		Edmond	
Mrs. A. B. Carter		2525 Poppy St.		Muskogee	
Mr. C. D. Evans		2626 Sunflower St.		Ada	
Mrs. E. F. Harris		2727 Zinnia St.		Bartlesville	
Mr. G. H. Clark		2828 Marigold St.		Pawnee	
Mrs. I. J. Lewis		2929 Begonia St.		Lawton	
Mr. K. L. Walker		3030 Petunia St.		Muskogee	
Mrs. M. N. Hall		3131 Geranium St.		Tulsa	
Mr. O. P. Young		3232 Fuchsia St.		Oklahoma City	
Mrs. Q. R. King		3333 Camellia St.		Norman	
Mr. S. T. Lee		3434 Hibiscus St.		Edmond	
Mrs. U. V. Scott		3535 Narcissus St.		Muskogee	
Mr. W. X. Adams		3636 Tulip St.		Bartlesville	
Mrs. Y. Z. Baker		3737 Daffodil St.		Pawnee	
Mr. A. B. Carter		3838 Crocus St.		Lawton	
Mrs. C. D. Evans		3939 Hyacinth St.		Muskogee	
Mr. E. F. Harris		4040 Iris St.		Tulsa	
Mrs. G. H. Clark		4141 Pansy St.		Oklahoma City	
Mr. I. J. Lewis		4242 Dandelion St.		Norman	
Mrs. K. L. Walker		4343 Sunflower St.		Edmond	
Mr. M. N. Hall		4444 Zinnia St.		Muskogee	
Mrs. O. P. Young		4545 Marigold St.		Bartlesville	
Mr. Q. R. King		4646 Begonia St.		Pawnee	
Mrs. S. T. Lee		4747 Petunia St.		Lawton	
Mr. U. V. Scott		4848 Geranium St.		Muskogee	
Mrs. W. X. Adams		4949 Fuchsia St.		Tulsa	
Mr. Y. Z. Baker		5050 Camellia St.		Oklahoma City	
Mrs. A. B. Carter		5151 Hibiscus St.		Norman	
Mr. C. D. Evans		5252 Narcissus St.		Edmond	
Mrs. E. F. Harris		5353 Tulip St.		Muskogee	
Mr. G. H. Clark		5454 Daffodil St.		Bartlesville	
Mrs. I. J. Lewis		5555 Crocus St.		Pawnee	
Mr. K. L. Walker		5656 Hyacinth St.		Lawton	
Mrs. M. N. Hall		5757 Iris St.		Muskogee	
Mr. O. P. Young		5858 Pansy St.		Tulsa	
Mrs. Q. R. King		5959 Dandelion St.		Oklahoma City	
Mr. S. T. Lee		6060 Sunflower St.		Norman	
Mrs. U. V. Scott		6161 Zinnia St.		Edmond	
Mr. W. X. Adams		6262 Marigold St.		Muskogee	
Mrs. Y. Z. Baker		6363 Begonia St.		Bartlesville	
Mr. A. B. Carter		6464 Petunia St.		Pawnee	
Mrs. C. D. Evans		6565 Geranium St.		Lawton	
Mr. E. F. Harris		6666 Fuchsia St.		Muskogee	
Mrs. G. H. Clark		6767 Camellia St.		Tulsa	
Mr. I. J. Lewis		6868 Hibiscus St.		Oklahoma City	
Mrs. K. L. Walker		6969 Narcissus St.		Norman	
Mr. M. N. Hall		7070 Tulip St.		Edmond	
Mrs. O. P. Young		7171 Daffodil St.		Muskogee	
Mr. Q. R. King		7272 Crocus St.		Bartlesville	
Mrs. S. T. Lee		7373 Hyacinth St.		Pawnee	
Mr. U. V. Scott		7474 Iris St.		Lawton	
Mrs. W. X. Adams		7575 Pansy St.		Muskogee	
Mr. Y. Z. Baker		7676 Dandelion St.		Tulsa	
Mrs. A. B. Carter		7777 Sunflower St.		Oklahoma City	
Mr. C. D. Evans		7878 Zinnia St.		Norman	
Mrs. E. F. Harris		7979 Marigold St.		Edmond	
Mr. G. H. Clark		8080 Begonia St.		Muskogee	
Mrs. I. J. Lewis		8181 Petunia St.		Bartlesville	
Mr. K. L. Walker		8282 Geranium St.		Pawnee	
Mrs. M. N. Hall		8383 Fuchsia St.		Lawton	
Mr. O. P. Young		8484 Camellia St.		Muskogee	
Mrs. Q. R. King		8585 Hibiscus St.		Tulsa	
Mr. S. T. Lee		8686 Narcissus St.		Oklahoma City	
Mrs. U. V. Scott		8787 Tulip St.		Norman	
Mr. W. X. Adams		8888 Daffodil St.		Edmond	
Mrs. Y. Z. Baker		8989 Crocus St.		Muskogee	
Mr. A. B. Carter		9090 Hyacinth St.		Bartlesville	
Mrs. C. D. Evans		9191 Iris St.		Pawnee	
Mr. E. F. Harris		9292 Pansy St.		Lawton	
Mrs. G. H. Clark		9393 Dandelion St.		Muskogee	
Mr. I. J. Lewis		9494 Sunflower St.		Tulsa	
Mrs. K. L. Walker		9595 Zinnia St.		Oklahoma City	
Mr. M. N. Hall		9696 Marigold St.		Norman	
Mrs. O. P. Young		9797 Begonia St.		Edmond	
Mr. Q. R. King		9898 Petunia St.		Muskogee	
Mrs. S. T. Lee		9999 Geranium St.		Bartlesville	

a - sample id refers to the number that was assigned to a sample when it was collected in the field. The id indicates the year the sample was collected, followed by a sequential number (e.g. 86-33 - the 33rd sample collected in 1986)

b - unit monikers are the same as those used on all maps and are defined in the text.

c - maj., min., acc.; major, minor, and accessory mineral constituents, respectively, of a sample.



APPENDIX 3.1

Geochronological Methods

Whole rock samples of between 15 and 30 kg were collected for the extraction of zircon and titanite separates. Sample locations are shown in Figure 3.1. Sample preparation followed Baadsgaard and Lerbeckmo (1983). Standard mineral separation techniques, including the use of a Wilfley table, a Frantz magnetic separator, and heavy liquids (ethylene-tetrabromide and methylene-iodide), were used to prepare zircon and titanite separates. Zircon separates were then acid washed, first by boiling in 7 N HNO₃ at 350 °C for 1 to 2 hours, and secondly by boiling in 12 N HCl at 275 °C for one hour. Finally, zircon separates were boiled in twice distilled 6 N HCl at 300 °C for one hour. Zircon separates processed at the GSC geochronology laboratory in Ottawa were strongly abraded prior to analysis (Krogh, 1982) to minimize the effects of Pb - loss related to surface weathering.

Samples analyzed at the University of Alberta were decomposed by heating in a Teflon bomb with an HF and HNO₃ solution (approximately 12:1 ratio) for 3 to 6 days at a temperature of 170 °C. The resulting solution was evaporated and the precipitate dissolved in 1 ml of 6 N HNO₃. To determine Pb and U concentrations a mixed ²⁰⁸Pb - ²³⁵U spike was added to the samples. In four of the samples (samples 2 - 5; Table 3.1; Appendix 3.2) Pb was separated out of solution by co-precipitation with Pb-free Ba(NO₃)₂ and was purified using a Dowex 1-X8 anion exchange resin in chloride form. Pb from the remaining samples was purified using an anion exchange column in chloride form. U from all samples was separated from solution using a cation exchange column in nitrate form. The Pb and U eluates were then evaporated. For mass spectrometric analysis, the Pb precipitate was taken up in phosphoric acid and was loaded on a silica gel substrate on single Re filaments. The U precipitate was taken up in nitric acid and loaded directly onto the side filament of a double Re filament. Pb and U were analyzed by conventional mass spectrometry using either a Micromass 30 or VG - 354 mass spectrometer. A Pb blank of less than 1.0 ng and a U blank of less than 0.4 ng was determined using repeated blank measurements. Accurate error analysis for bulk zircon separates, which are characterized by high and variable Pb blanks, is difficult, especially for ²⁰⁷Pb/²⁰⁶Pb. The values used here are provided by replicate analyses (n=11) of concordant Campanian zircon from a bentonite horizon (Baadsgaard and Lerbeckmo, 1983); at the one sigma level (1σ) they are: ²⁰⁶Pb/²³⁸U - .61%; ²⁰⁷Pb/²³⁵U - 1.00%; ²⁰⁷Pb/²⁰⁶Pb- 2.34%.

Zircon fractions A to E of the Nisling Assemblage orthogneiss, D to G of the Aishihik Batholith, and A to G of the pink quartz monzonite suite were analyzed at the GSC Geochronology Laboratory in Ottawa. Two titanite separates (fractions I and J, sample 86 - 82, Aishihik Batholith) were also analyzed at the GSC laboratory. Preparation techniques and analytical procedures have been described in Parrish et al. (1987). Measured blank levels were 0.016 to 0.043 ng for Pb, and less than 1 pg for U. Isotopic measurements were done on a Finnegan MAT 261 solid source mass spectrometer equipped with a fully adjustable multiple collector, electron multiplier, and operating software modified to permit simultaneous measurement of all five Pb masses.

All ages were calculated using the constants recommended by Steiger and Jager (1977). A numerical error propagation technique was used to calculate errors associated with individual analyses (Roddick, 1987). Discordia line fitting and calculation of concordia intercept ages and associated errors employed a modified York-II regression model (Parrish et al., 1987), and the algorithm of Ludwig (1980). All errors are quoted at the 2 σ level. Age assignments follow Harland *et al.* (1989)

APPENDIX 3.2

Locations of samples collected for geochronological study

SAMPLE no.	id	EASTING (m)	NORTHING (m)	LONGITUDE	LATITUDE	ELEV (masl)	UNIT
UTM grid zone - 8V							
<u>Nisling Assemblage two mica orthogneiss</u>							
1)	86-74	384052	6818033	61°28'49.5"N	137°10'36.9"W	914	PPo
<u>Aishihik Batholith - Foliated hornblende granodiorite</u>							
2)	86-82	376329	6826868	61°33'26.2"N	137°19'39.8"W	914	eJab
<u>Long Lake Suite - Pink Quartz Monzonite</u>							
3)	87-92	432693	6841067	61°41'55.2"N	136°16'21.0"W	777	eJll
<u>Ruby Range Batholith</u>							
4)	86-79	392783	6786205	61°11'50.6"N	136°59'41.6"W	922	KTr
5)	87-40	388278	6765137	61°00'25.6"N	137°03'58.5"W	762	KTr
6)	87-42	392422	6773358	61°04'55.3"N	136°59'39.5"W	914	KTr
7)	87-70	389889	6800302	61°19'23.0"N	137°03'25.0"W	968	KTr
8)	87-82	392945	6778026	61°07'26.6"N	136°59'14.1"W	1066	KTr
9)	87-83	393292	6775798	61°06'14.9"N	136°58'46.4"W	1036	KTr

1. Introduction

The purpose of this study is to investigate the effects of various factors on the growth of plants.

Methodology

Results

Conclusion

References

Appendix A: Data Collection

Appendix B: Statistical Analysis

Appendix C: Plant Growth Data

Appendix D: Soil Analysis

Appendix E: Water Analysis

Appendix F: Light Analysis

Appendix G: Temperature Analysis

Appendix H: Humidity Analysis

Appendix I: Nutrient Analysis

Appendix J: pH Analysis

Appendix K: Oxygen Analysis

Appendix L: Carbon Dioxide Analysis

Appendix M: Nitrogen Analysis

Appendix N: Phosphorus Analysis

Appendix O: Potassium Analysis

Appendix P: Magnesium Analysis

Appendix Q: Calcium Analysis

Appendix R: Sulfur Analysis

Appendix S: Zinc Analysis

Appendix T: Copper Analysis

Appendix U: Manganese Analysis

Appendix V: Iron Analysis

Appendix W: Boron Analysis

Appendix X: Chlorine Analysis

- 5) 87-40 unit: KTrr
 name: finely crystalline hornblende biotite granodiorite
 maj.: bi, fs, qt
 min.: hbl, op, sc
 acc.: zi, tt, ap
- 6) 87-42 unit: KTrr
 name: nebulitic biotite granite with minor mafic biotite rich
 enclaves
 maj.: bi, fs, qt
 min.: sc
 acc.: zi, tt, ap
- 7) 87-70 unit: KTrr
 name: hornblende granodiorite with mafic enclaves
 maj.: hbl, fs, qt
 min.: op, chl, sc
 acc.: zi, tt, ap
- 8) 87-82 unit: KTrr
 name: hornblende granodiorite
 maj.: hbl, fs, qt
 min.: op, bi
 acc.: zi, tt, ap
- 9) 87-83 unit: KTrr
 name: hornblende granodiorite
 maj.: hbl, fs, qt
 min.: op, bi
 acc.: zi, tt, ap

a - sample id refers to the number that was assigned to a sample when it was collected in the field. The id indicates the year the sample was collected, followed by a sequential number (e.g. 86-33 - the 33rd sample collected in 1986)

b - unit monikers are the same as those used on all maps and are defined in the text.

c - maj., min., acc.; major, minor, and accessory mineral constituents, respectively, of a sample.

APPENDIX 4.1

TRIPOD

TRIPOD (Charlesworth *et al.*, 1988) is a computer program designed for the analysis and display of drillhole, outcrop and seismic data from deformed sedimentary terrains. TRIPOD has three main functions. These are:

- i) to create databases using structural, stratigraphic and positional data from drillholes, outcrops and seismic sections, entered at the keyboard or imported as data files. Drillhole data can include deviation, intersection and dip-meter readings. Outcrop data can include coordinates, the exposed stratigraphic horizon, and the orientation of up to ten kinds of planar and linear structures (per outcrop).
- ii) to retrieve data from a database according to geographic position, stratigraphic horizon, structural unit, structural type, etc.
- iii) to display and analyze retrieved data. Orientations can be used, for example, to prepare contoured pi diagrams and rose diagrams and to calculate orientation parameters. Data can be displayed on maps. They can also be used to establish domains in which folding can be considered cylindrical, and to construct plots showing drillhole, outcrop and seismic data projected parallel to fold axes onto planes of any orientation and position. These plots can then be used to draw cross-sections. Data can be rotated before being processed which enables composite plots from areas with several cylindrically folded domains to be produced.

To use TRIPOD you begin with a Database Manager which enables you to create and edit a database and select which database is to be used. A Job Selector enables you to choose the way in which you want to display or analyze data. During a "worksession" you specify, by means of a Job Utility, what data are to be retrieved and how they are to be displayed and analyzed. The way you operate this Utility can be stored in a worksession record. The Worksession Manager enables you to create, copy and delete such records. A more complete description of the TRIPOD program is presented in Charlesworth *et al.* (1988).

The first part of the paper is devoted to a general discussion of the problem of the origin of life. It is shown that the problem is not only a scientific one, but also a philosophical one. The second part of the paper is devoted to a detailed discussion of the problem of the origin of life. It is shown that the problem is not only a scientific one, but also a philosophical one. The third part of the paper is devoted to a detailed discussion of the problem of the origin of life. It is shown that the problem is not only a scientific one, but also a philosophical one. The fourth part of the paper is devoted to a detailed discussion of the problem of the origin of life. It is shown that the problem is not only a scientific one, but also a philosophical one. The fifth part of the paper is devoted to a detailed discussion of the problem of the origin of life. It is shown that the problem is not only a scientific one, but also a philosophical one. The sixth part of the paper is devoted to a detailed discussion of the problem of the origin of life. It is shown that the problem is not only a scientific one, but also a philosophical one. The seventh part of the paper is devoted to a detailed discussion of the problem of the origin of life. It is shown that the problem is not only a scientific one, but also a philosophical one. The eighth part of the paper is devoted to a detailed discussion of the problem of the origin of life. It is shown that the problem is not only a scientific one, but also a philosophical one. The ninth part of the paper is devoted to a detailed discussion of the problem of the origin of life. It is shown that the problem is not only a scientific one, but also a philosophical one. The tenth part of the paper is devoted to a detailed discussion of the problem of the origin of life. It is shown that the problem is not only a scientific one, but also a philosophical one.

APPENDIX 5.1

Locations of Nisling Assemblage samples

SAMPLE no.	id	EASTING (m)	NORTHING (m)	LONGITUDE	LATITUDE	ELEV (masl)	UNIT
UTM grid zone - 8V							
1	85-9	395953	6806322	61°22'43.4"N	136°56'49.5"W	1234	Ppm
2	85-10	395349	6805542	61°22'17.7"N	136°57'28.6"W	1203	Ppo
3	85-11	395168	6805458	61°22'14.8"N	136°57'40.6"W	1188	Ppo
4	85-13	393551	6788195	61°12'55.6"N	136°58'54.2"W	917	Ppms
5	85-14	393438	6788454	61°13'03.9"N	136°59'02.3"W	917	Ppms
6	85-15	393364	6789172	61°13'27.0"N	136°59'08.7"W	917	Ppms
7	85-16	393418	6789694	61°13'43.9"N	136°59'06.1"W	917	Ppm
8	85-17	393364	6791063	61°14'28.1"N	136°59'12.5"W	917	Ppms
9	86-2	391830	6784551	61°10'56.2"N	137°00'41.9"W	1097	Ppms
10	86-3	397506	6798053	61°18'17.8"N	136°54'48.6"W	1295	Ppm
11	86-4	391081	6786401	61°11'55.2"N	137°01'35.9"W	1204	Ppha
12	86-16	391175	6813180	61°26'20.2"N	137°02'25.6"W	1059	Ppo
13	86-17	390560	6813110	61°26'17.3"N	137°03'06.9"W	1052	Ppo
14	86-24	378843	6822707	61°31'14.7"N	137°16'39.7"W	975	Ppo
15	86-30	378434	6822862	61°31'19.2"N	137°17'07.8"W	968	Ppo
16	86-31	378622	6822602	61°31'11.0"N	137°16'54.4"W	960	Ppo
17	86-36	383487	6818782	61°29'13.1"N	137°11'16.8"W	922	Ppo

18	86-38	383448	6818811	61°29'14.0"N	137°11'19.5"W	922	Ppo
19	86-39	383448	6818811	61°29'14.0"N	137°11'19.5"W	922	Ppo
20	86-40	383545	6818646	61°29'08.7"N	137°11'12.6"W	922	Ppo
21	86-41	383545	6818646	61°29'08.7"N	137°11'12.6"W	922	Ppo
22	86-42	393963	6805012	61°21'59.2"N	136°59'00.8"W	1059	Ppms
23	86-43	394594	6806180	61°22'37.5"N	136°58'20.7"W	1181	Ppo
24	86-46	397438	6804735	61°21'53.6"N	136°55'06.4"W	1311	Ppqtz
25	86-48	398075	6804303	61°21'40.2"N	136°54'22.7"W	1562	Ppo
26	86-52	398314	6849368	61°45'56.0"N	136°55'36.3"W	1402	Ppms
27	86-53	398460	6849473	61°45'59.5"N	136°55'26.6"W	1402	Ppms
28	86-54	400617	6848820	61°45'40.5"N	136°52'58.2"W	1425	Ppms
29	86-56	399272	6845466	61°43'50.9"N	136°54'23.2"W	1433	Ppa
30	86-57	399623	6845349	61°43'47.5"N	136°53'59.1"W	1425	Ppa
31	86-58	399516	6845355	61°43'47.5"N	136°54'06.4"W	1440	Ppa
32	86-60	393500	6857250	61°50'05.9"N	137°01'21.2"W	1227	Ppa
33	86-61	397922	6855329	61°49'08.2"N	136°56'15.1"W	1219	Ppms
34	86-63	397855	6852328	61°47'31.2"N	136°56'13.6"W	1288	Ppm
35	86-64	397363	6851898	61°47'16.8"N	136°56'46.3"W	1314	Ppa
36	86-65	397363	6851898	61°47'16.8"N	136°56'46.3"W	1314	Ppa
37	86-74	384052	6818033	61°28'49.5"N	137°10'36.9"W	914	Ppo
38	86-75	391650	6784348	61°10'49.5"N	137°00'53.6"W	1219	Ppms
39	86-76	391410	6784425	61°10'51.7"N	137°01'09.8"W	1249	Ppms
40	86-84	397775	6803837	61°21'24.9"N	136°54'41.9"W	1532	Ppa
41	87-1	393339	6787829	61°12'43.6"N	136°59'07.6"W	975	Ppms
42	87-2	393385	6787692	61°12'39.2"N	136°59'04.3"W	983	Ppms
43	87-5	393941	6787519	61°12'34.2"N	136°58'26.7"W	1021	Ppms
44	87-7	393481	6788688	61°13'11.5"N	136°58'59.9"W	983	Ppms
45	87-8	393481	6788688	61°13'11.5"N	136°58'59.9"W	983	Ppa

46	87-9	393511	6788810	61°13'15.4"N	136°58'58.1"W	975	Ppms
47	87-10	395327	6792516	61°15'16.9"N	136°57'03.9"W	991	Ppms
48	87-11	394693	6792384	61°15'12.0"N	136°57'46.1"W	1006	Ppms
49	87-12	394693	6792384	61°15'12.0"N	136°57'46.1"W	1006	Ppm
50	87-13	395261	6793073	61°15'34.8"N	136°57'09.4"W	1006	Ppa
51	87-14	397661	6791312	61°14'40.2"N	136°54'25.0"W	1067	Ppa
52	87-15	397987	6791083	61°14'33.1"N	136°54'02.7"W	1219	Ppa
53	87-16	397987	6791083	61°14'33.1"N	136°54'02.7"W	1219	Ppa
54	87-18	398437	6791264	61°14'39.4"N	136°53'32.9"W	1234	Ppm
55	87-19	399128	6793184	61°15'42.1"N	136°52'50.3"W	1387	Ppms
56	87-21	398300	6792000	61°15'03.1"N	136°53'43.5"W	1181	Ppms
57	87-22	397140	6793906	61°16'03.5"N	136°55'05.0"W	1052	Ppm
58	87-23	397592	6794468	61°16'22.1"N	136°54'35.8"W	1189	Ppms
59	87-24	397369	6795560	61°16'57.2"N	136°54'52.9"W	1303	Ppm
60	87-26	397188	6797678	61°18'05.4"N	136°55'09.3"W	1341	Ppm
61	87-27	393282	6789389	61°13'33.9"N	136°59'14.6"W	922	Ppms
62	87-28	393289	6789335	61°13'32.2"N	136°59'14.1"W	922	Ppms
63	87-29	393357	6789023	61°13'22.2"N	136°59'08.9"W	922	Ppm
64	87-30	393280	6790736	61°14'17.4"N	136°59'17.5"W	922	Ppms
65	87-31	393280	6790668	61°14'15.2"N	136°59'17.4"W	922	Ppm
66	87-33	392927	6790068	61°13'55.5"N	136°59'39.8"W	922	Ppa
67	87-34	393002	6789869	61°13'49.1"N	136°59'34.4"W	922	Ppms
68	87-37	393439	6796226	61°17'14.9"N	136°59'18.1"W	1158	Ppms
69	87-38	393563	6796375	61°17'19.8"N	136°59'10.0"W	1158	Ppa
70	87-39	394802	6795493	61°16'52.5"N	136°57'45.1"W	1219	Ppm
71	87-43	394569	6804046	72°26'19.7"N	138°07'54.4"W	1120	PPo
72	87-44	395106	6804739	61°21'51.5"N	136°57'43.3"W	1204	Ppo
73	87-45	395452	6805442	61°22'14.5"N	136°57'21.5"W	1273	Ppo
74	87-46	395328	6805530	61°22'17.2"N	136°57'30.0"W	1295	Ppms
75	87-47	395359	6805508	61°22'16.6"N	136°57'27.9"W	1295	Ppms

1840-1841 (1840-1841)

1841-1842 (1841-1842)

1842-1843 (1842-1843)

1843-1844 (1843-1844)

1844-1845 (1844-1845)

1845-1846 (1845-1846)

1846-1847 (1846-1847)

1847-1848 (1847-1848)

1848-1849 (1848-1849)

1849-1850 (1849-1850)

76	87-50	394902	6804413	72°28'18.5"N	138°07'39.3"W	1196	Ppms
77	87-51	395104	6805639	61°22'20.5"N	136°57'45.3"W	1219	Ppms
78	87-52	391289	6793934	61°15'58.7"N	137°01'37.6"W	1029	Ppms
79	87-53	391859	6793898	61°15'58.1"N	137°00'59.3"W	1036	Ppms
80	87-54	392877	6794601	61°16'21.8"N	136°59'52.4"W	1151	Ppms
81	87-55	393007	6795100	61°16'38.1"N	136°59'44.7"W	1196	Ppms
82	87-56	392951	6795322	61°16'45.2"N	136°59'49.0"W	1196	Ppa
83	87-57	392140	6794625	61°16'21.9"N	137°00'41.9"W	1097	Ppms
84	87-58	390970	6795435	61°16'46.9"N	137°02'02.1"W	945	Ppms
85	87-59	391465	6795536	61°16'50.6"N	137°01'29.1"W	975	Ppm
86	87-60	391662	6795458	61°16'48.3"N	137°01'15.7"W	1006	Ppms
87	87-62	392688	6796253	61°17'15.0"N	137°00'08.5"W	1219	Ppms
88	87-63	391787	6796528	61°17'23.0"N	137°01'09.6"W	1143	Ppm
89	87-64	391178	6796421	61°17'18.9"N	137°01'50.2"W	1021	Ppms
90	87-65	391147	6796368	61°17'17.2"N	137°01'52.2"W	1029	Ppms
91	87-66	390315	6799690	61°19'03.7"N	137°02'55.0"W	991	Ppms
92	87-67	390789	6799245	61°18'49.8"N	137°02'22.3"W	1021	Ppm
93	87-68	391580	6799457	61°18'57.4"N	137°01'29.6"W	1166	Ppms
94	87-69	391112	6800403	61°19'27.5"N	137°02'03.0"W	1082	Ppm
95	87-72	392319	6784989	61°11'10.8"N	137°00'10.1"W	945	Ppm
96	87-73	392347	6784874	61°11'07.2"N	137°00'08.0"W	975	Ppms
97	87-74	392377	6784539	61°10'56.4"N	137°00'05.3"W	1067	Ppms
98	87-75	392064	6784166	61°10'44.0"N	137°00'25.5"W	1143	Ppms
99	87-76	391442	6784530	61°10'55.1"N	137°01'07.8"W	1257	Ppms
100	87-77	391207	6784915	61°11'07.3"N	137°01'24.4"W	1250	Ppm
101	87-78	391395	6785139	61°11'14.8"N	137°01'12.2"W	1189	Ppms
102	87-80	385538	6817623	61°28'37.9"N	137°08'55.7"W	975	Ppms
103	87-84	396952	6803014	61°20'57.5"N	136°55'35.7"W	1280	Ppa
104	87-85	397552	6803092	61°21'00.6"N	136°54'55.5"W	1334	Ppms
105	87-86	397639	6803254	61°21'05.9"N	136°54'49.9"W	1417	Ppm



106	87-88	398029	6804301	61°21'40.1"N	136°54'25.8"W	1570	Ppa
107	87-100	393243	6845769	61°43'54.8"N	137°01'14.3"W	1394	Ppa
108	87-102	393670	6845497	61°43'46.5"N	137°00'44.7"W	1341	Ppa
109	87-103	393670	6845497	61°43'46.5"N	137°00'44.7"W	1341	Ppa
110	87-104	395537	6844285	61°43'09.2"N	136°58'35.1"W	1349	Ppms
111	87-105	395979	6844199	61°43'06.8"N	136°58'04.8"W	1173	Ppm
112	87-106	396123	6844216	61°43'07.5"N	136°57'55.0"W	1143	Ppm
113	87-114	368565	6827037	61°33'22.4"N	137°28'25.7"W	1212	Ppa
114	87-115	368772	6826275	61°32'58.0"N	137°28'09.7"W	1227	Ppm
115	87-116	368892	6826153	61°32'54.3"N	137°28'01.3"W	1234	Ppa
116	87-117	368836	6825728	61°32'40.5"N	137°28'04.0"W	1219	Ppqtz
117	87-118	368873	6825674	61°32'38.8"N	137°28'01.4"W	1219	Ppqtz
118	87-119	368560	6824234	61°31'51.9"N	137°28'18.8"W	1371	Ppms
119	87-121	368320	6824014	61°31'44.5"N	137°28'34.5"W	1402	Ppms
120	87-122	366500	6824930	61°32'11.8"N	137°30'40.0"W	1420	Ppms

1844-1845

1846-1847

1848-1849

1850-1851

1852-1853

1854-1855

1856-1857

1858-1859

1860-1861

1862-1863

1864-1865

1866-1867

1868-1869

APPENDIX 5.2
NISLING ASSEMBLAGE SAMPLES:
MINERAL ASSEMBLAGES

Sample no.	field id ^a	Description
1	85-9	unit ^b : PPm name: coarsely crystalline banded fetid tremolite diopside marble maj. ^c : cc, di min.: tr, ep, qt, fs, sc, op acc.: tt
2	85-10	unit: PPog name: biotite augan granite orthogneiss maj.: qt, pl, ks min.: bi, chl, sc, cc, ga, op acc.: zi
3	85-11	unit: PPog name: biotite hornblende granite orthogneiss maj.: qt, pl, ks min.: hbl, bi, chl, op acc.: zi, ap
4	85-13	unit: PPms name: mica schist maj.: qt, bi _{1,2} , mu _{1,2} , fs min.: chl, sc, op acc.: zi, to, ap
5	85-14	unit: PPms name: andalusite staurolite mica schist maj.: qt, bi _{1,2} , mu _{1,2} , fs min.: and ₂ , st, op, chl, sc acc.: ap
6	85-15	unit: PPms name: quartzose sillimanite mica schist maj.: qt min.: bi _{1,2} , mu _{1,2} , sil ₄ , fs, op, chl, sc

THE UNIVERSITY OF CHICAGO
LIBRARY

Author		Title		Date	
A. B. C.		The ABC of the ABC		1910	
D. E. F.		The DEF of the DEF		1911	
G. H. I.		The GHI of the GHI		1912	
J. K. L.		The JKL of the JKL		1913	
M. N. O.		The MNO of the MNO		1914	
P. Q. R.		The PQR of the PQR		1915	
S. T. U.		The STU of the STU		1916	
V. W. X.		The VWX of the VWX		1917	
Y. Z. A.		The YZA of the YZA		1918	
B. C. D.		The BCD of the BCD		1919	
E. F. G.		The EFG of the EFG		1920	
H. I. J.		The HIJ of the HIJ		1921	
K. L. M.		The KLM of the KLM		1922	
N. O. P.		The NOP of the NOP		1923	
Q. R. S.		The QRS of the QRS		1924	
T. U. V.		The TUV of the TUV		1925	
W. X. Y.		The WXY of the WXY		1926	
Z. A. B.		The ZAB of the ZAB		1927	
C. D. E.		The CDE of the CDE		1928	
F. G. H.		The FGH of the FGH		1929	
I. J. K.		The IJK of the IJK		1930	
L. M. N.		The LMN of the LMN		1931	
O. P. Q.		The OPQ of the OPQ		1932	
R. S. T.		The RST of the RST		1933	
U. V. W.		The UVW of the UVW		1934	
X. Y. Z.		The XYZ of the XYZ		1935	
A. B. C.		The ABC of the ABC		1936	
D. E. F.		The DEF of the DEF		1937	
G. H. I.		The GHI of the GHI		1938	
J. K. L.		The JKL of the JKL		1939	
M. N. O.		The MNO of the MNO		1940	
P. Q. R.		The PQR of the PQR		1941	
S. T. U.		The STU of the STU		1942	
V. W. X.		The VWX of the VWX		1943	
Y. Z. A.		The YZA of the YZA		1944	
B. C. D.		The BCD of the BCD		1945	
E. F. G.		The EFG of the EFG		1946	
H. I. J.		The HIJ of the HIJ		1947	
K. L. M.		The KLM of the KLM		1948	
N. O. P.		The NOP of the NOP		1949	
Q. R. S.		The QRS of the QRS		1950	
T. U. V.		The TUV of the TUV		1951	
W. X. Y.		The WXY of the WXY		1952	
Z. A. B.		The ZAB of the ZAB		1953	
C. D. E.		The CDE of the CDE		1954	
F. G. H.		The FGH of the FGH		1955	
I. J. K.		The IJK of the IJK		1956	
L. M. N.		The LMN of the LMN		1957	
O. P. Q.		The OPQ of the OPQ		1958	
R. S. T.		The RST of the RST		1959	
U. V. W.		The UVW of the UVW		1960	
X. Y. Z.		The XYZ of the XYZ		1961	
A. B. C.		The ABC of the ABC		1962	
D. E. F.		The DEF of the DEF		1963	
G. H. I.		The GHI of the GHI		1964	
J. K. L.		The JKL of the JKL		1965	
M. N. O.		The MNO of the MNO		1966	
P. Q. R.		The PQR of the PQR		1967	
S. T. U.		The STU of the STU		1968	
V. W. X.		The VWX of the VWX		1969	
Y. Z. A.		The YZA of the YZA		1970	
B. C. D.		The BCD of the BCD		1971	
E. F. G.		The EFG of the EFG		1972	
H. I. J.		The HIJ of the HIJ		1973	
K. L. M.		The KLM of the KLM		1974	
N. O. P.		The NOP of the NOP		1975	
Q. R. S.		The QRS of the QRS		1976	
T. U. V.		The TUV of the TUV		1977	
W. X. Y.		The WXY of the WXY		1978	
Z. A. B.		The ZAB of the ZAB		1979	
C. D. E.		The CDE of the CDE		1980	
F. G. H.		The FGH of the FGH		1981	
I. J. K.		The IJK of the IJK		1982	
L. M. N.		The LMN of the LMN		1983	
O. P. Q.		The OPQ of the OPQ		1984	
R. S. T.		The RST of the RST		1985	
U. V. W.		The UVW of the UVW		1986	
X. Y. Z.		The XYZ of the XYZ		1987	
A. B. C.		The ABC of the ABC		1988	
D. E. F.		The DEF of the DEF		1989	
G. H. I.		The GHI of the GHI		1990	
J. K. L.		The JKL of the JKL		1991	
M. N. O.		The MNO of the MNO		1992	
P. Q. R.		The PQR of the PQR		1993	
S. T. U.		The STU of the STU		1994	
V. W. X.		The VWX of the VWX		1995	
Y. Z. A.		The YZA of the YZA		1996	
B. C. D.		The BCD of the BCD		1997	
E. F. G.		The EFG of the EFG		1998	
H. I. J.		The HIJ of the HIJ		1999	
K. L. M.		The KLM of the KLM		2000	
N. O. P.		The NOP of the NOP		2001	
Q. R. S.		The QRS of the QRS		2002	
T. U. V.		The TUV of the TUV		2003	
W. X. Y.		The WXY of the WXY		2004	
Z. A. B.		The ZAB of the ZAB		2005	
C. D. E.		The CDE of the CDE		2006	
F. G. H.		The FGH of the FGH		2007	
I. J. K.		The IJK of the IJK		2008	
L. M. N.		The LMN of the LMN		2009	
O. P. Q.		The OPQ of the OPQ		2010	
R. S. T.		The RST of the RST		2011	
U. V. W.		The UVW of the UVW		2012	
X. Y. Z.		The XYZ of the XYZ		2013	
A. B. C.		The ABC of the ABC		2014	
D. E. F.		The DEF of the DEF		2015	
G. H. I.		The GHI of the GHI		2016	
J. K. L.		The JKL of the JKL		2017	
M. N. O.		The MNO of the MNO		2018	
P. Q. R.		The PQR of the PQR		2019	
S. T. U.		The STU of the STU		2020	
V. W. X.		The VWX of the VWX		2021	
Y. Z. A.		The YZA of the YZA		2022	
B. C. D.		The BCD of the BCD		2023	
E. F. G.		The EFG of the EFG		2024	
H. I. J.		The HIJ of the HIJ		2025	
K. L. M.		The KLM of the KLM		2026	
N. O. P.		The NOP of the NOP		2027	
Q. R. S.		The QRS of the QRS		2028	
T. U. V.		The TUV of the TUV		2029	
W. X. Y.		The WXY of the WXY		2030	
Z. A. B.		The ZAB of the ZAB		2031	
C. D. E.		The CDE of the CDE		2032	
F. G. H.		The FGH of the FGH		2033	
I. J. K.		The IJK of the IJK		2034	
L. M. N.		The LMN of the LMN		2035	
O. P. Q.		The OPQ of the OPQ		2036	
R. S. T.		The RST of the RST		2037	
U. V. W.		The UVW of the UVW		2038	
X. Y. Z.		The XYZ of the XYZ		2039	
A. B. C.		The ABC of the ABC		2040	
D. E. F.		The DEF of the DEF		2041	
G. H. I.		The GHI of the GHI		2042	
J. K. L.		The JKL of the JKL		2043	
M. N. O.		The MNO of the MNO		2044	
P. Q. R.		The PQR of the PQR		2045	
S. T. U.		The STU of the STU		2046	
V. W. X.		The VWX of the VWX		2047	

- acc.: rt
- 7 85-16 unit: PPM
 name: chloritized diopside marble
 maj.: cc
 min.: di, chl, op
 acc.:
- 8 85-17 unit: PPms
 name: andalusite cordierite staurolite sillimanite mica schist
 maj.: qt
 min.: fs, bi₂, mu₂, op, ga, st, si₄, ad₂, cd₂, sc
 acc.: tt, zi
- 9 86-2 unit: PPms
 name: sillimanite andalusite mica schist
 maj.: qt, bi
 min.: mu, fs, op, ad₄, sil₄
 acc.:
- 10 86-3 unit: PPM
 name: garnet diopside magnetite skarn
 maj.: ga, di, mt
 min.:
 acc.:
- 11 86-4 unit: PPa
 name: chloritized amphibolite breccia hosted in leucocratic
 pegmatite
 maj.: hbl, chl, qt, fs
 min.:
 acc.:
- 12 86-16 unit: PPog
 name: biotite granite orthogneiss
 maj.: qt, fs
 min.: bi, op
 acc.: al, tt, to
- 13 86-17 unit: PPog
 name: biotite granite orthogneiss
 maj.: qt, fs
 min.: bi, op
 acc.: al, ap

- | | | |
|----|-------|---|
| 14 | 86-24 | unit: PPog(?) or PPbs
name: fine grained quartzo-feldspathic biotite schist / biotite granite orthogneiss
maj.: bi, qt, fs
min.:
acc.: ap |
| 15 | 86-30 | unit: PPog
name: biotite hornblende granite orthogneiss
maj.: qt, fs
min.: bi, hb, op, sc
acc.: al, ap |
| 16 | 86-31 | unit: PPog
name: hornblende granodiorite orthogneiss
maj.: hb, fs
min.: qt, bi, op, ep, cc, chl, sc
acc.: ap |
| 17 | 86-36 | unit: PPog
name: blastomylonitic feldspar augan gneiss
maj.: qt, fs
min.: bi, op, gt, mu, sc
acc.: ap |
| 18 | 86-38 | unit: PPog
name: blastomylonitic feldspar augan gneiss
maj.: qt, fs
min.: bi, op
acc.: al |
| 19 | 86-39 | unit: PPog
name: blastomylonitic feldspar augan gneiss
maj.: qt, fs
min.: bi, op, gt, mu
acc.: |
| 20 | 86-40 | unit: PPog
name: altered hornblende granodiorite orthogneiss
maj.: hbl, fs, ep, qt
min.: bi, op, chl
acc.: ap |

- 21 86-41 unit: PPog
 name: hornblende granodiorite orthogneiss
 maj.: hbl, fs, qt
 min.: bi, ep, cc, chl, sc
 acc.: zi, ap
- 22 86-42 unit: PPms
 name: migmatitic sillimanite garnet mica schist
 maj.: qt, bi₂
 min.: sil_{2,4}, fs, op, gt, mu, ep, chl, sc
 acc.: tt, to, ap
- 23 86-43 unit: PPog
 name: garnetiferous hornblende granodiorite orthogneiss
 maj.: fs, hbl, qt
 min.: bi, gt
 acc.:
- 24 86-46 unit: PPqtz
 name: finely banded orthoquartzite
 maj.: qt
 min.: fs, op, ap, sc
 acc.:
- 25 86-48 unit: PPog
 name: finely crystalline hornblende biotite granite orthogneiss
 maj.: qt, gs, hb, bi
 min.: op, ch, sc
 acc.:
- 26 86-52 unit: PPms
 name: micaceous quartzite
 maj.: qt
 min.: bi, fs, op, mu, chl, sc
 acc.: zi, to, ap
- 27 86-53 unit: PPms
 name: sillimanite mica schist
 maj.: bi, mu, qt
 min.: qt, fs, ga, op, sil₂, sc
 acc.: zi, ap
- 28 86-54 unit: PPms
 name: quartzose garnet mica schist

- min.: hbl, ep, cc
acc.: ap
- 36 86-65 unit: PPa
name: augite hornblende amphibolite
maj.: hbl, ag
min.: chl
acc.: tt, ap
- 37 86-74 unit: PPog
name: two mica banded augan granite orthogneiss
maj.: qt, fs
min.: bi, mu, gt, sc
acc.:
- 38 86-75 unit: PPms
name: sillimanite garnet mica schist
maj.: bi_{1,2}, mu_{1,2}, qt, fs
min.: gt, op, sil_{2,4}, chl, sc
acc.:
- 39 86-76 unit: PPms
name: quartzose garnet biotite schist
maj.: qt, fs
min.: bi, op, ga, chl, sc
acc.: zi, ap
- 40 86-84 unit: PPa
name: mafic biotite hornblende amphibolite
maj.: hbl, bi
min.: pl, op, ep, chl, sc
acc.: tt
- 41 87-1 unit: PPms
name: micaceous garnetiferous grey quartz gneiss
maj.: qt
min.: bi, fs, ga, op, chl
acc.: zi, ap
- 42 87-2 unit: PPms
name: migmatitic garnet biotite schist
maj.: qt, fs, bi_{1,2}
min.: ga, chl, sc
acc.: ap, al

- 43 87-5 unit: PPms
 name: andalusite biotite schist
 maj.: bi_{2,3}, fs, qt
 min.: op, ad₂, chl, sc
 acc.:
- 44 87-7 unit: PPms
 name: sillimanite (?) mica schist
 maj.: qt, fs, bi_{1,2}
 min.: mu_{1,2}, sil₄, chl, sc
 acc.: zi, to, ap, tt
- 45 87-8 unit: PPa
 name: hornblende amphibolite gneiss
 maj.: hbl
 min.: bi, pl, qt, ep, cc, chl, sc
 acc.: tt
- 46 87-9 unit: PPms
 name: migmatitic mica schist
 maj.: qt, fl
 min.: bi_{1,2}, mu_{1,2}, chl, sc
 acc.: zi, to
- 47 87-10 unit: PPms
 name: quartzose sillimanite garnet mica schist
 maj.: qt, mu, bi
 min.: fs, op, ga, sil_{2,4}, chl, sc
 acc.: zi, to, ap
- 48 87-11 unit: PPms
 name: quartzose kyanite garnet mica schist
 maj.: qt, bi, mu
 min.: fl, op, ga, ky, ch, sc
 acc.:
- 49 87-12 unit: PPM
 name: garnetiferous diopside calc-silicate
 maj.: cc, di
 min.: gt, ep, tr, chl
 acc.: tt
- 50 87-13 unit: PPa

1	100	100	100
2	100	100	100
3	100	100	100
4	100	100	100
5	100	100	100
6	100	100	100
7	100	100	100
8	100	100	100
9	100	100	100
10	100	100	100
11	100	100	100
12	100	100	100
13	100	100	100
14	100	100	100
15	100	100	100
16	100	100	100
17	100	100	100
18	100	100	100
19	100	100	100
20	100	100	100
21	100	100	100
22	100	100	100
23	100	100	100
24	100	100	100
25	100	100	100
26	100	100	100
27	100	100	100
28	100	100	100
29	100	100	100
30	100	100	100
31	100	100	100
32	100	100	100
33	100	100	100
34	100	100	100
35	100	100	100
36	100	100	100
37	100	100	100
38	100	100	100
39	100	100	100
40	100	100	100
41	100	100	100
42	100	100	100
43	100	100	100
44	100	100	100
45	100	100	100
46	100	100	100
47	100	100	100
48	100	100	100
49	100	100	100
50	100	100	100
51	100	100	100
52	100	100	100
53	100	100	100
54	100	100	100
55	100	100	100
56	100	100	100
57	100	100	100
58	100	100	100
59	100	100	100
60	100	100	100
61	100	100	100
62	100	100	100
63	100	100	100
64	100	100	100
65	100	100	100
66	100	100	100
67	100	100	100
68	100	100	100
69	100	100	100
70	100	100	100
71	100	100	100
72	100	100	100
73	100	100	100
74	100	100	100
75	100	100	100
76	100	100	100
77	100	100	100
78	100	100	100
79	100	100	100
80	100	100	100
81	100	100	100
82	100	100	100
83	100	100	100
84	100	100	100
85	100	100	100
86	100	100	100
87	100	100	100
88	100	100	100
89	100	100	100
90	100	100	100
91	100	100	100
92	100	100	100
93	100	100	100
94	100	100	100
95	100	100	100
96	100	100	100
97	100	100	100
98	100	100	100
99	100	100	100
100	100	100	100

- name: hornblende amphibolite gneiss
 maj.: hbl
 min.: pl, bi, qt, op, py, chl, sc
 acc.: tt, zi, ap
- 51 87-14 unit: PPa
 name: hornblende amphibolite gneiss
 maj.: hbl
 min.: bi, fs, qt, op, chl, sc
 acc.: al, ap
- 52 87-15 unit: PPa
 name: blastomylonitic hornblende amphibolite
 maj.: hbl
 min.: bi, fs, qt, op, ep, cc, chl, sc
 acc.: ap
- 53 87-16 unit: PPa
 name: hornblende amphibolite with biotite schist laminae
 maj.: qt, fs, bi, hbl
 min.: op, ep, sc
 acc.: tt, zi, ap
- 54 87-18 unit: PPm
 name: banded fetid tremolite marble
 maj.: cc
 min.: tr, qt, fs, op, chl, sc
 acc.: tt
- 55 87-19 unit: PPms
 name: micaceous grey sillimanite quartz gneiss
 maj.: qt, fs
 min.: bi_{2,4}, mu_{2,4}, sil₄, chl, sc
 acc.:
- 56 87-21 unit: PPms
 name: quartzose garnet mica schist
 maj.: qt
 min.: bi, fs, op, ga, mu, chl, sc
 acc.: tt, zi
- 57 87-22 unit: PPm
 name: tremolite diopside calc-silicate
 maj.: di, tr, qt

THE HISTORY OF THE

REIGN OF

CHARLES THE FIRST

BY

JOHN BURNET

OF THE UNIVERSITY OF OXFORD

IN TWO VOLUMES

THE FIRST

OF THE REIGN

OF

CHARLES THE FIRST

BY

JOHN BURNET

OF THE UNIVERSITY OF OXFORD

IN TWO VOLUMES

THE SECOND

OF THE REIGN

OF

CHARLES THE FIRST

BY

JOHN BURNET

OF THE UNIVERSITY OF OXFORD

IN TWO VOLUMES

THE THIRD

OF THE REIGN

OF

CHARLES THE FIRST

BY

JOHN BURNET

OF THE UNIVERSITY OF OXFORD

IN TWO VOLUMES

min.: cc, fs, sc
acc.: tt

- | | | |
|----|-------|---|
| 58 | 87-23 | unit: PPms
name: tourmaline mica schist
maj.: bi _{1,2} , qt, fs
min.: op, mu _{1,2} , chl, sc
acc.: zi, to, ap |
| 59 | 87-24 | unit: PPm
name: banded garnet diopside skarn
maj.: ga, di, qt, fs
min.: tr, chl sc,
acc.: tt |
| 60 | 87-26 | unit: PPm
name: garnet tremolite diopside calc-silicate
maj.: di
min.: phl, fs, qt, ga, tr, chl, sc
acc.: tt |
| 61 | 87-27 | unit: PPms
name: biotite schist
maj.: bi _{1,2,4}
min.: qt, fs, gt, cd ₂₂ , chl, sc, op
acc.: zi, ap |
| 62 | 87-28 | unit: PPms
name: andalusite mica schist
maj.: qt, bi
min.: fs, op, mu, ad ₂₂ , sil ₄ , chl, sc
acc.: zi, ap |
| 63 | 87-29 | unit: PPm
name: coarsely crystalline banded diopside marble
maj.: cc
min.: phl, qt, tr, di, chl, sc
acc.: |
| 64 | 87-30 | unit: PPms
name: mica schist
maj.: bi _{1,2} , mu _{1,2} , qt
min.: fs, op, sc
acc.: zi, to, ap |

- 65 87-31 unit: PPm
 name: tremolite diopside calc-silicate
 maj.: qt, tr, di
 min.: fs, ep, cc, chl, sc
 acc.: tt
- 66 87-33 unit: PPa
 name: fine grained hornblende amphibolite
 maj.: hbl, fs
 min.: bi, qt, chl, sc
 acc.: ap
- 67 87-34 unit: PPms
 name: kyanite mica schist
 maj.: bi, qt, fs
 min.: mu, st, ky, cd₂, sc
 acc.: rt
- 68 87-37 unit: PPms
 name: crenulated mica schist
 maj.: qt, mu_{2,3}
 min.: bi₂, fs, op, chl, sc
 acc.: tt
- 69 87-38 unit: PPa
 name: banded hornblende amphibolite
 maj.: hbl
 min.: bi, pl, qt, op, ep, chl, sc
 acc.: tt
- 70 87-39 unit: PPm
 name: altered diopside marble
 maj.: cc
 min.: qt, di, sc, chl
 acc.:
- 71 87-43 unit: PPo
 name: biotite muscovite graniteorthogneiss
 maj.: qt, fs
 min.: mu, bi, op, sc, chl, cc
 acc.: ap, zi
- 72 87-44 unit: PPog

- name: leucocratic two mica granite orthogneiss
maj.: qt, fs
min.: bi, mu, op, sc
acc.:
- 73 87-45 unit: PPog
name: chloritized biotite feldspar orthogneiss
maj.: qt, fs
min.: bi, chl, op, chl
acc.:
- 74 87-46 unit: PPms
name: garnet mica schist
maj.: bi, qt, fs
min.: mu, op, ga, chl, sc
acc.: tt, zi, ap
- 75 87-47 unit: PPms
name: mica schist with thin amphibolite laminae
maj.: qt, fs, bi
min.: hbl, op, gt, mu
acc.:
- 76 87-50 unit: PPa
name: calc-silicate gneiss
maj.: di, cc, qt
min.: bi, bhl, op, fs, sc, chl, ep
acc.: tt, ap, zi
- 77 87-51 unit: PPms
name: sillimanite garnet mica schist
maj.: bi, fs, qt
min.: mu, op, gt, sil_{2,4}, chl
acc.: zi, to
- 78 87-52 unit: PPms
name: garnet mica schist
maj.: bi, qt
min.: fs, op, mu, ga
acc.: zi, to, ap
- 79 87-53 unit: PPms
name: kyanite garnet mica schist
maj.: bi_{1,2,3}, qt, mu_{1,2,3}

1. The first part of the report
describes the general situation
of the country.

2. The second part of the report
describes the economic situation
of the country.

3. The third part of the report
describes the social situation
of the country.

4. The fourth part of the report
describes the political situation
of the country.

5. The fifth part of the report
describes the cultural situation
of the country.

6. The sixth part of the report
describes the environmental situation
of the country.

7. The seventh part of the report
describes the international situation
of the country.

8. The eighth part of the report
describes the future prospects
of the country.

- min.: fs, op, ga, ky, chl
acc.: zi, to, ap
- 80 87-54 unit: PPms
name: interfoliated garnet mica schist and amphibolite
maj.: qt, bi, hbl, fs
min.: op, ga, ep, chl, sc
acc.: tt, zi, ap
- 81 87-55 unit: PPms
name: garnet biotite schist
maj.: bi, qt, ga
min.: fs, op, chl, sc
acc.: zi, to
- 82 87-56 unit: PPa
name: banded amphibolite gneiss
maj.: hbl, qt
min.: fs, bi, op, ep, chl, sc
acc.: tt, ap
- 83 87-57 unit: PPms
name: garnet mica schist
maj.: qt, fs
min.: bi, gt, mu, op, ep, chl, sc
acc.: zi, ap
- 84 87-58 unit: PPms
name: mica schist
maj.: bi, qt, fs
min.: mu, op, chl, sc
acc.:
- 85 87-59 unit: PPM
name: coarsely crystalline banded grey and white marble
maj.: cc
min.: qt, op, di(?), sc
acc.:
- 86 87-60 unit: PPms
name: micaceous quartzite
maj.: qt
min.: fs, mu, chl
acc.:

- 87 87-62 unit: PPms
 name: garnet mica quartzite
 maj.: qt
 min.: bi, fs, op, mu, gt, chl, sc
 acc.: zi, to, ap
- 88 87-63 unit: PPm
 name: gneissic diopside hornblende marble - calc silicate
 maj.: hbl, qt, di
 min.: ph, ep, cc, chl, sc
 acc.: tt, zi, ap
- 89 87-64 unit: PPms
 name: micaceous quartzite
 maj.: qt, mu
 min.: bi, fs, op
 acc.: zi
- 90 87-65 unit: PPms
 name: andalusite mica schist
 maj.: qt, fs, mu_{2,3}, bi₂
 min.: op, ad₂₇, ep, sc
 acc.: zi, to
- 91 87-66 unit: PPms
 name: garnet mica schist
 maj.: qt, mu_{1,2}
 min.: bi_{1,2}, fs, op, gt, chl, sc
 acc.: zi, to, ap
- 92 87-67 unit: PPm
 name: interfoliated hornblende amphibolite and marble
 maj.: hbl, cc
 min.: qt, fs, chl, sc
 acc.:
- 93 87-68 unit: PPms
 name: quartzose sillimanite garnet mica schist
 maj.: qt
 min.: bi, fs, op, mu, ga, sil₂, chl, sc
 acc.: zi, to, ap
- 94 87-69 unit: PPm

- name: coarsely crystalline banded white and grey tremolite
marble
maj.: cc
min.: qt, tr, ph
acc.: tt
- 95 87-72 unit: PPm
name: coarsely crystalline banded green and white tremolite
diopside marble
maj.: cc
min.: fs, qt, tr, di, sc
acc.: tt
- 96 87-73 unit: PPms
name: andalusite staurolite kyanite sillimanite garnet mica schist
maj.: qt, mu_{2,4}
min.: bi_{2,4}, fs, op, ga, st, ky, ad_{2,4}, sil₄, chl, sc
acc.: zi, to
- 97 87-74 unit: PPms
name: andalusite staurolite garnet mica schist
maj.: qt, fs, mu
min.: bi, op, ga, st, ad_{2,4}, chl, sc
acc.:
- 98 87-75 unit: PPms
name: crenulated sericitized porphyroblastic mica schist
maj.: qt, fs, mu
min.: bi, chl, sc
acc.: to, ap
- 99 87-76 unit: PPms
name: sericitized andalusite mica schist
maj.: qt
min.: bi, fs, mu, sil₄?, ad, chl, sc
acc.: tt, zi, to
- 100 87-77 unit: PPm
name: coarsely crystalline banded garnet tremolite diopside
marble
maj.: cc
min.: qt, fs, gt, tr, di, chl, sc
acc.: tt

THE UNIVERSITY OF CHICAGO

PHYSICS DEPARTMENT

PHYSICS 341

LECTURE 1

MECHANICS

1.1

1.2

1.3

1.4

1.5

1.6

1.7

1.8

- 101 87-78 unit: PPms
 name: andalusite staurolite sillimanite garnet mica schist
 maj.: qt, mu
 min.: bi, fs, op, ga, st, ad_{2,4}, sil₄, chl, sc
 acc.: tt, zi, to, ap
- 102 87-80 unit: PPms
 name: mica schist
 maj.: qt, fs
 min.: bi, mu, wp, gt, chl, sc
 acc.:
- 103 87-84 unit: PPa
 name: massive hornblende amphibolite
 maj.: hbl, fs
 min.: qt, op, ep, chl, sc
 acc.:
- 104 87-85 unit: PPms
 name: sillimanite garnet mica schist
 maj.: qt, fs
 min.: bi, mu, ga, op, sil₂, chl, sc
 acc.:
- 105 87-86 unit: PPM
 name: banded calcite marble and garnet diopside hornblende
 calc-silicate
 maj.: cc, hbl
 min.: fs, qt, ga, ep, cc, tr, di, chl, sc
 acc.:
- 106 87-88 unit: PPa
 name: sericitized feldspar amphibolite gneiss
 maj.: hbl, fs, sc
 min.: qt, bi, chl
 acc.:
- 107 87-100 unit: PPa
 name: biotite amphibolite gneiss
 maj.: hbl, fs, qt
 min.: bi, cc, sc
 acc.: tt, ap
- 108 87-102 unit: PPa

1. The first part of the report
describes the general situation
of the country.

2. The second part of the report
describes the economic situation
of the country.

3. The third part of the report
describes the social situation
of the country.

4. The fourth part of the report
describes the political situation
of the country.

5. The fifth part of the report
describes the cultural situation
of the country.

6. The sixth part of the report
describes the environmental situation
of the country.

7. The seventh part of the report
describes the international situation
of the country.

8. The eighth part of the report
describes the future prospects
of the country.

- name: garnet biotite hornblende amphibolite
maj.: hbl, fs
min.: qt, bi, op, ga, chl, sc
acc.:
- 109 87-103 unit: PPa
name: feldspar augan hornblende amphibolite
maj.: hlb, fs
min.: qt, op, chl, sc
acc.:
- 110 87-104 unit: PPms
name: sillimanite garnet mica schist
maj.: qt, mu
min.: bi, fs, op, sil₄, chl, sc
acc.: tt, zi to
- 111 87-105 unit: PPM
name: brown weathering diopside marble breccia
maj.: cc
min.: di, op, ep, chl
acc.:
- 112 87-106 unit: PPM
name: diopside marble
maj.: cc, di
min.: ph, fs, qt, op, ep, tr, sc
acc.: tt, ap
- 113 87-114 unit: PPa
name: leucocratic micaceous augan mylonite
maj.: qt, fs
min.: bi, mu, op, chl, sc
acc.:
- 114 87-115 unit: PPM
name: mylonitized calcite marble
maj.: cc
min.: qt
acc.:
- 115 87-116 unit: PPa
name: biotite hornblende blastomylonite
maj.: hbl, fs, qt

		min.: bi, op, ep, cc, chl, sc acc.: tt, ap
116	87-117	unit: PPms name: brown graphitic quartzite maj.: qt min.: bi _{1,2} , fs, op acc.:
117	87-118	unit: PPms name: micaceous brown graphitic quartzite maj.: qt min.: bi, fs, qp, mu, chl, sc acc.:
118	87-119	unit: PPms name: sericitized and altered mica schist maj.: qt, sc min.: bi, fs, chl acc.: to
119	87-121	unit: PPms name: quartzose staurolite mica schist maj.: qt min.: bi, fs, op, st, chl, sc acc.:
120	87-122	unit: PPms name: crenulated sillimanite staurolite kyanite garnet mica schist maj.: bi, mu, qt min.: fs, op, ga, st, sil ₄ , ky, chl, sc acc.: zi, to

a - sample id refers to the number that was assigned to a sample when it was collected in the field. The id indicates the year the sample was collected, followed by a sequential number (e.g. 86-33 - the 33rd sample collected in 1986)

b - unit monikers are the same as those used on all maps and are defined in the text.

c - maj., min., acc.; major, minor, and accessory mineral constituents, respectively, of a sample.

THE UNIVERSITY OF CHICAGO

1900

THE UNIVERSITY OF CHICAGO

1900

THE UNIVERSITY OF CHICAGO

1900

THE UNIVERSITY OF CHICAGO

1900

THE UNIVERSITY OF CHICAGO

1900

THE UNIVERSITY OF CHICAGO

1900

THE UNIVERSITY OF CHICAGO

1900

THE UNIVERSITY OF CHICAGO

1900

THE UNIVERSITY OF CHICAGO

1900

THE UNIVERSITY OF CHICAGO

1900

THE UNIVERSITY OF CHICAGO

1900

THE UNIVERSITY OF CHICAGO

1900

THE UNIVERSITY OF CHICAGO

1900

THE UNIVERSITY OF CHICAGO

1900

THE UNIVERSITY OF CHICAGO

1900

THE UNIVERSITY OF CHICAGO

1900

THE UNIVERSITY OF CHICAGO

1900

APPENDIX 5.3
MICROPROBE DATA BASE

Garnet Analyses

sample no.	48	48	48	75	75	75	77	77	79
analysis	core	int	rim	core	int	rim	core	rim	core
SiO ₂	37.22	36.89	37.64	37.24	37.17	37.07	37.30	37.62	37.40
Al ₂ O ₃	19.74	20.14	19.91	20.89	20.68	20.33	20.26	20.80	20.48
FeO	35.29	36.08	35.28	32.22	31.52	30.23	30.90	33.46	35.39
MnO	0.44	0.14	0.93	4.66	7.09	8.98	5.70	2.22	0.20
MgO	1.43	1.93	2.14	3.49	2.57	1.99	1.47	2.45	2.82
CaO	6.42	5.12	4.95	1.93	1.86	1.75	5.41	5.00	4.82
Total	100.54	100.30	100.85	100.43	100.89	100.35	101.04	101.55	101.11

Cations per 12 oxygen

Si	3.01	2.99	3.03	2.99	2.99	3.01	3.00	2.99	2.99
Al	1.88	1.95	1.89	1.96	1.95	1.95	1.92	1.94	1.92
Fe++	2.34	2.45	2.37	2.16	2.12	2.05	2.08	2.23	2.37
Mn	0.03	0.01	0.06	0.32	0.48	0.62	0.39	0.15	0.01
Mg	0.17	0.23	0.26	0.42	0.31	0.24	0.18	0.29	0.34
Ca	0.56	0.45	0.43	0.17	.16	0.15	0.47	0.43	0.41
Pyr	0.05	0.07	0.08	0.14	0.10	0.08	0.06	0.09	0.11
Alm	0.76	0.78	0.76	0.71	0.69	0.67	0.67	0.72	0.76
Sp	0.01	0.00	0.02	0.10	0.16	0.20	0.12	0.05	0.00
Gro	0.18	0.14	0.14	0.05	0.05	0.05	0.15	0.14	0.13

Garnet Analyses

sample no.	79	79	89	89	89	91	91	91	99
analysis	int	rim	core	int	rim	core	int	rim	core
SiO ₂		37.46	36.92	37.04	37.17	37.61	37.80	37.46	37.84
Al ₂ O ₃		20.75	20.60	20.24	20.72	20.72	20.93	20.92	20.22
FeO		36.53	33.12	37.66	36.74	33.91	34.67	35.66	35.70
MnO		0.17	2.75	0.21	0.40	2.04	1.10	1.83	0.11
MgO		3.36	0.91	1.65	2.10	2.09	2.16	2.26	2.38
CaO		2.71	5.65	3.11	3.07	4.58	4.78	3.01	5.25
Total		100.98	99.95	99.91	100.20	100.95	101.44	101.14	101.50
									101.47

Cations per 12 oxygen

Si	2.993	3.00	3.02	3.01	3.01	3.01	3.01	3.00	3.02	2.99
Al	1.95	1.97	1.94	1.97	1.97	1.95	1.96	1.97	1.90	1.96
Fe	2.44	2.25	2.57	2.48	2.48	2.27	2.31	2.39	2.38	2.32
Mn	0.01	0.19	0.01	0.03	0.03	0.14	0.07	0.12	0.01	0.11
Mg	0.40	0.11	0.20	0.25	0.25	0.25	0.26	0.27	0.28	0.29
Ca	0.23	0.49	0.27	0.27	0.27	0.39	0.41	0.26	0.45	0.34
Pyr	0.13	0.04	0.07	0.08	0.08	0.08	0.08	0.09	0.09	0.10
Alm	0.79	0.74	0.84	0.82	0.82	0.74	0.76	0.79	0.76	0.76
Sp	0.00	0.06	0.00	0.01	0.01	0.05	0.02	0.04	0.00	0.03
Gro	0.08	0.16	0.09	0.09	0.09	0.13	0.13	0.08	0.14	0.11

1000	1000	1000	1000
1000	1000	1000	1000
1000	1000	1000	1000
1000	1000	1000	1000
1000	1000	1000	1000
1000	1000	1000	1000
1000	1000	1000	1000
1000	1000	1000	1000
1000	1000	1000	1000

1000 1000 1000 1000

Garnet Analyses

sample no.	102	102	108	108	120	120
analysis	core	rim	core	rim	core	rim
SiO ₂	37.30	37.01	37.21	36.73	37.49	37.39
Al ₂ O ₃	20.92	20.80	20.58	20.33	20.56	20.50
FeO	34.77	34.90	34.05	34.08	33.88	34.68
MnO	3.66	3.83	3.52	4.87	1.31	1.44
MgO	2.52	2.09	2.67	1.76	1.06	1.95
CaO	1.87	1.86	2.34	2.01	6.50	4.32
Total	101.04	100.49	100.37	99.78	100.80	100.28

Cations per 12 oxygen

Si	2.99	2.99	3.00	3.00	3.01	3.02
Al	1.97	1.98	1.96	1.96	1.97	1.95
Fe	2.33	2.36	2.30	2.33	2.27	2.34
Mn	0.25	0.26	0.24	0.34	0.08	0.10
Mg	0.30	0.25	0.32	0.21	0.13	0.23
Ca	0.16	0.16	0.20	0.18	0.56	0.37
Pyr	0.10	0.08	0.10	0.07	0.04	0.08
Alm	0.77	0.78	0.75	0.76	0.75	0.77
Sp	0.08	0.09	0.08	0.11	0.03	0.03
Gro	0.05	0.05	0.07	0.06	0.18	0.12

Biotite Analyses

sample no.	48	48	48	75	75	77	77	79	79	89
analysis	core	int	rim	core	rim	core	rim	core	rim	core
SiO ₂	34.76	42.88	34.46	35.45	35.37	35.99	35.27	34.37	35.23	34.04
TiO ₂	2.08	0.95	2.02	2.91	2.84	1.71	0.84	1.75	0.94	2.43
Al ₂ O ₃	19.63	30.61	19.55	19.87	20.34	20.37	20.83	18.89	19.40	18.97
FeO	21.87	7.32	22.38	20.41	20.20	18.65	19.33	22.22	22.35	22.88
MnO	0.04	0.05	0.06	0.28	0.43	0.20	0.26	0.03	0.01	0.04
MgO	8.21	2.87	8.00	8.01	7.89	10.20	10.07	9.81	9.45	6.98
CaO	0.01	0.04	0.02	0.00	0.16	0.00	0.01	0.18	0.17	0.00
Na ₂ O	0.17	0.04	0.14	0.10	0.13	0.21	0.06	0.28	0.19	0.14
K ₂ O	9.43	8.00	9.37	9.77	9.90	9.59	10.16	8.71	8.85	9.64
F	0.34	0.18	0.32	0.17	0.17	0.35	0.32	0.27	0.32	0.30
H ₂ O	3.28	6.79	3.38	2.78	2.42	2.43	2.66	3.26	2.88	4.32
Total	99.72	99.73	99.70	99.75	99.85	99.70	99.81	99.77	99.79	99.74
Total - F	99.58	99.65	99.57	99.68	99.78	99.55	99.68	99.66	99.66	99.61
Cations per 22 oxygen										
Si	5.31	6.01	5.29	5.34	5.31	5.36	5.30	5.26	5.35	5.31
Al ^{iv}	2.69	1.989	2.71	2.66	2.69	2.65	2.71	2.75	2.65	2.69
Ti	0.24	0.10	0.23	0.33	0.32	0.19	0.10	0.20	0.11	0.29
Al	0.84	3.07	0.83	0.87	0.91	0.93	0.98	0.66	0.82	0.79
Fe ₂	2.79	0.86	2.87	2.57	2.54	2.32	2.43	2.84	2.84	2.98
Mn	0.01	0.01	0.01	0.04	0.06	0.03	0.03	0.00	0.00	0.01
Mg	1.87	0.60	1.83	1.80	1.77	2.26	2.25	2.24	2.14	1.62
Ca	0.00	0.01	0.00	0.00	0.01	0.00	0.00	0.01	0.01	0.00
Na	0.05	0.01	0.04	0.03	0.04	0.06	0.02	0.08	0.01	0.42
K	1.84	1.43	1.83	1.88	1.90	1.82	1.95	1.70	1.71	1.92
F	0.16	0.08	0.16	0.08	0.08	0.17	0.15	0.13	0.15	0.15
OH	3.84	3.92	3.85	3.92	3.92	3.84	3.85	3.87	3.85	3.85
Phl	0.40	0.41	0.39	0.41	0.41	0.49	0.47	0.44	0.43	0.35
Ann	0.60	0.59	0.61	0.58	0.58	0.50	0.52	0.56	0.57	0.64
Mn	0.00	0.00	0.00	0.01	0.01	0.01	0.01	0.00	0.00	0.01

Biotite Analyses

sample no.	89	91	91	99	99	102	102	108	108	120
analysis	rim	core	rim	core	rim	core	rim	core	rim	core
SiO ₂	32.46	34.44	34.60	34.73	34.49	34.56	33.24	34.77	34.02	34.66
TiO ₂	1.48	1.95	1.78	1.90	1.71	2.65	2.54	1.98	1.99	1.96
Al ₂ O ₃	19.13	19.89	20.55	19.98	20.39	19.07	20.34	19.46	19.55	19.42
FeO	25.14	22.85	22.56	22.16	21.98	22.56	23.37	21.72	22.29	22.12
MnO	0.09	0.08	0.07	0.10	0.10	0.08	0.17	0.13	0.18	0.12
MgO	7.36	7.24	7.09	8.06	7.93	7.42	7.12	7.48	7.42	7.43
CaO	0.04	0.00	0.02	0.24	0.28	0.00	0.04	0.03	0.05	0.00
Na ₂ O	0.08	0.20	0.23	0.20	0.14	0.24	0.14	0.12	0.12	0.11
K ₂ O	9.14	9.06	8.94	9.26	9.02	9.21	8.02	9.36	8.97	9.60
F	0.34	0.25	0.25	0.32	0.37	0.29	0.39	0.37	0.36	0.40
H ₂ O	4.53	3.71	3.56	2.86	3.35	3.62	4.33	4.35	4.79	3.87
Total	99.79	99.67	99.65	99.81	99.76	99.70	99.70	99.77	99.74	99.69
Total - F	99.65	99.56	99.54	99.68	99.60	99.58	99.54	99.61	99.59	99.52
Cations per 22 oxygen										
Si	5.14	5.30	5.30	5.29	5.27	5.32	5.16	5.40	5.30	5.35
Al ^{iv}	2.86	2.70	2.70	2.71	2.73	2.68	2.85	2.63	2.71	2.65
Ti	0.18	0.23	0.21	0.22	0.20	0.31	0.30	0.23	0.23	0.23
Al	0.71	0.91	1.01	0.88	0.95	0.78	0.87	0.91	0.88	0.88
Fe ₂	3.33	2.94	2.89	2.82	2.81	2.90	3.03	2.81	2.90	2.86
Mn	0.01	0.01	0.01	0.01	0.01	0.01	0.02	0.02	0.02	0.02
Mg	1.74	1.66	1.62	1.83	1.81	1.70	1.65	1.72	1.72	1.71
Ca	0.01	0.00	0.00	0.01	0.02	0.0	0.01	0.01	0.01	0.00
Na	0.03	0.06	0.07	0.06	0.04	0.07	0.04	0.04	0.04	0.03
K	1.85	1.78	1.75	1.80	1.76	1.81	1.59	1.84	1.78	1.89
F	0.17	0.12	0.12	0.15	0.18	0.14	0.19	0.18	0.17	0.20
OH	3.83	3.88	3.88	3.85	3.82	3.86	3.81	3.82	3.82	3.81
Phl	0.34	0.36	0.36	0.39	0.39	0.37	0.35	0.38	0.37	0.37
Ann	0.66	0.64	0.64	0.61	0.61	0.63	0.64	0.62	0.63	0.62
Mn	0.00	0.00	0.00	0.00	0.00	0.00	0.01	0.00	0.00	0.01

1. The first part of the document is a list of names and addresses.

2. The second part of the document is a list of names and addresses.

3. The third part of the document is a list of names and addresses.

4. The fourth part of the document is a list of names and addresses.

5. The fifth part of the document is a list of names and addresses.

6. The sixth part of the document is a list of names and addresses.

7. The seventh part of the document is a list of names and addresses.

8. The eighth part of the document is a list of names and addresses.

9. The ninth part of the document is a list of names and addresses.

10. The tenth part of the document is a list of names and addresses.

11. The eleventh part of the document is a list of names and addresses.

12. The twelfth part of the document is a list of names and addresses.

Biotite Analyses

sample no.	120
analysis	rim
SiO ₂	34.90
TiO ₂	2.03
Al ₂ O ₃	19.43
FeO	23.39
MnO	0.13
MgO	6.22
CaO	0.17
Na ₂ O	0.03
K ₂ O	8.83
F	0.31
H ₂ O	4.35
Total	99.79
Total - F	99.66
Cations per 22 oxygen	
Si	5.41
Al ^{iv}	2.59
Ti	0.24
Al	0.96
Fe ₂	3.03
Mn	0.02
Mg	1.44
Ca	0.01
Na	0.01
K	1.75
F	0.15
OH	3.85
Phl	0.32
Ann	0.67
Mn	0.01



Plagioclase Analyses

sample no.	48	48	75	75	77	77	91	91	99	102
analysis	core	rim	core	rim	core	rim	core	rim	core	core
SiO ₂	59.72	59.43	61.25	63.23	63.64	62.44	59.57	59.63	61.54	60.49
Al ₂ O ₃	25.23	25.83	24.26	22.96	22.75	23.90	24.87	25.04	23.96	24.81
FeO	0.12	0.17	0.04	0.12	0.12	0.20	0.28	0.22	0.21	0.11
CaO	6.87	7.12	6.06	4.95	3.94	5.01	6.55	6.49	5.66	6.31
Na ₂ O	7.70	7.67	8.07	8.52	9.20	8.69	7.75	7.82	8.48	7.98
K ₂ O	0.13	0.13	0.21	0.17	0.17	0.18	0.15	0.13	0.07	0.15
Total	99.77	100.35	99.89	99.95	99.82	100.42	99.17	99.33	99.92	99.85
Cations per 8 oxygen										
Si	2.67	2.64	2.72	2.80	2.82	2.76	2.68	2.68	2.74	2.70
Al	1.33	1.35	1.27	1.20	1.19	1.24	1.32	1.32	1.26	1.30
Fe	0.00	0.01	0.00	0.00	0.00	0.01	0.01	0.01	0.01	0.00
Ca	0.33	0.34	0.29	0.24	0.19	0.24	0.32	0.31	0.27	0.30
Na	0.67	0.66	0.70	0.73	0.79	0.74	0.68	0.68	0.73	0.69
K	0.01	0.01	0.01	0.01	0.01	0.01	0.01	0.01	0.00	0.01
An	0.33	0.34	0.29	0.24	0.19	0.24	0.31	0.31	0.27	0.30
Ab	0.66	0.65	0.70	0.75	0.80	0.75	0.68	0.68	0.73	0.69
Or	0.01	0.01	0.01	0.01	0.01	0.01	0.01	0.01	0.00	0.01

121 30119 1 30119 1 3

122 30120 1 30120 1 3

123 30121 1 30121 1 3

124 30122 1 30122 1 3

125 30123 1 30123 1 3

126 30124 1 30124 1 3

127 30125 1 30125 1 3

128 30126 1 30126 1 3

129 30127 1 30127 1 3

130 30128 1 30128 1 3

131 30129 1 30129 1 3

132 30130 1 30130 1 3

Plagioclase Analyses (cont.)

sample no.	102	108	120
analysis	rim	core	core
SiO ₂	60.50	59.18	63.07
Al ₂ O ₂	24.51	25.28	22.95
FeO	0.05	0.08	0.20
CaO	4.42	7.01	4.24
Na ₂ O	7.61	7.61	9.00
K ₂ O	1.28	0.14	0.10
Total	98.37	99.30	99.56

Cations per 8 Oxygen

Si	2.73	2.66	2.80
Al	1.30	1.34	1.20
Fe	0.00	0.00	0.01
Ca	0.21	0.34	0.20
Na	0.67	0.66	0.78
K	0.07	0.01	0.01
An	0.22	0.33	0.20
Ab	0.70	0.66	0.79
Or	0.08	0.01	0.01

RY
CANICS

SSEM

P Pb

P Pm

P Pa

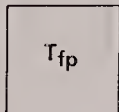
P Pms

LEGEND

PLUTONIC ROCKS

METAMORPHIC ROCKS

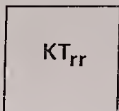
TERTIARY



FELDSPAR PORPHYRY

heterogeneous igneous suite which includes plugs and small plutons of orange and pink weathering, flesh colored, miarolitic, massive, felspar and quartz - feldspar porphyry; and dykes of brown and dark green weathering, green to buff colored, feldspar and hornblende feldspar porphyry.

CRETACEOUS & TERTIARY



RUBY RANGE BATHOLITH

grey to tan weathering, grey to dark grey, medium to coarsely crystalline, massive to mildly foliated, hornblende and biotite hornblende diorite and granodiorite to nebulitic hornblende biotite granite.

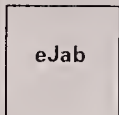
EARLY JURASSIC



LONG LAKE PLUTONIC SUITE

orange weathering, orange and pink colored, coarsely crystalline to porphyritic, massive, miarolitic, quartz and biotite quartz monzonite.

STIKINE TERRANE

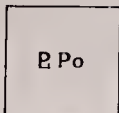


AISHIHIK BATHOLITH

grey to light grey weathering, grey to dark grey colored, coarsely crystalline, equigranular to K-feldspar megacrystic, hornblende and biotite hornblende granodiorite to quartz diorite. A foliation, defined by the alignment of mineral grains, is commonly developed. A second foliation, defined by protomylonitic, and gneissic banding, is locally developed and overprints the mineral foliation

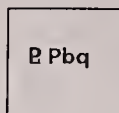
NISLING ASSEMBLAGE

DEVONO-MISSISSIPPIAN



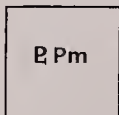
ORTHOGNEISS

tan weathering, light grey colored, medium to coarsely crystalline, feldspar augan, muscovite and biotite muscovite orthogneiss; and dark grey weathering, dark grey colored, medium grained, hornblende and biotite hornblende diorite and quartz diorite orthogneiss.



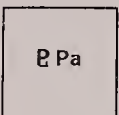
BROWN QTZITE

dark to light brown weathering, brown to buff colored, medium to fine grained, locally graphitic, micaceous and feldspathic quartzite. Includes thin and discontinuous marble, amphibolite and micaschist lenses.



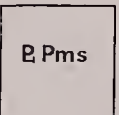
MARBLE

light grey to light brown weathering, white to grey colored, fetid, coarsely crystalline, laminated calcite marble. Includes minor skarn, amphibolite, and calc-silicate



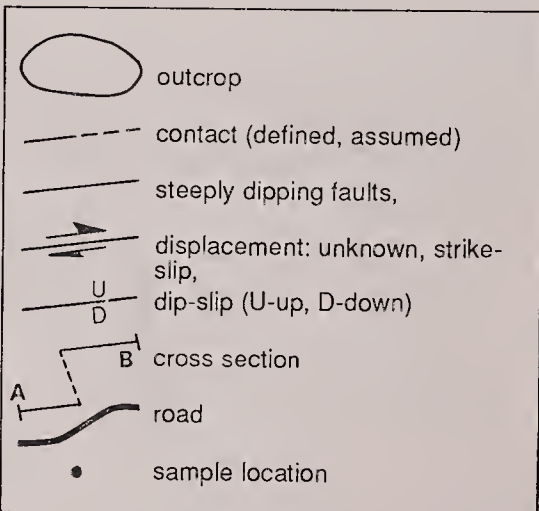
AMPHIBOLITE

dark green to black weathering, green colored, fine to coarsely crystalline, gneissic to well foliated, hornblende and biotite hornblende quartzite, micaschist and marble, and significant amounts of pistachio green, epidote hornblende diopside calc-silicate

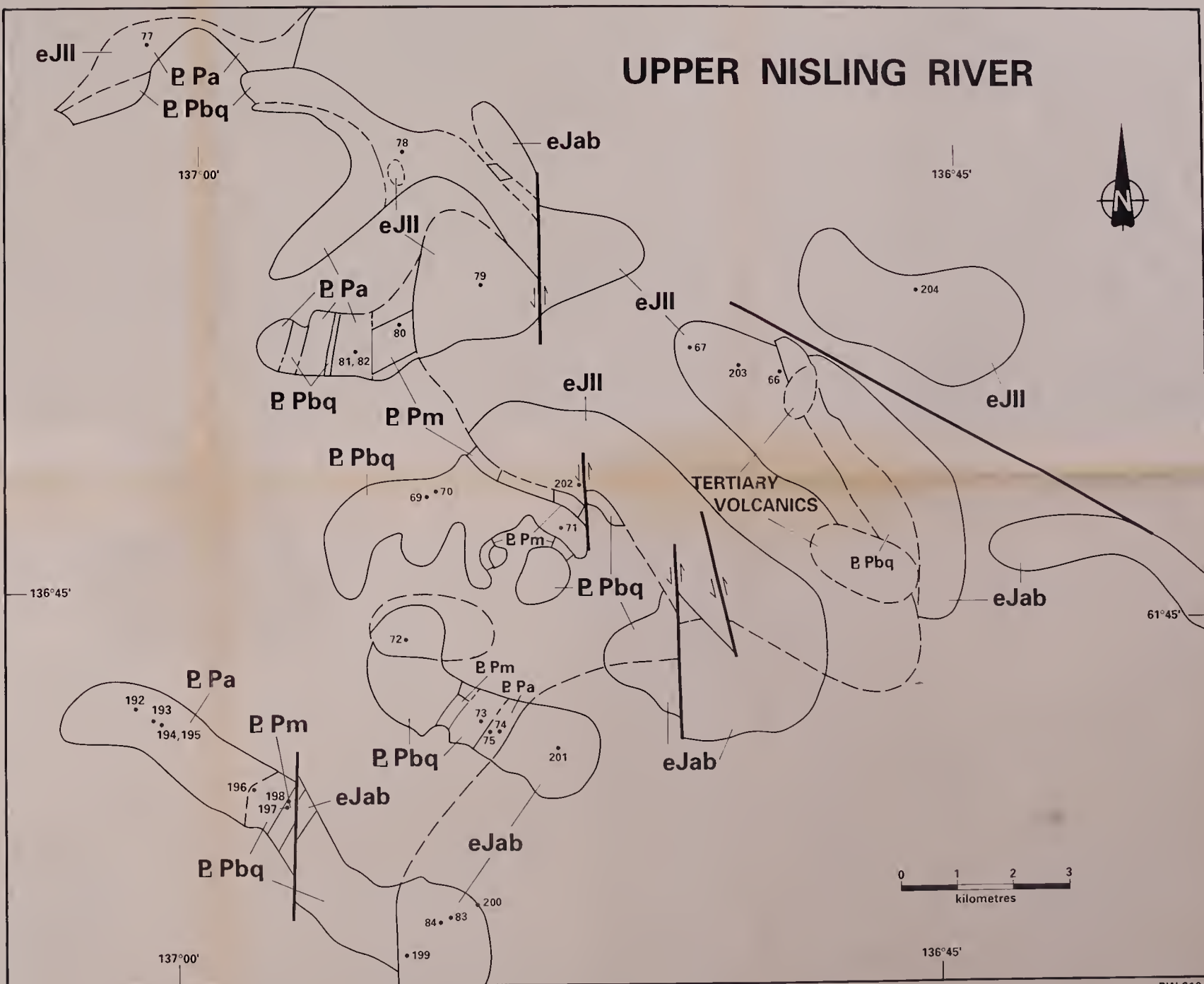


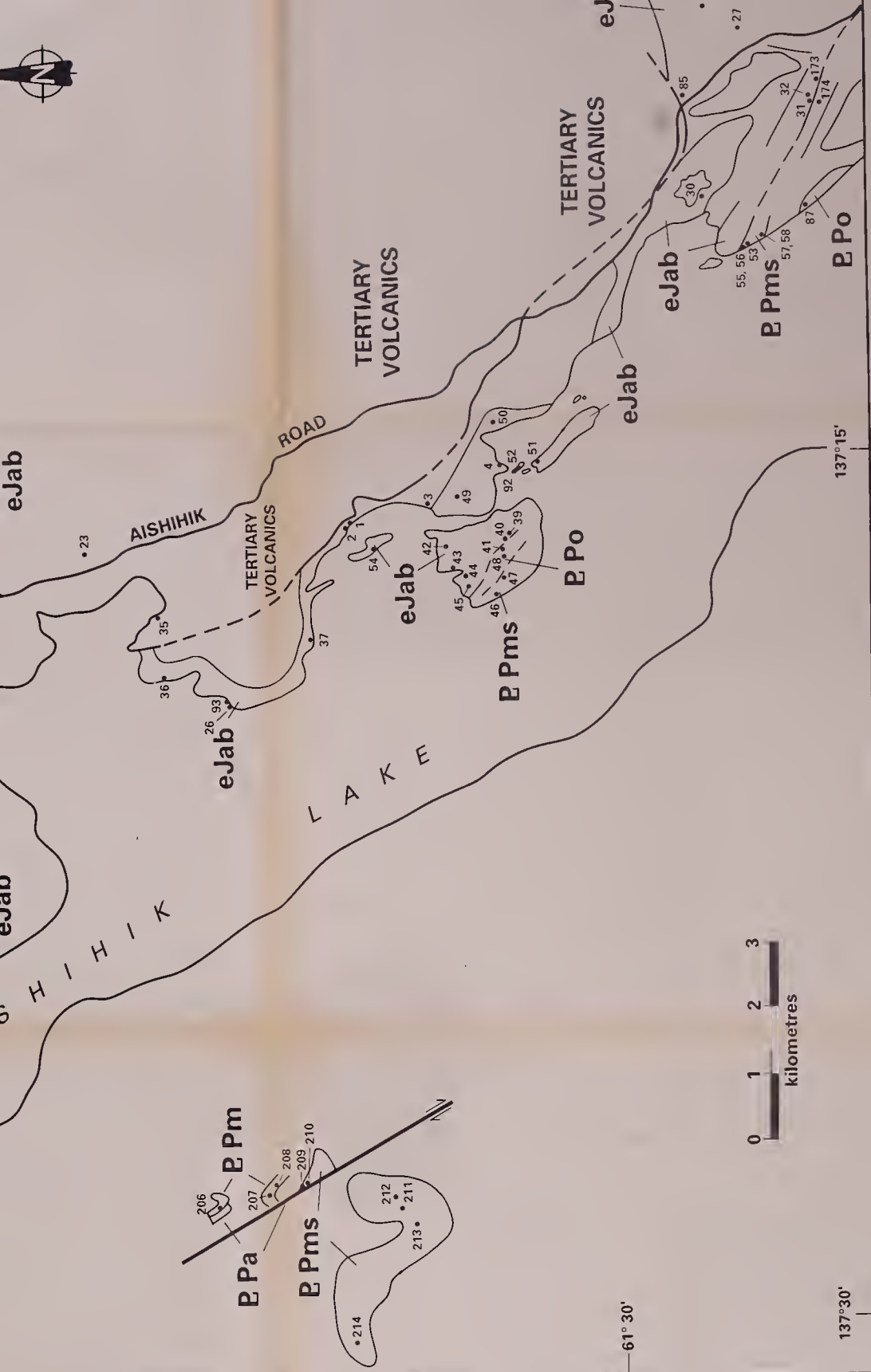
MICASCHIST

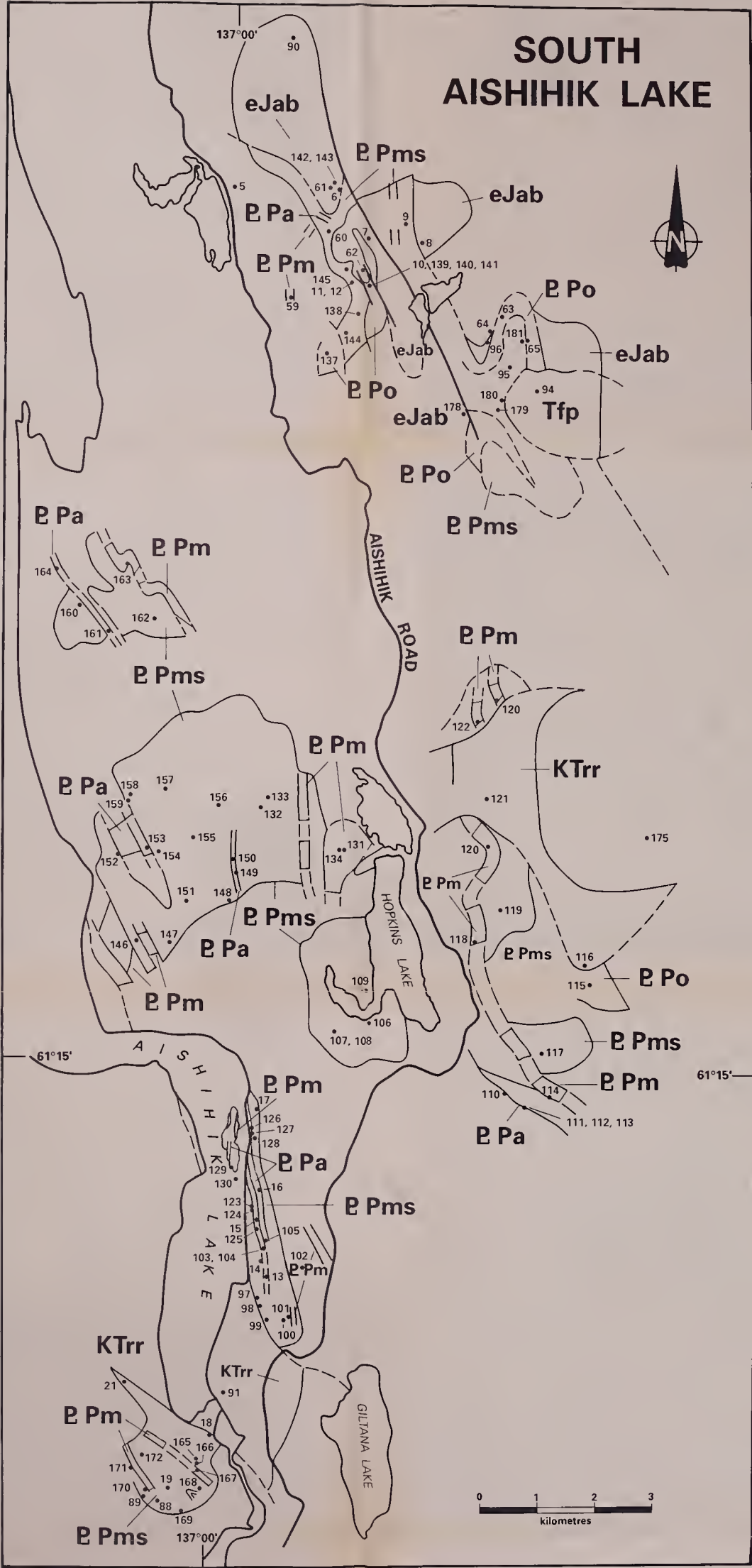
Brown weathering, dark to light grey colored, medium to coarsely crystalline, well foliated to gneissic, migmatitic, muscovite biotite schist with minor grey quartz gneiss and brown weathering, tan colored, medium grained, foliated, micaceous & feldspathic quartzite. Includes minor amphibolite and marble.



UPPER NISLING RIVER







University of Alberta Library



0 1620 0110 6531

B44938